NASA CONTRACTOR REPORT 166187

Determination of Wind Tunnel Constraint Effects by a Unified Pressure Signature Method

Part II: Application to Jet-In-Crossflow Cases

J.E. Hackett
S. Sampath
C.G. Phillips

Lockheed-Georgia Company

CONTRACT NAS2-9883(Mod 3)
June 1981

NASA

NASA CONTRACTOR REPORT 166187

Determination of Wind Tunnel Constraint Effects by a Unified Pressure Signature Method

Part II: Application to Jet-In-Crossflow Cases

J.E. Hackett
S. Sampath
C.G. Phillips

Lockheed-Georgia Company
Marietta, Georgia 30060

Prepared for
Ames Research Center
under Contract NAS2-9883 (Mod 3)

NASA
National Aeronautics and Space Administration
Ames Research Center
Moffett Field, California 94035

CONTENTS

LIST OF FIGURES

LIST OF SYMBOLS

a	vortex core
A_j	measured jet exit area
b	vortex span
B	tunnel width
C	tunnel area
C_Q	jet mass flow coefficient defined as $\dot{m}/\rho_c U_c S$
C_μ	jet momentum flux coefficient defined as $\int_{A_j} \rho_j V_j^2 dA_j / \frac{1}{2}\rho_c U_c^2 S$
D	jet diameter
H	tunnel height
H_o	mainstream total pressure
I_1	radius-weighted, normalized jet-velocity integral
I_2	radius-weighted, normalized jet-velocity-squared integral
M	line source strength, $ft^3/sec/ft$
$\dot{m}$	measured mass flow rate, from initial flow nozzle
M_{jet}	jet exit Mach number from equation (3.5)
p_c	jet exit static pressure from equation (3.4)
p_p	measured jet plenum pressure
q_o	calibrated empty tunnel dynamic pressure at the model location
q_c	blockage-corrected dynamic pressure at the model location
Q	point source strength, ft^3/sec.
R	ratio of jet velocity to mainstream velocity, corrected by $\sqrt{\rho_j/\rho_c}$
R	universal gas constant
R_m	mean jet inside radius at jet exit

R_{NOM}	nominal true velocity ratio used for test control
S	model reference area
T	jet thrust from momentum flux
T_{jet}	jet exit temperature from equation (3.6)
T_p	measured plenum temperature
U_o, U_∞	calibrated empty tunnel velocity at the model location
U_c	blockage-corrected true tunnel velocity at the model location
V_E	effective jet velocity: transport velocity of $\dot{m}$ to achieve thrust T
U_j	jet velocity
$\bar{V}_j$	mean true jet velocity from mass flow meter and ρ_j
V_{jm}	true local jet exit velocity, from rake measurement
V_{th}	theoretical jet exit velocity from equation (3.8)
X, Y, Z	streamwise, spanwise and vertical coordinates
α	angle of attack
$\Delta\alpha$	angle-of-attack correction for tunnel constraint effects
γ	ratio of specific heats
Γ	vortex circulation $ft^2/sec.$
ΔC_{pt}	difference between tunnel plenum and test section entry pressure coefficient
Δpt	pressure difference corresponding to ΔC_{p_t}
ΔU	tunnel-induced supervelocity in test section
ϵ_s	solid blockage velocity correction factor
ϵ_w	wake blockage velocity correction factor
η_1, η_2	temporary calibration factors (see eqns. 3.12 and 3.13)
λ	ratio between mean jet velocities derived from rake and mass flow measurements
μ	line doublet strength, $ft^3/sec.$

ρ	density
ρ_c	mainstream density
ρ_j	jet density, at exit, from equation (3.7)
χ	inclination of line doublet from vertical (in Heyson's method, Appendix C)
Ψ	stream function

SUMMARY

The development is described of an improved jet-in-crossflow model for estimating wind tunnel blockage and angle-of-attack interference. Experiments showed that the simpler existing models fall seriously short of representing far-field flows properly. A new, vortex-source-doublet (VSD) model was therefore developed which employs curved trajectories and experimentally-based singularity strengths. The new model is consistent with existing and new experimental data and it predicts tunnel wall (i.e. far-field) pressures properly. It is implemented as a preprocessor to the wall-pressure-signature-based tunnel interference predictor described in Part I of the present report.

The supporting experiments and theoretical studies revealed some new results. Comparative flow field measurements with 1-inch "free-air" and 3-inch impinging jets showed that vortex penetration into the flow, in diameters, was almost unaltered until 'hard' impingement occurred. In modeling impinging cases, a 'plume redirection' term was introduced which is apparently absent in previous models. The effects of this term were found to be very significant.

A copy of this document is retained in the Lockheed-Georgia Company Engineering Report Files. The identifying number is LG81ER0167.

1.0 INTRODUCTION

1.1 Aims of the present work

The aim of the work described in this report is to adapt or develop a jet-in-crossflow model for estimating wind tunnel interference, with primary emphasis upon non-impinging cases. A corresponding computer program is required which can be used on an optional basis with the Part 1 program for tests involving models with lifting jets or fans.

1.2 Background

Part 1 of this report describes a method for calculating wind tunnel blockage and angle-of-attack corrections from pressure measurements made along the tunnel surfaces. Theoretical flow models employed are constructed from line singularities which represent the model and it's wake as 'perceived' by the tunnel. The flow models can accommodate wing sweep, angle-of-attack and offset from the tunnel center, though in many cases it has been found that an unswept planar model suffices. The approach may be considered semi-inverse since the details mentioned are user-specified yet the singularity strengths and their axial locations are determined from wall pressures using influence matrices.

It would be very useful if the above approach could be extended along the same lines to lifting jets and allow trajectory shape, for example, to be implied from the wall pressures. However, on reviewing the logistics needed for doing this - particularly the likely size and conditioning of the influence matrices concerned - it soon became apparent that a more explicit approach was preferable. Subsequent experience, described later, has shown that use of an explicit model for the jet plume is probably essential.

It appeared initially that, with the exception of wall pressure measurements, most of the needed experimental data and flow modeling experience would be available in existing literature. However an extensive review of experimental data revealed that most experiments concerned jets emergent from a plane or from models which are relatively complex. Jet-from-pipe data, which was considered more suitable, was relatively scarce. New experiments were therefore planned, using jets-from-pipes, to determine wall pressures and to find parametric relationships between the new jet-from-pipe and the existing jet-from-plane flow field data.

A review was made of the very many theoretical models which have been proposed for the jet-in-crossflow. Most had to be rejected because they are too complex for the present application. However the models proposed by Fearn (Ref. 1), by Heyson (Ref. 2) and by Williams and Wood (Ref. 3) included at least some of the necessary physics and were reasonably simple. These were therefore prime candidates in the earlier stage of the work and it was hoped that one or more could be used directly.

The principal flow model property required for the present work is the ability to predict far-field flows. A good test of this is to attempt to predict tunnel wall pressures. It will be seen later that all of the candidate methods failed this test quite badly. In retrospect, it is apparent that all were suitable only for near-field applications.

As originally perceived, the main tasks were to interpret and organize existing experimental data and modeling techniques for tunnel interference prediction. It has turned out that significant new studies were needed in both areas in order to build upon existing technology. These studies are the subject of the rest of this report.

1.3 Layout of the Present Report

Section 2 will describe, in broad terms, the way in which jet-in-crossflow and "rest of model" interference effects are determined and combined. Sections 3 and 4 concern test details and results for jet-from-pipe tests conducted as part of the present study. Jet hardware and calibration procedures are described in more-than-usual detail because the extra attention given to these aspects paid off well. The development of a new flow model, designated the 'VSD' model for Vortex/Source/Doublet, is described in Section 5 and comparisons are made with predictions using other methods. Section 6 gives the fairly comprehensive conclusions which arose from the present work.

In the interest of shortening the main part of this report, the majority of the experimental traverse data is presented as Appendices A and B. For similar reasons, comments concerning Heyson's method for interference estimation appear in Appendix C. Program documentation and listings are given in Appendix D.

2.0 INTERFACE TO THE PART I PROGRAM

For the reasons mentioned above, the jet-in-crossflow modeling program developed here is used as a pre-processor to the main, Part I program. Figure 2.1 depicts the general principles of operation of the Part I program. Prior to a test, a theoretical flow model is constructed using model span, sweep and angle-of-attack details, as needed. An influence matrix derived from this model is used in conjunction with wall, roof and floor pressure data to determine source and vortex strength distributions as a function of X. Tunnel-induced angle-of-attack and blockage increments are then calculated.

For jet- or fan-lift models the general approach is the same but the above routine is preceded by explicit jet-in-crossflow calculations (see Figure 2.2). These accomplish two objectives. Firstly, a direct estimate is made of the distributions of Δu and $\Delta \alpha$, for subsequent addition to corresponding 'rest-of-model' data. Secondly, the effect of the jet-in-crossflow (or jets) is removed from the measured wall pressure signatures prior to further processing. This step is very important because it removes substantial non-planar effects from the data which would otherwise cause errors due to 'cross' effects. In particular, offset blockage effects of a strongly penetrating jet would be returned eventually as tunnel-induced angle-of-attack in the absence of the preprocessing step.

3.0 TEST RIGS AND PROCEDURES

3.1 Introduction

Figures 3.1 and 3.2 give a general view and dimensions of the test rig for the jet-in-crossflow experiments. The main test measurements comprised in-plume three-component velocity traverses, using the rake of 5-holed pitch yaw probes shown, and wall pressures along the test section walls and roof (see subsection 3.4). Boundary layer tangential blowing was available at the roof, from a location 13-inches ahead of the jet exit, and was applied when surface pressures on the roof centerline indicated the presence of flow breakdown. Sufficient blowing was applied to remove the standing vortex, ahead of the jet impingement point, when it occurred. This parallels the approach discussed in detail in Part I of the present report for jet-flapped wings. In practice, the tangential blowing was needed only with the 3-inch jets at high jet velocity ratios.

Figure 3.3 tabulates the jet configurations used and typical mainstream and jet velocities for the nominal test velocity ratios. With the 3-inch jets at velocity-ratio 8, a reduced mainstream speed was necessary because of supply limitations.

3.2 On-line Tunnel Blockage Corrections

The conventional solid-plus-wake blockage equation has the form

$$U_c = U_o \, (1 + \varepsilon_s + \varepsilon_w) \tag{3.1}$$

where U_c is the corrected velocity at the model location

U_o is the calibrated empty tunnel velocity at the model

ε_s, ε_w are solid and wake blockage factors.

The above form was used because the full wall pressure signature approach cannot be implemented without the flow model which will be developed from the present experiments. A predecessor of the pressure signature method, formerly designated the 'q-pot' approach, was used to determine ε_w. A conventional calculation was used for ε_s, the solid blockage, based upon jet pipe dimensions. The velocity increase ΔU, due to wake blockage, is inferred via linear assumptions from the pressure decrease ΔC_{pt}, between the contraction exit piezometer ring and the (atmospheric) breather slots at the start of the first diffuser. Thus

$$\varepsilon_w = \left(\frac{\Delta U}{U_o}\right)_{x=o} = \frac{1}{2} \left(\frac{\Delta U}{U_o}\right)_{x=\infty} = \frac{1}{4} \, (\Delta C_{pt}) \tag{3.2}$$

On supplying the necessary calibration constants and removing the empty-section value of ΔC_{pt}, a working equation for blockage-corrected velocity is obtained at the model location as

$$q_c = \frac{1}{2}\rho U_c^2 = 1.0182\ \{1 + \varepsilon_s + 0.25\ (\Delta C_{pt} - .04903)\}\ \Delta p$$

$$= 1.0182\ (q_c / q_o)\ \Delta p \qquad (3.3)$$

where Δp is the measured contraction pressure drop

and $\Delta C_{pt} = \Delta p_t / 1.0182\ \Delta p$.

The corresponding corrected static pressure at the model is

$$p_c = H_o - \frac{1}{2}\rho U_c^2 \qquad (3.4)$$

where H_o is obtained from the tunnel calibration, based upon contraction entry piezometer pressures. Figure 3.4 shows typical values of blockage ratio as a function of nominal jet velocity ratio R_{NOM}.

To complete the free stream data, tunnel density is obtained using p_c, the measured tunnel temperature and the equation of state. Tunnel pressure ratio (to p_c), true speed and and blockage ratio (i.e. U_c / U_o) are also calculated.

3.3 Jet Hardware and Its Calibration

Hardware

Figure 3.5 shows a longitudinal section through the jet plenum and flow conditioning system with a 3-inch transition piece to a 1-inch inclined jet fitted. For verticaljets, the transition piece is omitted. In the latter cases plenum-to-jet pipe contraction ratios are 12.8 and 115 for the 3-inch and 1-inch pipes respectively. Pre-straightening, from the supply cones at the base of the plenum (Figure 3.6) is accomplished by a 2-inch thick honeycomb of $\frac{1}{4}$-inch cell size. When installing the inclined, 1-inch pipes the plenum position was adjusted to keep the jet exit location constant.

Calibration runs, using a total pressure rake at the jet exits, showed a need to correct the 3-inch jet profile to match the more fully developed 1-inch jet profile. Figure 3.7 shows an adjustable, profile-modification device used to increase the velocity deficit around the 3-inch pipe. A good match was obtained, after two adjustments, for the configuration shown. The profiles themselves will be discussed in Section 4.

Jet calibration

Pressure ratio, to corrected tunnel static, p_c, was the primary jet control variable. Mass flow was also measured but this included roof boundary layer control air, during forward speed runs with the larger jets at high velocity ratio. The main calibrations were therefore made on the basis of jet plenum-to-exit pressure ratio.

A rake of total pressure probes at 0.1-inch spacing was employed to determine the thrust of the partially developed pipe flow profiles at jet exit. Data were obtained across two diameters at right angles and integrations were performed to determine mass flow, for comparison with direct measurements, and thrust. Checks on the thrust gave good agreement, for

partially developed pipe flow skin friction, with data quoted by Ower and Pankhurst

The following calculation procedure was employed during data reductions:

$$M_{jet}^{2} = \frac{2}{\gamma - 1}\left\{\frac{P_p}{P_c}^{\frac{\gamma-1}{\gamma}} - 1\right\} \tag{3.5}$$

$$T_{jet} = T_p / (1 + \frac{\gamma - 1}{2} M_{jet}^{2}) \tag{3.6}$$

$$\rho_J = \frac{P_c}{R\, T_{jet}} \tag{3.7}$$

$$V_{th} = M_{jet} \sqrt{\gamma R\, T_{jet}} \tag{3.8}$$

The mean jet velocity $\bar{V}_J$ was obtained during calibration from the measured mass flow in via:

$$\bar{V}_J = \frac{\dot{m}}{\rho_J A_J} \tag{3.9}$$

A shape parameter, λ, was defined as

$$\lambda = \frac{\bar{V}_J}{V_{th}} \tag{3.10}$$

λ is obtained during jet calibration and is used routinely to obtain the flow coefficient C_Q using

$$C_Q \frac{S}{A_J} = \frac{\dot{m}}{\rho_c U_c S} \cdot \frac{S}{A_J}$$

$$= \frac{\rho_J \bar{V}_J A_J}{\rho_c U_c S} \cdot \frac{S}{A_J}$$

$$= \lambda \frac{\rho_J}{\rho_c} \frac{V_{th}}{U_c} \tag{3.11}$$

where λ is a function of jet pressure ratio (see Figure 3.8)

As net jet thrust could not be measured directly, I_1 and I_2, defined via equations 3.12 and 3.13 below, were evaluated from calibration rake data:

$$\dot{m} = \eta_1 \, 2\pi\rho_J \int_0^{R_m} V_{J_m}^2 \, r \, dr = \eta_1 \, 2\pi\rho_J \, R_m^2 \bar{V}_J \int_0^1 \frac{V_{J_m}}{\bar{V}_J} \, \frac{r}{R_m} \, d\frac{r}{R_m} = \eta_1 2\pi\rho_J \bar{V}_J I_1 \qquad (3.12)$$

$$T = \eta_2 \, 2\pi\rho_J \int_0^{R_m} V_{J_m}^2 \, r \, dr = \eta_2 \, 2\pi\rho_J \, R_m^2 \bar{V}_j^2 \int_0^1 \left(\frac{V_{J_m}}{\bar{V}_J}\right)^2 \frac{r}{R_m} \, d \, \frac{r}{R_m} = \eta_2 2\pi\rho_J \bar{V}_J^2 I_2 \qquad (3.13)$$

η_1 and η_2 are calibration factors which allow for the differences, due to traverse coverage and other reasons, between rake integrations and true values. Since $\dot{m}$ is known, we may find η_1 via (3.12), from

$$\eta_1 = \frac{\dot{m}}{2\pi\rho_J \bar{V}_J I_1} \qquad (3.14)$$

The final step contains the main assumption of the present calibration, that η_1 and η_2 are equal; i.e. the calibration factors for mass flow and momentum flux are the same. This assumption is supported by the fact that good pipe skin friction estimates were obtained from the present calibration data.

$$\text{If } \eta_1 = \eta_2 \qquad (3.15)$$

we may combine (3.14) and (3.15) and substitute for η_1 in (3.13) to obtain

$$T = \frac{\dot{m}}{2\pi\rho_J \bar{V}_J I_1} \cdot 2\pi\rho_J \bar{V}_J^2 I_2$$

$$= \dot{m}\bar{V}_J \frac{I_2}{I_1}$$

$$= \dot{m}V_E$$

$$\text{From (3.10)} \quad T = \dot{m}\lambda V_{th} \frac{I_2}{I_1} \qquad (3.16)$$

Finally, we may obtain the momentum flux coefficient $C_\mu \, S/A_J$ from

$$C_\mu \frac{S}{A_j} = \frac{\dot{m}V_E}{\frac{1}{2}\rho_c U_c^2 S} \frac{S}{A_J}$$

$$= \frac{\dot{m}V_{th}}{\frac{1}{2}\rho_c U_c^2 A_J} \lambda \frac{I_2}{I_1} \qquad (3.17)$$

$\frac{I_2}{I_1}$, and $\frac{V_E}{V_{th}}$ (i.e. $\lambda \cdot I_2/I_1$) are shown for the three individual configurations in Figure 3.8, as a function of jet pressure ratio. It will be noticed that λ and V_E/V_{th} are much lower for the modified 3-inch jet than for the clean pipes. This is because of the extra pressure drop caused by the flow shaper in the former case.

3.4 Jet Mass and Momentum Flux Coefficients at Forward Speed

Figure 3.9 shows the nominal true velocity ratio, R_{NOM}, as a function of jet pressure ratio, for typical runs at forward speed. Decreased pressure ratios, for 3-inch jet cases at $R_{NOM} = 8$, reflect the fact that these tests were run at a lower mainstream speed than the others.

In the case of the modified 3-inch and the 1-inch jets, R_{NOM} was found to be a very close approximation to the effective true velocity ratio V_E/U_c. This was also true for the clean 3-inch jet, up to $R_{NOM} = 4$, but thereafter V_E/U_c increased faster than R_{NOM}, to 8.25 at $R_{NOM} = 8.0$.

Differences between jets were noticeable for both the flow coefficient C_Q (Figure 3.10) and the momentum flux coefficient C_μ (Figure 3.11) when plotted as functions of the true velocity ratio R_{NOM}. However, these are the true test values applicable to R_{NOM} values used in comparisons of jet trajectory and vortex strength information.

It has been found that the spread between large- and small-jet curves in Figures 3.10 and 3.11 is due predominantly to the fact that the large jets ran 10° - 15° F cooler. The effects on density ratio are shown in Figure 12. If R_{NOM} and R_{NOM}-squared are weighted by the density ratio, as in Figures 3.13 and 3.14, a much improved correlation is obtained between the modified 3-inch and the 1-inch jets. The differences which remain reflect firstly the fact that there are some slight inconsistencies amongst the interim jet calibrations used for the various pipes during test runs. Secondly, C_μ, in particular, should not correlate on an R_{NOM}-squared basis for differing profile shapes: the distinctions between average, RMS, and jet transport velocities become involved.

It may have been noticed that the calibrations and analyses described above were made with especial care. This was necessary to insure that comparisons between large and small jets will truly reflect tunnel effects rather than differences between the jets themselves.

3.5 Wall Pressure and Jet Traverse Measurements

Five sets of pressure orifices were installed, as indicated in Figure 3.15, in rows which extended for most of the test section length. Symmetry checks were possible using rows 3 and 5. However it was not possible at the time of the test to install orifices on the right hand wall, because it was all-glass.

Figure 3.1 shows the rake of seven pitch-yaw, five-holed pressure probes used for jet flow traverses. This rake was mounted with the probes horizontal and the rake axis vertical for all tests. This limited in-jet traverses to locations no less than 6-diameters aft of the jet axis for the velocity ratios of interest. Other traverses, just aft of the jet (Figure 3.2), were restricted to a small region centered in the plane of the jet exit.

The traverse measurements fell into two distinct sets. The in-plur measurements at X = 6D were for the determination of vortex strength and location in the plume. The remaining measurements, in the jet exit plane at X = D and 6D were for use in matching jet velocities during plume modeling. The two X-locations may be regarded as representing "wing" and "tail" locations.

Data were recorded and reduced using standard techniques, though second-stage analyses-involving stream function and circulation calculations - were fairly elaborate. These will be described more fully in Section 4.

4.0 TEST RESULTS

4.1 Similitude Between 1- and 3-inch Jets

Jet velocity profiles

Figure 4.1 shows typical velocity profiles, measured during static calibration, for the unmodified and the modified 3-inch jets. For the 3-inch, unmodified configuration, the core flow profile was tilted. The axis of the tilt could be changed by biasing the supply (Figure 3.6) but it could not be eliminated. Nonetheless, the velocity in the central core was uniform to within about ±2% and the difference between the clean and matched profiles was sufficient to be useful for investigations into the effects of profile shape.

Figure 4.2 gives a comparison between the modified 3-inch jet profile and the 1" pipe profile to which it was matched. It is evident that a good match was obtained.

Base pressures on jet cylinders

The cylinder diameters and forward speeds used were such that the Reynolds numbers for both pipes lay in the high-C_D, pre-transitional range. However, the possibility was recognized that finite length effects might reduce the drag coefficient of the 3-inch pipe (see Prandtl and Tietjens - Applied Hydro and Aeromechanics, p 97). So checks were made on cylinder base pressures.

Figure 4.3 shows the base pressure distributions down each pipe for three typical velocity ratios. Good matches are achieved between the 1-inch jet and the with-BLC, 3-inch jet data. The base pressures attain the two dimensional value about 5- to 7-diameters below the jet exit. The reason for the shift in the no-BLC, 3-inch jet cases is not understood. However, the magnitude of the shift is not enough for it to be of great concern.

It appears that end-effects, on the 3-inch cylinder, do not cause serious flow changes, relative to the 1-inch data. Cylinder-induced effects upon the jet development should therefore be the same in both cases.

4.2 Traverse Results: Flow Distributions

Measurements were made on a sample basis in the longitudinal and horizontal planes and on a comprehensive basis in a transverse plane at $x = 6D$. The longitudinal and vertical runs were to explore the general nature of the flow. The transverse traverses provided vortex location and strength information for flow modeling purposes: the traverse boundaries were selected accordingly. Downwash data, in the jet exit plane, intended for use in modeling, will be summarized below.

Longitudinal plane ($Y = 0$)

An initial series of traverses, not mentioned previously, were made in the longitudinal center plane of the jet using a laser velocimeter. Anomalies found in these data, which were traced subsequently to a loose mirror in the LV system, made retesting necessary using the pressure probe system described above. The change restricted quite severely the choice of practical traverses.

Though the LV data were useless as 'hard' data, for finding cross-flow vorticity distributions, etc., they did give general guidance concerning jet-trajectory in side view.

Figure 4.4 shows velocity vectors for the 1-inch jet at $R_{NOM} = 3$. A good impression of the flow structure is obtained, both in the jet bending region and behind the cylinder. The flow vectors aft of the cylinder suggest clearly that the increase in cylinder base suction towards the jet exit (Figure 4.3), is associated with jet-induced vertical flow. It is noted that Figure 4.4 shows only the upper four diameters of the 1-inch cylinder.

Total velocity contour plots corresponding to Figure 4.4 were compared with published total pressure data at the same velocity ratio for a jet emergent from a flat plate. The comparisons made, at several R_{NOM} values for the 1-inch jet, indicated that the trajectory shapes were similar and suggested that the form of the trajectory equations developed for jets-from-surfaces should be applicable to the present data.

Horizontal plane (Z = 0)

Axial velocity distributions near the sides of the cylinder (Figure 4.5(a)) show the expected, doublet-like character. The wake region fills and spreads quite rapidly opposite to the jet, which induces a strong downwash component there (Figure 4.5(b)). The downwash reaches a maximum about three diameters aft of the jet. The zero downwash contour at X = 6-inches lies just to the outside of the plan-view of the vortex trajectory (see below).

Figure 4.6(a) shows downwash at four locations in the jet exit plane as a function of R_{NOM}. The upper plots are for a location one diameter aft of the jet, representing the near field; the lower plots are at 6 diameters aft of the jet. The span locations were chosen so that comparable data were available for both 1- and 3-inch jets. Downwash values quoted are means of left- and right-side data in all cases.

On a simplified basis of classical angle-of-attack correction theory, about one degree of downwash reduction should be experienced by the 3-inch jet at $R_{NOM} = 3$. At higher jet velocities three dimensional and impingement effects make such estimates inappropriate. Though Figure 4.6(a) exhibits significant data scatter, it is apparent that the anticipated downwash reduction for the 3-inch jet is absent. In three of the four plots the 3-inch jet experiences more downwash, not less, than the 1-inch jet.

Figure 4.6(b) shows similar data for the inclined and vertical 1-inch jets. The differences between jets are more marked, probably because of changes in vortex spacing (see below).

Transverse plane (X = 6D)

The main 'production' measurements were made in transverse planes six diameters aft of the center of the jet exit for five configurations (1" vertical, two 3" vertical and two 1" inclined jets) at five velocity ratios (R = 2,3,4,6 and 8). The primary flow measurements were total pressure, static pressure, axial velocity, vertical velocity and lateral velocity. Axial vorticity distributions (the curl of the transverse velocity field) and source strength distributions (the divergence) were derived. Streamlines were

calculated from the axial vorticity distributions: this was a more convenient procedure and gave more intelligible results than working directly with measured cross-flow velocity data.

First-stage 'production' plots for the twenty-five configuration/velocity ratio combinations comprised: total pressure, vertical velocity and lateral velocity contours, cross-flow velocity vectors, vorticity and source strength contours.

Only the more useful plots, of total pressure, vertical velocity, lateral velocity and streamlines are presented in this report. These are consolidated to show the effects of jet inclination in Appendix A and to show the effects of profile shape and jet size in Appendix B. Summary data, taken from these plots, will be presented in subsection 4.3.

Figure 4.7 repeats selected data from Appendix B and shows the effect of jet size upon cross-flow streamline patterns as R_{NOM} is increased. The effects of profile shape were found to be secondary. Length scales in Figure 4.7 are measured in diameters. The tunnel roof location, indicated by the 'hatched' regions, consequently appears closer to the jet exit for the 3-inch jet cases. Negative stream function contours are denoted by broken lines and the contour values are listed to the left of each plot, starting with the innermost negative contour. The integers to the upper left of each plot are run numbers. (Test MTF68).

At R = 2 and 3 (Figure 4.7(a) and (b)) the vortex penetration into the flow has apparently not been affected by the proximity of the tunnel roof to the plume for the 3-inch jet though there is somewhat less vertical elongation of the vortex streamlines. At R = 4 (Figure 4.7(c)), both a reduction in vortex penetration and a marked flattening of the streamlines is evident for the 3-inch jet. Another indication of roof-induced interference is the reduced magnitudes of the stream function values at the vortex centers - a consequence of a reduction in vertical velocity between them.

In the R = 6 and 8 cases (Figures 4.7(d) and (e)) the 3" jet impinges strongly upon the tunnel roof and the flattening and the other effects noted above are very pronounced At R = 8 there was significant flow unsteadiness not only for the 3-inch but also for the 1-inch jet. Application of tangential blowing of the roof reduced the unsteadiness, though a tendency for the 3-inch jet to bend sideways may still be seen.

The data of Figure 4.7, taken with data in Appendixes A and B and elsewhere, indicate that the structures of the 1-inch and modified 3-inch jets are qualitatively similar at low values of jet-to-mainstream velocity ratio. It may also be inferred from experience with the 3-inch pipe, that streamlines for the 1-inch pipe at R = 9 are sufficiently far from the tunnel roof, as in Figure 4.7(e), so that tunnel-induced local distortion may be assumed to be negligible.

4.3 Traverse Results: Data Summary

Vortex location at X = 6D

Having calculated the streamline patterns, vortex centers, defined as

maximum- or minimum-ψ points, may be found quite readily. Figure 4.8(a) shows that vortex penetration into the flow, for the 1-inch jet, is very nearly proportional to R_{NOM}. Comparison with Weston's data (Ref. 4) shows less penetration for his data, which are for a jet emergent from a plane: this seems reasonable. However, it is pointed out that there are differences between the present analysis and Weston's in the definition of vortex center.

The two sets of 3-inch jet data differ only slightly from each other, mainly in vortex span, confirming the insensitivity to profile shape, mentioned earlier. The jet penetration curve for the 3-inch jets diverges from the 1-inch data at about $R_{NOM} = 3$ as the tunnel roof causes increased jet turning. It appears that the 3-inch curve will asymptote to about 0.7D below the roof at high jet velocity ratios.

Figure 4.8(b) shows that forward inclination of the 1-inch jet causes increased spreading of the vortex pair, but reduced penetration into the flow. It will be seen later that the increased spreading is accompanied by reduced strength, relative to the vertical jet, at high R_{NOM}. At $R_{NOM} = 2$, 3 and 4 vortex penetration for aft-inclined and vertical jets is almost the same. Thereafter the aft-inclined and forward-inclined jet data are the more similar. Vortex spreading is less for the aft-inclined jet than for the others.

Vortex strength at X = 60

After considering a number of alternatives, a method of determining vortex strength was selected based upon line integrals of velocity around the streamline patterns derived from crossflow vorticity data. This is consistent with the vortex center determination procedure, just described, and also permits an economical description of diffuse vortex cores. By plotting vortex strength as a function of the stream function (Figure 4.9) a family of similar curves is obtained with R_{NOM} as a parameter. Intercepts on the horizontal axis are vortex center locations, in terms of ψ. The maximum circulation strength is usually associated with the zero or a nearby streamline and is of prime interest in the present work because tunnel effects relate to the far-field. Central streamlines sometimes intersect the traverse boundary, which is used to complete the integration circuit in such cases. This provides the opportunity to calculate both clockwise and anticlockwise circuits for the same central streamline and can give rise to the overlap region (both open and filled points at given ψ) which is evident in Figure 4.9 at $R_{NOM} = 6$. The occurrence of such a discrepancy is an indication of net circulation around the outer boundary of the traverse. Both Γ_{max} points will be shown subsequently.

Figure 4.10 shows maximum values of vortex strength obtained from Figure 4.9 and other, similar plots. It should be noted that the data represent the axial component of the vortex strength, not the total. Despite differing exit conditions and differing methods for finding vortex strength, it is found that the present results are quite similar to corresponding data, derived from Ref. 4, for jet-from-surface cases. Since vortex strength is greater in the present case, and spacing is less, their product - which is proportional to lift - tends to correlate better. Two apparently 'bad' points, at R = 8 in Figure 4 10(a), were derived from a [illegible] curve which had an inverted peak, unlike any other data. This probably reflects an out-of-range condition for the pitch probe, so these points have been ignored.

The 3-inch jet circulations in Figure 4.10(a) agree well with the 1-inch data at $R_{NOM} = 2$ but are somewhat lower at $R_{NOM} = 3$ and 4. As impingement intensifies, a circulation plateau is reached at about 2.5 $U_\infty D$.

Complementary behavior between vortex strength and span is again observed for inclined jet cases (Figures 4.10(b) and 4.8(b)). After behaving similarly to the vertical jet at R = 2, 3 and 4, vortices in the swept-forward jet display increased span but decreased strength. Conversely, vortices in the swept-aft jet plume are less widely spaced but stronger than for the vertical jet.

Vortex-lift correlation

The vertical component of jet reaction lift is given by

$$L_1 = \rho_j A_j V_j^2 \cos\delta \text{ where } \delta \text{ is jet inclination to the vertical}$$

and

$$2C_{z_1} \equiv \frac{L_1}{\frac{1}{2}\rho U_\infty^2 A_j} = 2\frac{\rho_j}{\rho_\infty}\left(\frac{V_j}{U_\infty}\right)^2 \cos\delta = 2\frac{\rho_j}{\rho_\infty} R^2 \cos\delta \qquad (4.1)$$

Vortex-lift, from the wake measurements, is given by

$$L_2 = \rho_\infty U_\infty \Gamma_{max} \Delta Y$$

and

$$2C_{z_2} \equiv \frac{L_2}{\frac{1}{2}\rho U_\infty^2 A_j} = \frac{2\rho_\infty U_\infty \Gamma_{max} \Delta Y}{\rho_\infty U_\infty^2 \frac{\pi}{4} D^2} = 2.\frac{4}{\pi}\frac{\Gamma_{max}}{U_\infty D}\frac{\Delta Y}{D} \qquad (4.2)$$

It is evident from Figure 4.11 that, for the 1-inch vertical jet, $C_{z_1} = C_{z_2}$ to a reasonable approximation, i.e. all of the jet reaction lift is represented by the vortex pair. For the inclined jets $C_{z_2} > C_{z_1}$. The implication may be that the vortex pair represents total jet thrust rather than the lift component. Removal of the cosδ factor from C_{z_1} improves the correlation in Figure 4.11 but does not collapse the data entirely.

The above result is significant in relation to jet-in-crossflow modeling because it provides a rationale by which vortex strength may be estimated if the spacing is known.

4.4 Tunnel Surface Pressures

Datum runs at $R_{NOM} = 0$

Figure 4.12(a) shows tunnel surface pressures with the 3-inch jet pipe installed but with both the blowing air and the ground BLC turned off. The upper part of the figure is an empty-tunnel-plus pipe case and shows suction peaks, corresponding to the maximum cylinder/separation bubble diameter, followed by a pressure rise towards an asymptote proportional to wake displacement thickness. On installing the traverse gear (lower plot) this pressure recovery is largely lost and further flow acceleration occurs opposite to the traverse gear location. Figure 4.12(b) shows how the previous distribution is modified when 'ground' BLC is applied. Figure 4.12(c) shows corresponding data for the vertical 1-inch jet pipe. Here, the effect of the pipe itself is quite small, as expected, and the traverse gear 'signature' predominates. The effects of sweeping the jet pipe 30-degrees forward or aft are found to be small.

In subsequent figures the appropriate jet-off datum values, depicted in Figure 4.12, have been removed in most cases. Certain exceptions occur in strong impingement regions where greater-than-mainstream total pressures invalidate the $\sqrt{(1 - C_p)}$ superposition technique which was used. These regions are recognized readily since $C_p \geq 1$ at impingement.

3-inch jet: effects at the 'ground'

This jet impinges at about $R_{NOM} = 3$. By $R_{NOM} = 4$, strong ground impingement is present (Figure 4.12) and there is evidence of a separation vortex ahead of the X = 0 station in the three no-BLC cases shown. Applying BLC (triangles) destroys this vortex and may reduce the impingement pressure. Comparisons between sets of octagonal points show good repeatability between runs and comparison of these points with the 'plus' points suggests that the effects of jet profile shape are not very great.

Figure 4.14 shows similar, no-BLC data for various R_{NOM} VALUES. At $R_{NOM} = 6$ and 8 the vortex suction peaks move forward and becomes strong. It is also evident that impingement C_p's become very high. There was considerable unsteadiness in the flow at $R_{NOM} = 8$, which caused scatter in the data.

3-inch jet: tunnel wall pressures

At $R_{NOM} = 2$, Figure 4.15(a) shows that the wall pressures are blockage-dominated: there is a continuous acceleration along the test section. Superimposed upon this, comparison between rails 1 and 3 or 5 shows, firstly, the anticipated difference signature associated with positive jet lift but then, downstream of about X = 0.2, a reversal which corresponds to negative jet lift. This may be due to the fact that jet blockage effects are offset towards the "ground" (i.e. the tunnel roof). Comparison between the upper and lower plots in Figure 4.15(a) shows that ground BLC has little effect at R = 2.

At R_{NOM} = 4 (Figure 4.15(b)), spreading between rails 1, 2 and 3 becomes more noticeable as lift effects increase. Application of 'ground' BLC (lower plot) reduces the spread significantly. This may be due to entrainment into the BLC jet sheet, which will have an accelerating effect upon the flow at rails 3 and 5.

By R_{NOM} = 6 (Figure 4.15(c)) tunnel flow breakdown is well advanced and the locus of the characteristic impingement "footprint" and the vortex ahead of it may be deduced quite readily. Since the vortex is undoubtedly skewed quite strongly, the X/B-length scales in the pressure plots may exaggerate the vortex size. Rail 3 and 5 data, at R_{NOM} = 6 suggest that separation, vortex center and reattachment are at X/B = -0.20, + 0.15 and + 0.70 approximately. At mid-sidewall (Rail 2 - triangles) the same features may be identified, shifted downstream, but only the vortex peak location can be estimated, at about X/B = 1.0 (upper plot, Figure 4.15(c)). This was changed somewhat by 'ground' BLC (lower plot) but otherwise the BLC produced no great effect. Some differences are observed between right and left sides (Rails 3 and 5) at the two highest R_{NOM} values (Figures 4.15(c) and (d)). This is most likely caused by the jet bending sideways (see also Figures 4.7(d) and (e)).

Effect of profile shape

Comparisons between corresponding plots in Figure 4.15, which is for 'square' profiles, and Figure 4.16 ('pipe' profiles) show that differences due to profile shape are almost negligible.

1-inch jet: effects at the "ground"

Figures 4.17(a) and (b) comprise four pressure plots for R_{NOM} values of 3, 4 and 6, respectively. Curves for several jet inclination ang'es are shown on each. The overall magnitude of the signatures are small prior to impingement but the general trends are the same as those described above. As might be suspected, the forward-inclined jet (δ = -30-degrees) produces greater effects at the walls than the vertical jet and the aft-inclined jet produces smaller effects.

Figures 4.18 and 4.19 include data for other rails at R_{NOM} = 4 and 8, respectively. In the R_{NOM} = 4 case the magnitudes of the signature are starting to become comparable with measurement accuracy and flow unsteadiness effects. Nonetheless, the anticipated trends are present. The R_{NOM} = 8 cases (Figure 4.19) may involve impingement and both lift and blockage effects are starting to become noticeable.

5.0 THE 'VSD' FLOW MODEL AND IT'S DEVELOPMENT

5.1 Introduction

The present aim is to identify or develop a realistic theoretical model of a jet-in-crossflow which is suitable for tunnel interference estimation. The model will be applied with the standard wall pressure signature procedures, firstly to extract jet effects from powered-model-signatures and then to provide jet-related interference velocities for addition later to those determined for other parts of the test model.

Any flow model used for these purposes must be reasonably simple: this eliminates the finite difference and the detailed vortex lattice techniques used for many near-field studies. It was thought at first that an extension of Heyson's work, probably towards the Fearn, curved trajectory model would be adequate. However, both were found to have serious shortcomings and considerable development work was needed to produce a theoretical model which was reasonably simple, yet reproduced observed flow features properly. The new flow model, designated the 'VSD' model (Vortex,Source, Doublet) will be described in subsection 5.2.

Impingement cases

The terms of reference for the present work exclude impingement cases. However, cases in which the theoretical plume strikes a tunnel surface cannot just be ignored. Appropriate geometric changes have therefore been made, for impinging cases, which parallel Heyson's treatment. Though this approach appears reasonable, detailed studies have not been made of the impingement region itself or of ways to model it properly. Results obtained here for impinging cases must therefore be considered speculative.

5.2 Description of the 'VSD' Model

Geometry

The data found most useful for modeling purposes were measured vortex strengths and locations - augmented by the 'Fearn' vortex model - and tunnel wall pressures for the 3-inch jet.

As the work progressed, it became apparent that twin vortex models such as Fearn's contributed only weakly to the wall pressure signatures: Sources and/or curved lines of axially-directed doublets were needed to match the observed tunnel blockage effects. As the main body of the jet penetrates further than the vortices, the source/doublet lines were given the greater penetration into the flow, as sketched in Figure 5.1 (a) and (b). On the basis of measured data at $X/D = 6$ and $2 \leq R \leq 8$, the 'Fearn' and the 'Williams and Wood' trajectories respectively were selected for vortex and source/doublet elements (see Figure 5.1(c)).

The line vortex and line source/doublet trajectories are defined for the 'VSD' model via the equations:

$$Z/D = 0.352\ (X/D)^{0.429}\ R^{1.122} \qquad (5.1)$$

for the vortex pair.

$$Z/D = 0.758\ (X/D)^{0.333}\ R^{1.000} \qquad (5.2)$$

for the source/doublet pair.

and

$$Y/D = 0.0769\ (X/D)^{0.440}\ R^{1.000} \qquad (5.3)$$

for both vortex and source/doublet pairs.

Vortex strength

Since the Fearn equation for vortex strength agreed well with the present data, this is used directly in the 'VSD' model, i.e.

$$\frac{\Gamma}{U_\infty D} = 0.600 \frac{R^2}{(X/D)}\ (1 - e^{-0.035(X/D)^2}) \qquad (5.4)$$

Source strength

The source system is selected so as to model the physics of the observed wakes. The system described is the original one, derived as stated: no adjustments to constants were used to improve the match to the wall pressure signature.

For elements of the initial part of the plume, the data show that an almost parallel-sided wake is required (e.g. Figure A1, all R). The total volume Q_{12} emanating from a line source between points 1 and 2 in the initial plume may be written

$$Q_{12} = U_\infty\ \Delta Y\ (Z_2 - Z_1) \qquad (5.5)$$

where ΔY is the far-wake displacement width. For the initial plume, a value $\Delta Y = D$ (i.e. $C_d = 1$) appears to be appropriate. For a plume developing without a crossflow, entrainment adds to the mass flow in the jet at about a 23% rate. An improved approximation for ΔY is therefore

$$\Delta Y = D \sqrt{(1+0.23\ Z/D)}$$

Recognizing that mixing depends upon path length, S, the flow physics is better represented by

$$\Delta Y = D \sqrt{(1+0.23\ S/D)}$$

Substituting into (5.5) we obtain

$$Q_{12} = U_\infty D\ (Z_2 - Z_1) \sqrt{(1+0.23\ S_{12}/D)}$$

The local source strength, per unit length along the plume, is then given by

$$m_{12} = \frac{Q_{12}}{\Delta S_{12}} = \frac{U_\infty D\ (Z_2 - Z_1)}{\Delta S_{12}}\ \sqrt{1+0.23\ S_{12}/D} \qquad (5.6)$$

Doublet strength

In addition to the sources, a doublet system was introduced in response to features observed in the wall pressure signatures. In this case, local peaks made it apparent that solid blockage was present, which requires either a source-sink model or a set of upstream-directed axial doublets. These are sized to match the jet diameter at exit and grow at the same rate as for the sink system. The axial doublet strength distribution is then given by:

$$\mu_{12} = -\frac{\pi}{2} U_\infty D^2 \sqrt{(1+0.23\ S_{12}/D)} \qquad (5.7)$$

No vertical doublets are required because lift is represented by the vortex system. In evaluating (5.6) and (5.7) the approximation $S_{12} = X_{12}$ is made.

5.3 Tunnel Surface Pressures

Synthesis of the 'VSD' model

The development of the VSD model and the reasons for it's final form are best illustrated in terms of measured and predicted wall pressures. The case with the 3-inch jet at R = 2 (i.e. no impingement) will be used to demonstrate the matching procedure.

Figure 5.3(a) shows that Fearn's vortex model causes almost negligible effects at the tunnel sidewall (Rails 1 to 2) and represents rail 4 conditions poorly. It may be inferred that the jet lift, and the vortex drag implied by the Fearn model affect the wall pressures very little. A separate estimate was made of vortex drag and used to size axial doublets in a flow model like Heysons (see Appendix C). The results (Figure 5.3(b)) were similar to those for the Fearn model.

In view of this failure of established methods to predict wall pressures, the properties of line sources and line doublets were investigated when laid out along a curved jet trajectory. Use of constant-strength sources or constant strength axially-directed doublets, sized to give far wake width D and cylinder diameter D, respectively (Equations (5.6 and (5.7)), gave the triangle and circle results in Figure 5.4. The plus symbols, for graded sources (Equation 5.6 with S_{12}/D term removed) reflect reducing line source strength along the plume as needed to maintain constant wake width far downstream. The latter results are remarkably similar to those for the doublets.

Comparison of Figure 5.4 results with experimental data (Figures 5.2 and 5.3) showed clearly that at least sources are needed to complete the flow model. On the basis of wall pressure comparisons, there is a temptation at this point to omit the vortex system. However, this would be incorrect because the associated upwash inteference would be lost.

Figure 5.5 shows measured wall pressures and predictions from a vortex pair/split line source model, with constant strength sources. The comparisons are encouraging. However, Figure 5.6 shows that some improvement is possible by grading the source strengths as indicated earlier. Because of their similar properties, it is evidently possible either to increase the source strengths or introduce upstream-directed doublets to improve the correlation. The latter choice was made on physical grounds.

Figure 5.7 shows that the introduction of doublets, which completes the VSD model, generally improves the wall pressure correlations. Further fine tuning is obviously possible but was not considered worthwhile on the basis of one flow case. Comparison of Figure 5.8 with Figure 5.7 shows that the changes in wall pressures on removing the vortex system from the VSD model are almost negligible. However, the full VSD model was retained for the reasons indicated earlier.

Other flow cases

Figures 5.9(a) and (b) show wall pressures for the 1-inch jet at R = 2 and R = 4, respectively. As the measured pressures are of very low level and are a residue which remains after removing the (larger) traverse gear effects, good comparisons are unlikely. With a single exception, however, the predictions appear qualitatively correct. The exception concerns Rail 4 at R = 4 (Figure 5.9(b), which has obvious problems at large X/B. Figures 5.10(a) and (b) show VSD and SD results respectively for an impingement case: the 3-inch jet at R = 4. Rails 1 and 2 correlate quite well but the Rail 3 and 4 results show that the impingement flow is not well represented by the VSD model.

Bi-energy flow effects

In converting flow velocities generated by the theoretical models to pressures, it is necessary to use Bernoulli's equation and assume that the flow next to the wall has mainstream total pressure. This not so in the jet impingement region, as evidenced by experimental points near X/B = 0 for Rail 4 in Figure 5.10. It is apparent from the experimental curves that a stagnation pressure of about three times mainstream is present here. It appears highly likely that the Rail 3 pressures are also directly affected by impingement total pressure effects, which are not modeled by the present scheme.

5.4 Interference Velocities

The tunnel interference flow, at the model centerline, comprises velocities due to the image system of the model and it's wake as it exists in the tunnel and velocities associated with any redirection of the model

wake caused by tunnel surfaces. The second effect is usually ignored. Figure 5.11 illustrates this breakdown for an impinging jet-in-crossflow. Generally, in-tunnel measurements, term (i), are corrected by removing image effects, term (ii), on the assumption that the wake is unchanged. We have seen in Section 4 that this is well justified for jets prior to impingement. However if terms (i) and (ii) are combined for the impinged case shown, the result obtained is for a 'kinked' plume. Terms (iii) and (iv) may be introduced to estimate the effects of redirecting the plume so as to straighten out the kinked region. Though these effects will be evaluated and discussed below, it is again emphasized that the present work is incomplete because no systematic attempt has been made either to measure or to model the impingement region itself.

The remainder of this subsection will comprise a description, within the above framework, of interference predictions first for the 1-inch and then for the 3-inch jet using the VSD flow model. Comparisons will then be made with similar predictions using other methods.

One-inch jet (Figure 5.12)

The R = 2, 4 and, to a large degree the R = 6 cases for the 1-inch jet are of primary interest in the present work because impingement is not involved. For this reason, the complications connected with plume impingement and redirection (see above) do not arise. Though small, the blockage and angle-of-attack increments at R = 2 and 4 increase with X/B in the expected way and asymptote appropriately far downstream (Figures 5.12(a), (b), and (d)).

At R = 6, non-planar effects become important for this jet. In particular, first-image trailers, which are offset towards the tunnel model, gives rise to large local angle-of-attack increments (Figures 5.12(a) and (b)).

Figure 5.12(c) shows the increments associated with plume redirection, to be added to the previous, image-induced effects. Redirection at R = 6 involves swinging the plume through about 7-degrees about the impingement point, which is at X = 2.54B. At R = 8 impingement is at 1.05B and the angular change is 14-degrees. The effect of redirection is to increase the local blockage correction somewhat (Figure 5.12(c), upper), because the trailing vortex pair moves further from the tunnel centerline during redirection.

The 'bottom line' for angle-of-attack is shown in Figure 5.12(d). At low R, the interference is as expected for simple- planar cases. As a result of non-planar image effects, $\Delta\alpha$ increases faster than R-squared, the rate for planar assumptions.

Three-inch jet (Figure 5.13)

For this jet, only the R = 2 case is non-impinging: most of the previous comments apply in this case. For the remaining, impinging cases, the previous cautionary remarks apply. The data will be further discussed because of some interesting findings concerning the redirection term.

In the absence of the along-surface elements (Figure 5.13(a)) the interference effects are quite insensitive to R. Once impingement occurs (R = 4, 6 and 8), the VSD model comprises a curved cylinder joining the jet exit to the impingement point, which has limited movement over this R-range. Blockage effects are therefore almost the same at R = 4, 6 and 8 (Figure 5.13(a)). The movement of the angle of attack peak follows that of the impingement point as it progresses forward with increasing R.

The introduction of along-surface elements (Figure 5.13(b)) and their subsequent redirection (Figures 5.13(c) and (d)) have major, but opposing, effects upon the corrections. The two corrections illustrate the importance of redirection vividly. Figure 5.13(b) shows apparent interference calculated for a 'kinked-plume' case (Figure 5.11, sketch (i)). Here the plume is held next to the tunnel surface artificially and high angle-of-attack increments result (compare Figures 5.13(a) and (b)). Since the true plume position is much further from the tunnel centerline, most of the spurious trailer-induced effect in Figure 5.13(b) is removed when the plume redirection term (Figure 5.13(c)) is applied. As a result, the magnitude of the net interference (Figure 5.13(d)) is several times less than some of it's constituents. This is not a reflection of any real effect but rather a demonstration that the intermediate, along surface model of Figure 5.13(b) (or Figure 5.11, sketch (ii)) is inappropriate. Methods which fail to pick up the redirection term must be considered suspect or, at best, incomplete.

5.5 Comparisons Between Methods

Comparisons will be made firstly on the basis of effective source and doublet distributions (Figure 5.14), then in terms of interference predicted by the VSD, Heyson and other methods (Figures 5.15 and 5.16) and finally in relation to results calculated directly from wall pressures using the program from Part I of the present report (Figure 5.17). Further comments on Heyson's method, as interpreted herein, are given in Appendix C.

Effective source and doublet distributions

To illustrate the nature of the 'VSD' and Heyson flow models, Figure 5.14(a) and (b) expresses doublet effects in terms of equivalent circular cylinder diameter, plotted with the trajectory in the upper parts of the figures and expresses source effects in terms of displacement.

For the 'VSD' model (Figure 5.14(a)), the effective cylinder diameter (upper plot) is essentially that of the jet: the spreading term is weak. In the lower plot, the full line shows continuously increasing mass flow due to the (explicit) line sources. The broken line shows the implied mass flow due to the point source effects at the joints between doublet lines (see also Appendix C). For the VSD model, this effect is related only to drag.

The total source effect is shown by the chained line. It is evident that a rapid increase occurs in the first few diameters to a level somewhat exceeding the jet volume flow. Thereafter the rate of increase declines as the jet bends.

In Figure 5.14(b) a comparable Heyson case is illustrated for the same lift and for the same effective cylinder diameter. The source effects are much weaker because only doublet-related sources are present. The drag-related source effect, in the vicinity of the model is weakened by a sink-effect at the jet exit caused by the lifting doublet system.

Despite having forced the Heyson model to match the VSD cylinder diameter, it is evident that it suffers from serious shortcomings regarding source effects and their distribution.

Blockage interference

Figures 5.14 and 5.15 show blockage and angle-of-attack interference increments respectively for the 3-inch jet at various values of R. The 'Fearn'-vortex model and the 'SD' source-doublet model combine to form the 'VSD' model. Comparison is also made with results from the present interpretation of Heyson's method.

Figure 5.15(a) shows u-component blockage interference, due to the tunnel image sets, for several theoretical jet-in-crossflow models. At R = 2 and R = 4, the interference predicted by the present method is an order of magnitude greater than that of Heyson. This reflects the fact that, being largely drag-based for blockage the Heyson results have strong R-dependence. The SD and VSD present results, on the other hand, depend heavily upon measured wall pressures which have much less R dependence. The R = 2 and R = 4 results are not affected greatly by the redirection term so the results shown in Figures 5.15(a) and (b) are almost the same.

In Figure 5.15(b) it is evident that the vortex 'cross' effects upon blockage become more significant as R increases. With no redirection term (Figure 5.15(a)) this effect is very strong, but spurious. However, the Figure 5.15(a) result at high-R shows how important it is to include the redirection term for vortex models.

Angle-of-attack interference

The R = 4 case in Figure 5.16(a) or (b) characterizes the various methods quite well. Though the SD model has no vertical doublets, the angle-of-attack curve is very similar in form and magnitude to that of Heyson, except that the SD impingement point is located (more correctly) further forward.

As a result of vortex inclination near the jet exit and in the early plume, the vortex contribution (i.e, the Fearn result) is shifted aft at medium R-values. This causes an angle-of-attack plateau to occur where negative $d\Delta\alpha/dx$ for the SD model and positive $d\Delta\alpha/dx$ for the vortex models are about equal. This local detail is undoubtedly very sensitive to modeling assumptions and should not be taken too seriously.

As R increases, the vortex contribution (Fearn) to angle-of-attack dominates increasingly, particularly prior to redirection (Figure 5.16(a)). It is interesting to note that the magnitudes of the image-effect corrections are comparable with corrections calculated on a simple, $\delta(S/C)C_L$ basis. The fact that redirection reduces the angle-of-attach correction by a factor

of three or four (Figures 5.16(a) and (b), lower parts) may explain the preference of some V/STOL experimentalists not to apply (image-based) tunnel corrections.

Direct use of wall pressures and the Part I method

It is obviously possible to ignore the non-planar aspects of the jet-in-crossflow problem and use the Part I program directly to obtain a rough estimate of interference. If the jet is small enough or if R is low enough this should produce acceptable results. Figure 5.17(a) confirms this for one-inch jet tests at low R values. The blockage level is low (about 0.6% at most) and wall pressure signals are subject to scatter. Nonetheless the 'VSD' model predictions (crosses) are in quite good agreement with the results from the matrix method of Part I. This agreement also confirms that the 'VSD' method operates properly as planar conditions are approached.

Figure 5.17(b) shows the corresponding results for the three-inch jet. Here, the blockage is an order of magnitude greater. These comparisons are particularly interesting because, though the previous comments largely apply at R = 2, by R = 4 the non-planar effects have become significant. The full, 'VSD' treatment gives a blockage curve which levels out as the jet bends (crosses). However, for the early part of the characteristic, where the jet penetration is incomplete, the results from the planar and non-planar predictions are in remarkable agreement.

It is tempting to conclude that, if impingement is absent, direct use of the Part I method will produce good interference estimates. This is probably true for blockage at the model position, though not aft of this. However, serious problems can be anticipated in estimating angle-of-attack interference on the basis of the Part I method if used with an influence matrix for center-tunnel elements. Runs paralleling those for Figure 5.17 confirmed that the latter procedure yields entirely spurious angle-of-attack estimates. This occurs because (as seen previously) true jet lift effects are almost "invisible" at the tunnel wall. The Part I method would respond predominantly to the "cross" effects of offset blockage and return corresponding, spurious angle-of-attack predictions.

6.0 CONCLUSIONS

6.1 Scope of the Present Work

The aim of the work described, to adapt or develop a jet-in-crossflow model for estimating wind tunnel interference, has been met successfully. A study of measured and predicted wind tunnel surface pressure signatures shows that the two most likely existing candidates - the models of Fearn and of Heyson - fall seriously short of representing the flow physics properly for the present application. A new, vortex-source-doublet (VSD) model was therefore developed with significantly improved flow physics. This incorporates:

- a curved, varying-strength vortex pair based upon the 'Fearn' near-field jet-in-crossflow model.
- a pair of curved, varying-strength source-doublet lines extending beyond the vortex pair but with the same horizontal development.
- source-doublet strengths based upon viscous wake measurements, jet cylinder diameter, and jet growth considerations.

The 'VSD' flow model is employed in a pre-processor program which removes jet effects from whole-model wall pressure signatures and provides jet-induced tunnel interference data. The revised wall pressure signatures and the interference data become input to the subsequent "rest-of-model" interference calculation described in Part I of this report.

The above development was backed experimentally (see 6.2, below) and by a number of theoretical studies (see 6.3, below). It is not easy to validate methods such as the present one: 6.4, below, deals with this topic. Subsection 6.5 considers the special topic of impingement cases.

6.2 Experimental Studies

Though a great volume of jet-from-surface data exists, its relevence to the tunnel interference problem was in doubt: a jet-from-cylinder represents a typical V/STOL configuration better. Experiments were therefore carried out on jets emergent from chimney-like cylinders mounted on the tunnel floor. The jets, of 1- and 3-inch diameter, emerged from 15-inch high cylinders mounted in the Lockheed-Georgia 30- by 43-inch wind tunnel.

Three component velocity measurements were made in the planes $X = 6D$ and $Z = 0$ over a range of jet velocity ratios, $2 \leq R \leq 8$. Two jet profile shapes were investigated for the (vertical) 3-inch jet and three jet angles were investigated for the 1-inch case (30-degrees forward, vertical and 30-degrees aft). Especial care was taken in calibrating the jets. The experiments lead to the following main conclusions:

- The jet flow measurements at $X = 6D$ showed that jet-from-cylinder vortex trajectories and strengths, for non-impinging cases, were in general agreement with jet-from-surface data.

- Results for square and pipe jet exit velocity profiles, were essentially indistinguishable at the same C_μ.

- Comparisons of 1- and 3-inch jet data showed that vortex penetration (in diameters) into the flow was almost unaltered, during tests at increasing velocity ratio R, until 'hard' impingement occurred.

- Careful integrations of the X = 6D cross flow data showed that the product of trailing vortex axial strength and lateral spacing closely approximated the jet lift. This demonstration is believed to be a 'first'.

- The above three facts were helpful when developing the flow model.

Tunnel wall pressure 'signatures' were measured along five longitudinal 'rails' for all of the above conditions. The 3-inch jet data provided the primary checks during VSD-model development.

6.3 Theoretical Studies

The 'VSD' and planar models

Studies with the completed 'VSD' flow model revealed the following:

- The contribution to the wall pressure signatures of the vortex portion of the VSD model is almost negligible: the lifting system is essentially 'invisible' to the tunnel walls.

- Angle-of-attack corrections due to the jet-in-crossflow must therefore be estimated entirely on the basis of the jet-in-cross-flow theoretical model.

Demonstration runs were made by submitting jet-in-crossflow wall pressure signatures to the (planar) Part I analysis program. These revealed the following:

- At low-R for the 1-inch jet, the VSD and planar programs gave blockage estimates which agreed well with each other, as should be expected.

- For the 3-inch jet the agreement was good in the vicinity of the jet but, aft of the jet, a continuously rising blockage correction for the planar analysis was replaced by asymptotic behavior for the full, VSD model. The latter is more credible on the basis of previous experience.

- Predicted angle-of-attack corrections, using the planar method, were entirely erroneous. This was because the method interpreted offset blockage interference in terms of angle-of-attack.

These results of the theoretical studies prove that the pre-processor approach to handling jet-in-crossflow interference is not just expeditious; it is essential.

Studies using the 'Heyson' model

Both Heyson's program itself and a new, equivalent program which extends it for wall pressure calculations were implemented. At a qualitative level the studies were fairly successful. Source-like properties of line doublets in Heyson's model were identified and interpreted and some inherent shortcomings, relative to the present, flow-based model, were uncovered. Quantitatively, the present studies with Heyson's model were unsatisfying, largely because no balance data were available. The problem was compounded by difficulties in deciding upon ground rules for comparing force-based and flow-based methods.

6.4 Validation

A direct validation of a jet-in-crossflow interference model is likely to be difficult because of the presence of other components for any practical jet-powered configuration. The VSD model, in contrast to others reviewed, is supported by the following facts:

- Wall pressures are matched quite well for the 3-inch jet.
- For the 1-inch jet, wall pressure matching is qualitatively correct and of the right magnitude: this is the most that can be expected of the data.
- It follows that far-field predictions by the method, and hence tunnel blockage predictions, are of the correct order.
- Downwash differences, between Z = 0 data for 1- and 3-inch jets, were too small to be of practical use in validating angle-of-attack inteference estimates.
- Angle-of-attack interference estimates, therefore, rest heavily upon Fearn's vortex model, which is incorporated in the 'VSD' model. The Fearn model is supported by extensive test data gathered by the original authors and by more limited experiments described herein.
- Comparisons with the planar method (see above), show that the VSD method performs properly as this limit is approached.

6.5 Cases with Jet Impingement

The experimental studies included a significant number of impinged cases. Here, floor tangential blowing was applied as required to remove the vortex induced suction peak ahead of impingement. The theoretical studies acknowledged impingement but did not make any attempt to model it explicitly except with regard to a jet 'redirection' effect (see below). The following conclusions were reached:

- By simplifying the floor flow, tangential blowing is likely to have eased the task of modeling impingement cases.

- The use of a 'kinked' theoretical jet plume, with line elements along the tunnel floor, may cause spurious interference effects, particularly if vortices are used in the flow model.

- The introduction of a theoretical 'plume redirection term (Figure 5.11), which restores the plume from it's kinked form to a free air trajectory, can reduce the apparent interference by a factor of three or four.

The last finding is considered very significant.

REFERENCES

1. Fearn, R. L. and Weston, R. P., "Velocity Field of a Round Jet in a Cross Flow for Various Jet Injection Angles and Velocity Ratios," NASA Technical Paper 1506, Oct., 1979.

2. Heyson, H. H., "General Theory of Wall Interference for Static Stability Tests in Closed Rectangular Test Sections and in Ground Effect," NASA Technical Report, NASA TR R-364, Sept. 1971.

3. Williams, J. and Wood, M. N., "Aerodynamic Interference Effects with Jet-Lift V/STOL Aircraft under Static and Forward-Speed Conditions," Zeitschrift für Flugwissenschaften, Vol 15, Sec 7, pp. 237-256, July 1967.

4. Weston, R. P., "Vorticity in the Jet in a Crossflow," Paper G9, presented to the AIAA South Eastern Regional Student Conference: April 1973. (See also NASA TP 1087 "Induced Velocity Field of a Jet in a Crossflow," May 1978, by Fearn and Weston).

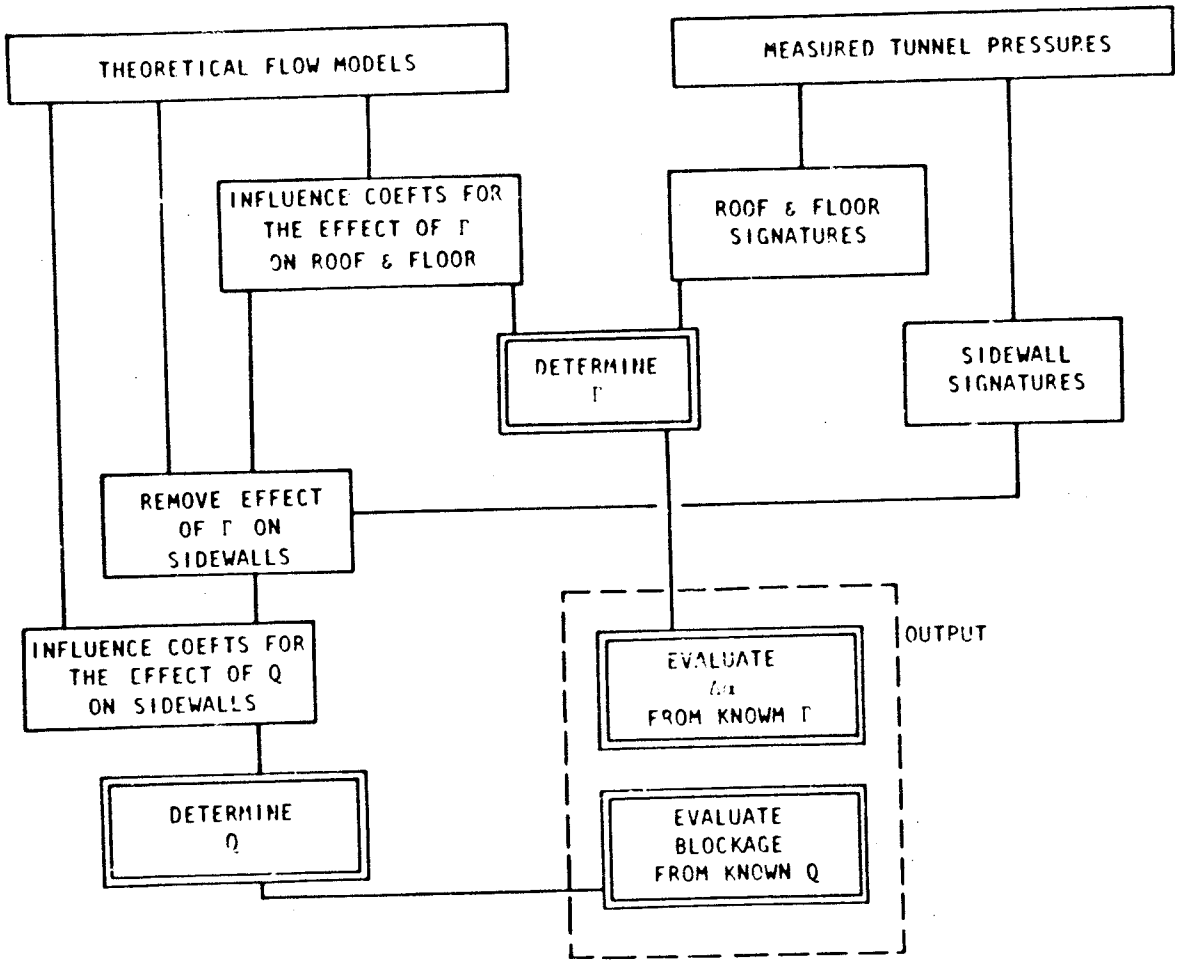

Figure 2.1 Operating principles of the Part I, wall-pressure-signature analysis program for conventional configurations.

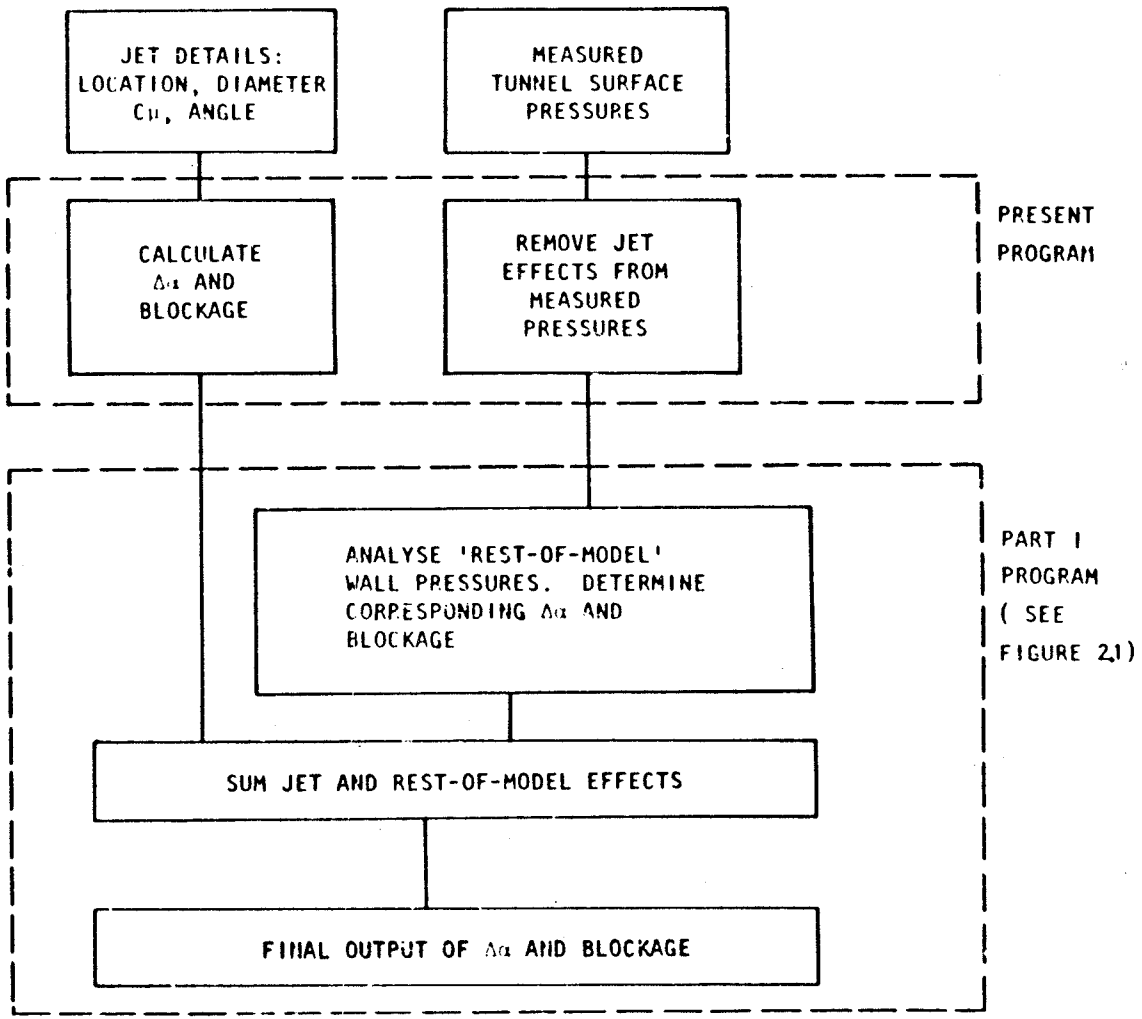

Figure 2.2 Interface between the present and Part 1 programs.

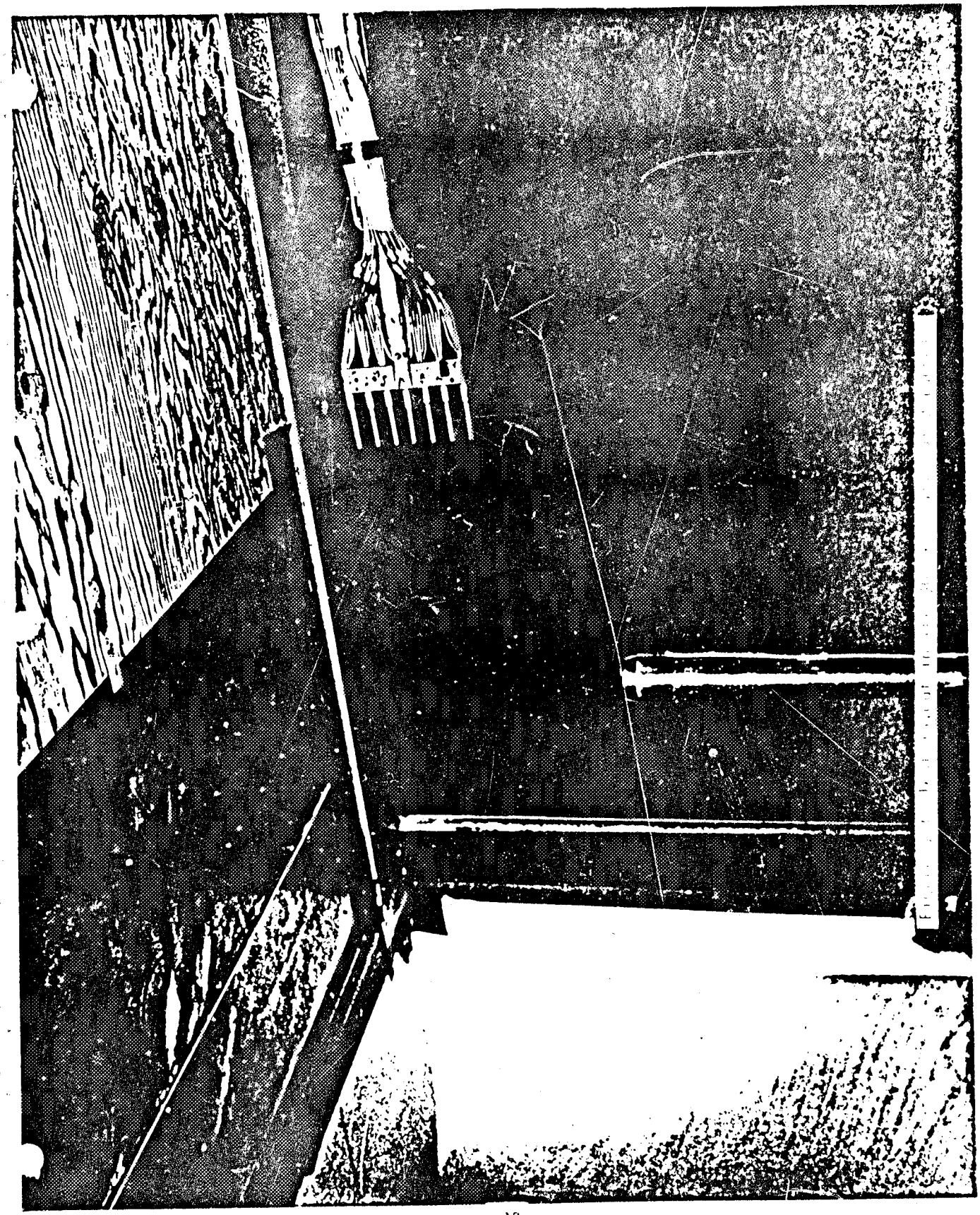

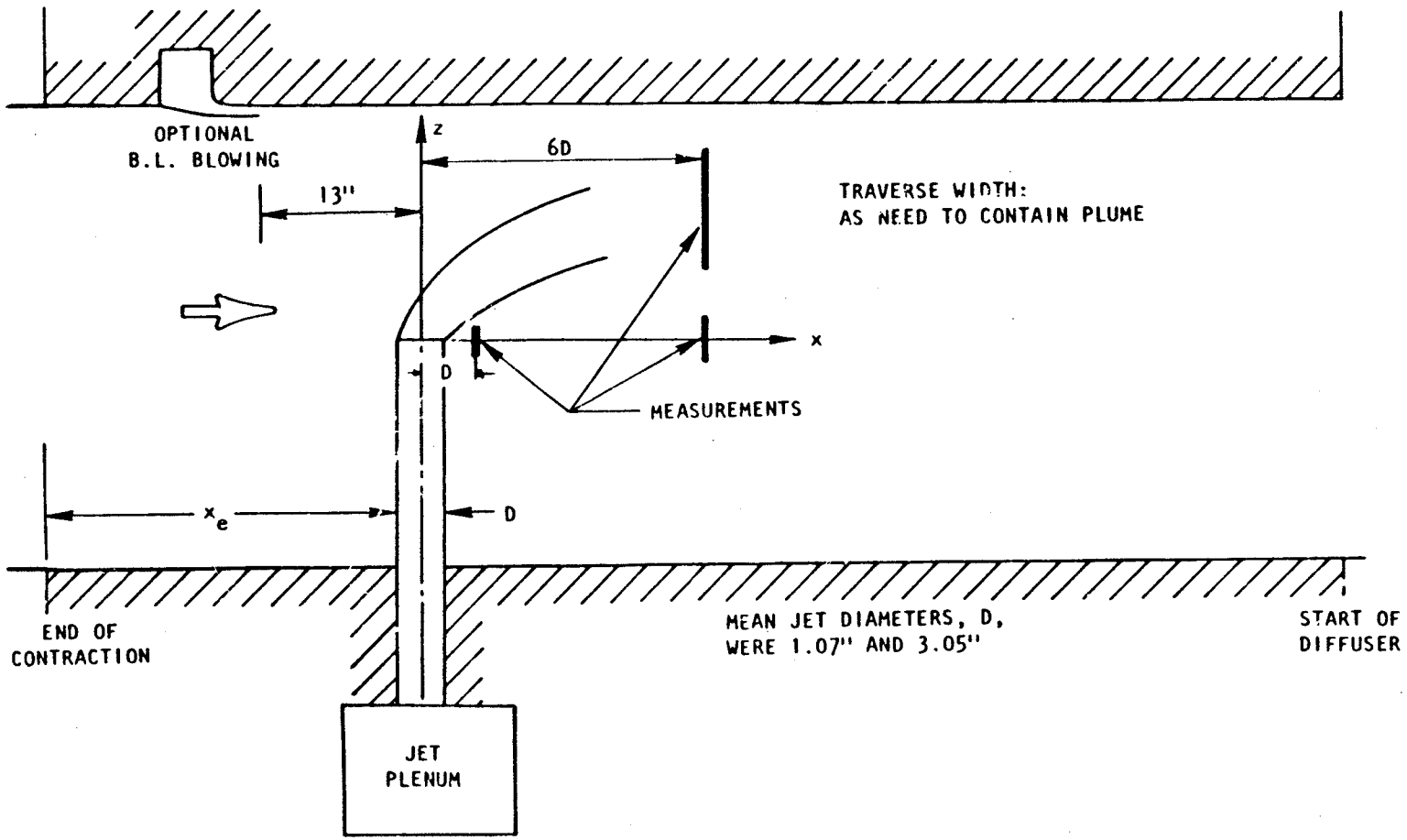

Figure 3.2 Pertinent rig dimensions (3-inch jet shown)

JET ANGLE	JET DIAMETER		
	1"	3"	3"(Mod)
VERTICAL	√	√	√
30° FWD	√		
30° AFT	√		

R_{NOM}		2	3	4	6	8
V_J/U_c	1" Jet	150/75	225/75	300/75	450/75	600/75
FT/SEC	3" Jet	150/75	225/75	300/75	450/75	400/50

Figure 3.3 Jet configurations and velocity conditions of tests.

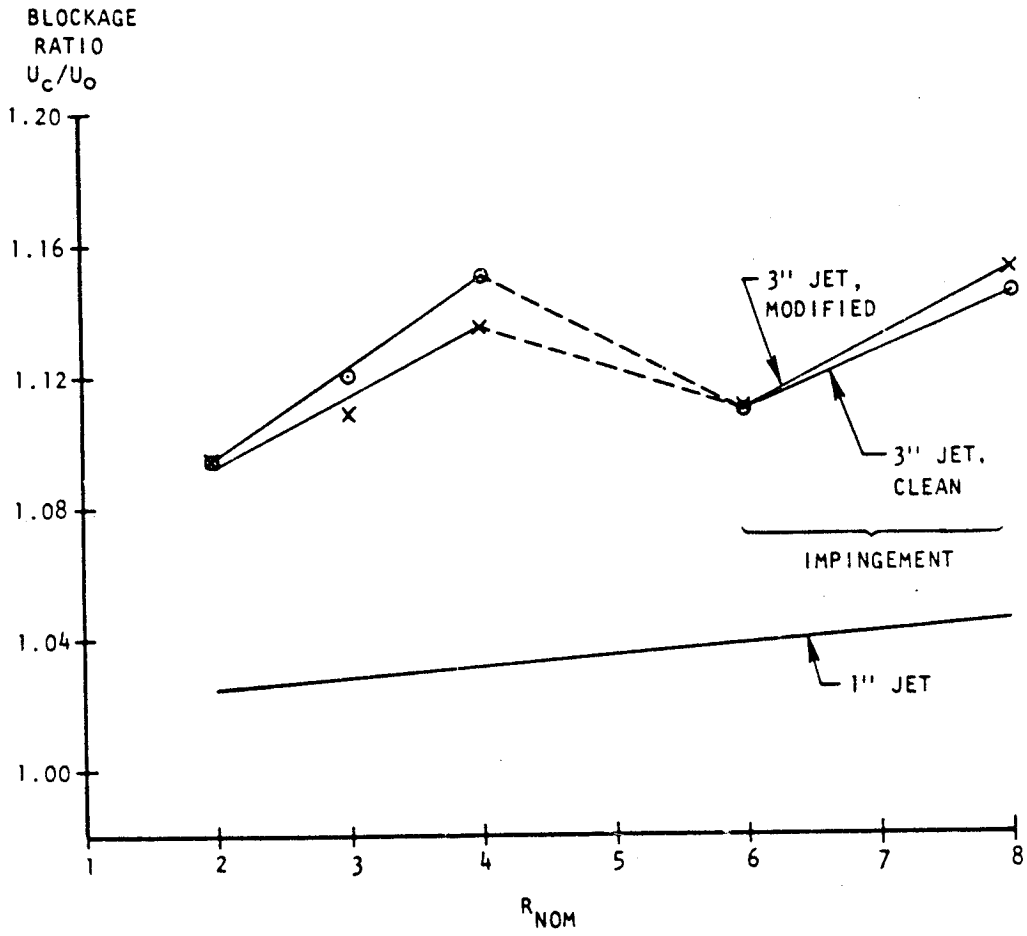

Figure 3.4 Typical on-line blockage corrections

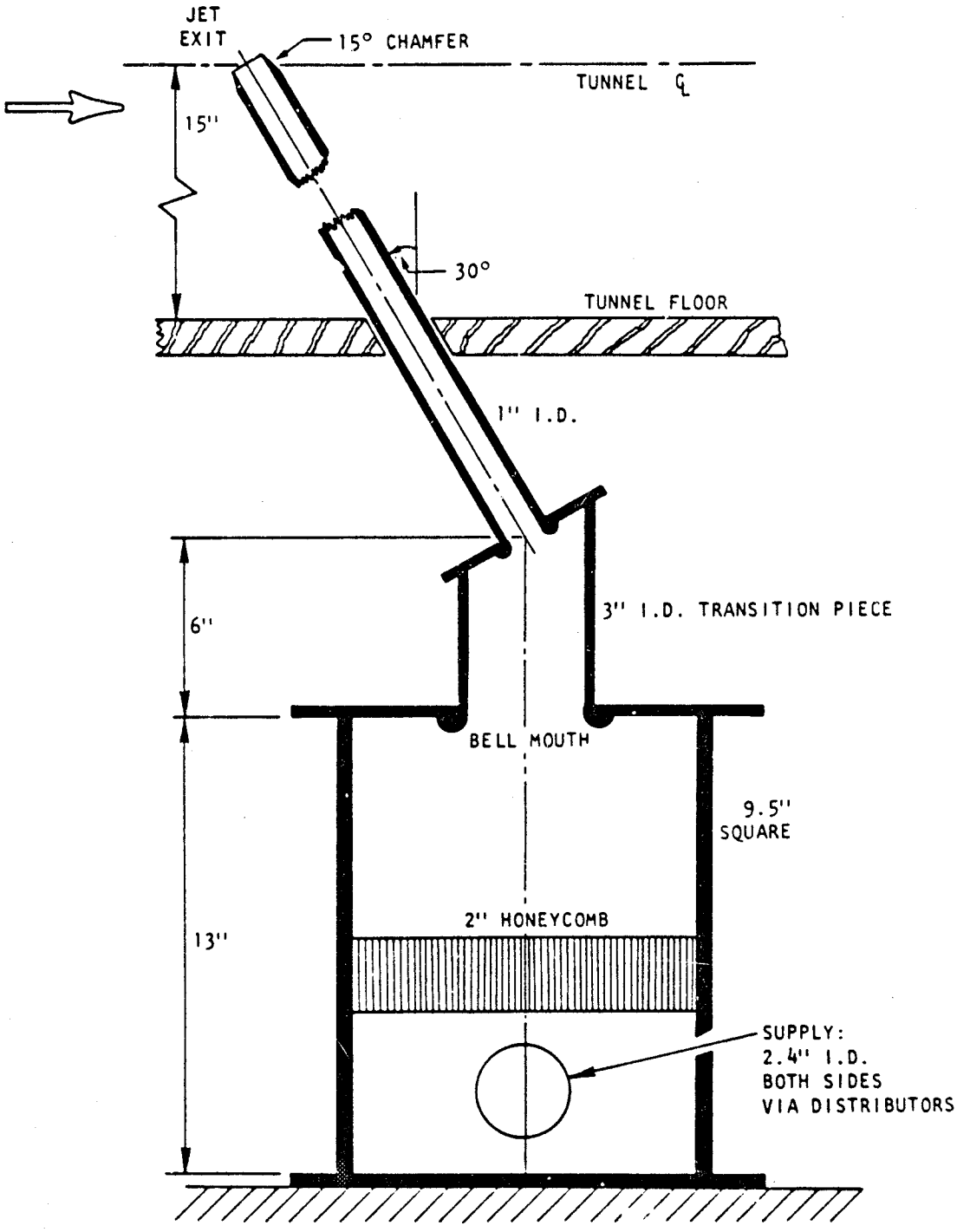

Figure 3.5 Supply plenum and flow conditioning for jet.

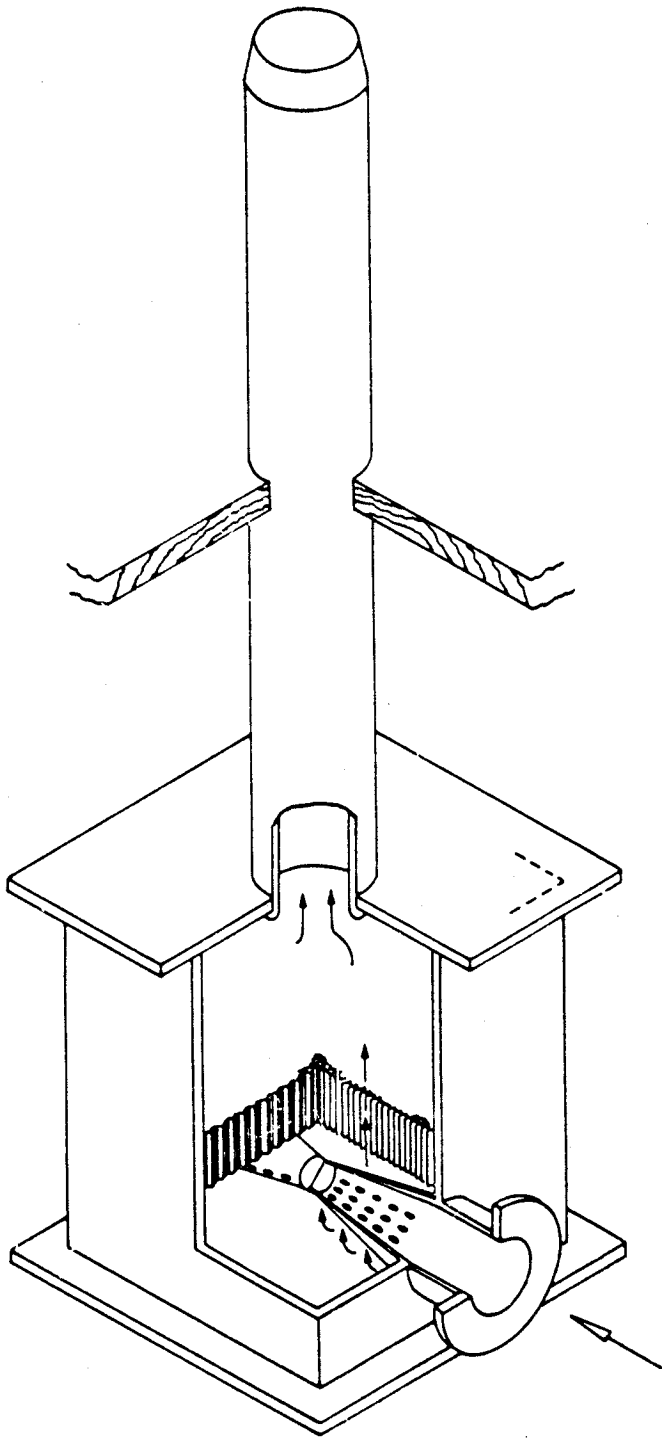

Figure 3.6 Oblique view of jet rig, showing supply details.

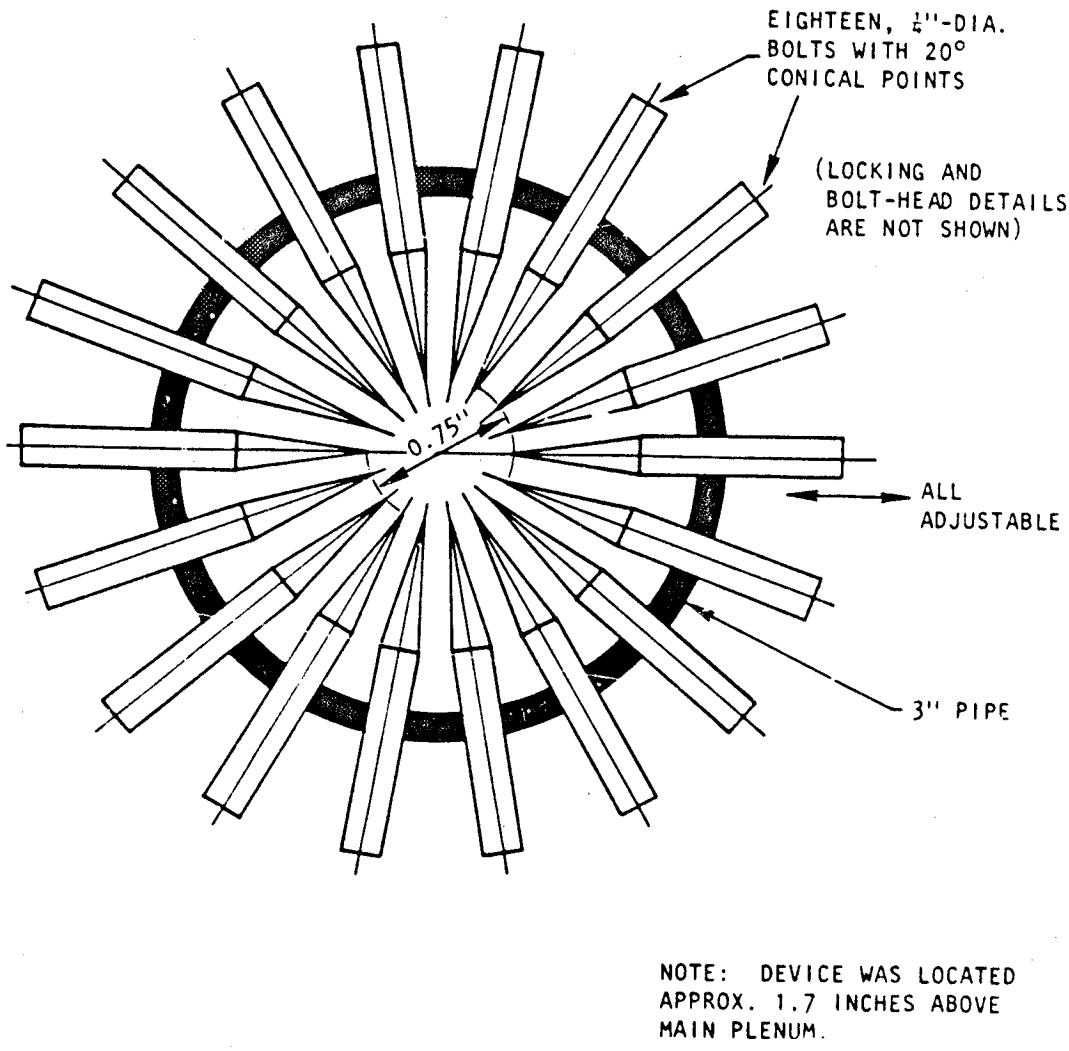

Figure 3.7 Modification to 3-inch jet pipe for profile adjustment.

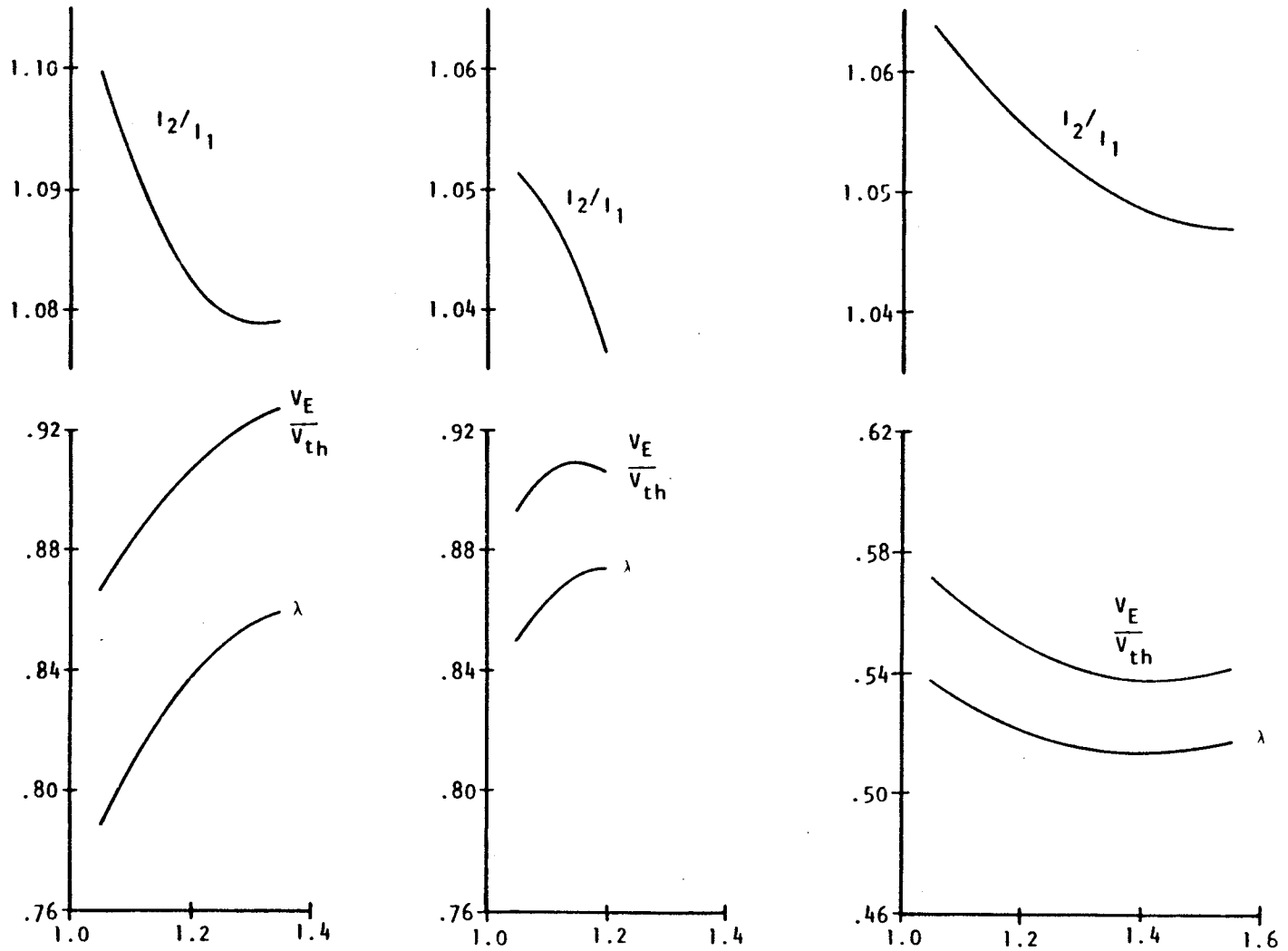

Figure 3.8 Jet calibration parameters as a function of jet pressure ratio. (fitted curves)

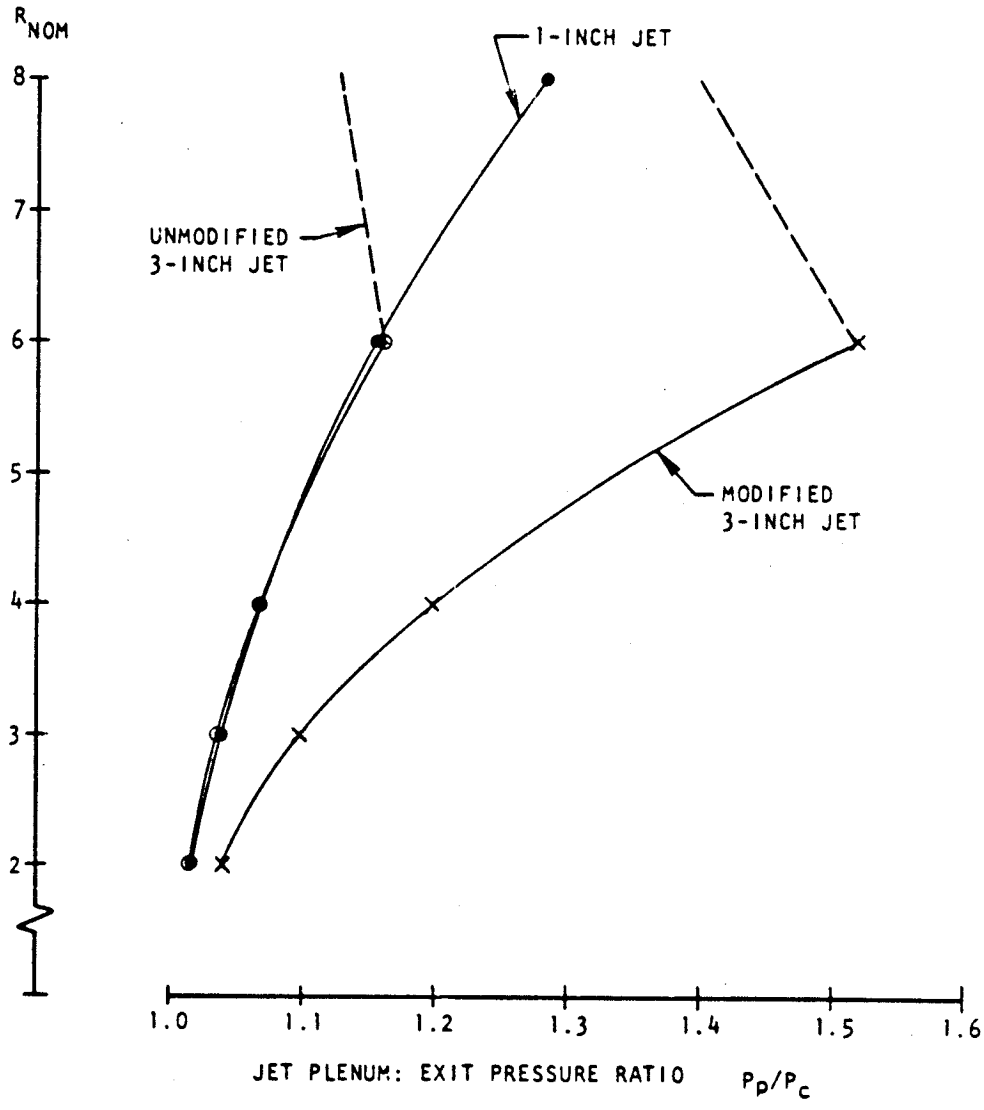

Figure 3.9 Nominal velocity ratio as a function of plenum pressure ratio.

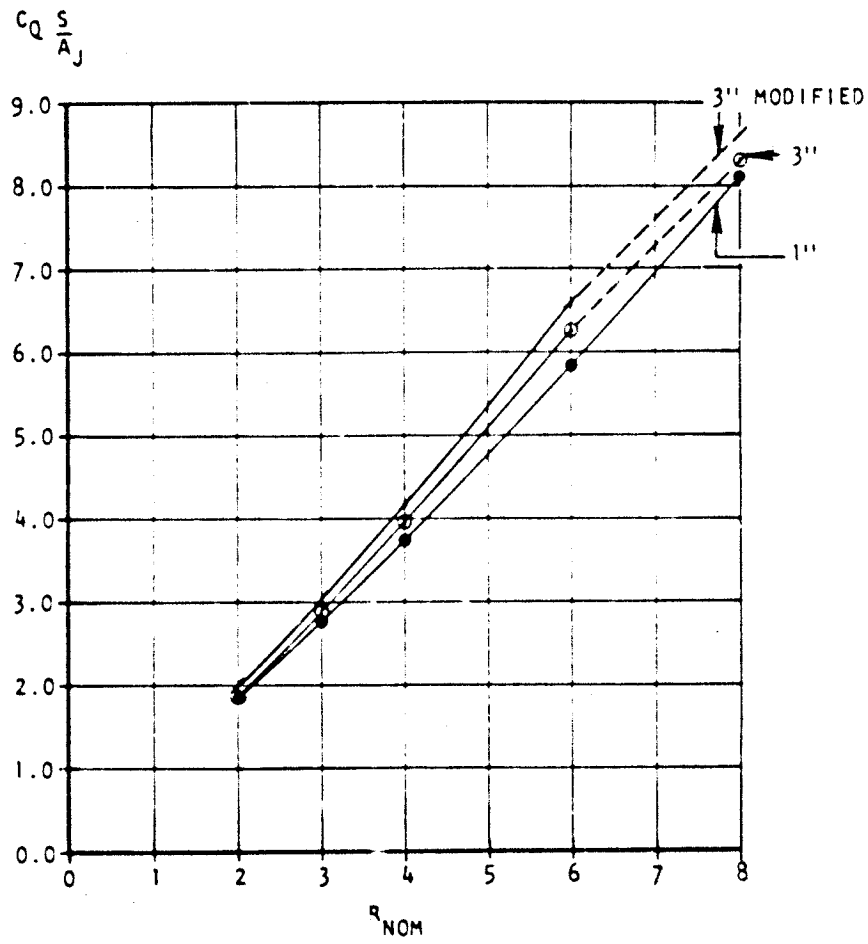

Figure 3.10 Flow coefficients for 1- and 3-inch jets.

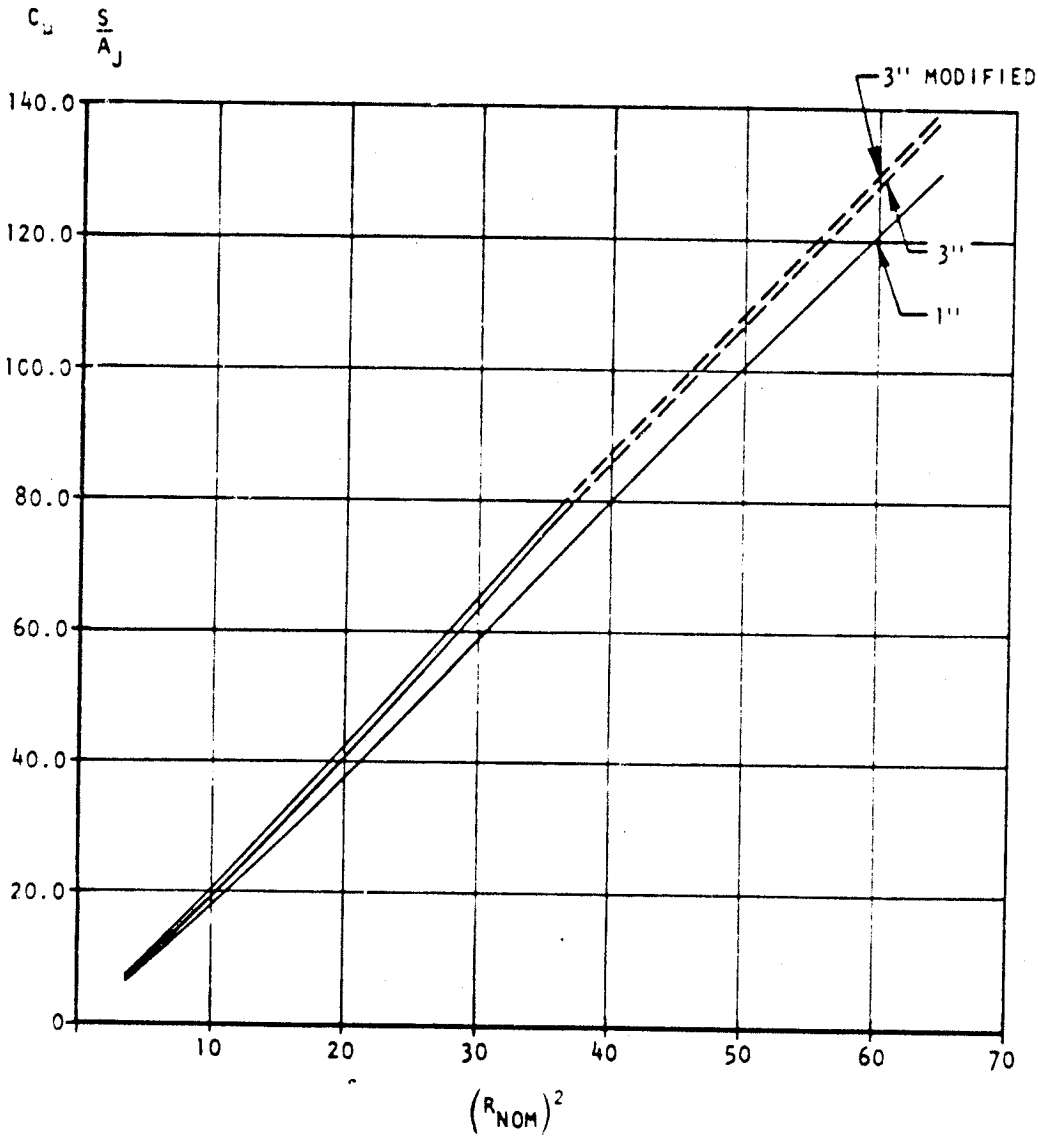

Figure 3.11 Momentum flux coefficients for 1- and 3-inch jets.

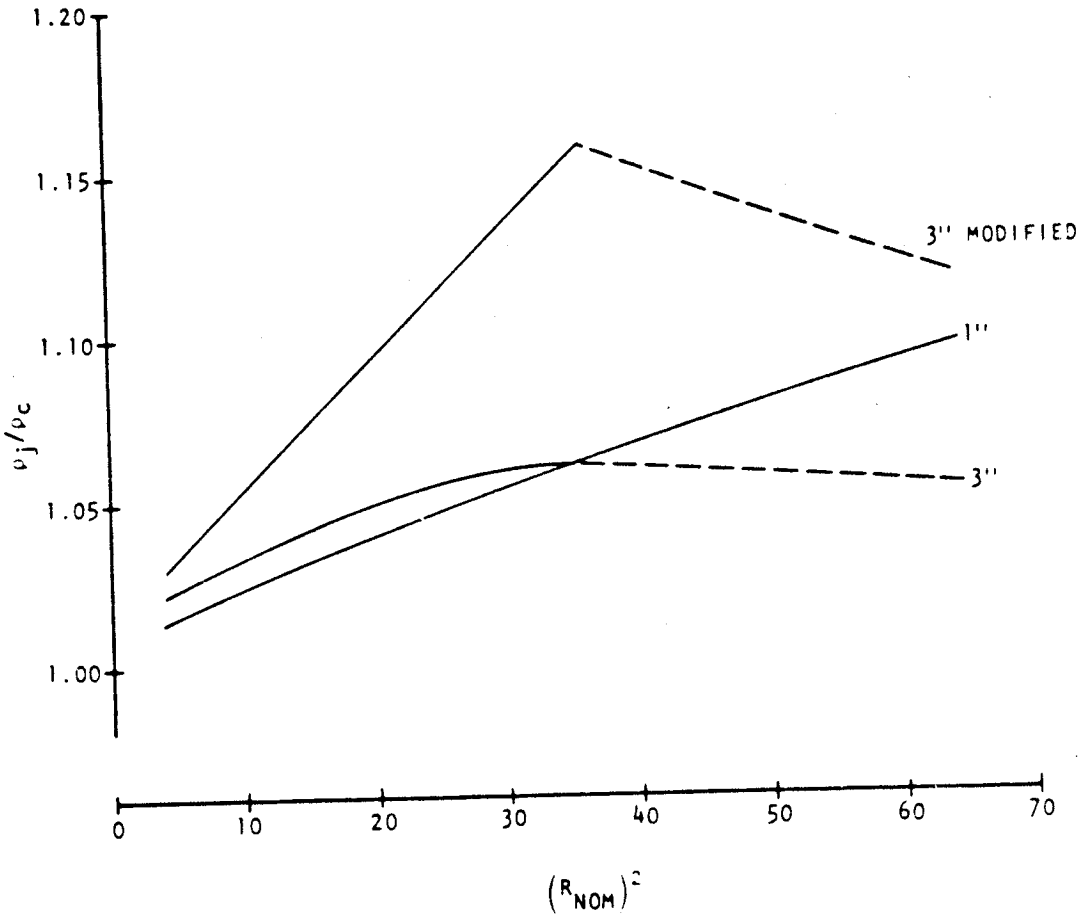

Figure 3.12 Jet: mainstream density ratio.

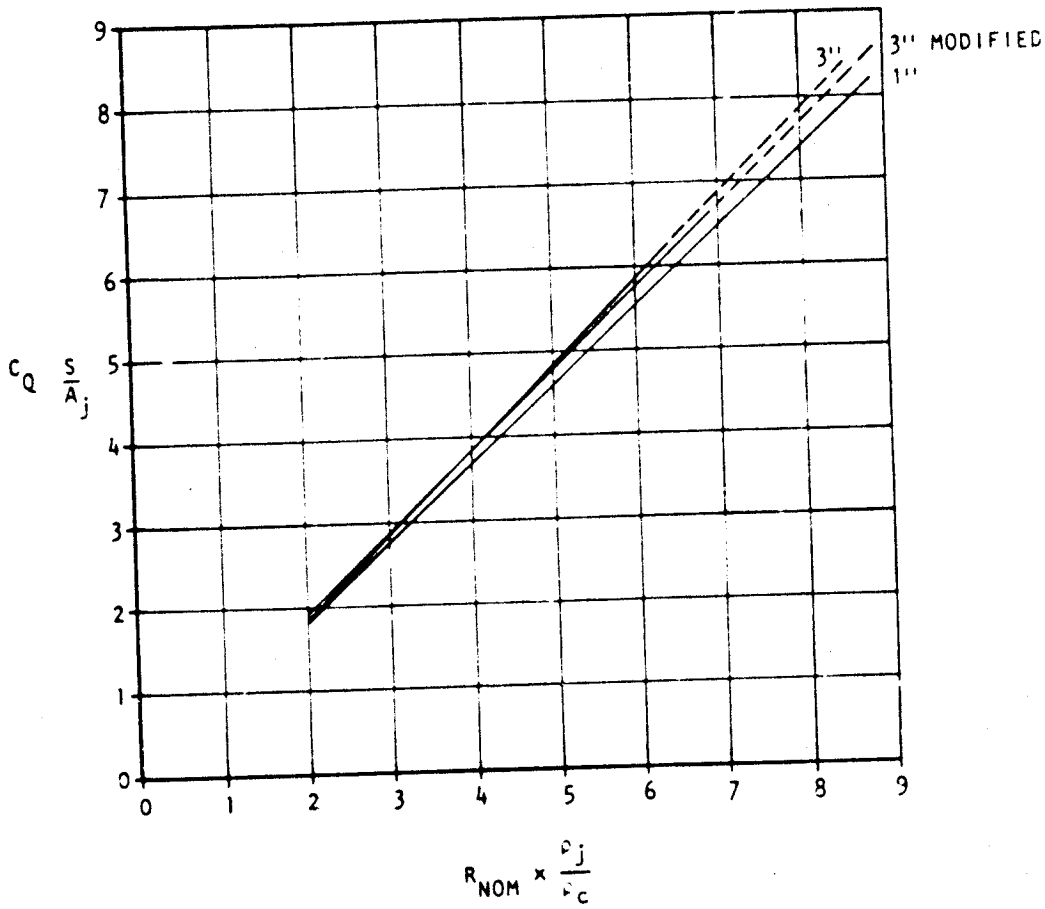

Figure 3.13 Effect of density ratio on flow coefficient correlations.

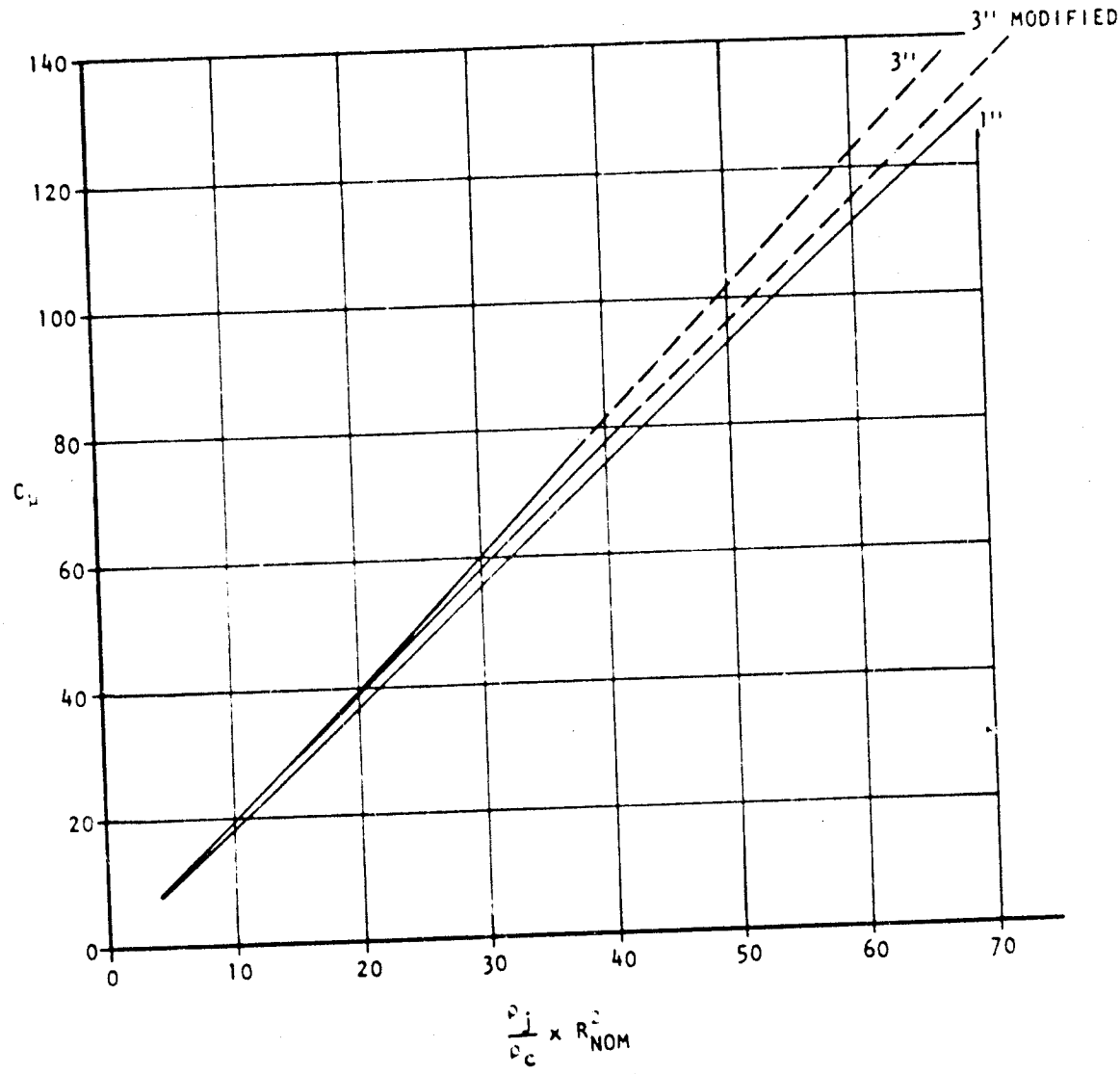

Figure 3.14 Effect of density ratio on momentum flux correlations.

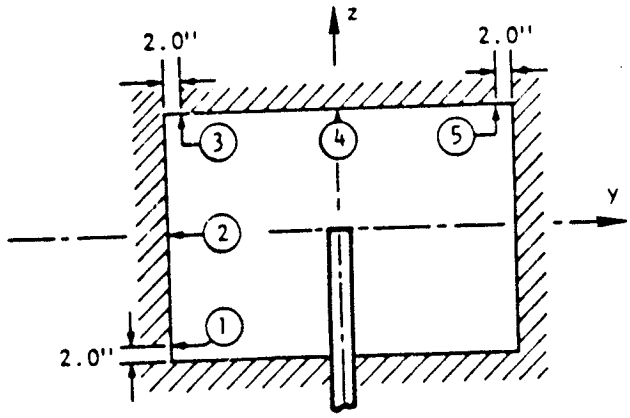

#	Rows 1 THRU 5
1	-0.814
2	-0.465
3	-0.372
4	-0.279
5	-0.186
6	-0.093
7	0.000
8	0.070
9	0.140
10	0.209
11	0.279
12	0.349
13	0.419
14	0.488
15	0.587
16	0.698
17	0.837
18	0.977
19	1.116
20	1.256
21	1.395

← TUNNEL REFERENCE STATIC

TABLE SHOWS
X/B VALUES
(B = 43.0")

Figure 3.15 Wall pressure orifice locations for jet-in-crossflow experiments.

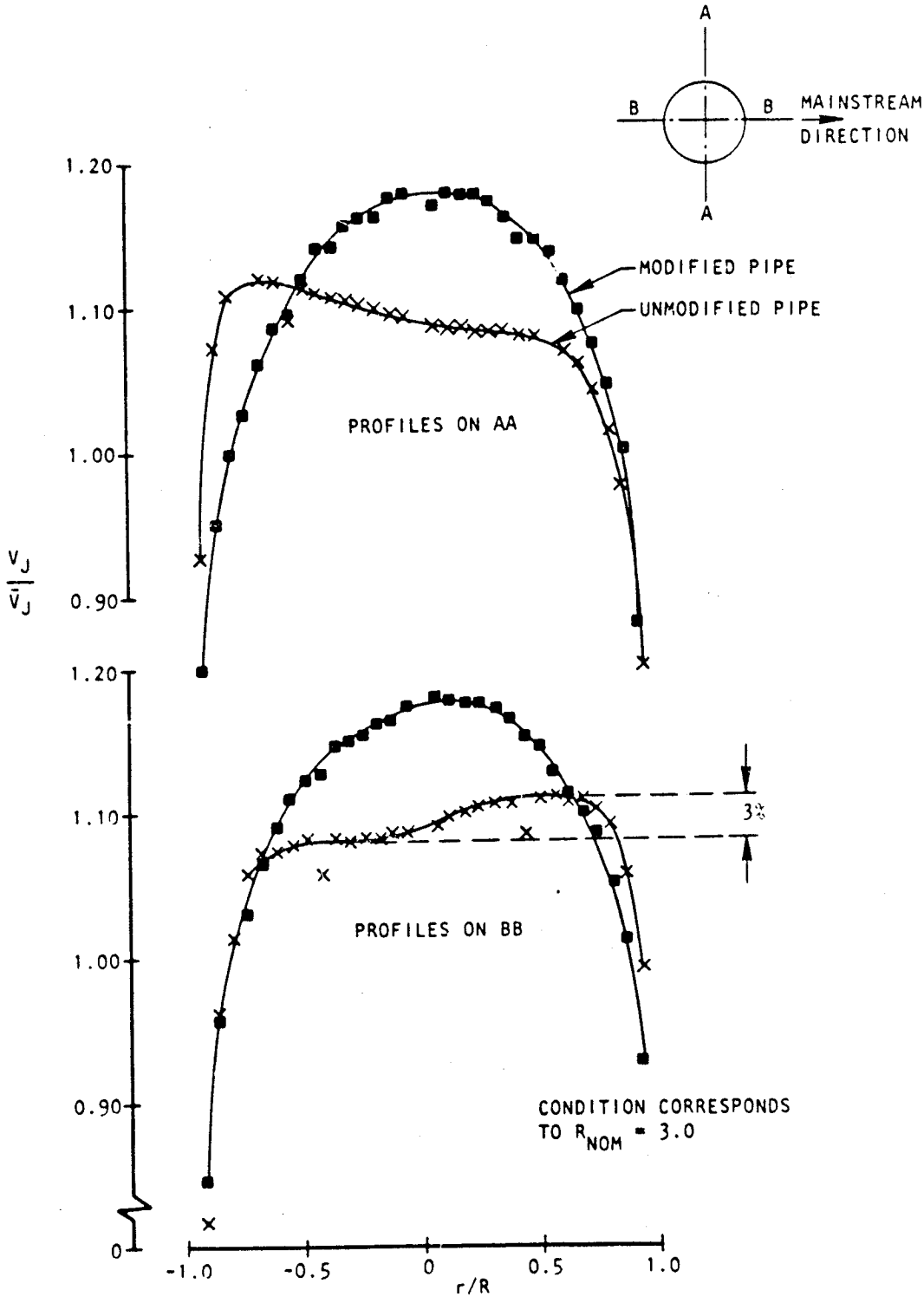

Figure 4.1 Comparison of clean and modified jet profiles for the 3-inch jet

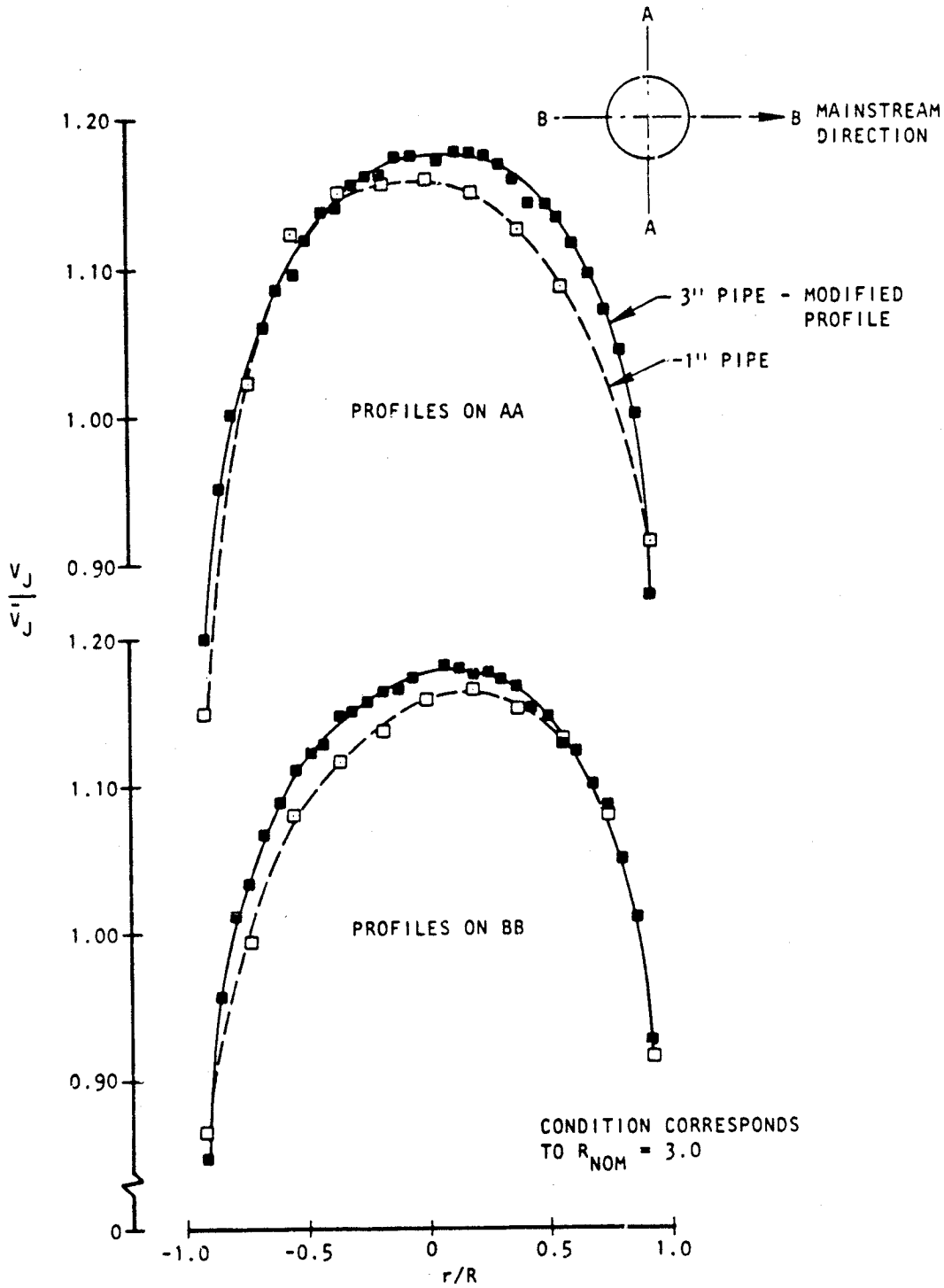

Figure 4.2 Comparison of 1-inch clean and 3-inch modified jet profiles.

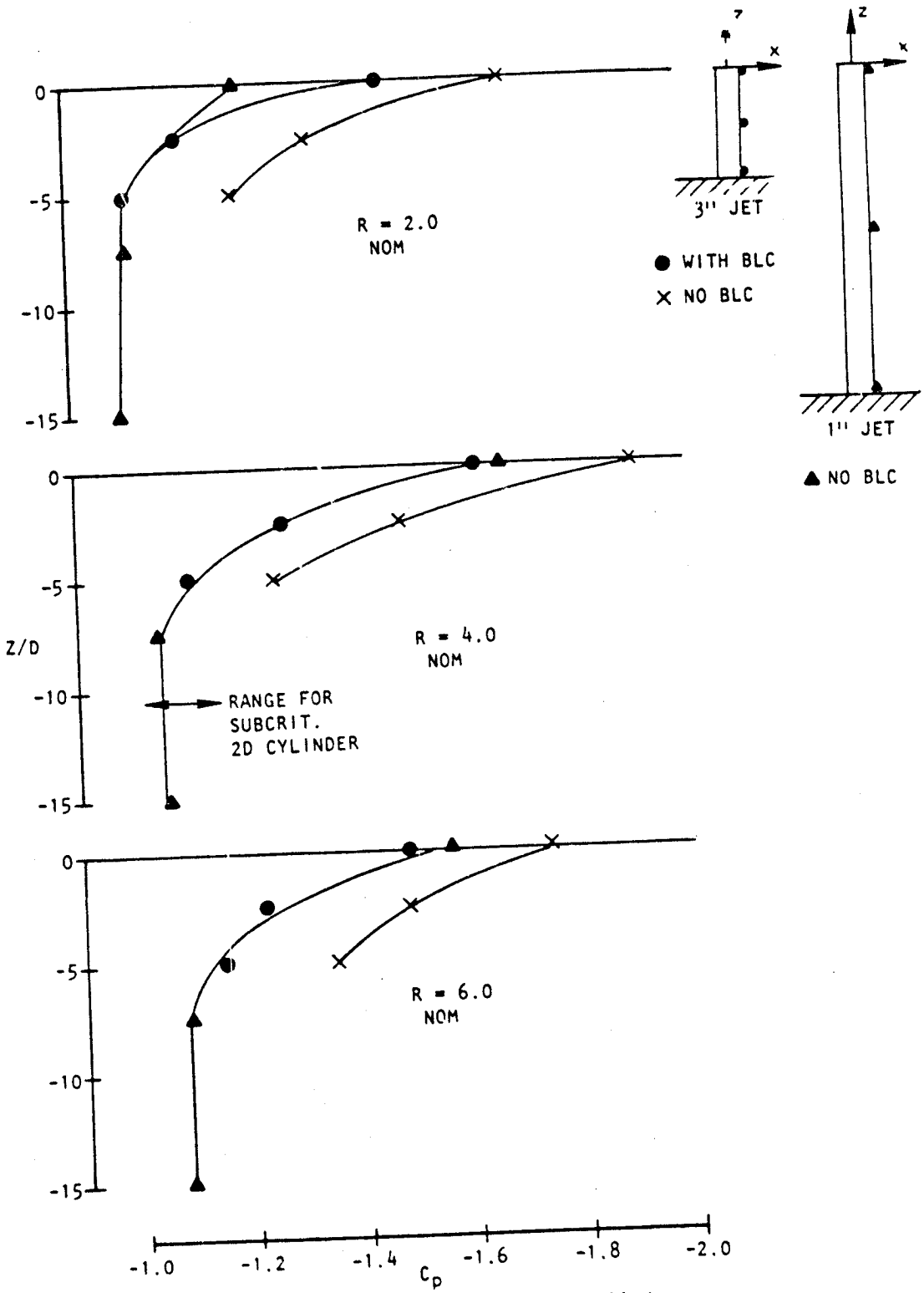

Figure 4.3 Base pressures on jet cylinders

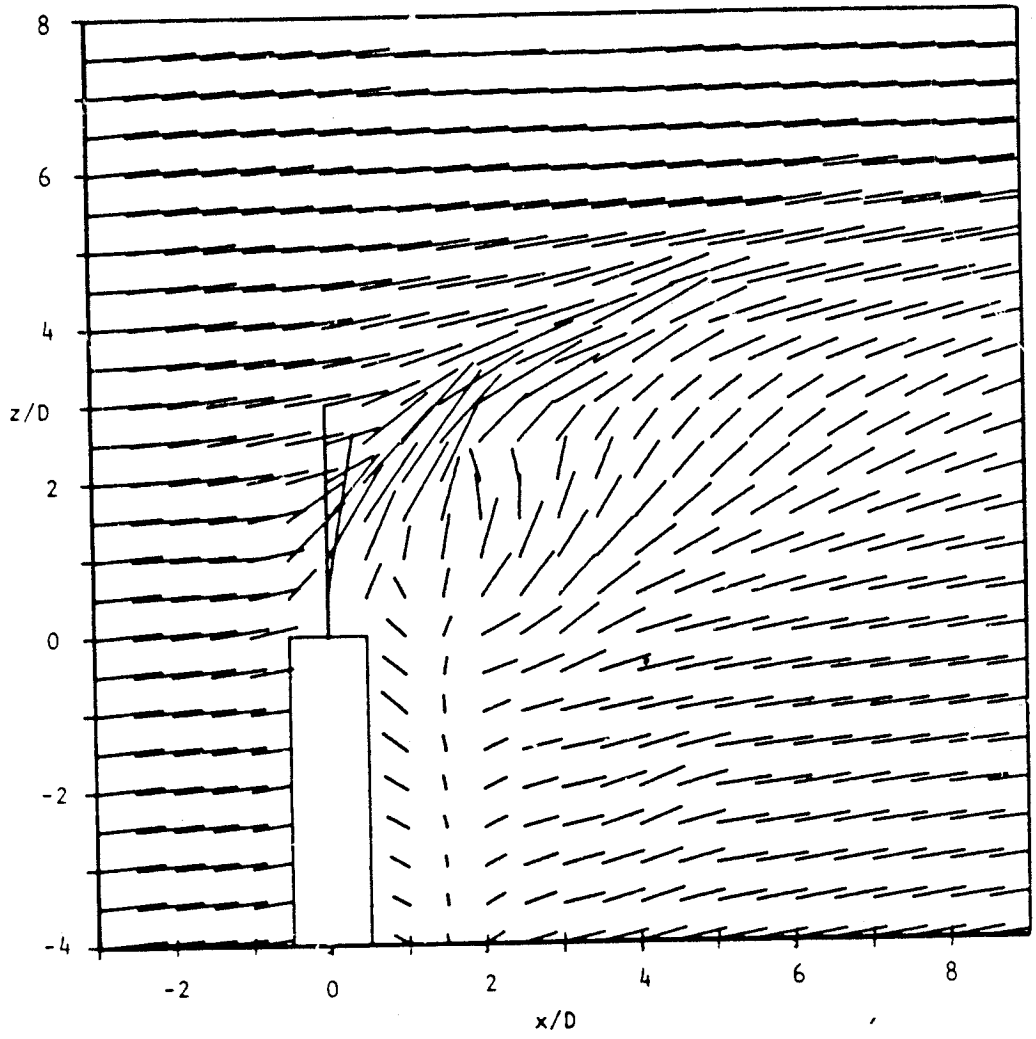

Figure 4.4 Laser-velocimeter measurements of flow vectors at center-plane of 1-inch jet: $R_{NOM} = 3$

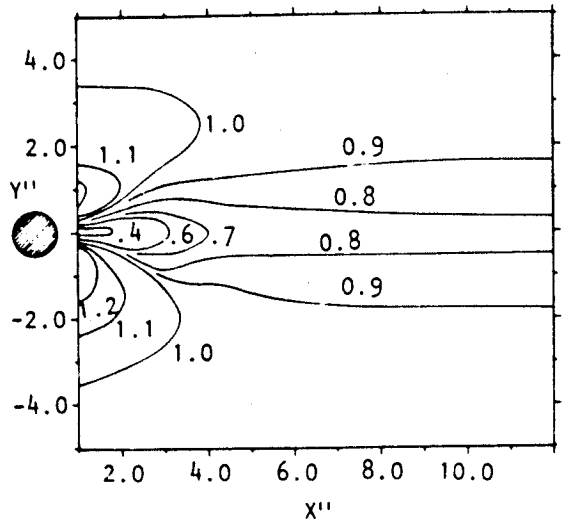

a) Axial velocity distribution

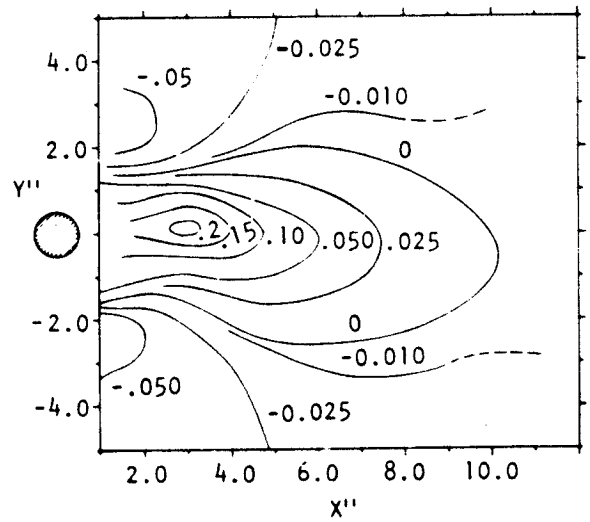

b) Downwash distribution

Figure 4.5 Exit velocity contours for the 1-inch jet: $R_{nom} = 3$

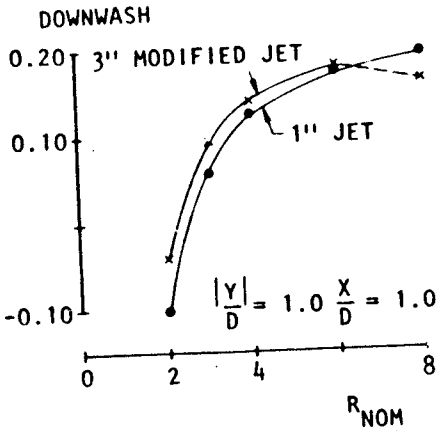

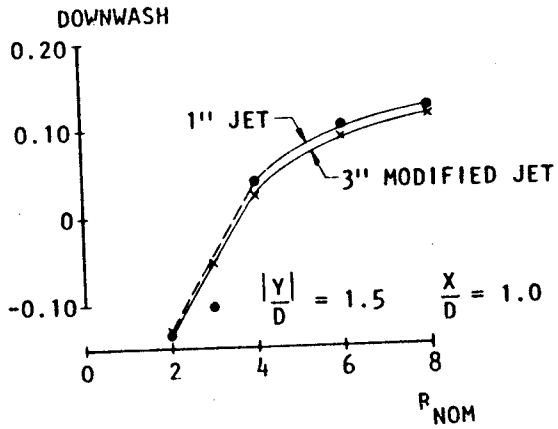

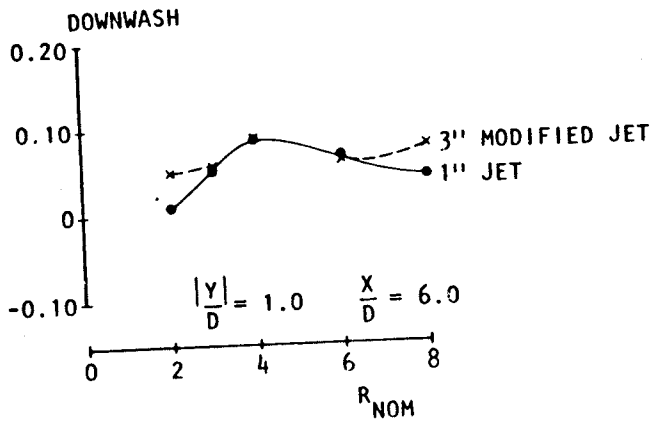

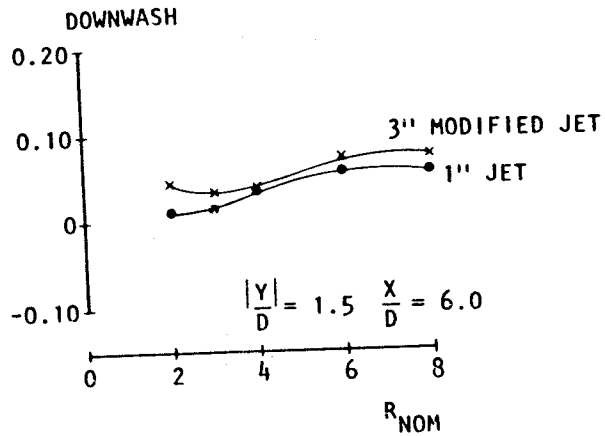

Figure 4.6 Exit plane downwash as a function of jet velocity ratio
a) Effect of jet diameter

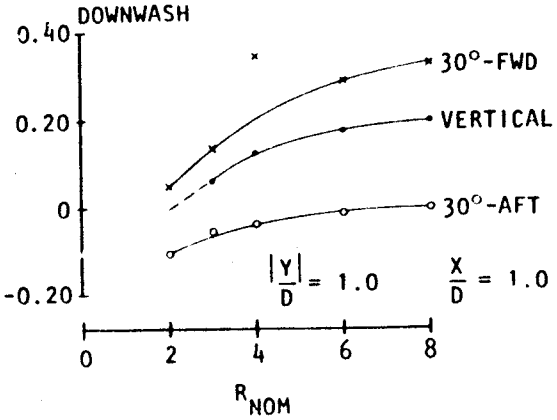

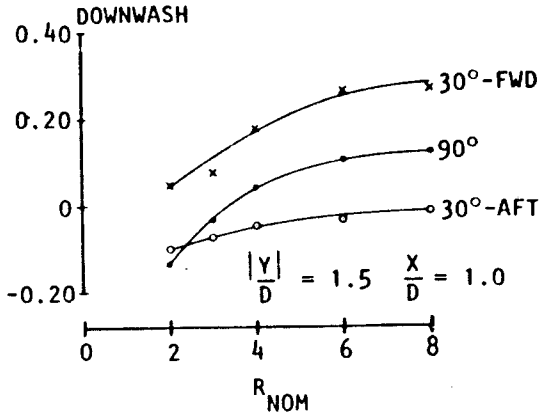

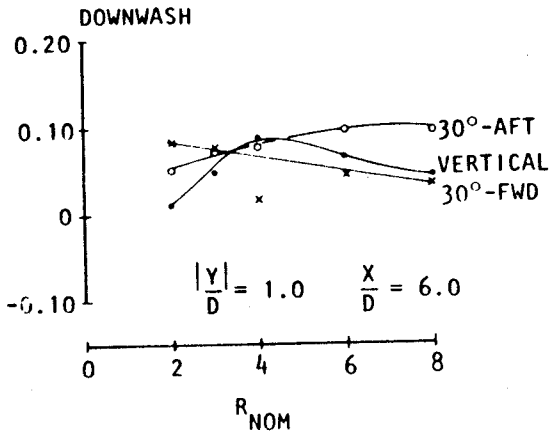

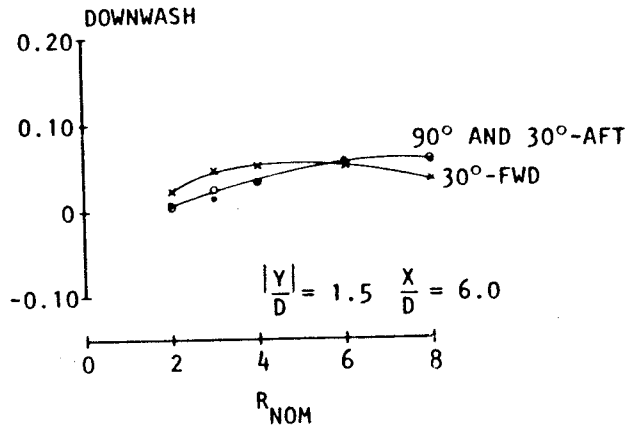

Figure 4.6 (concluded) Exit plane downwash as a function of jet velocity ratios
b) Effect of jet angle

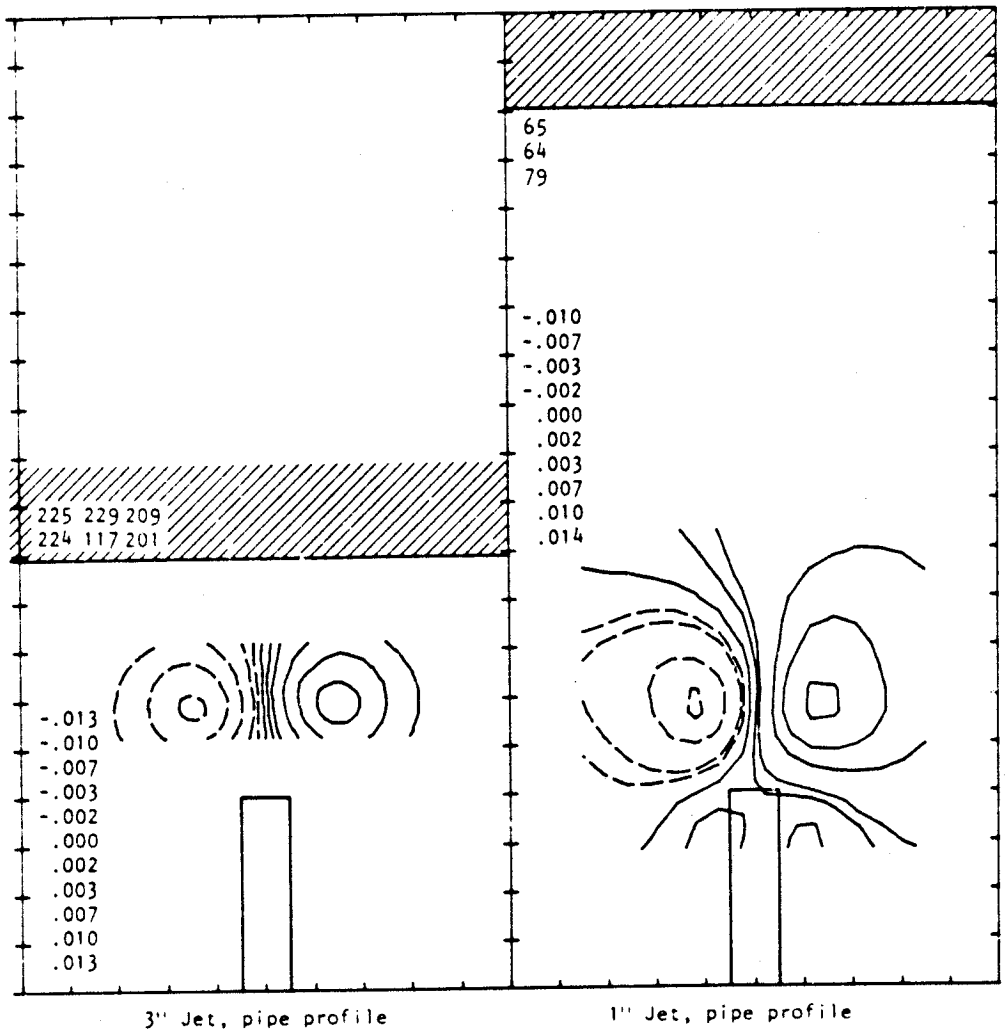

Figure 4.7 Effect of jet size on cross flow streamlines
a) R = 2

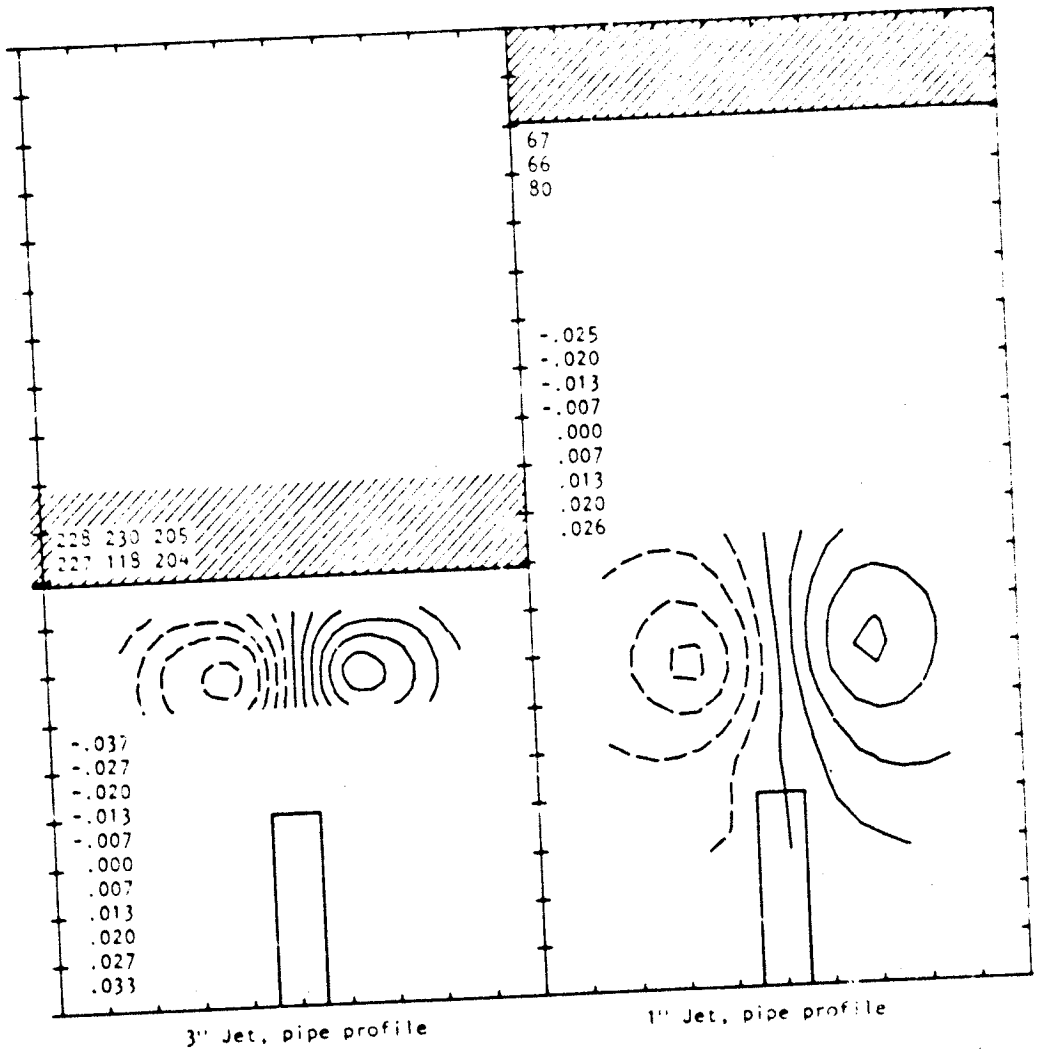

Figure 4.7 (Continued) b) R = 3

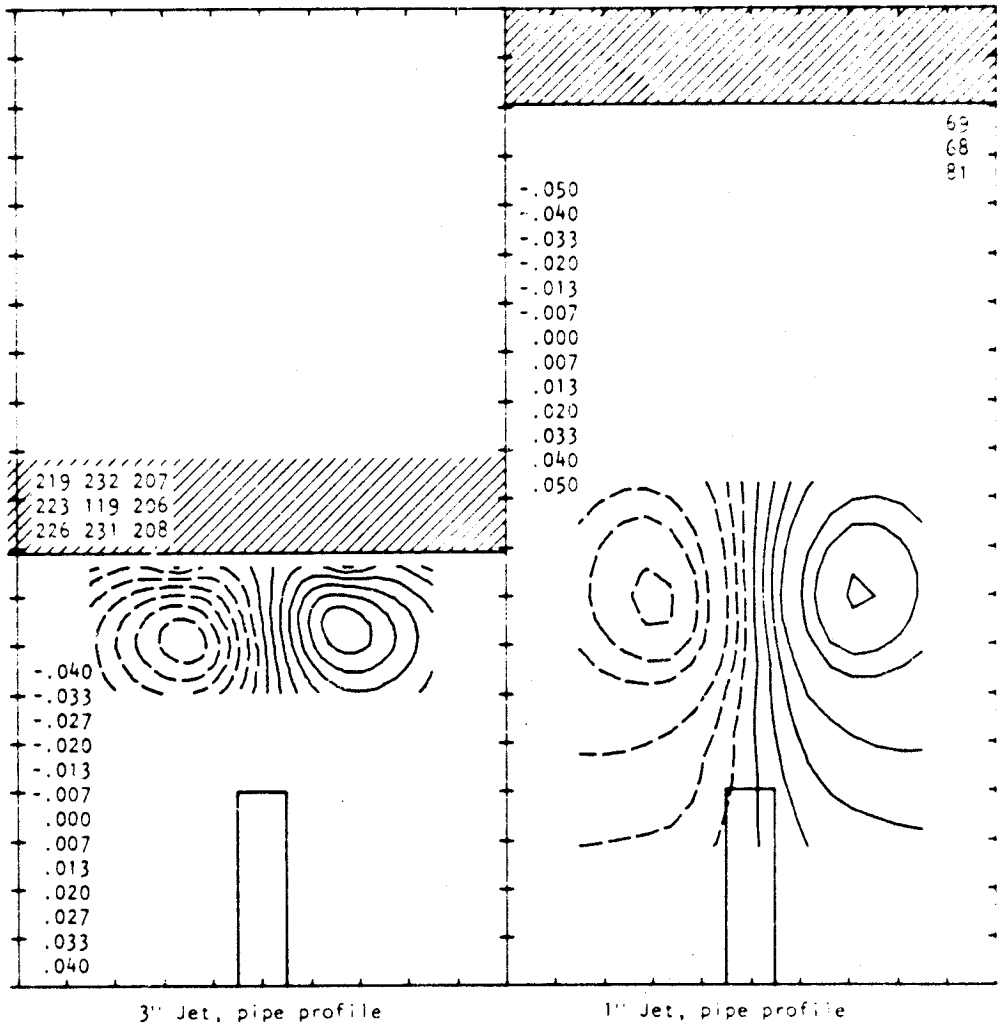

Figure 4.7 (Continued) c) R = 4

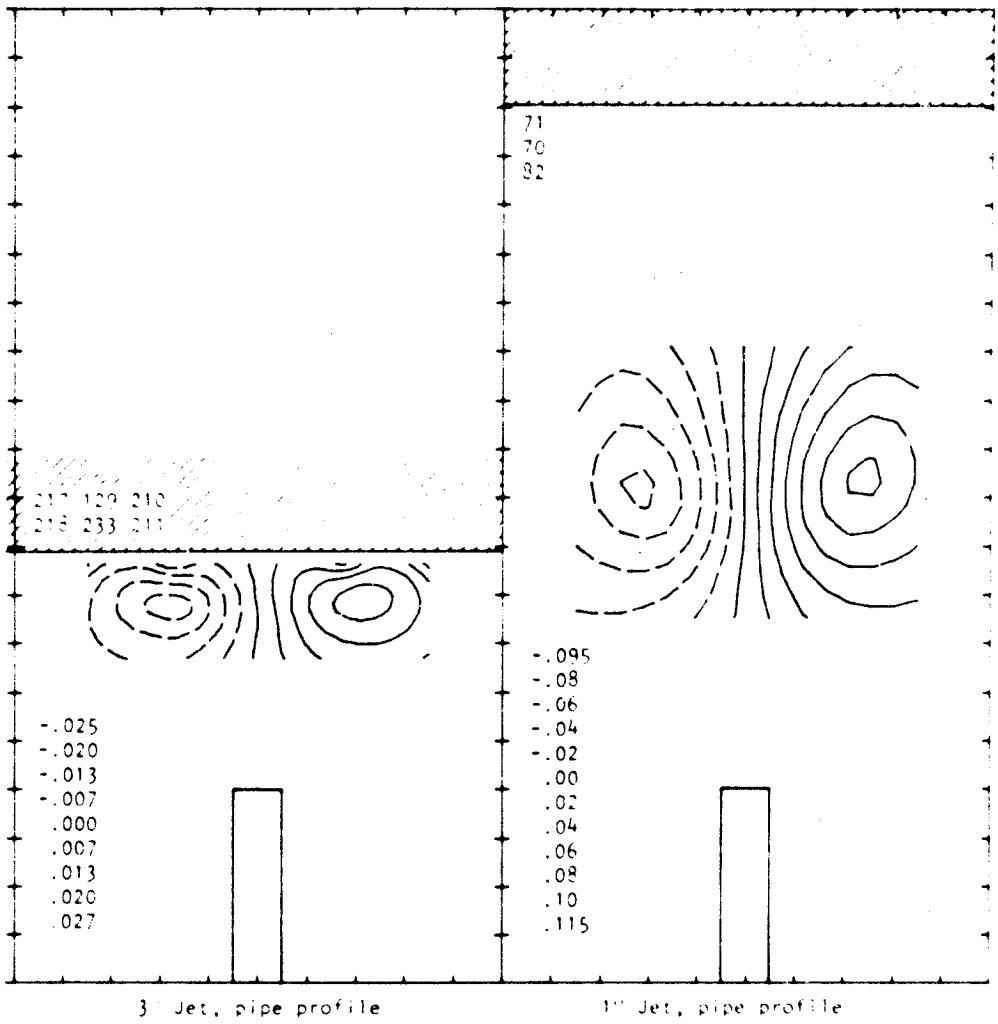

Figure 4.7 (Continued) d) R = 6

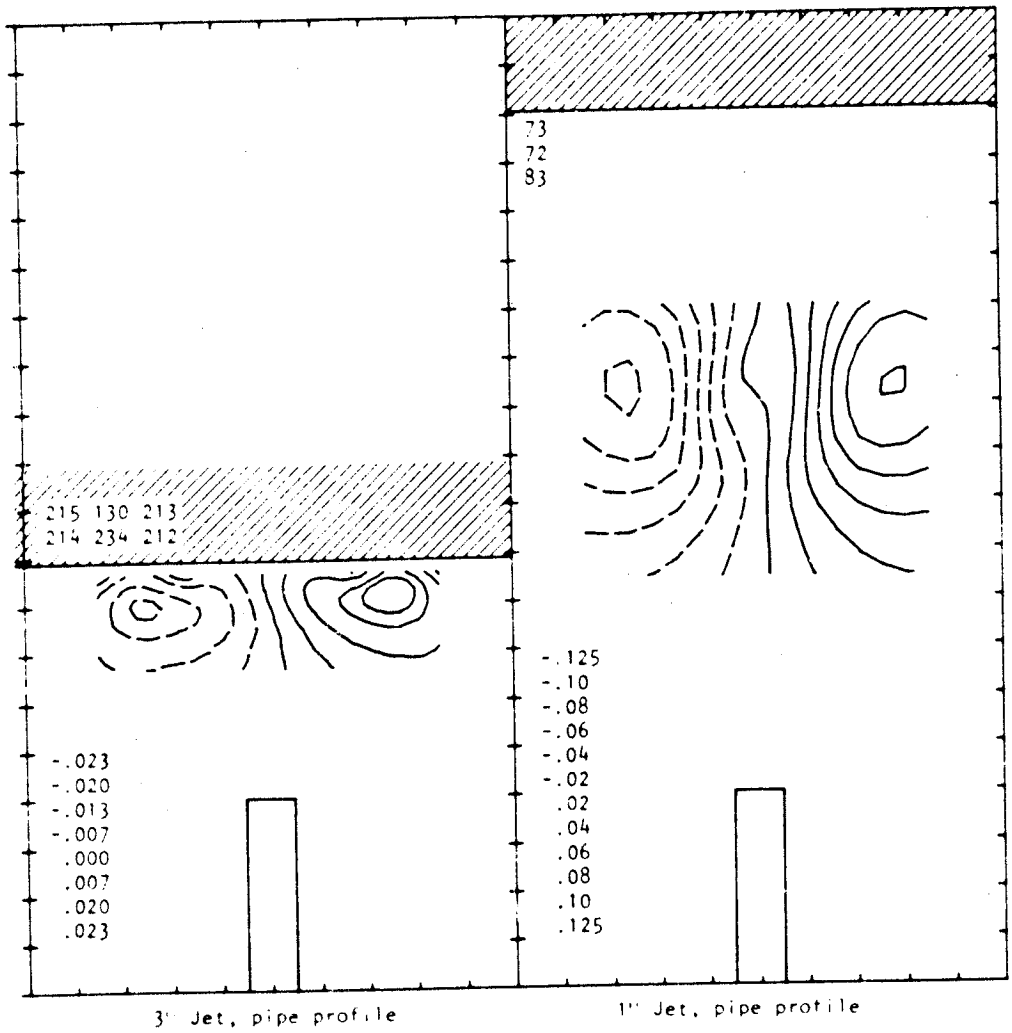

Figure 4.7 (Concluded) e) R = 8

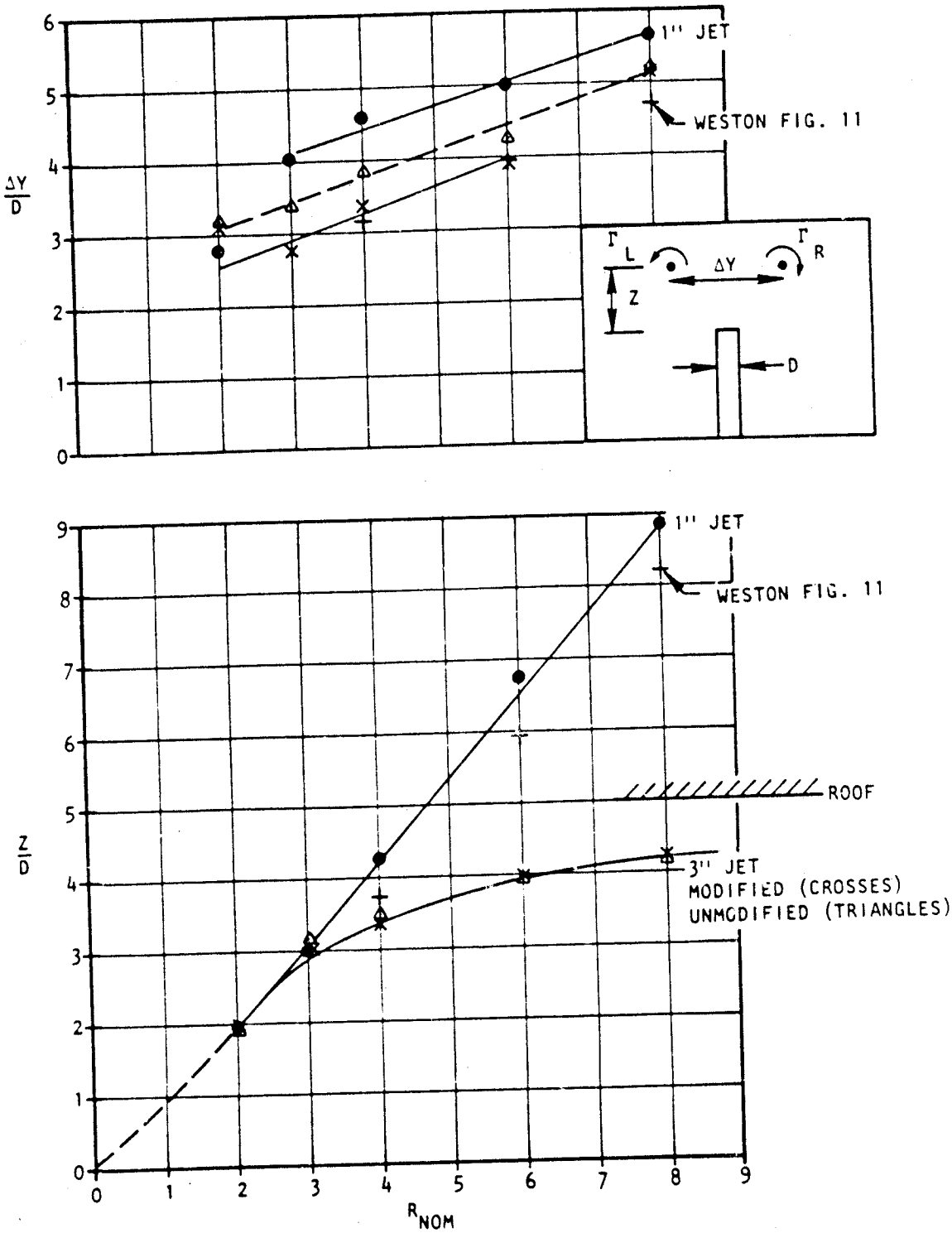

Figure 4.8 Vortex location as a function of jet velocity ratio
a) Effect of jet diameter and profile shape

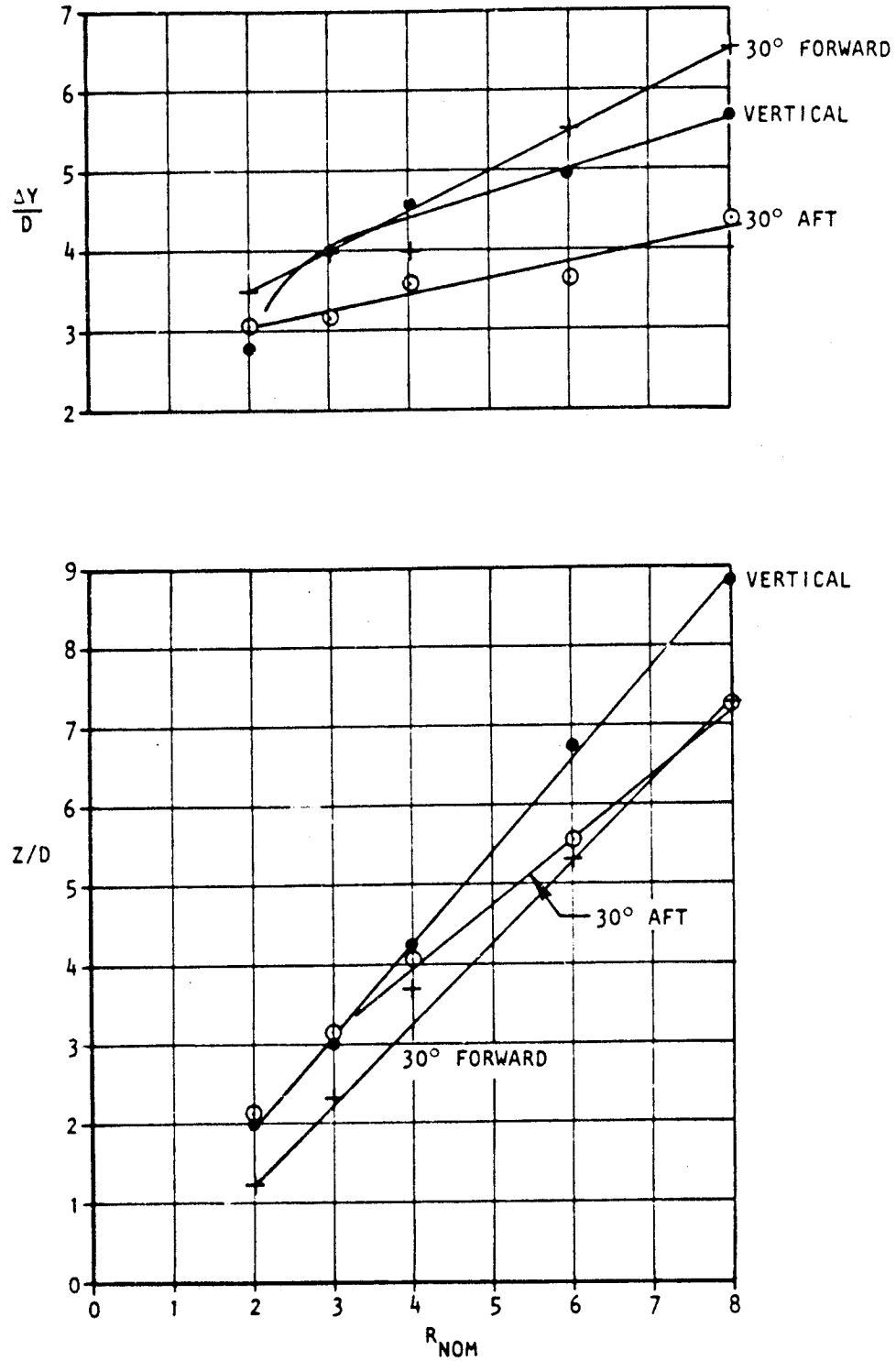

Figure 4.8 (concluded) Vortex location as a function of jet velocity ratio
b) Effect of jet angle

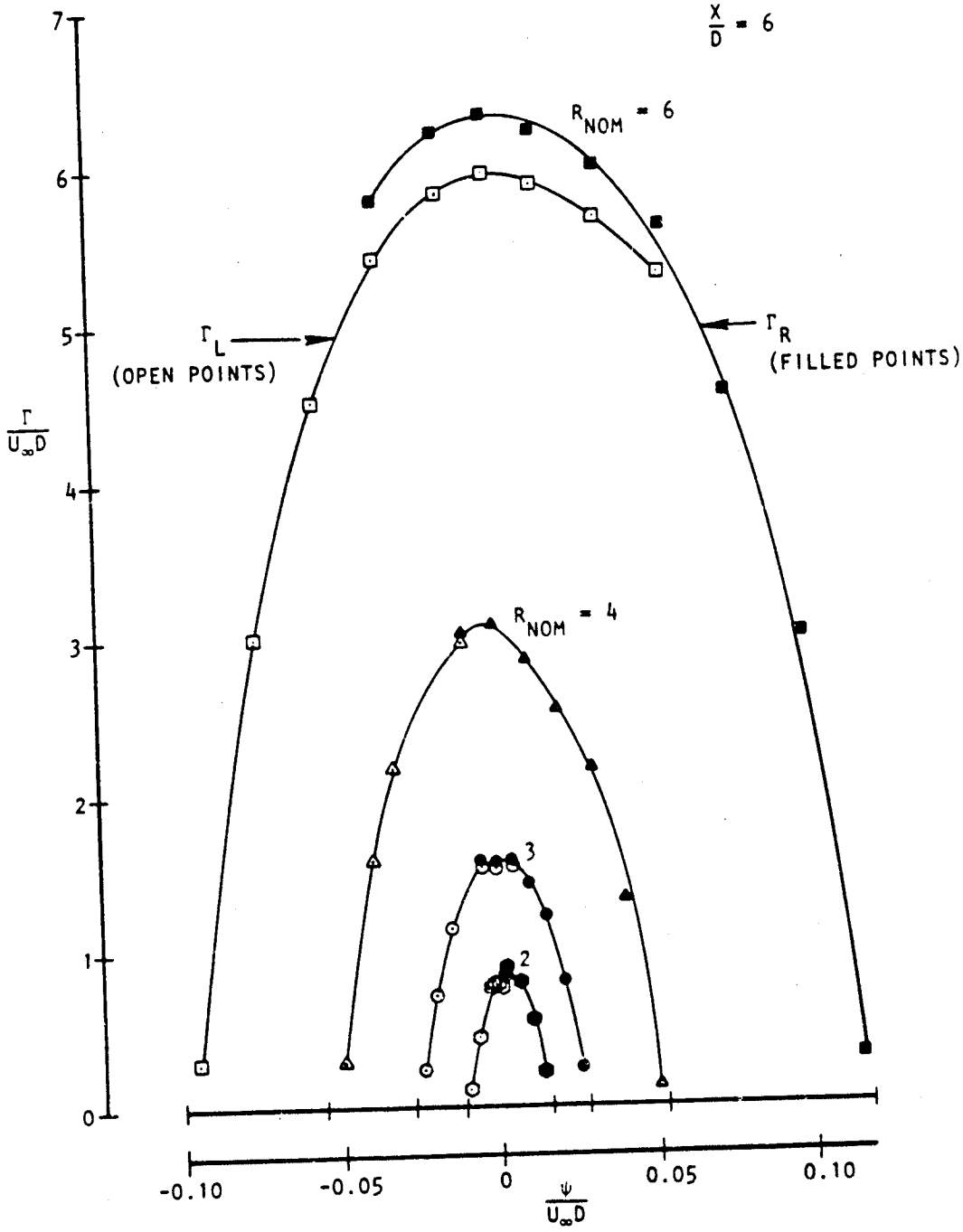

Figure 4.9 Variation of circulation, between vortex centers, for 1-inch vertical jet.

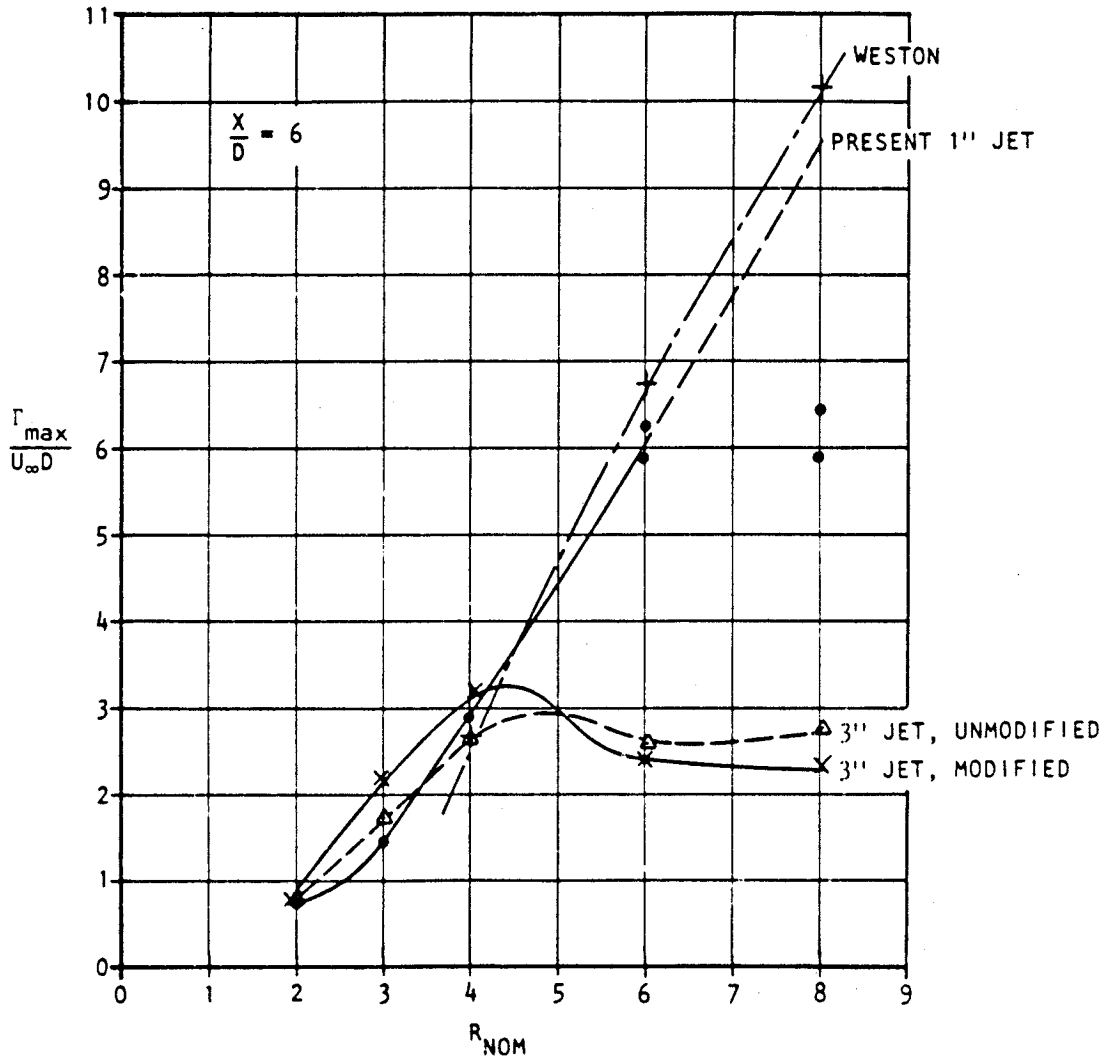

Figure 4.10 Vortex strength as a function of jet velocity ratio
a) Effect of jet diameter and profile shape

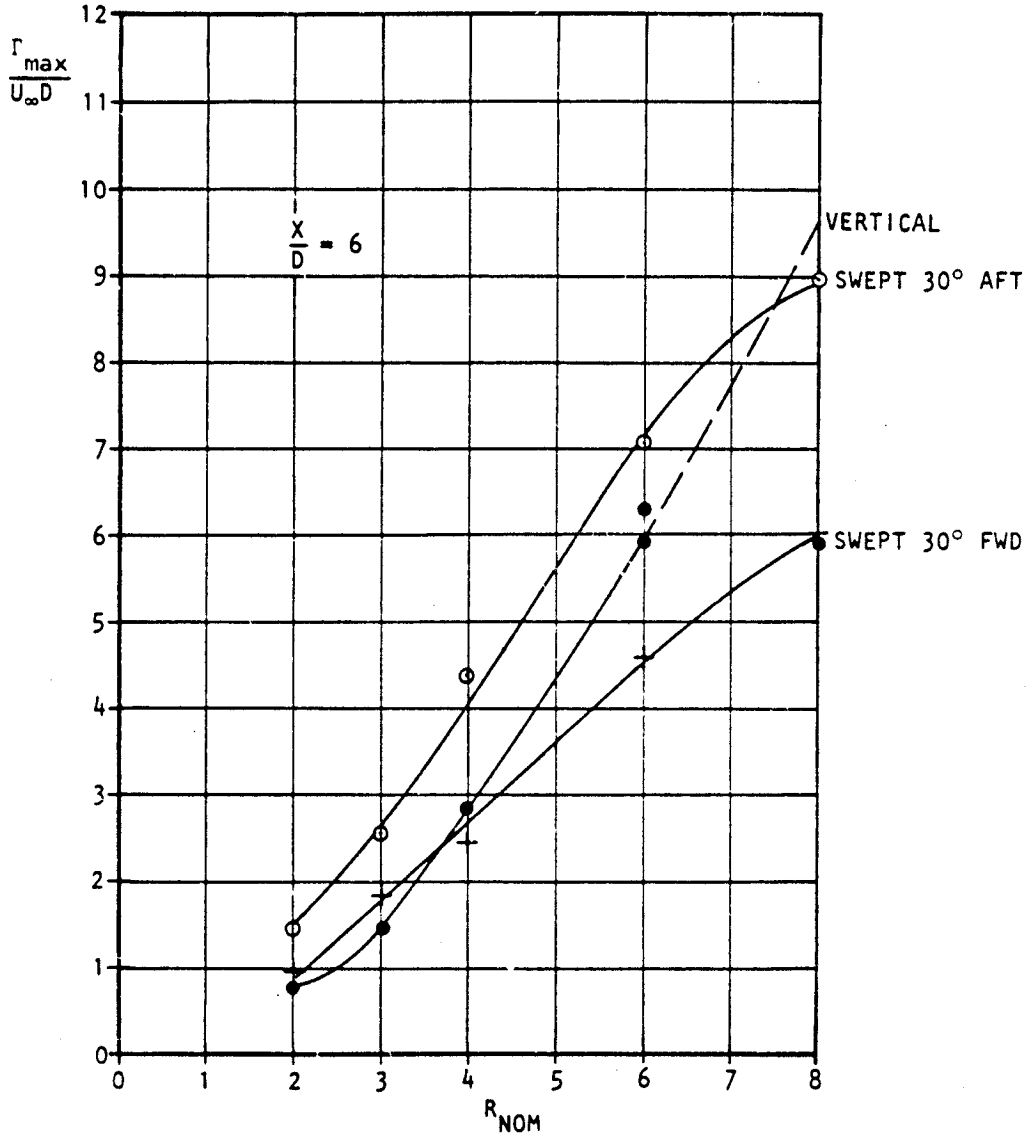

Figure 4.10 (concluded) Vortex strength as a function jet velocity ratio
b) Effect of jet angle

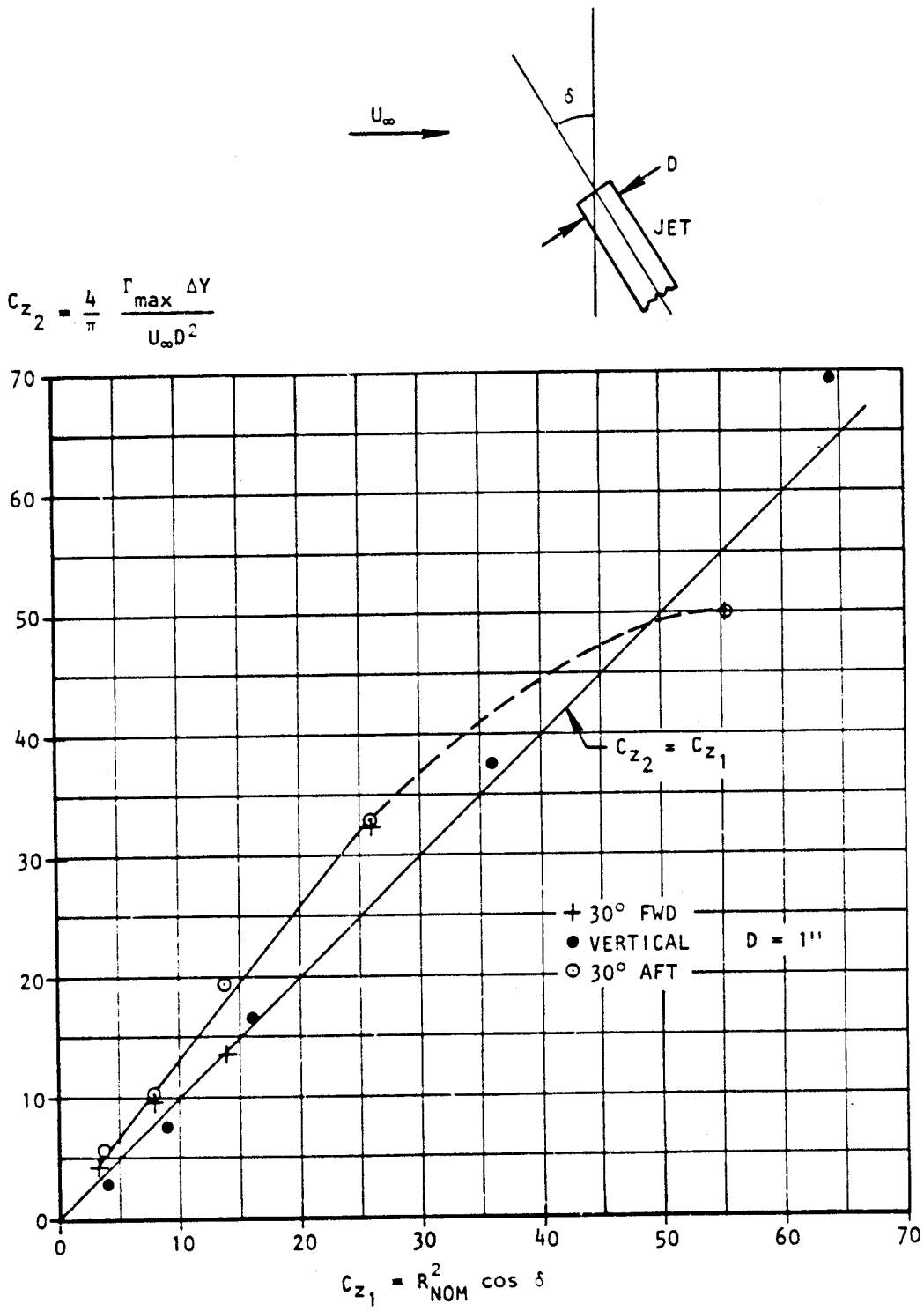

Figure 4.11 Vortex-lift correlation for 1-inch jets

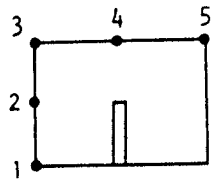

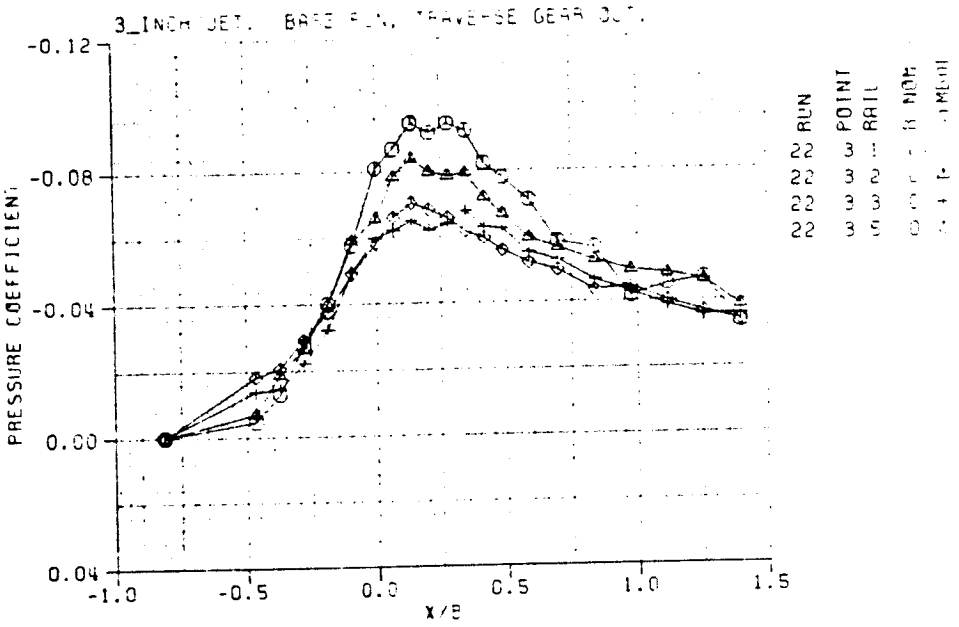

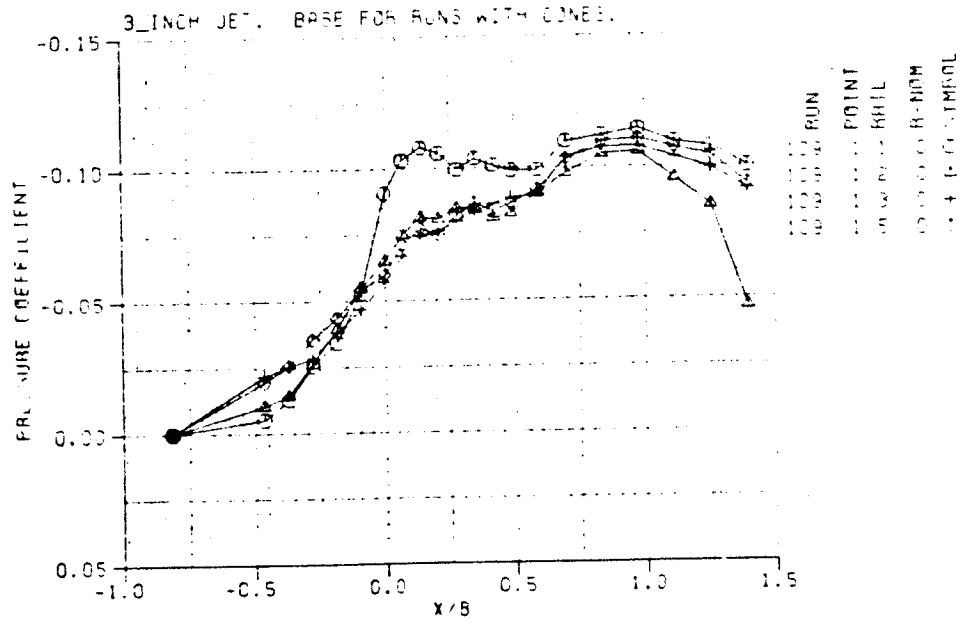

Figure 4.12 Jet pipe datum runs at $R_{NOM} = 0$
(a) 3-inch jet pipe

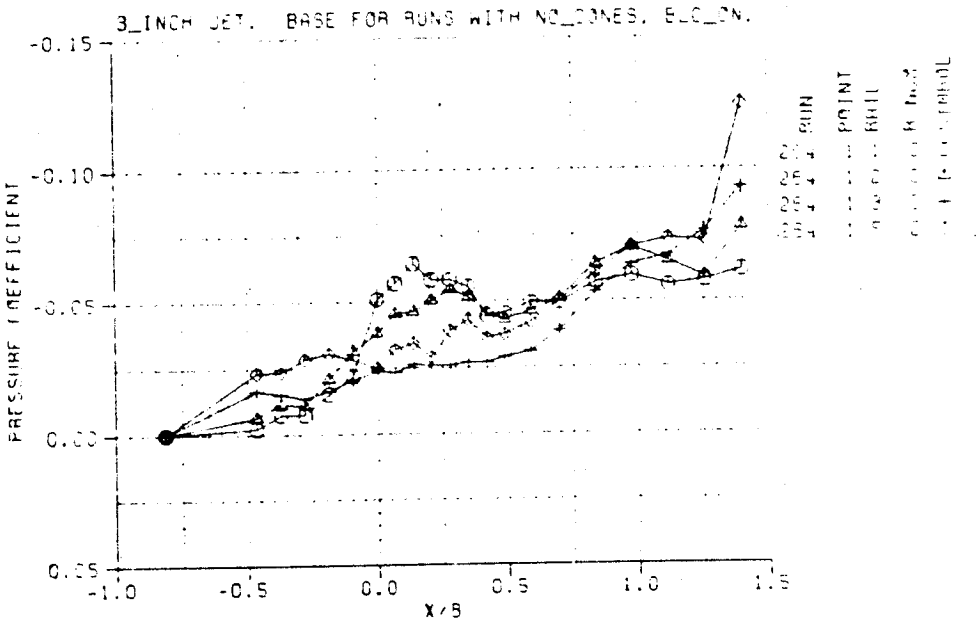

Figure 4.12 (Continued) Jet pipe datum runs at $R_{NOM} = 0$
(b) 3-inch jet pipe with 'ground' BLC

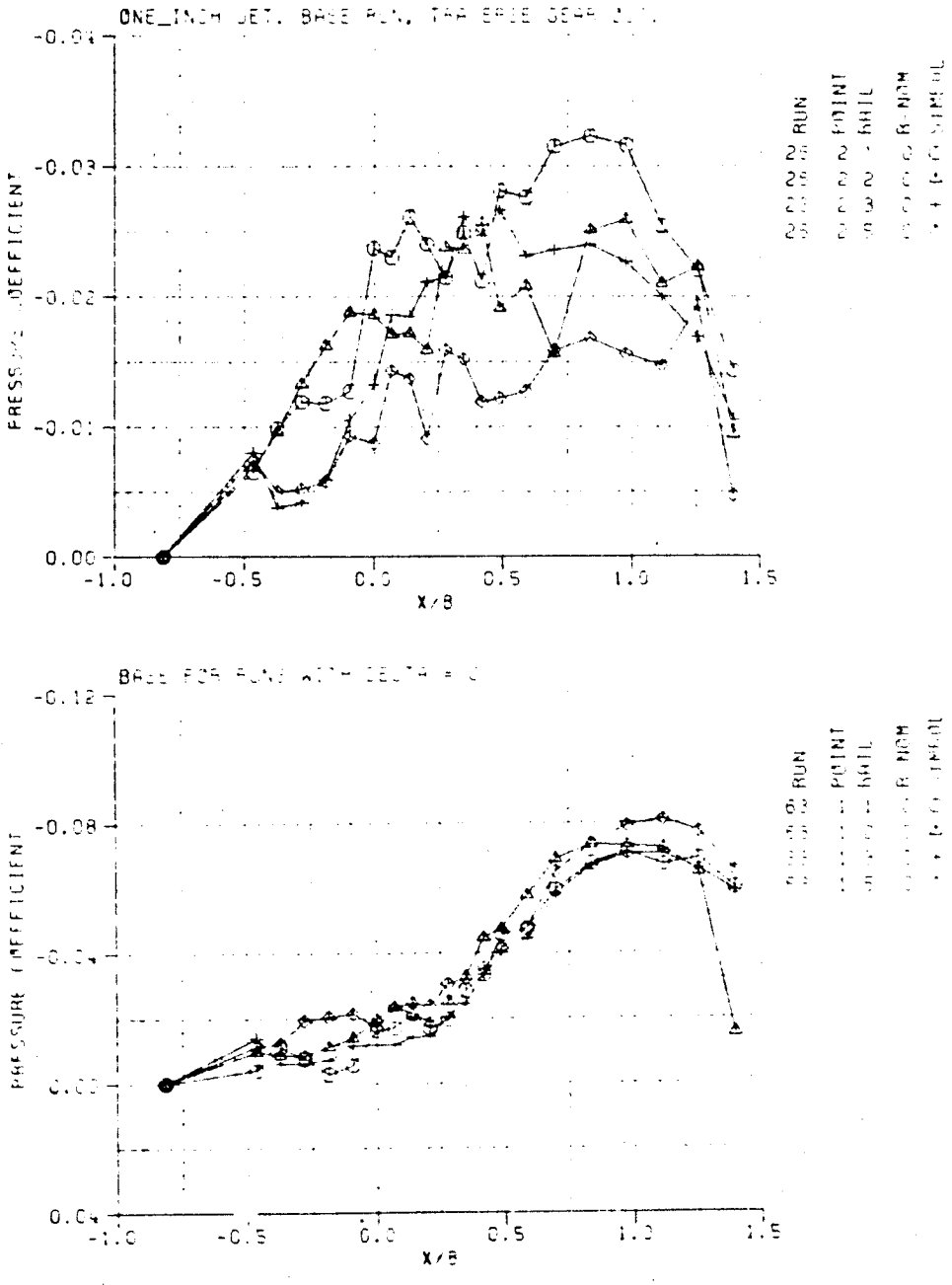

Figure 4.12 (Concluded) Jet pipe datum runs at R = 0
(c) 1-inch jet pipe

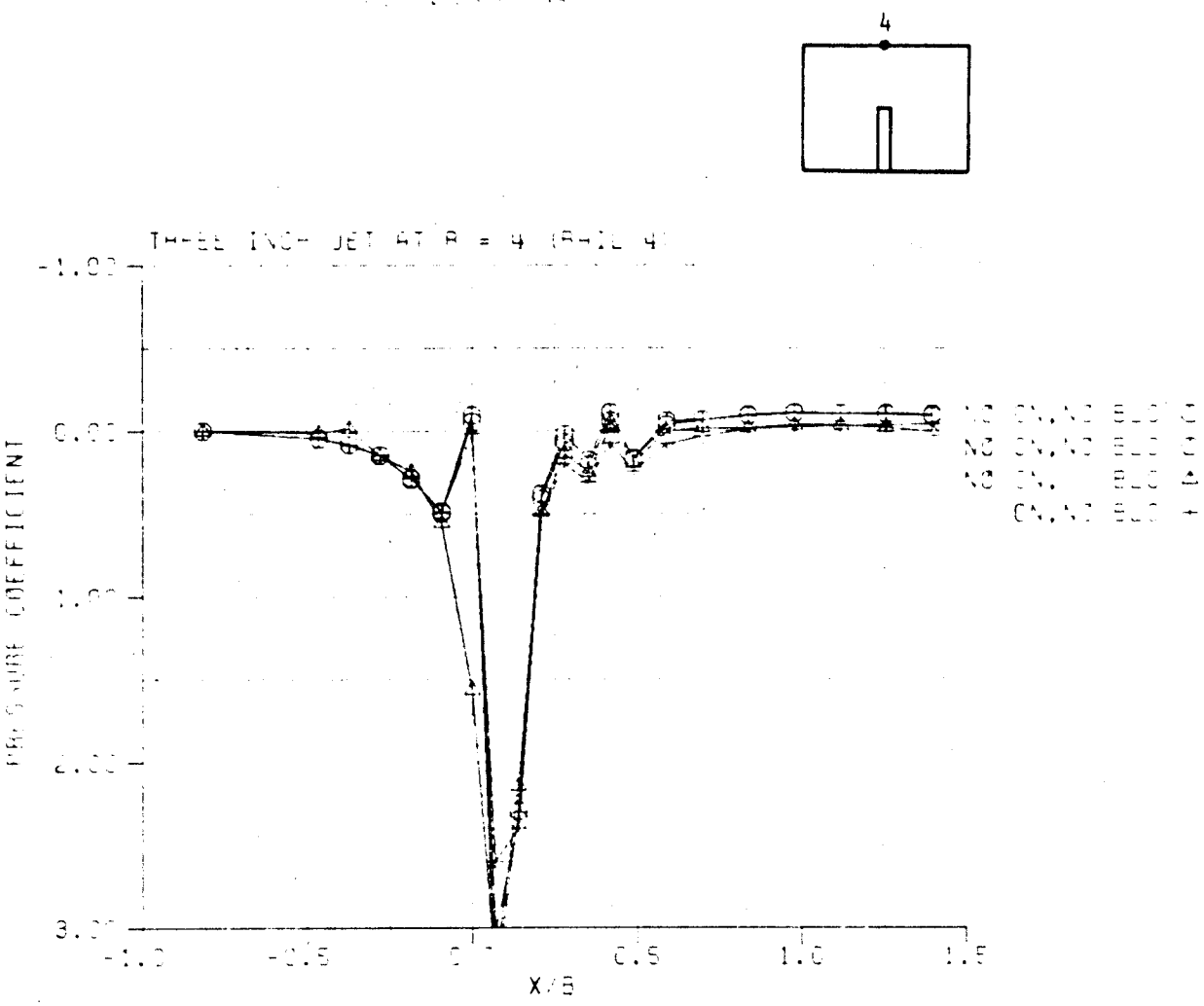

Figure 4.13 Effect of ground BLC and jet profile shape upon ground pressures (R_{NOM} = 4)

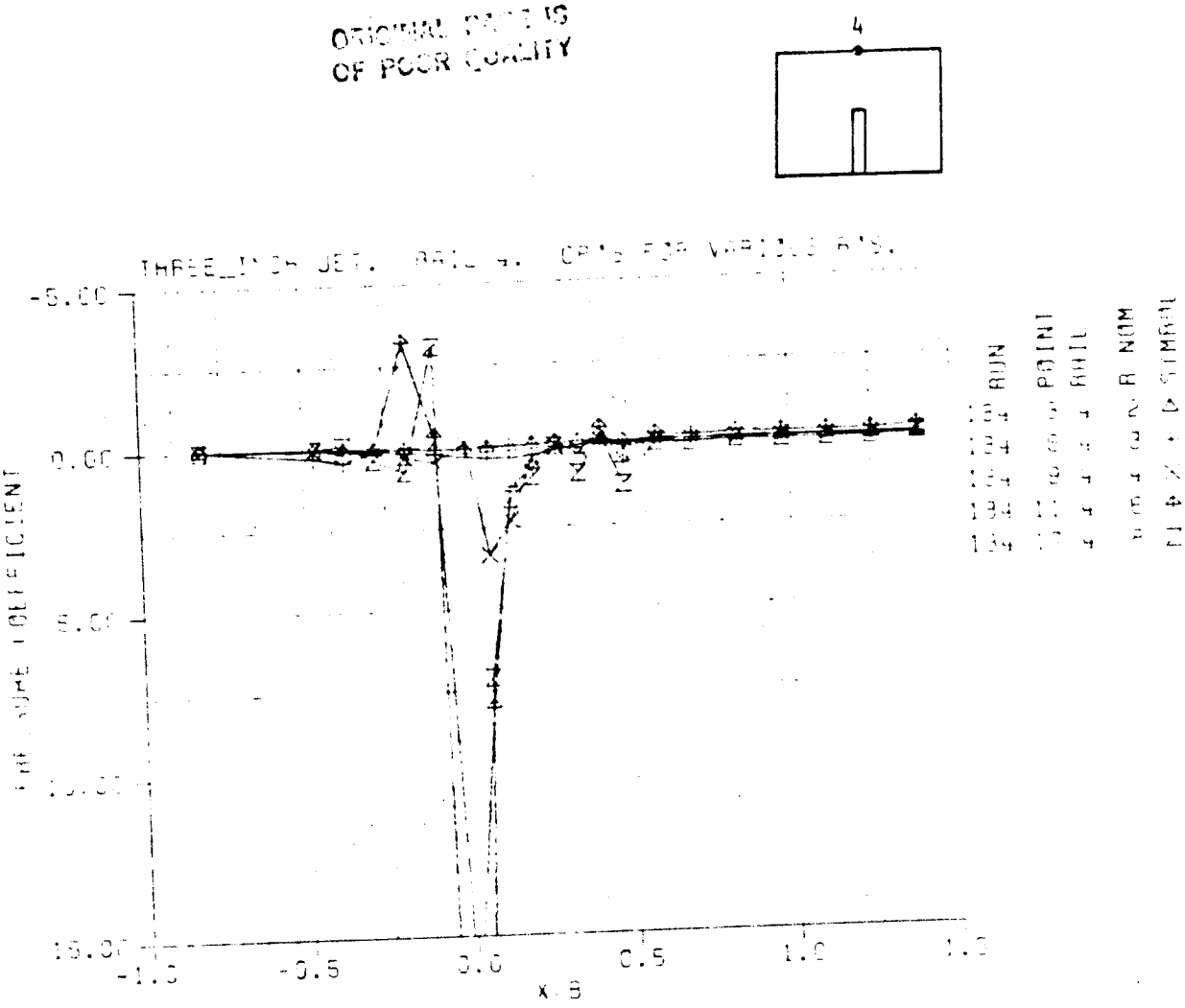

Figure 4.14 Effect of jet velocity ratio upon ground pressures
(No BLC applied)

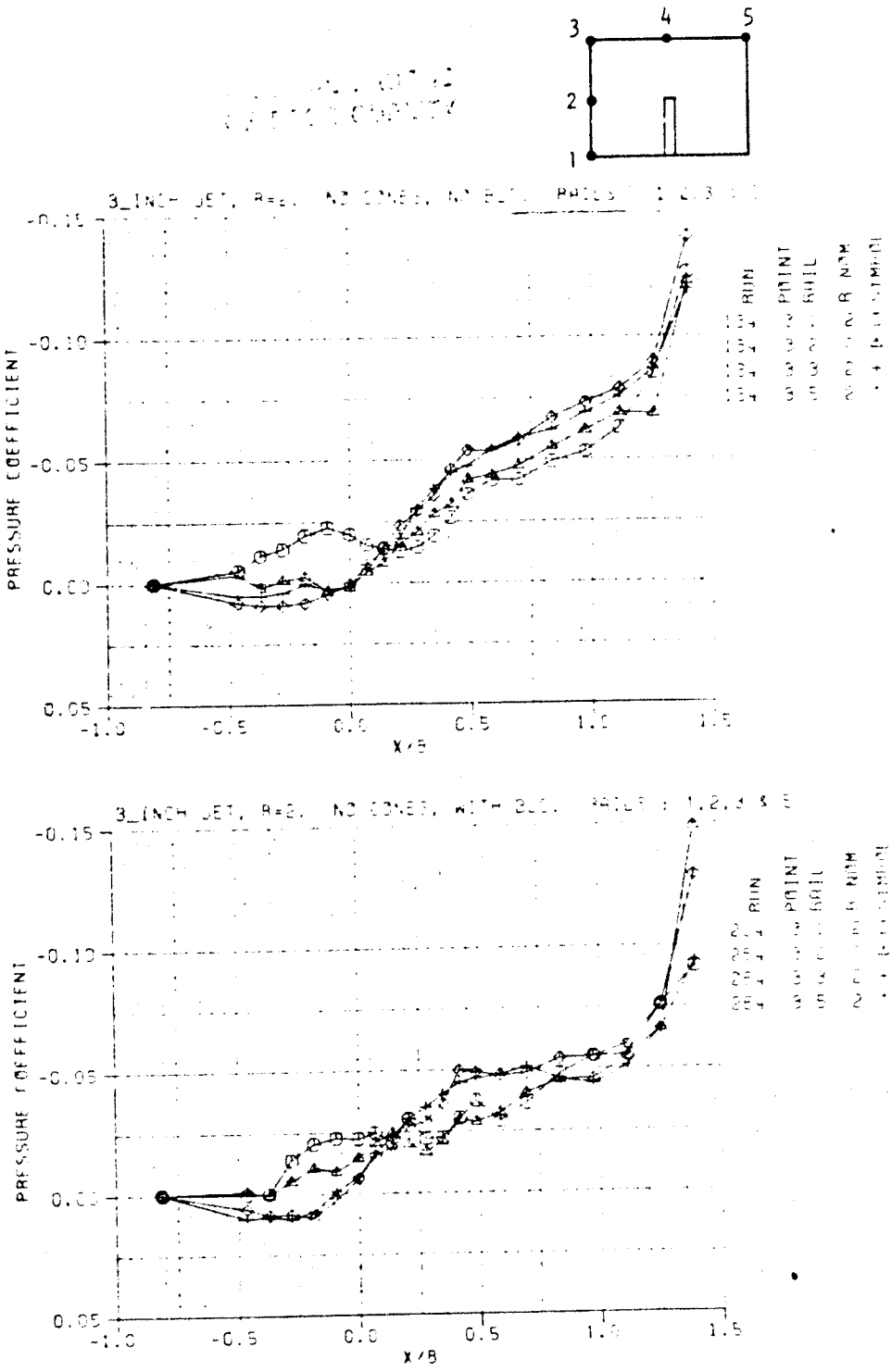

Figure 4.15 Wall pressures for 3-inch jet 'square' profile
(a) $R_{NOM} = 2$

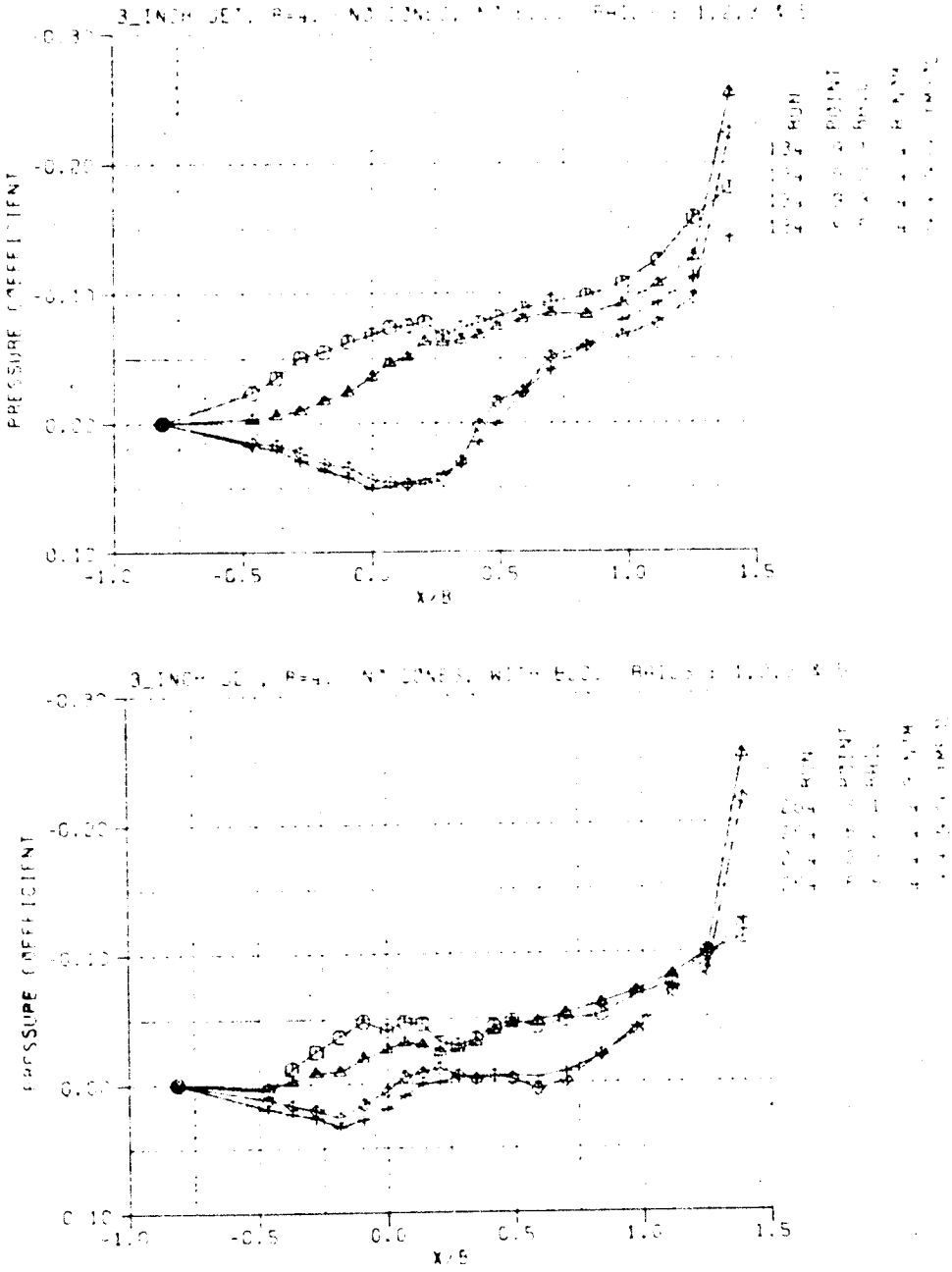

Figure 4.15 (Continued) Wall pressures for 3-inch jet 'square' profile
(b) $R_{NOM} = 4$

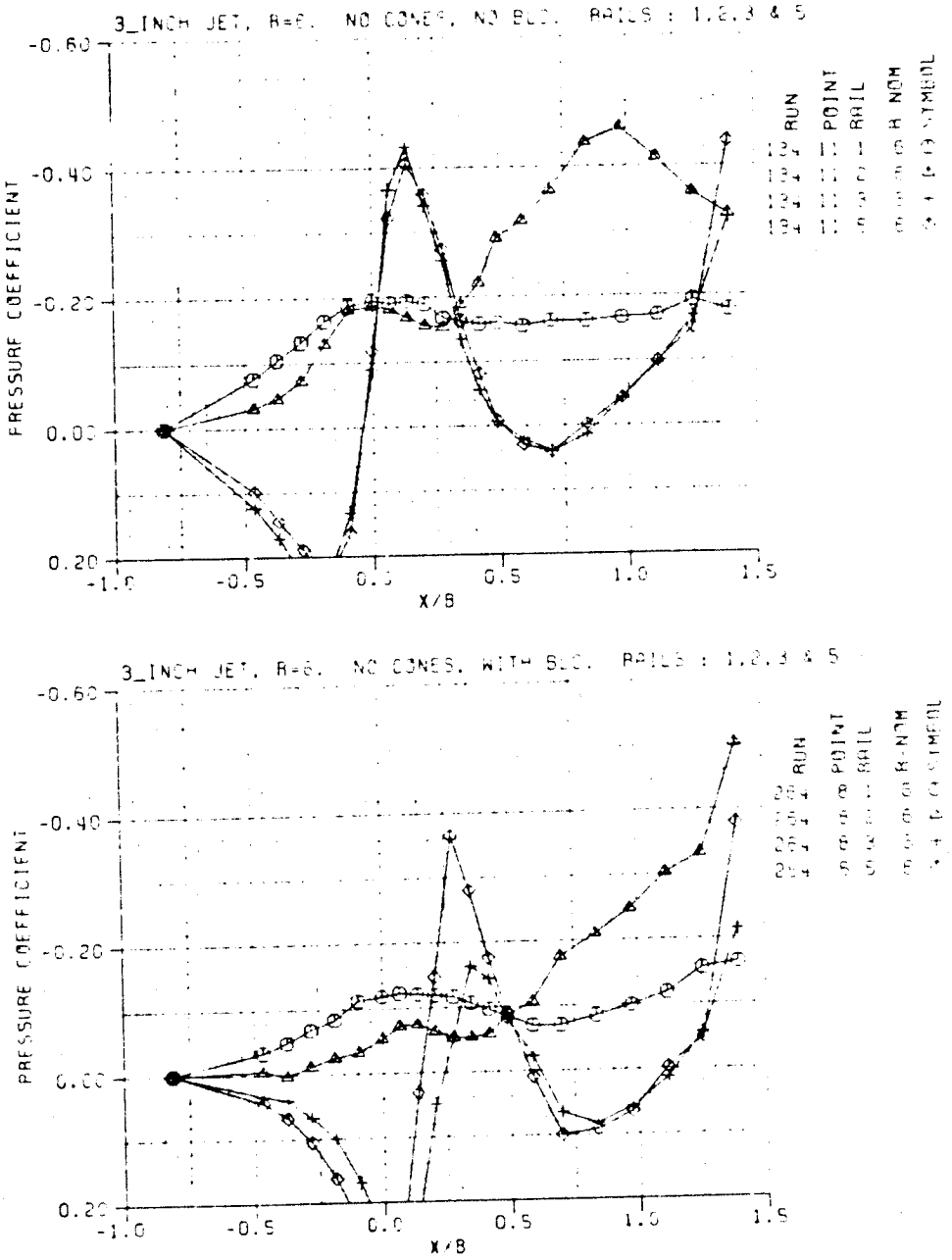

Figure 4.15 (Continued) Wall pressures for 3-inch jet 'square' profile
(c) R = 6

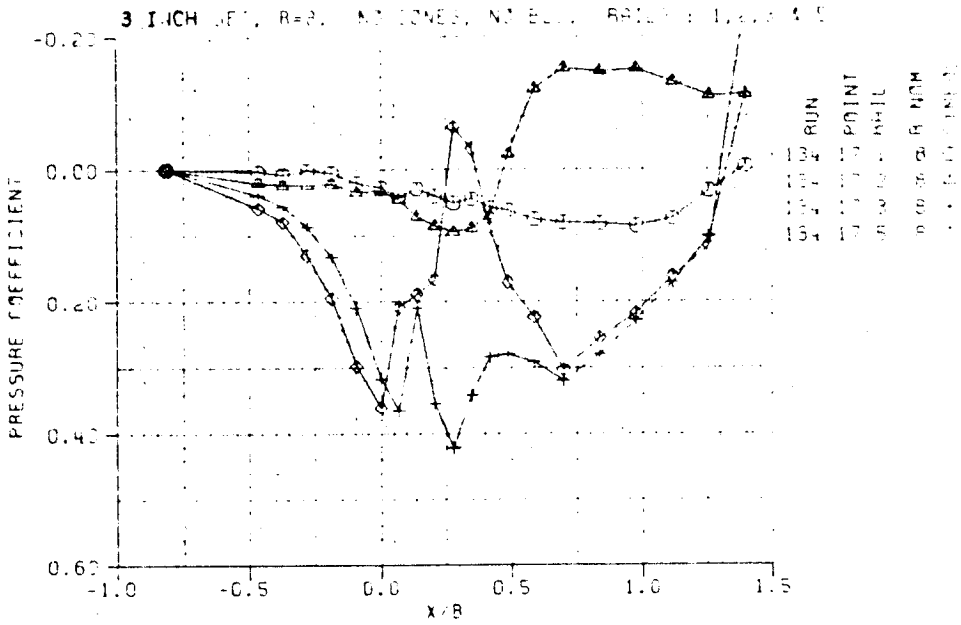

NO DATA AVAILABLE

Figure 4.15 (Concluded) Wall pressures for 3-inch jet 'square' profile
(d) R = 8

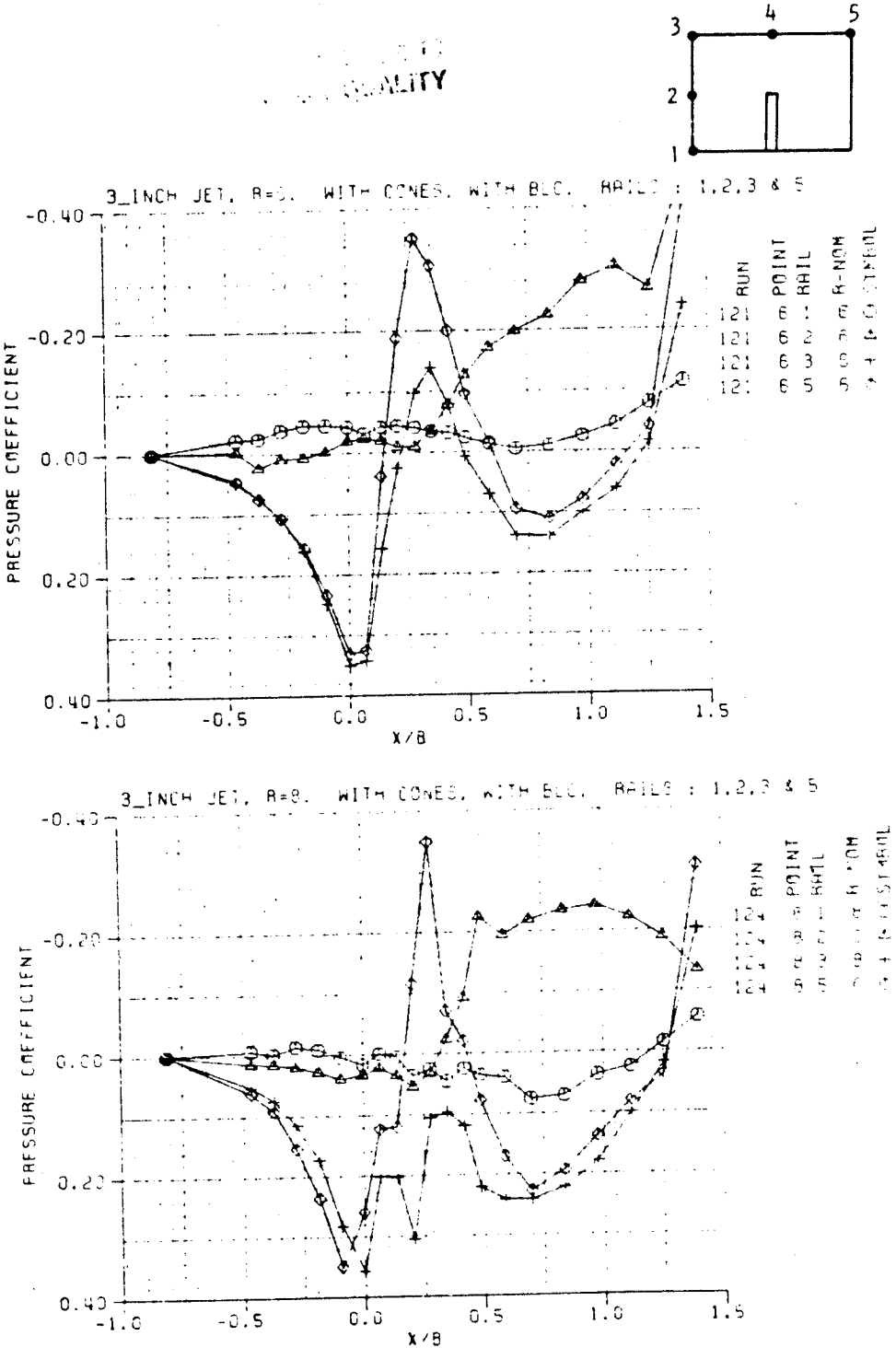

Figure 4.16 Wall pressures for 3-inch jet 'pipe' profile for R = 6 and R = 8, with 'ground' BLC applied

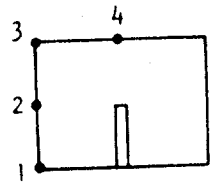

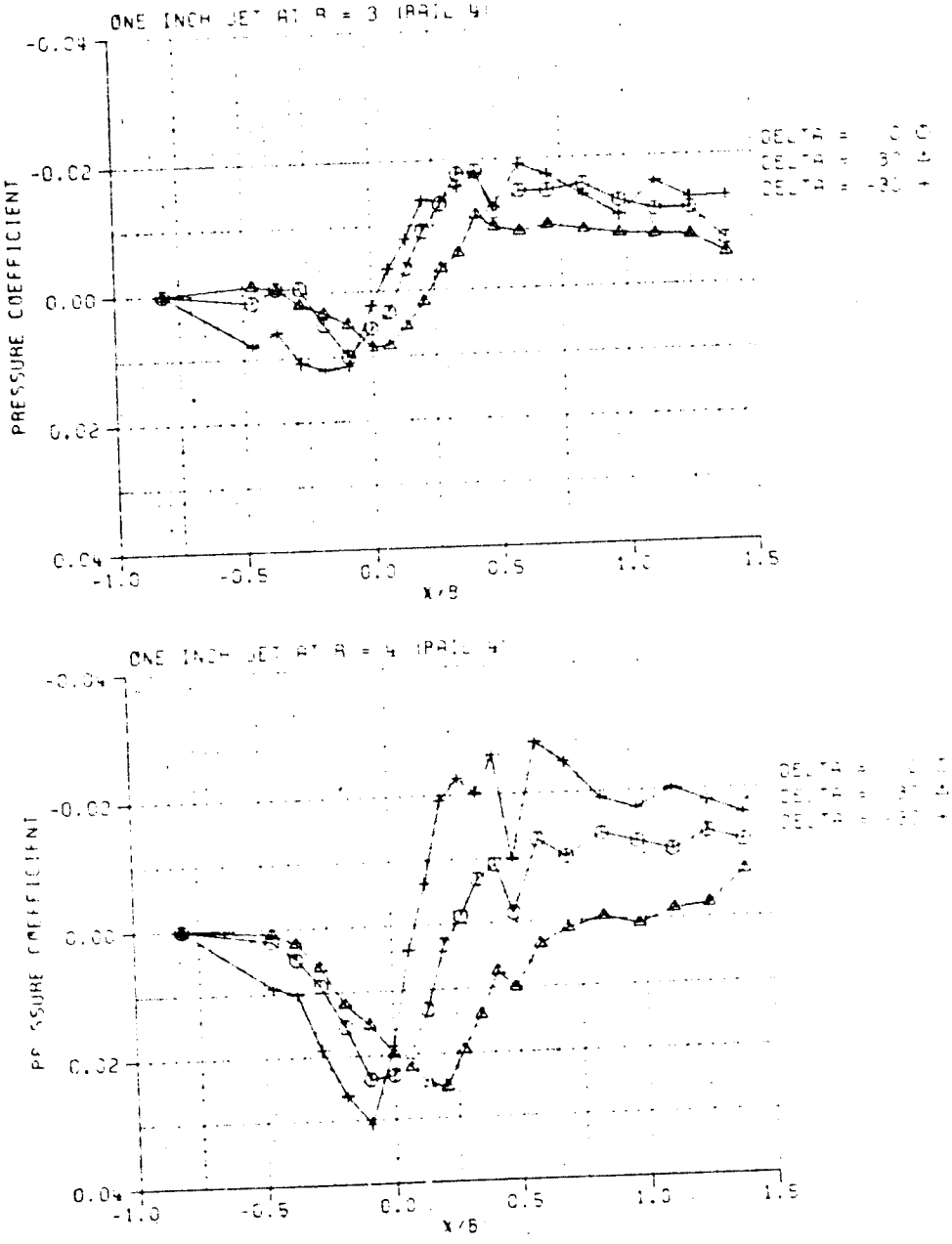

Figure 4.17 'Ground' pressures for vertical and inclined 1-inch jets
(a) $R_{NOM} = 3$ and $R_{NOM} = 4$

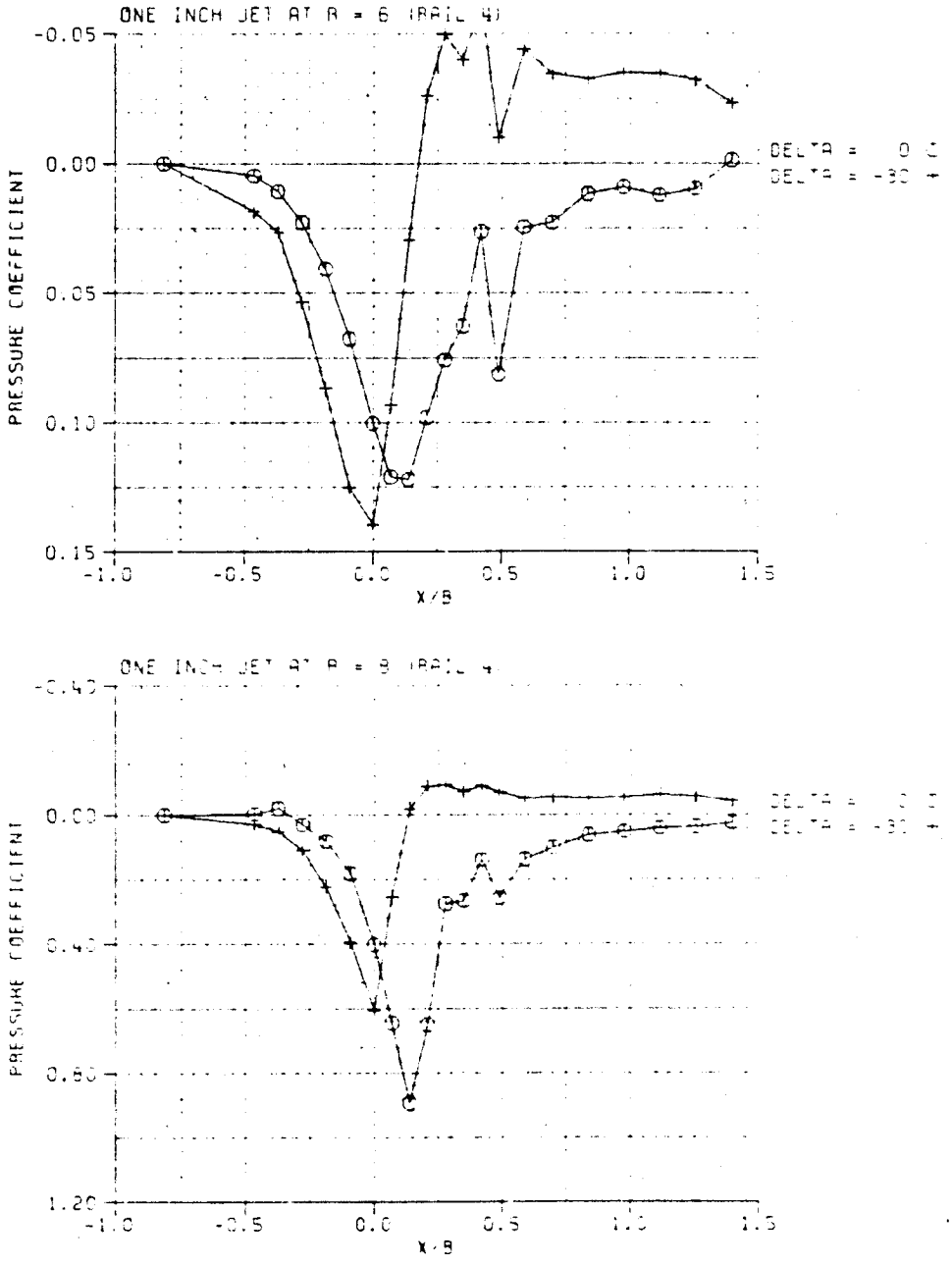

Figure 4.17 (Concluded) 'Ground' pressures for vertical and inclined 1-inch jets. (b) $R_{NOM} = 6$ and $R_{NOM} = 8$

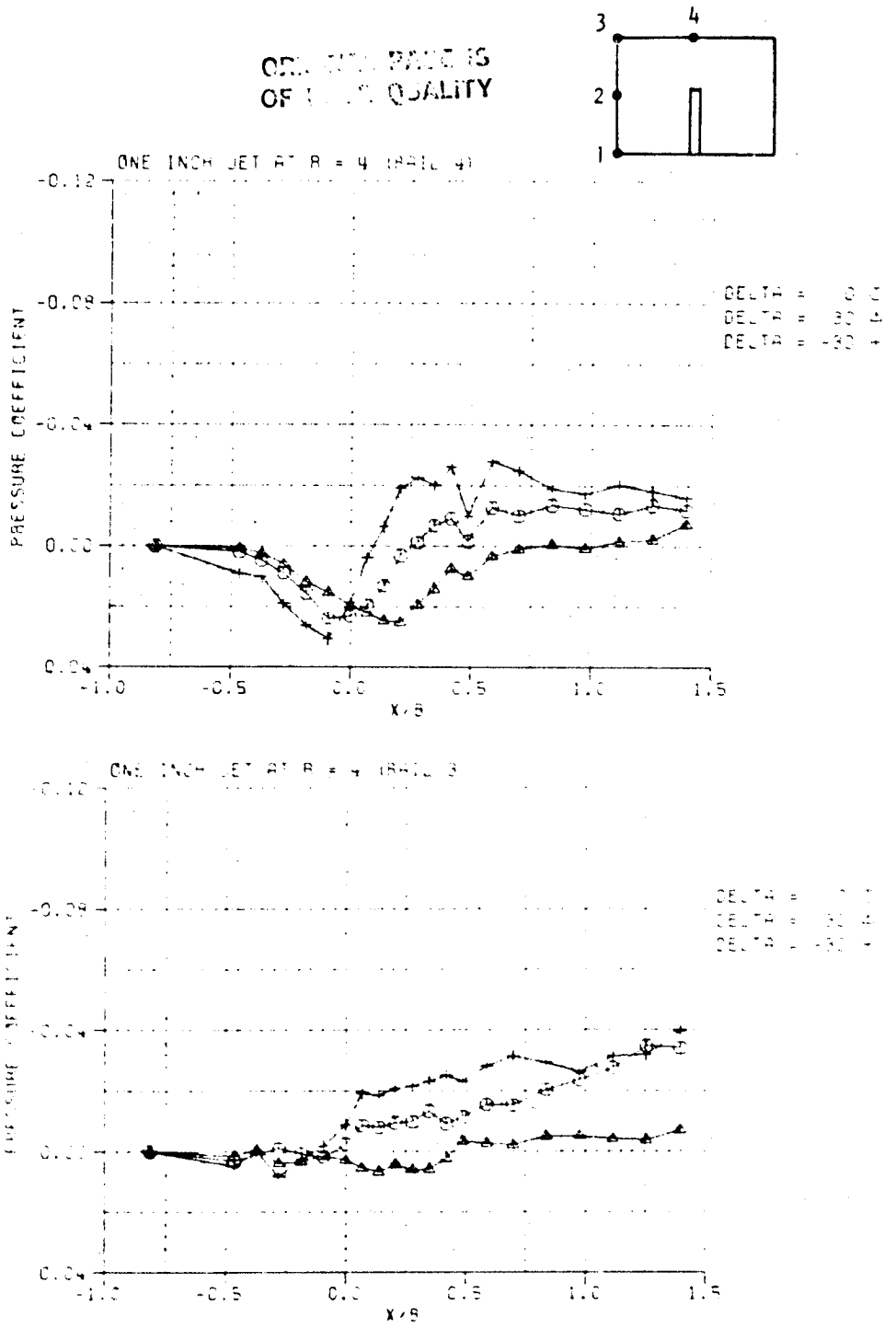

Figure 4.18 Wall pressures for vertical and inclined jets at $R_{NOM} = 4$
(a) Rails 4 and 3

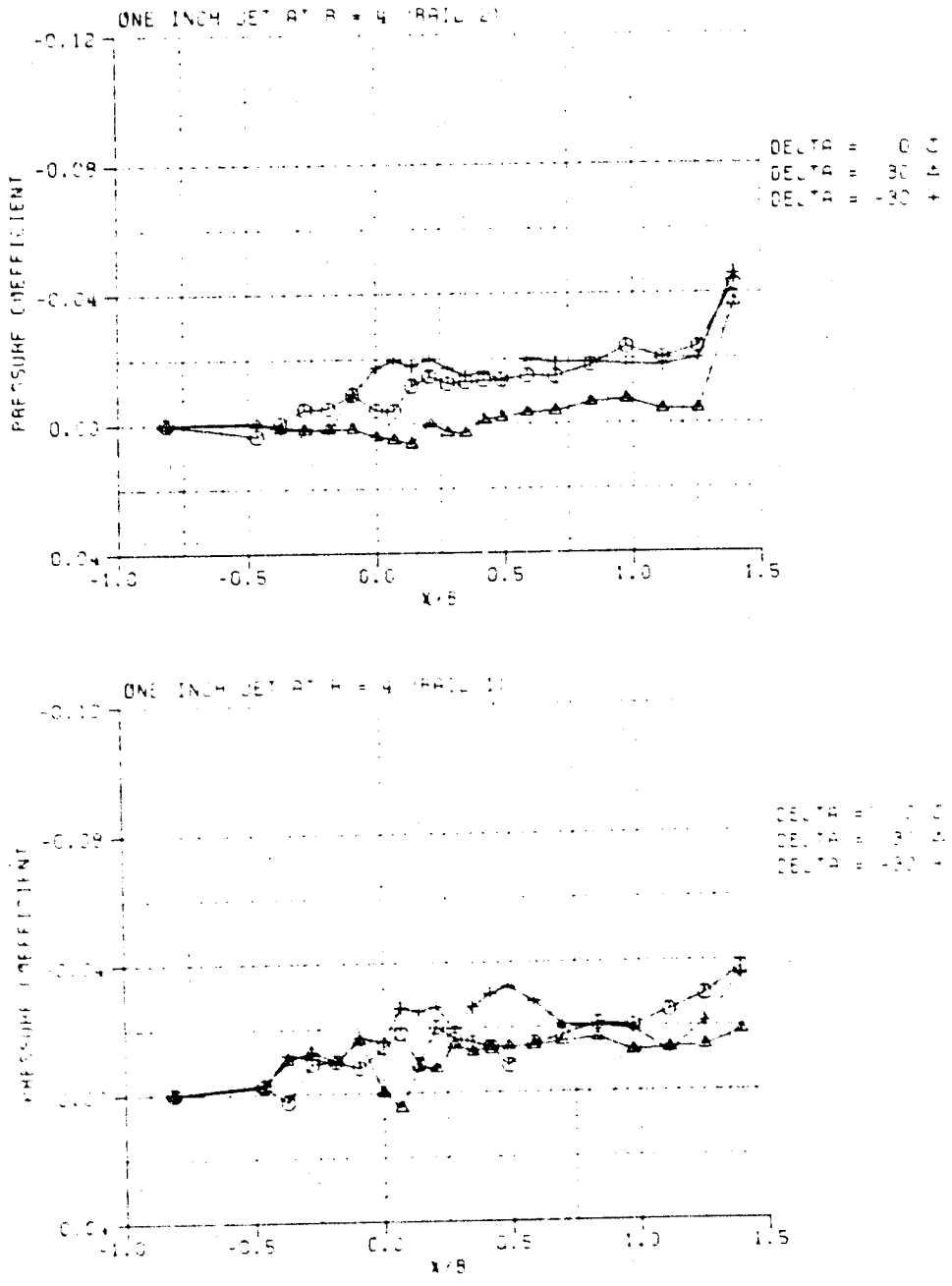

Figure 4.18 (Concluded) Wall pressures for vertical and inclined jets at R = 4
(b) Rails 2 and 1

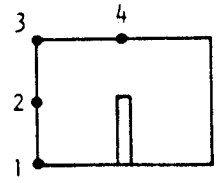

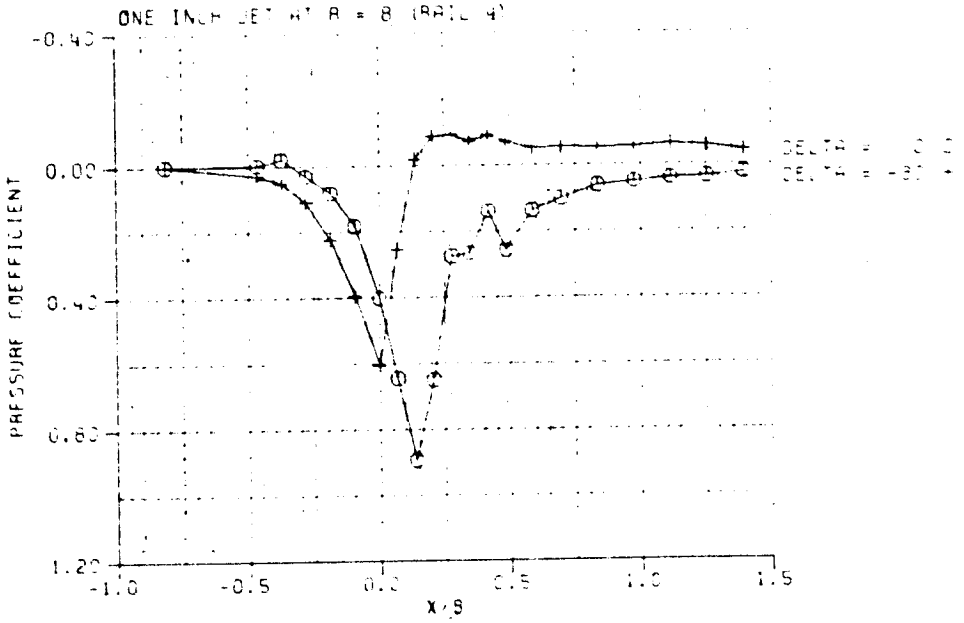

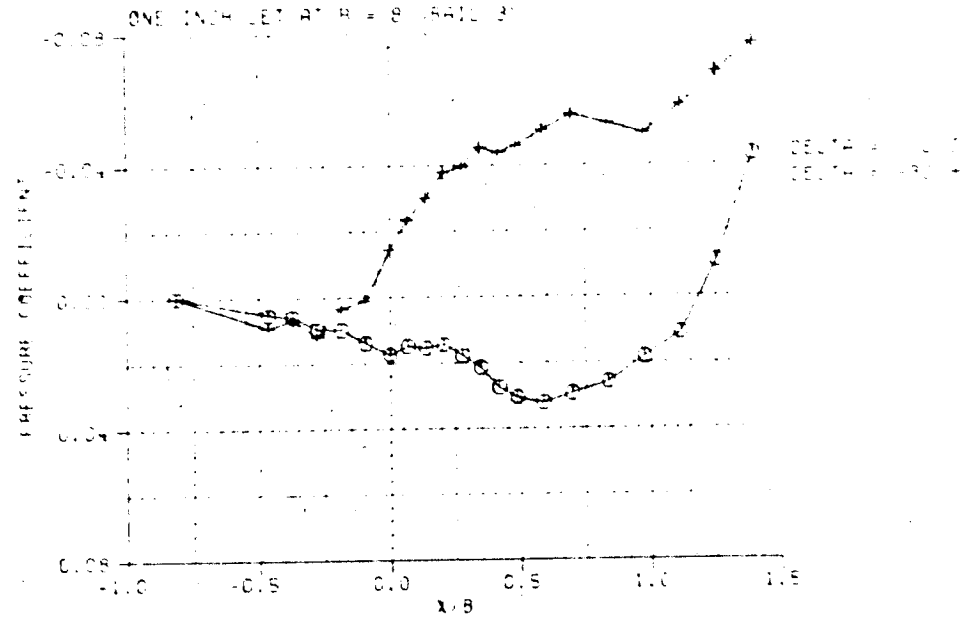

Figure 4.19 Wall pressures for vertical and inclined jets at R = 8
(a) Rails 4 and 3

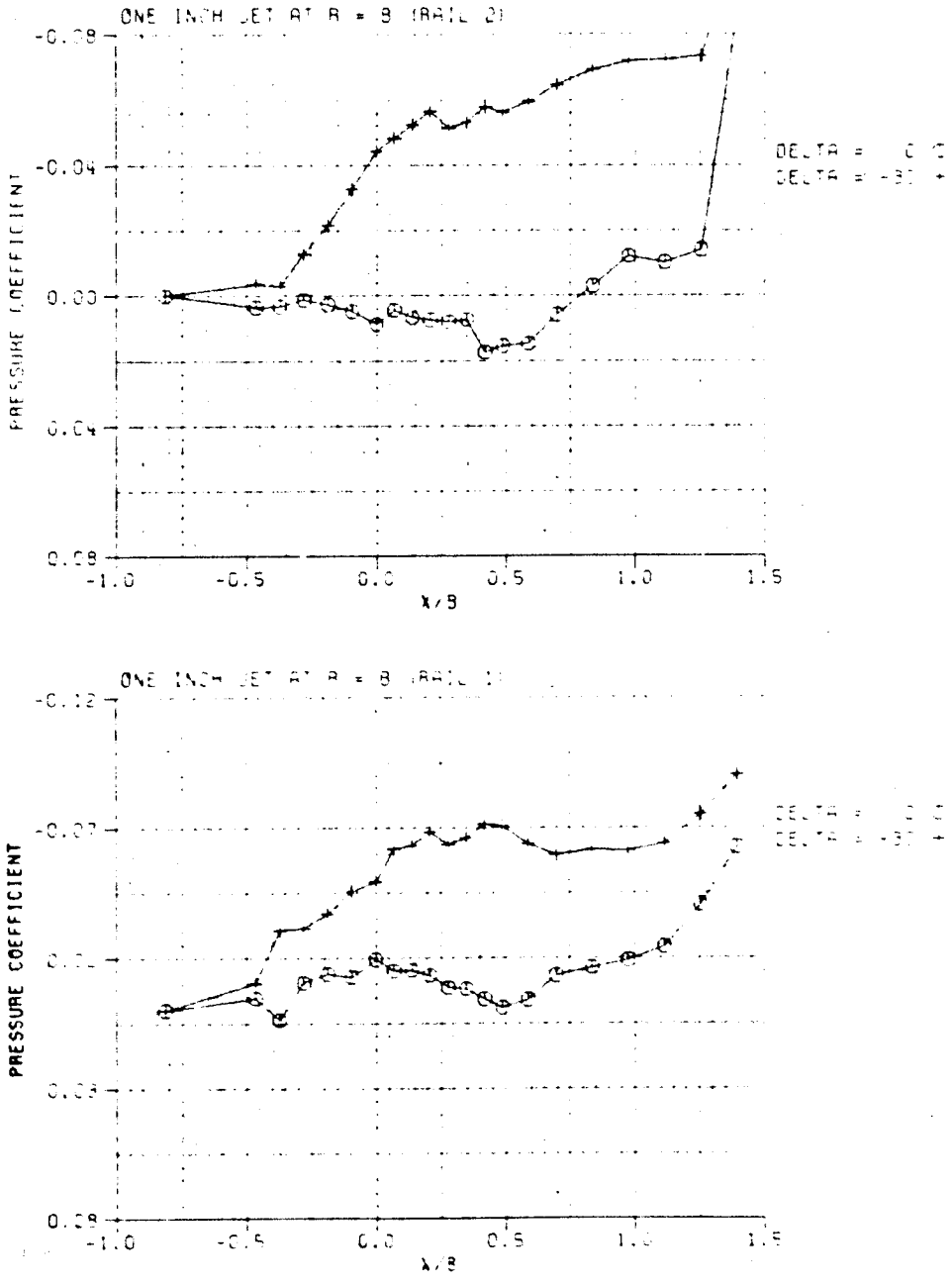

Figure 4.19 (Concluded) Wall pressures for vertical & inclined jets at R = 8
(b) Rails 2 and 1

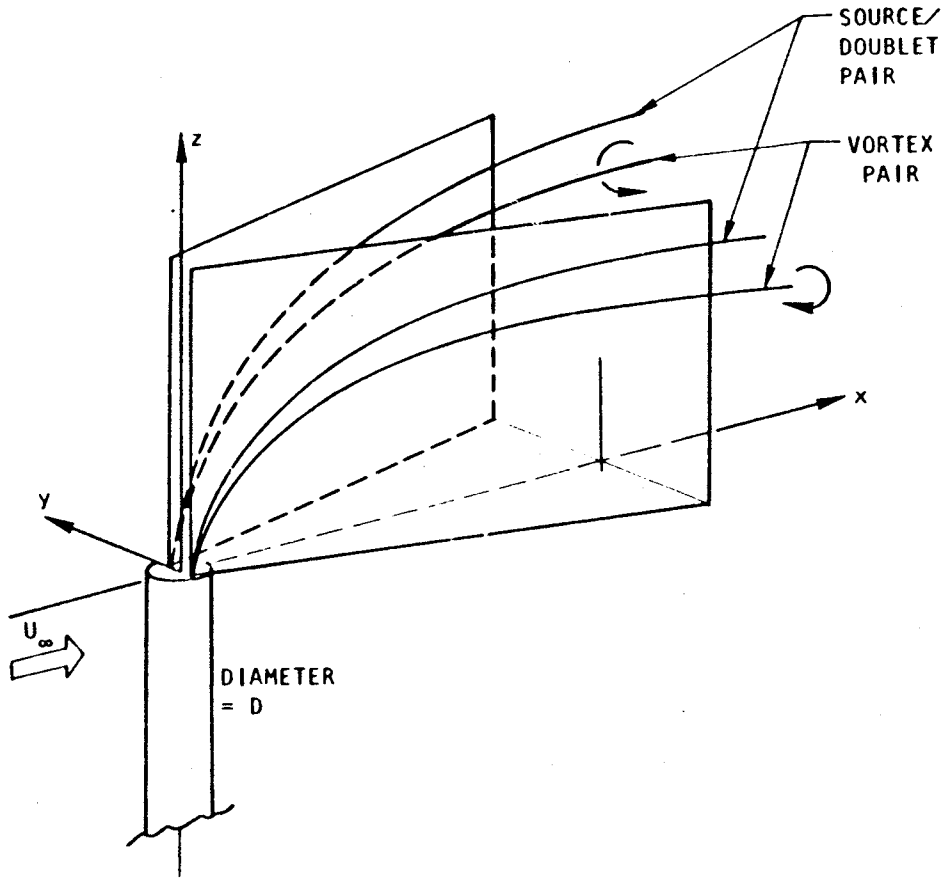

Figure 5.1 Flow model geometry
(a) General layout

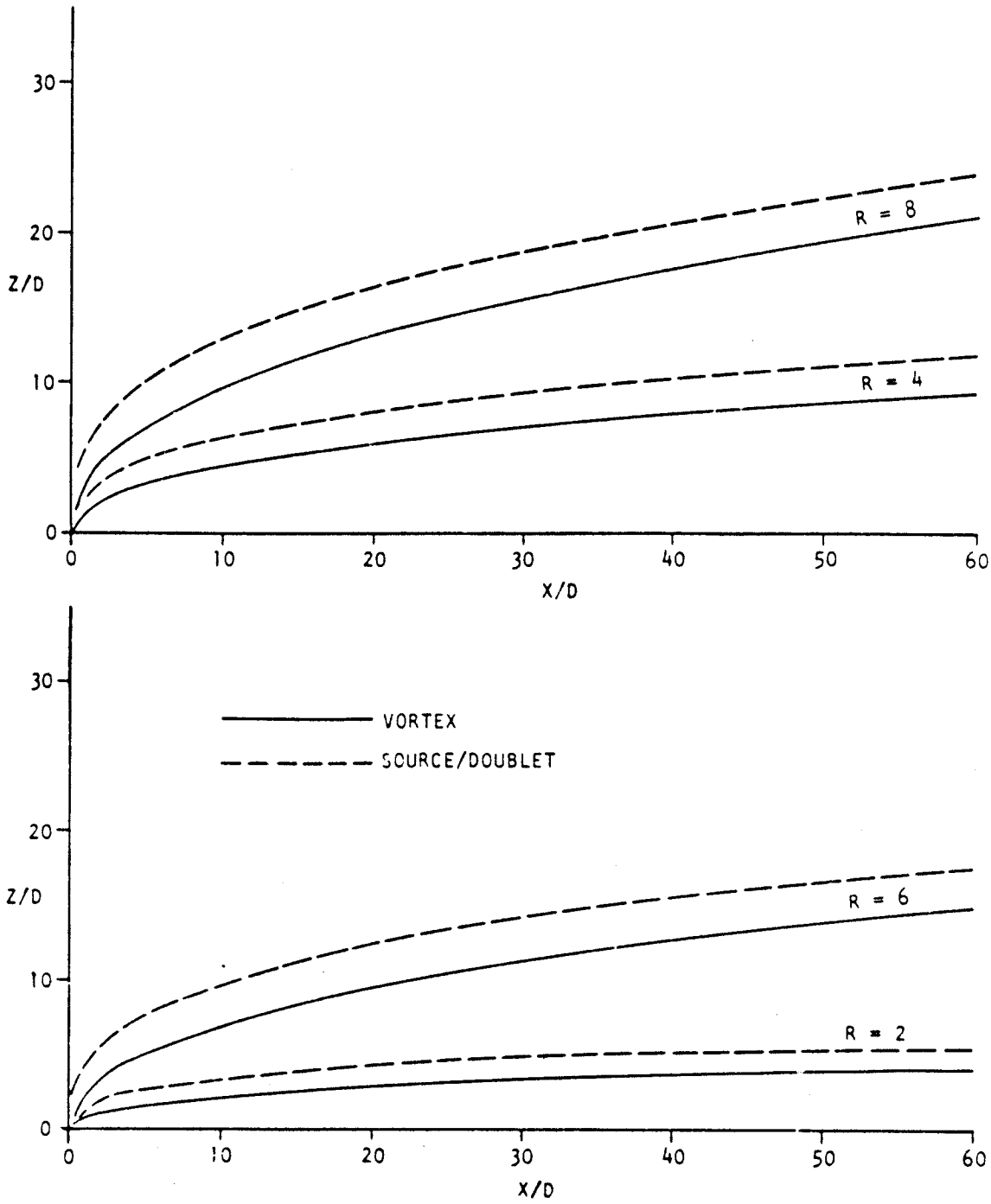

Figure 5.1 (Continued) Flow model geometry
(b) Trajectory shapes

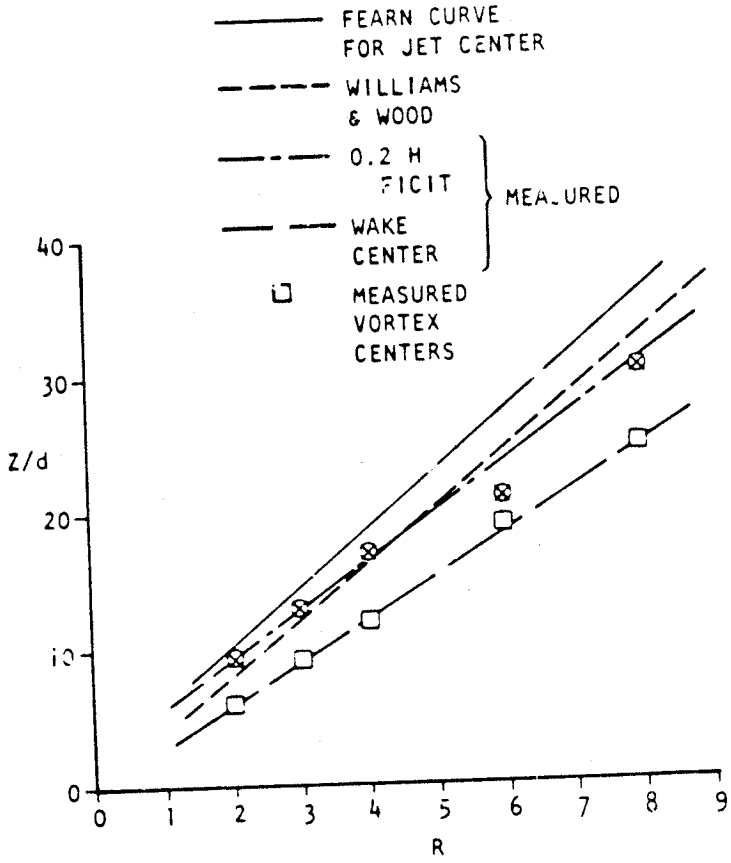

Figure 5.1 (Concluded) Flow model geometry
(c) Selection of trajectories

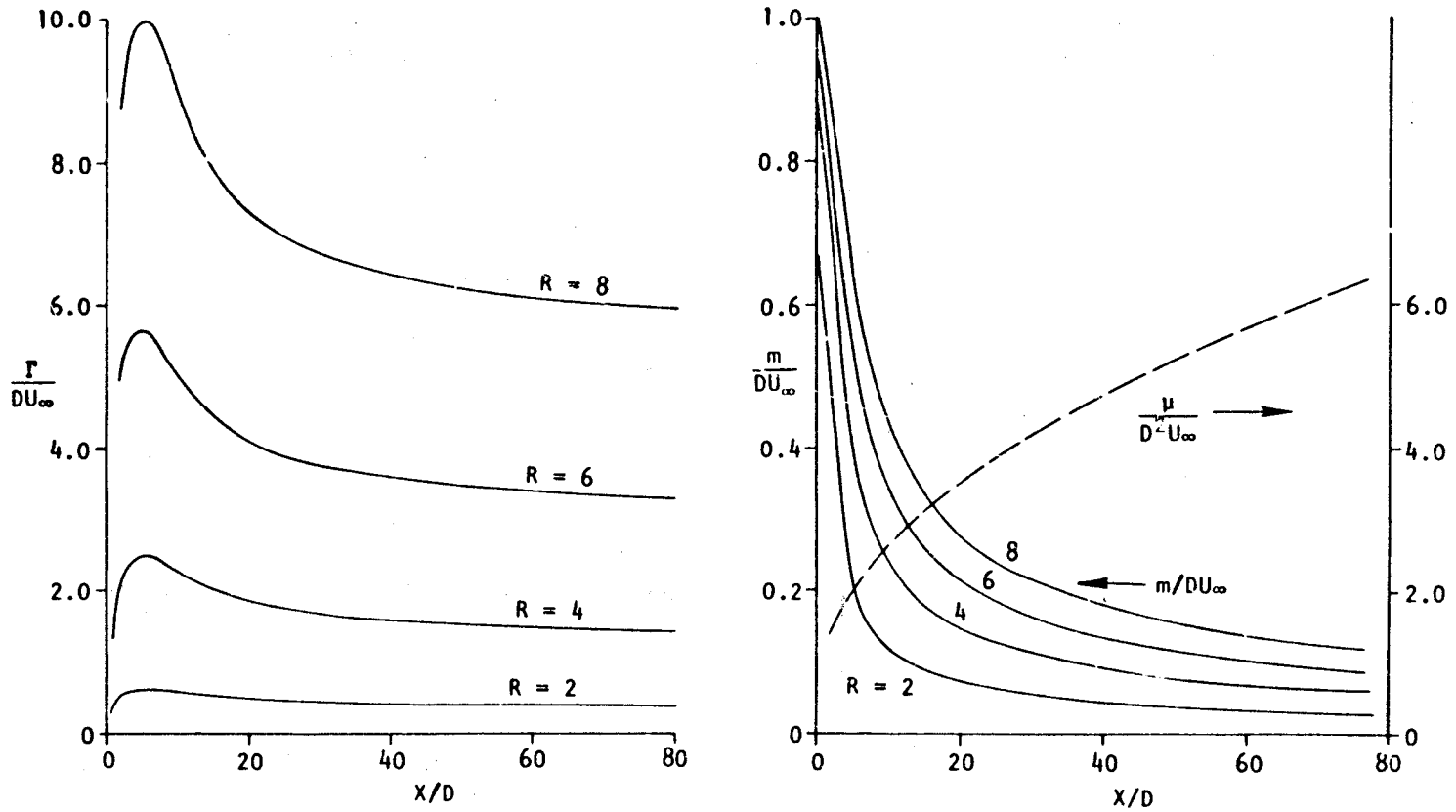

Figure 5.2 Singularity distributions for the 'VSD' flow model

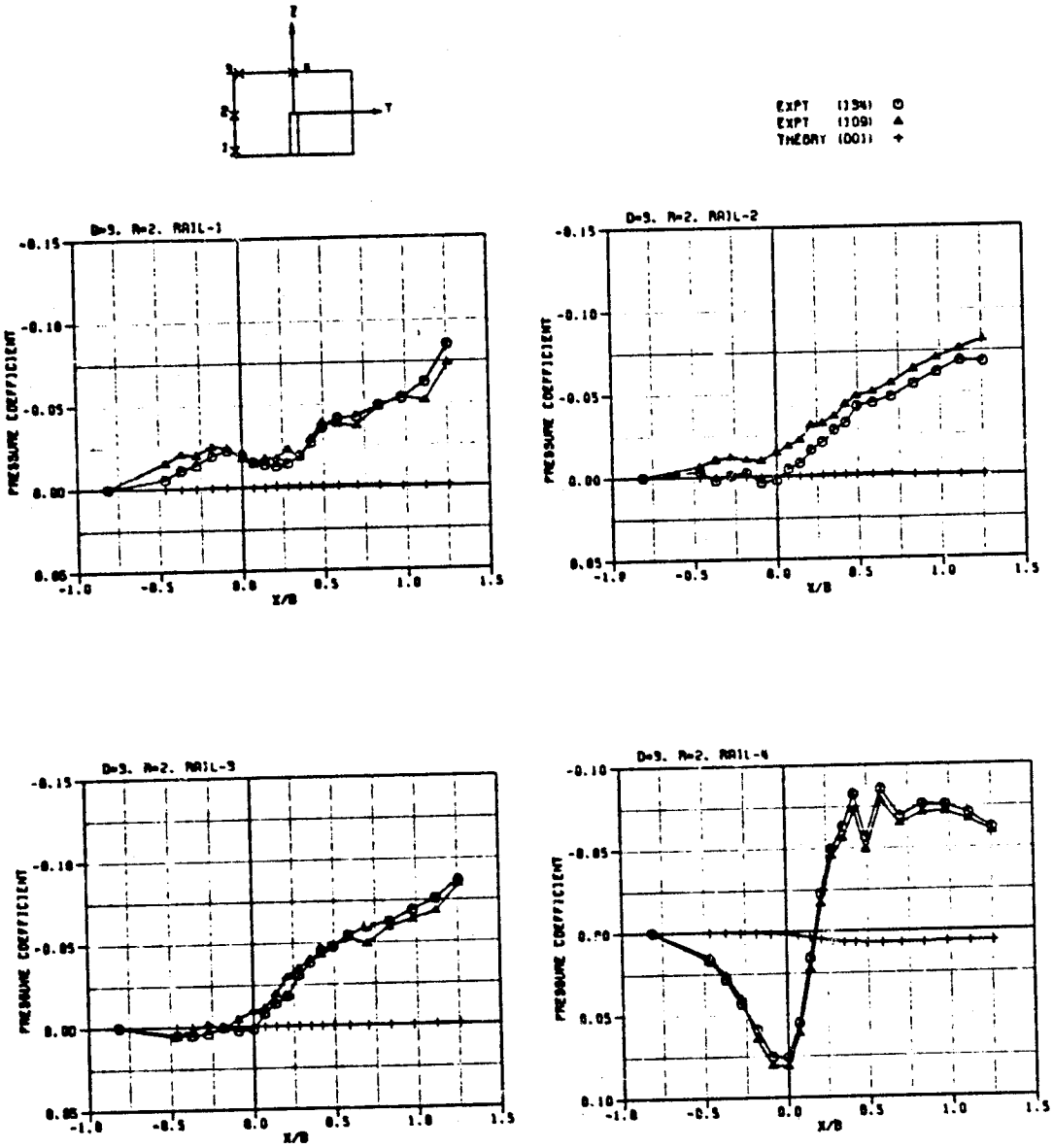

Figure 5.3 Wall pressures for two available flow models: D = 3", R = 2.
(a) The "Fearn" , vortex model.

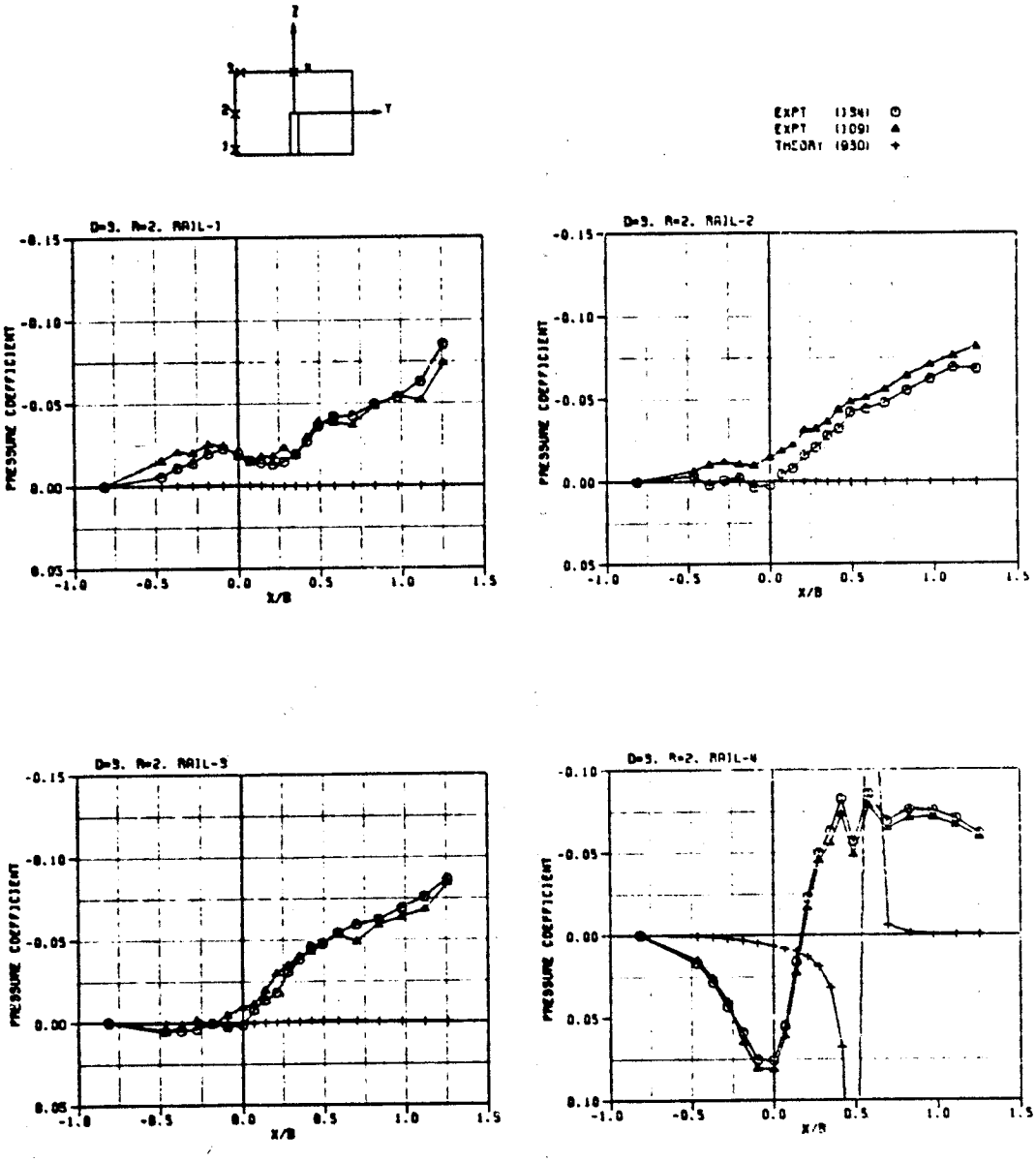

Figure 5.3 (Concluded) Wall pressures for two available flow models:
D = 3", R = 2.
(b) The "Heyson", lifting-doublet model.

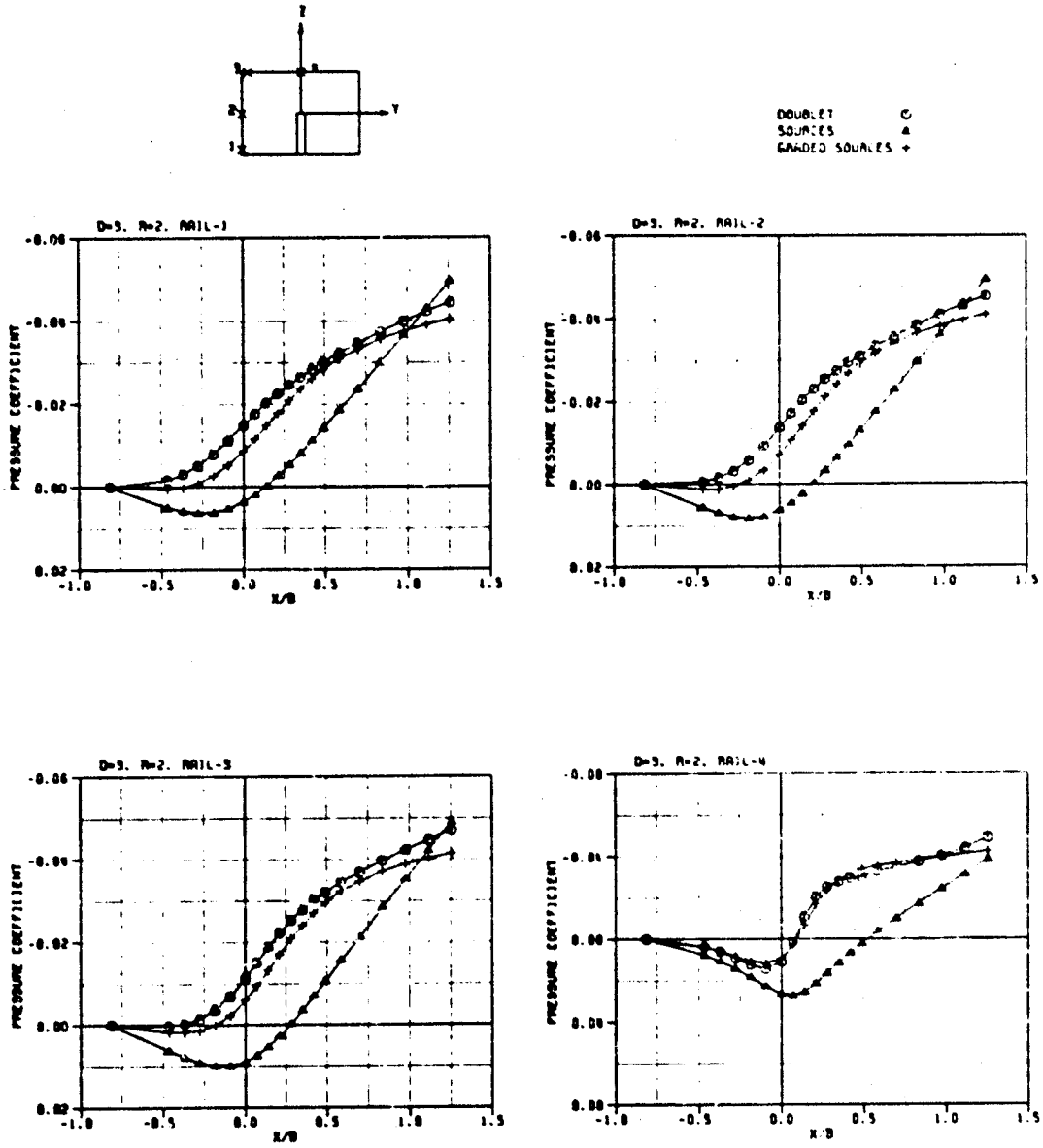

Figure 5.4 Individual effects of line sources and line doublets: D = 3", R = 2.

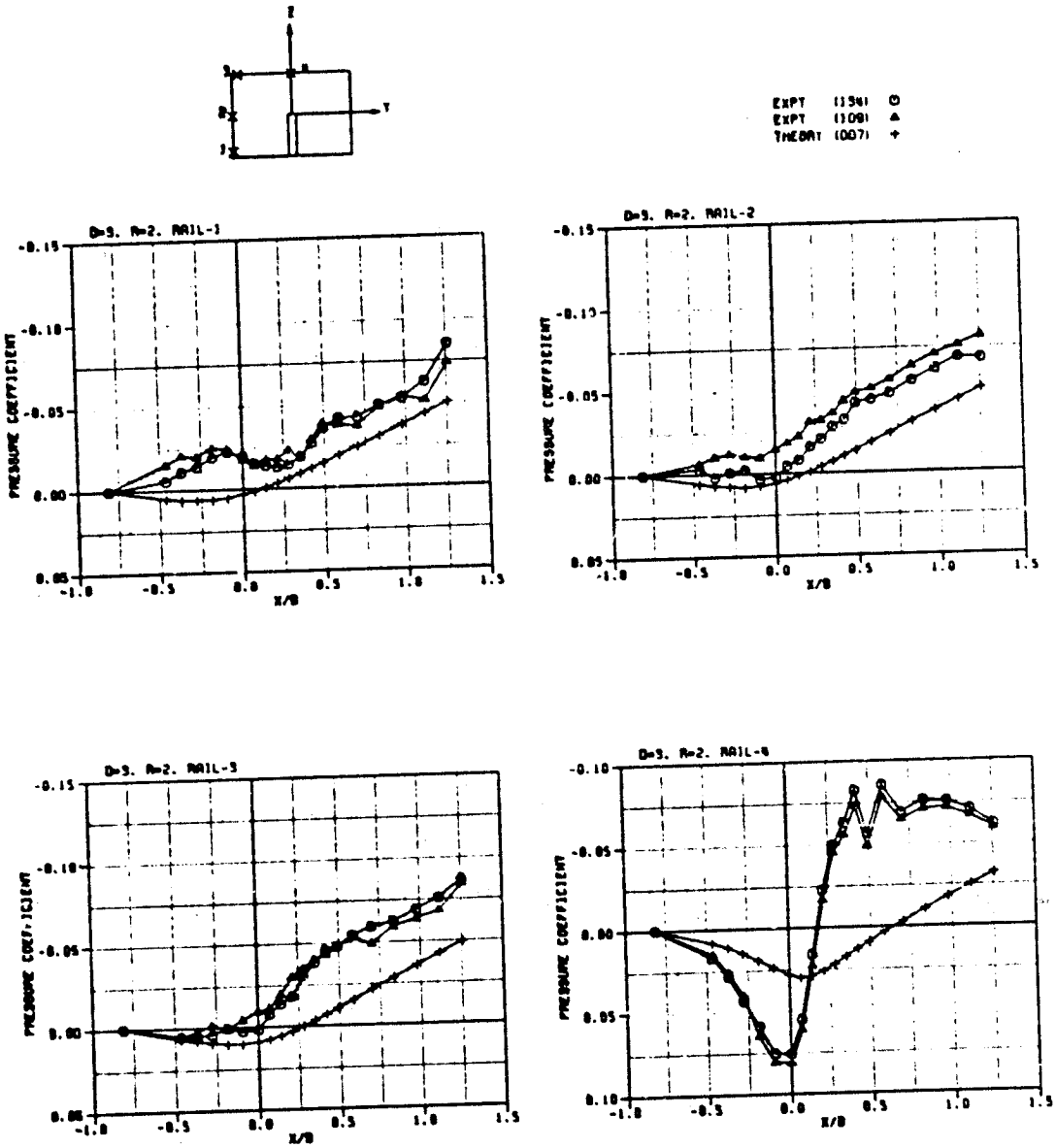

Figure 5.5 Wall pressure correlations for the Vortex/Line-Source model: D = 3", R = 2.

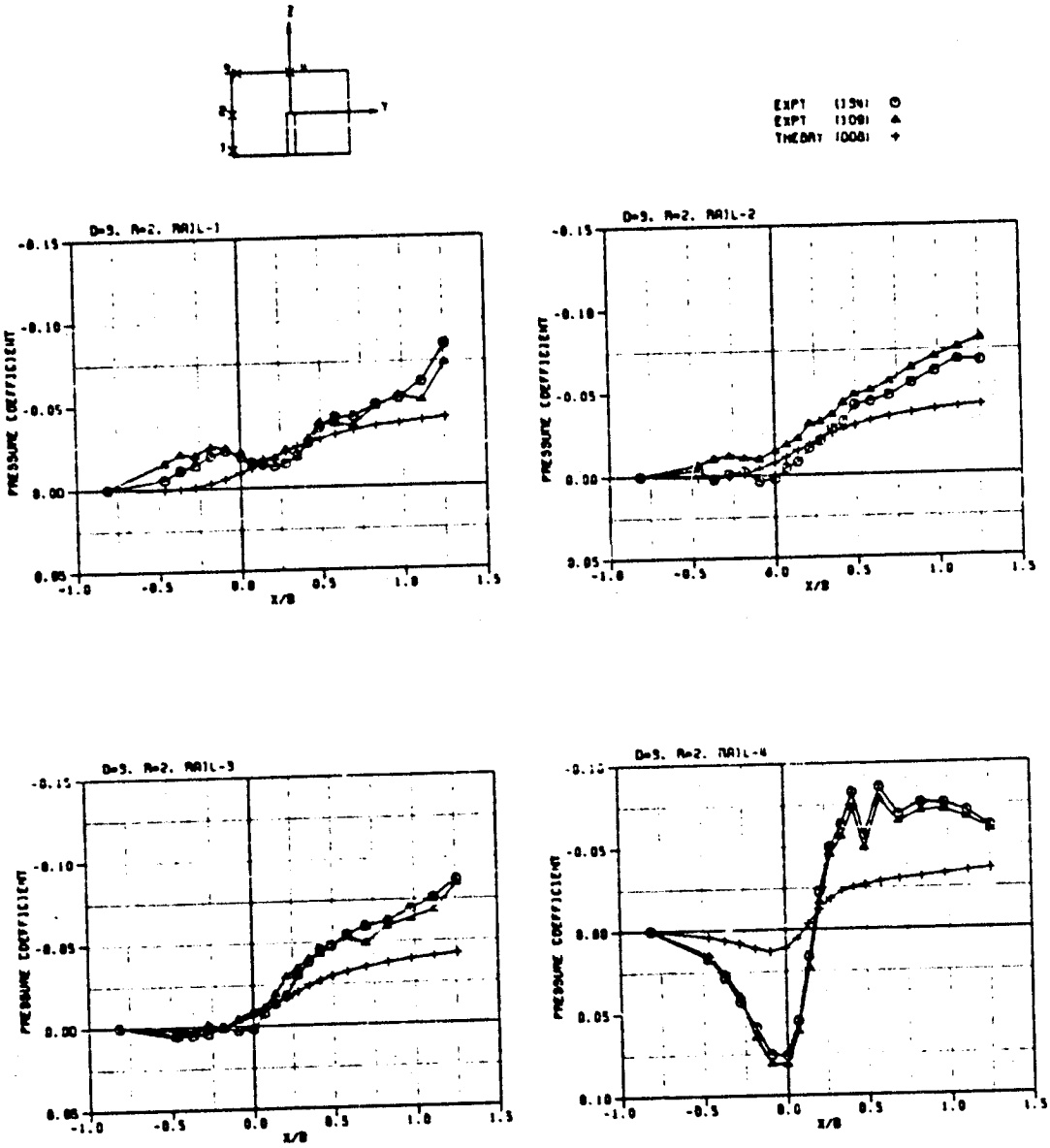

Figure 5.6 Wall pressure correlations for the Vortex/Graded-Source model: D = 3", R = 2.

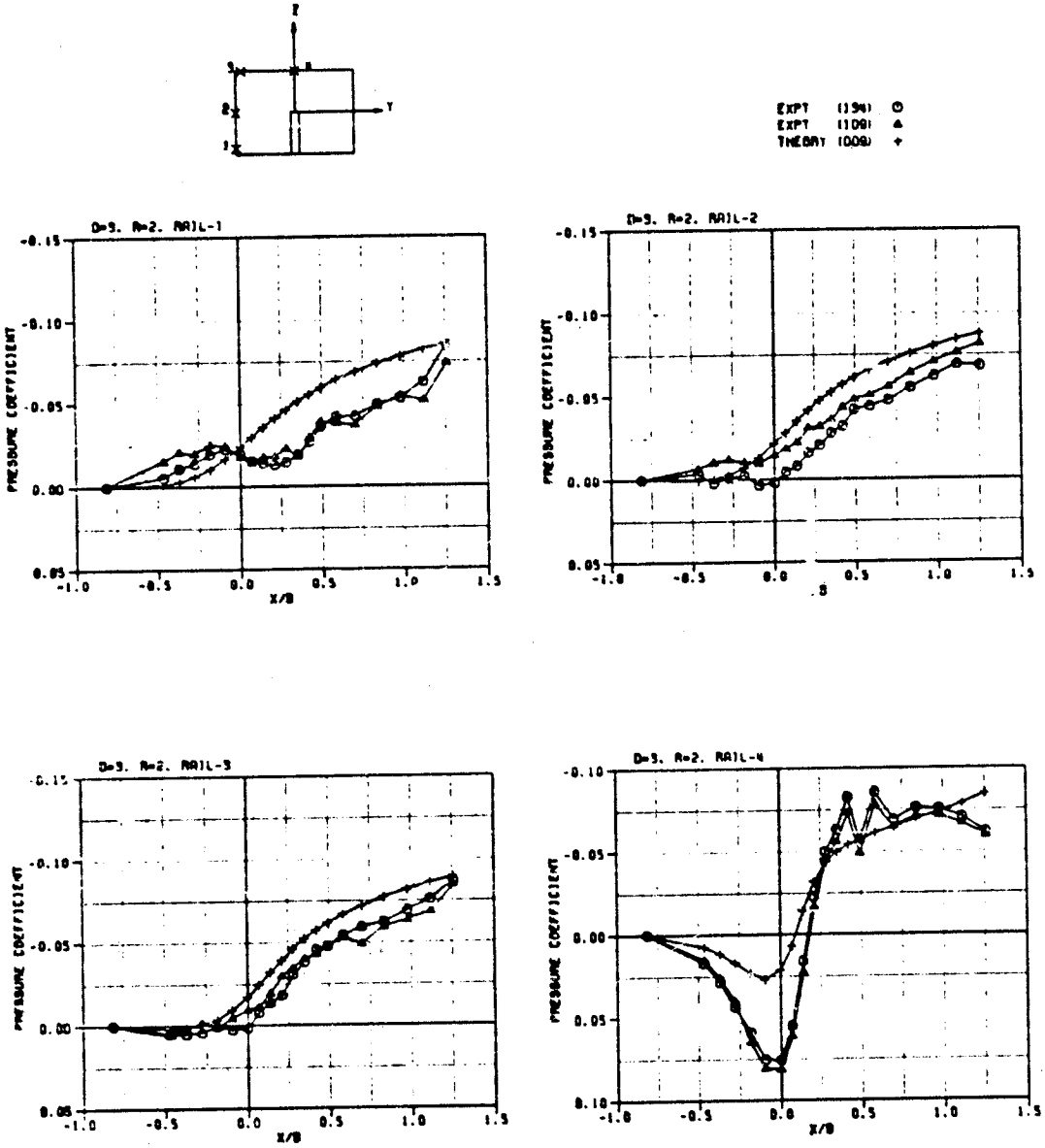

Figure 5.7 Wall pressure correlations for the Vortex/Graded-Source/Doublet model: D = 3", R = 2.

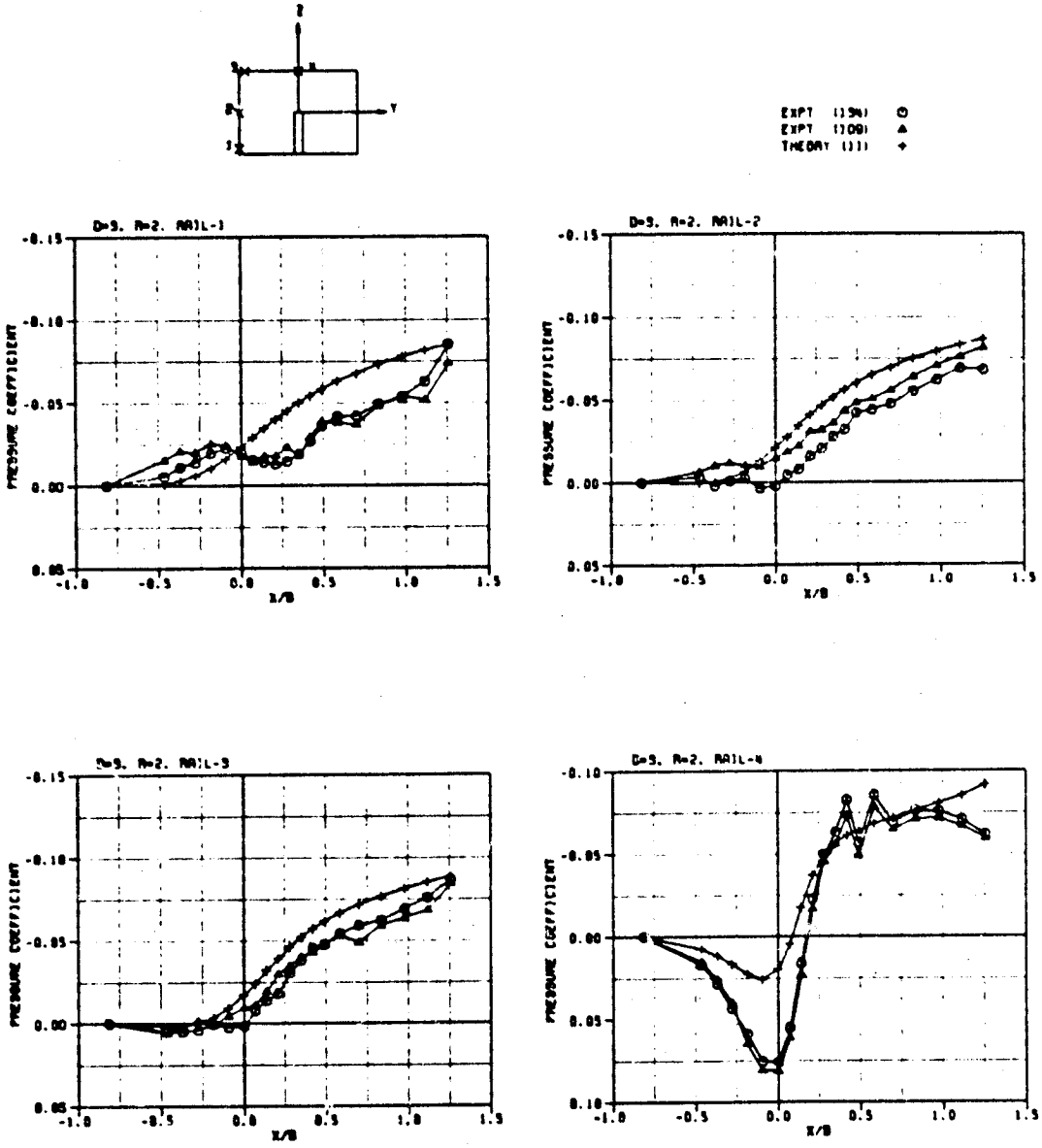

Figure 5.8 Wall pressure correlations for the Graded Source/Doublet model: D = 3", R = 2.

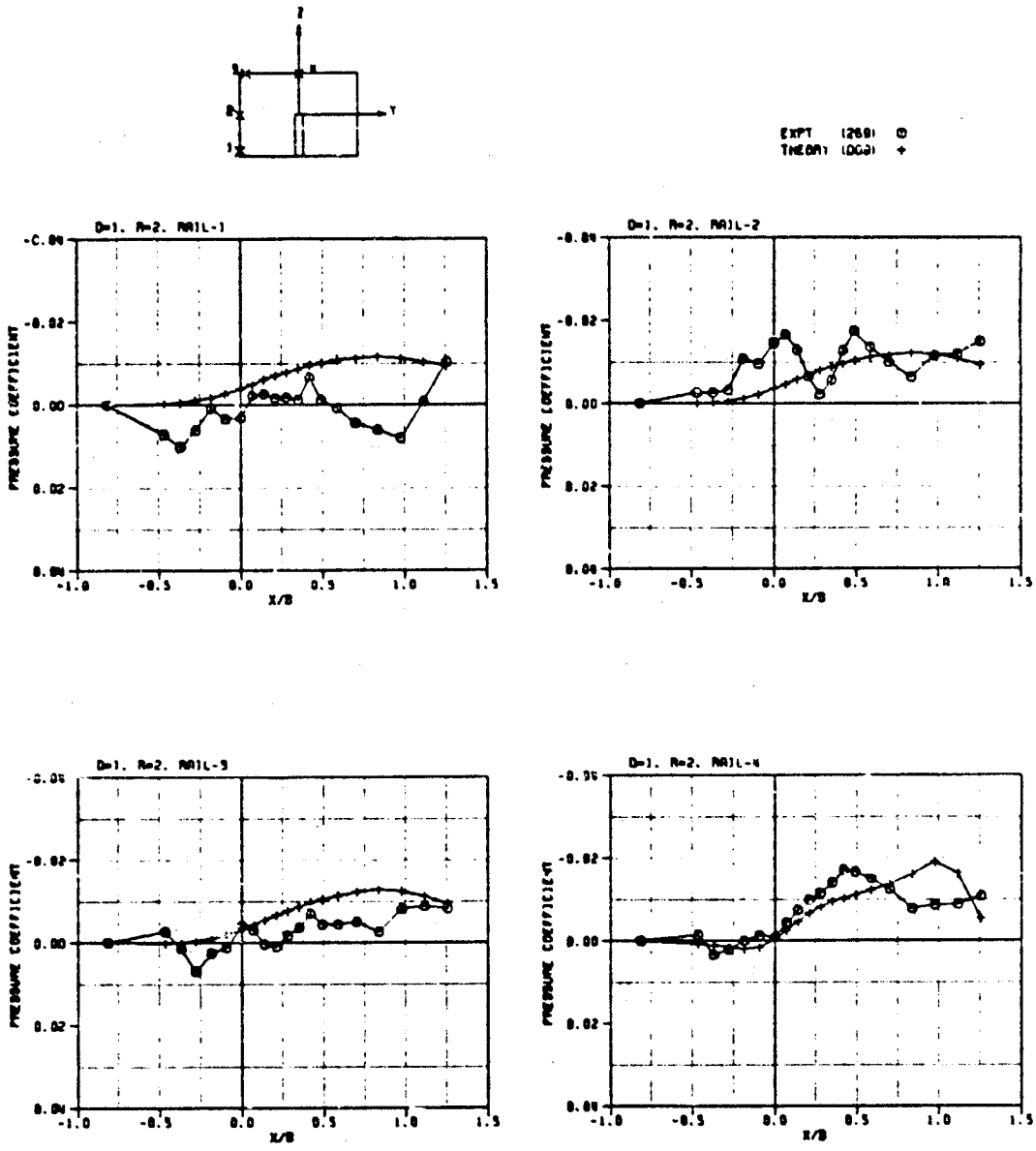

Figure 5.9 Wall pressure correlations for other, non-impinging cases: (a) D = 1", R = 2.

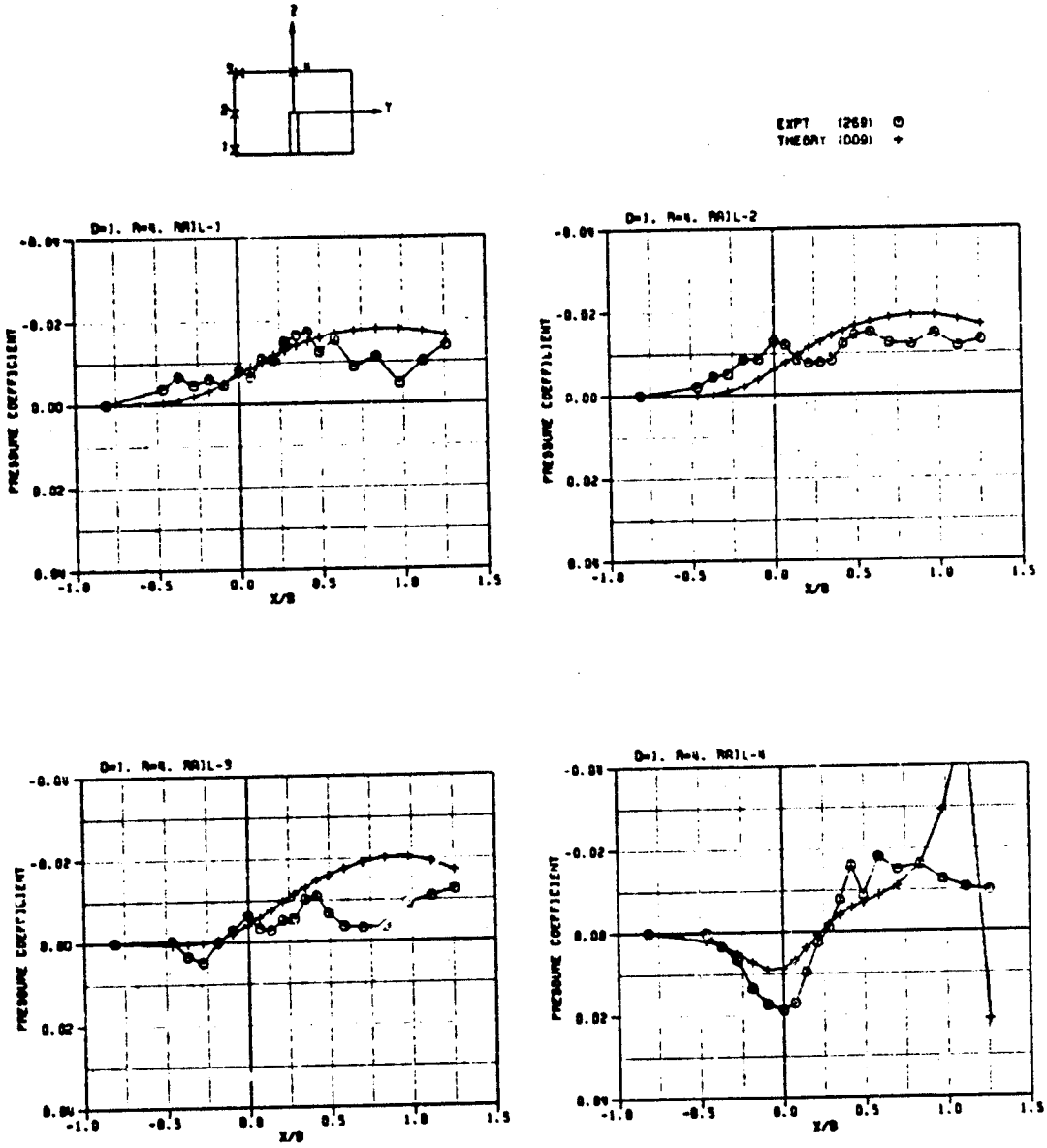

Figure 5.9 (Concluded) Wall pressure correlations for other, non-impinging cases: (b) D = 1", R = 4.

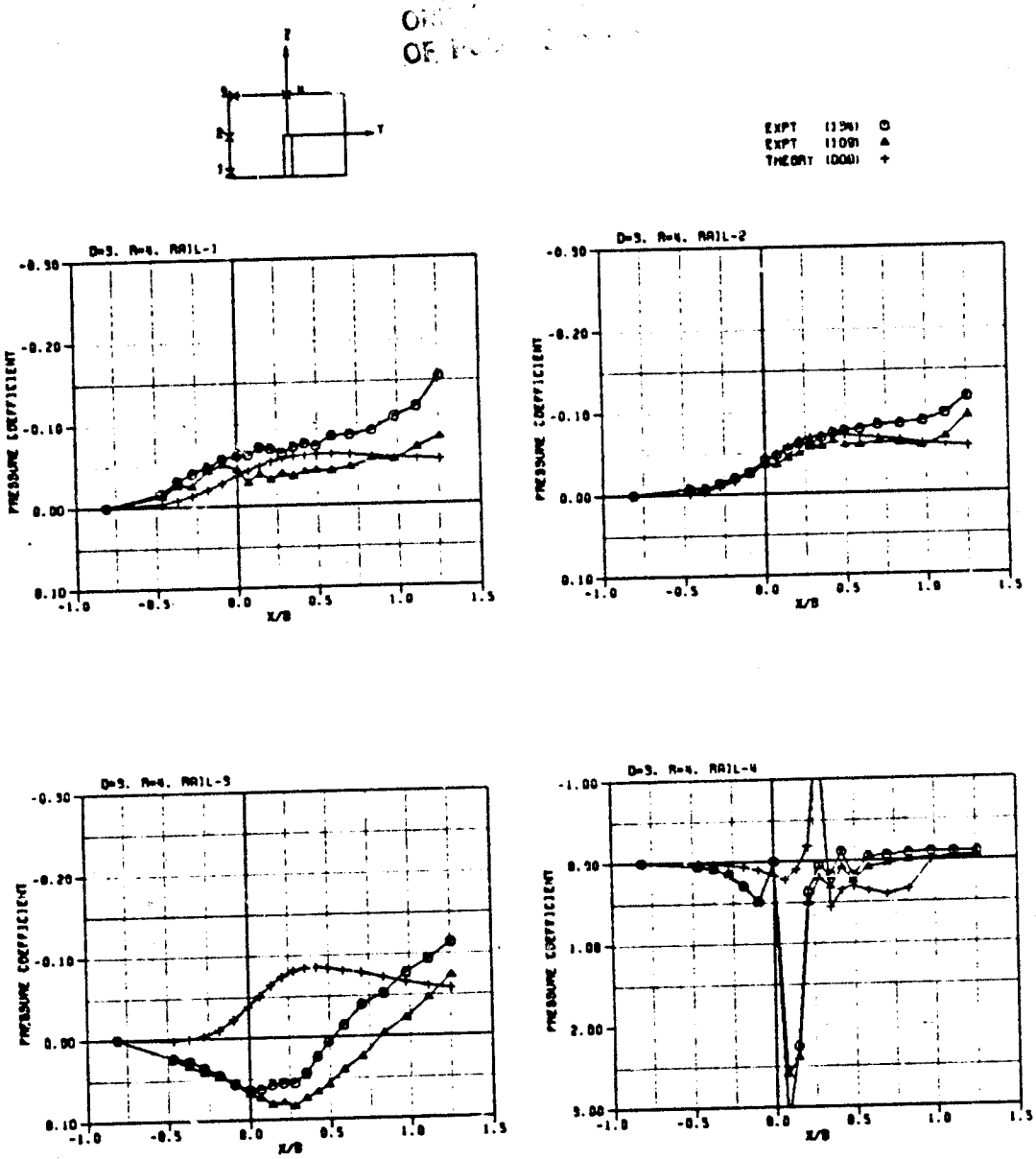

Figure 5.10 Wall pressure correlations for an impinging case:
(a) D = 3", R = 4: VSD model.

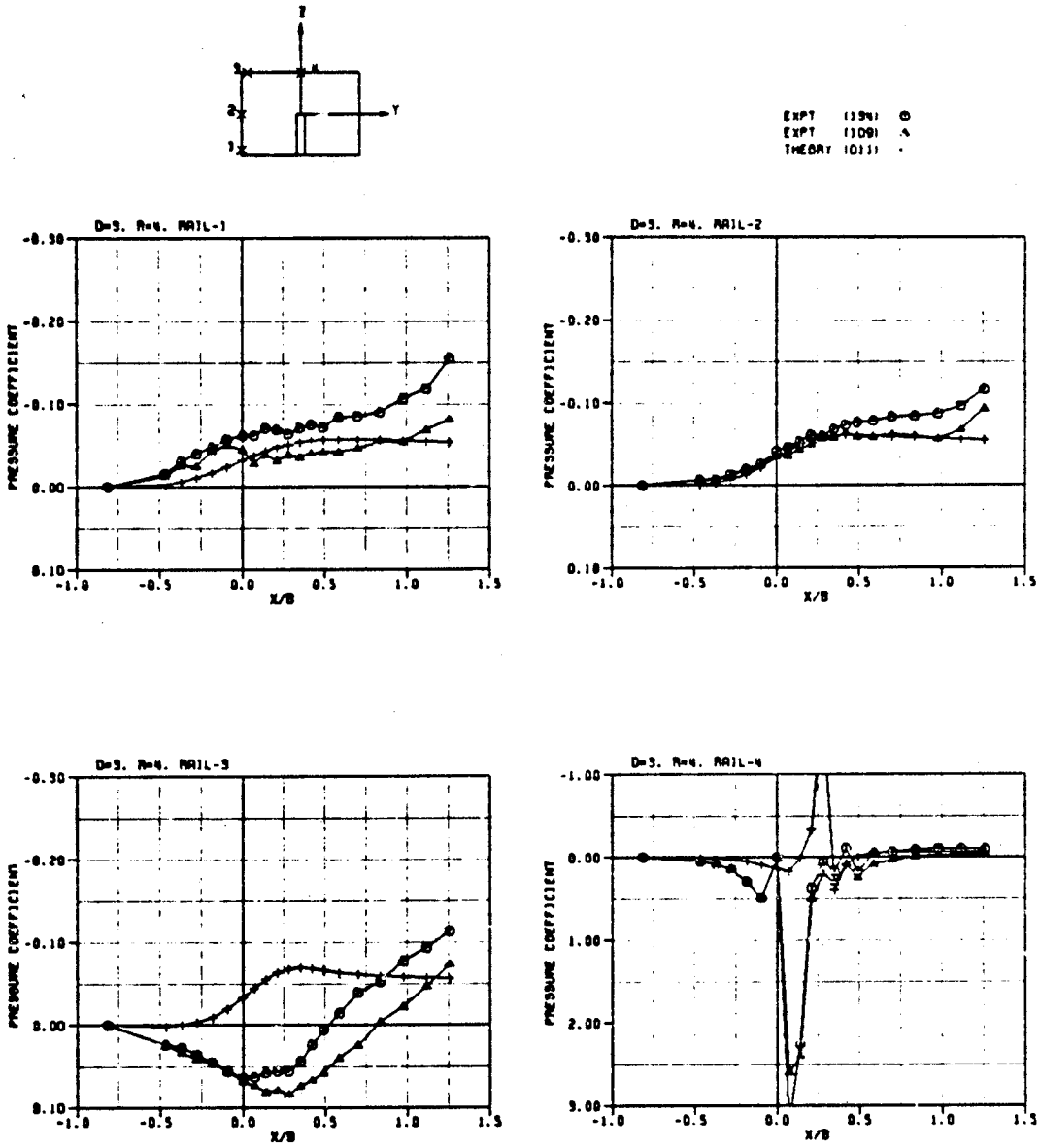

Figure 5.10 (Concluded) Wall pressure correlations for an impinging case: (b) D = 3", R = 4: SD model.

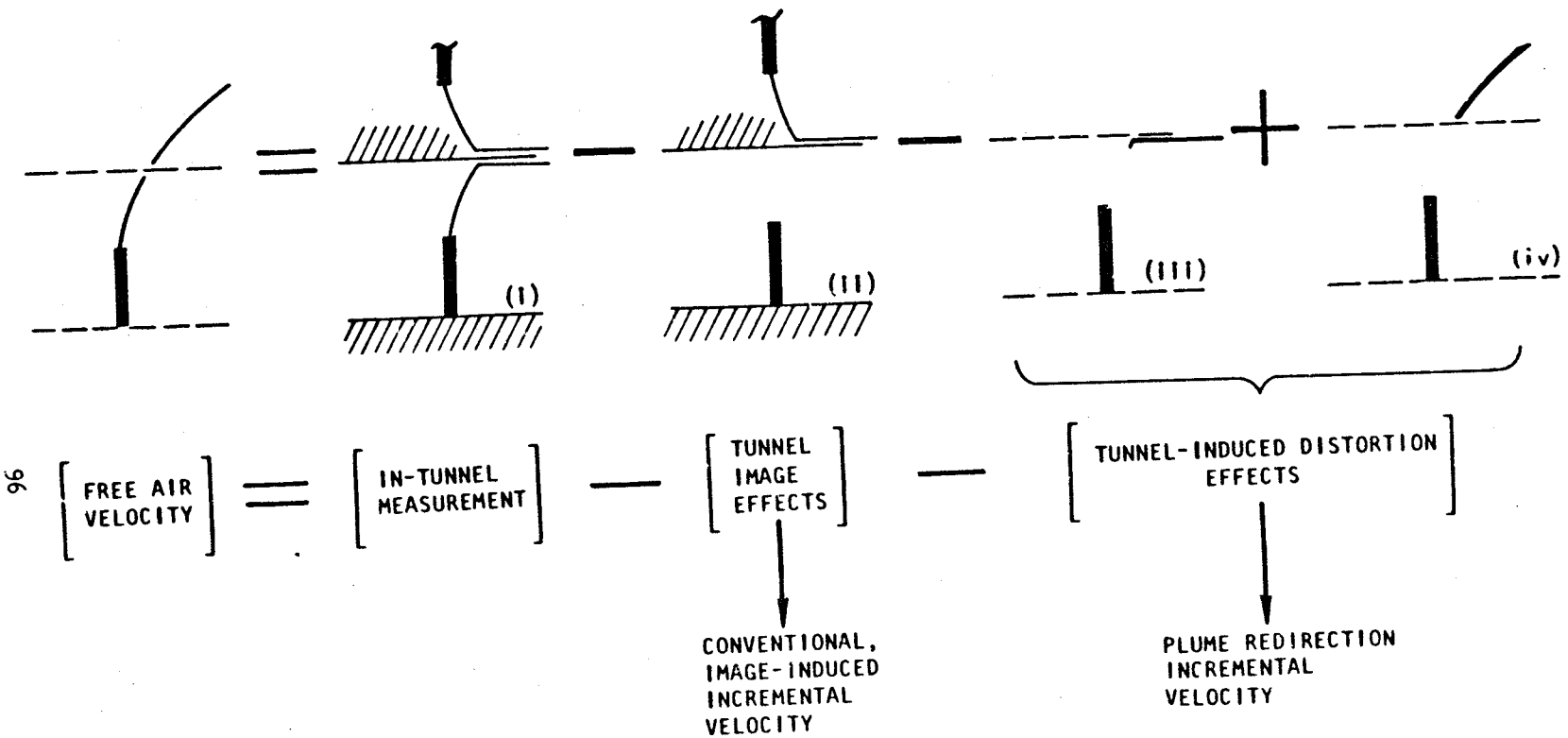

Figure 5.11 Build-up of free air flow field from tunnel image and plume redirection effects: schematic.

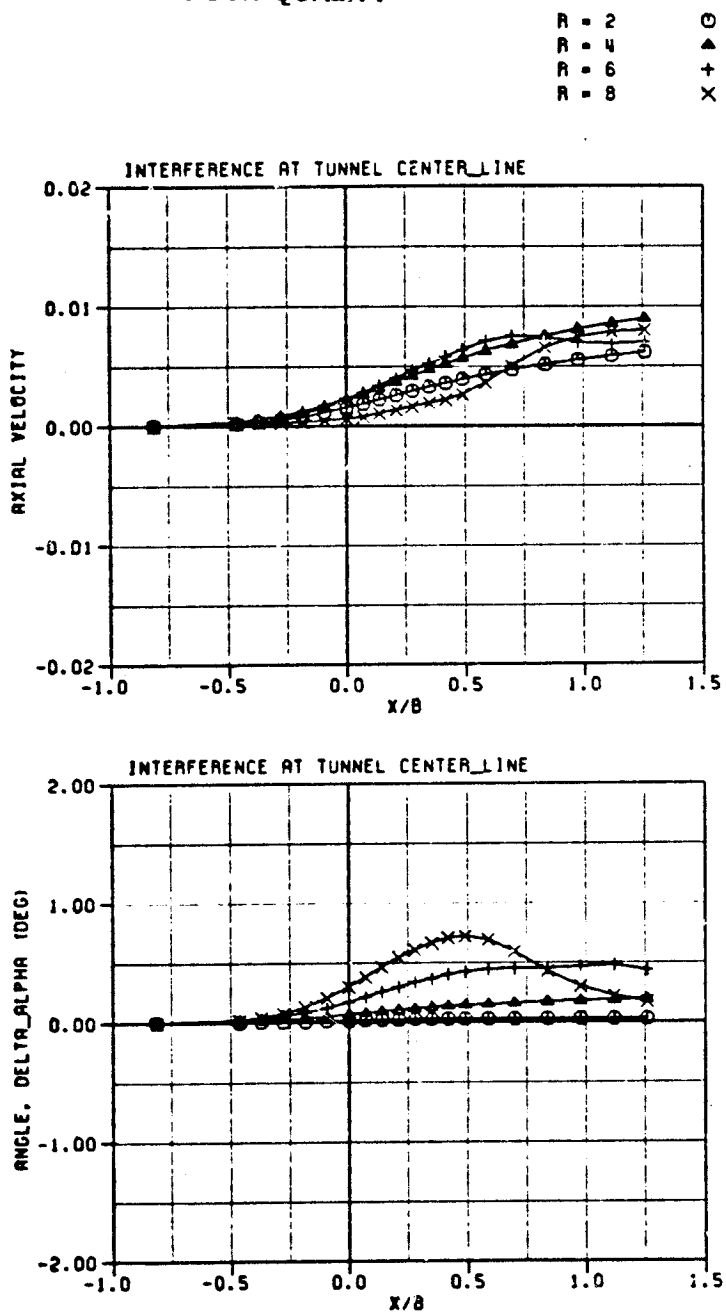

Figure 5.12 Build-up of total tunnel effect for the 1-inch jet.
(a) Effect of within-tunnel images.

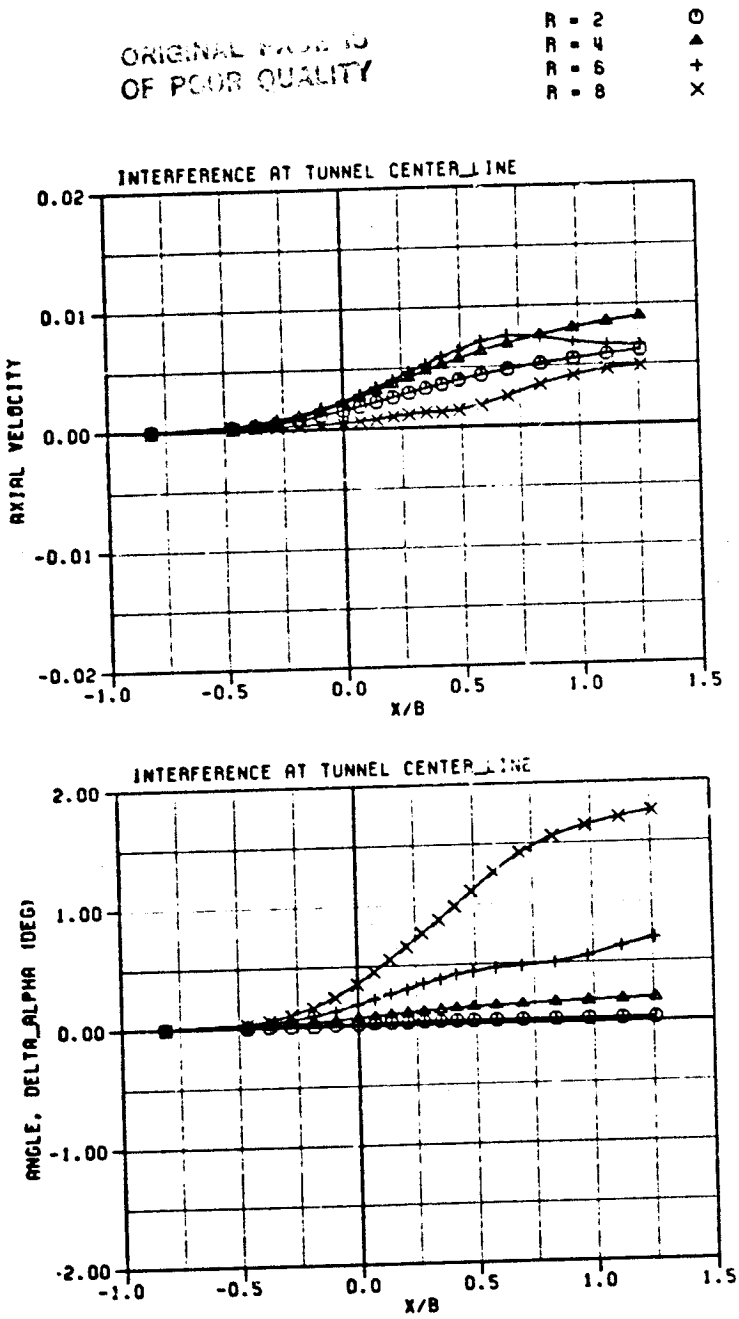

Figure 5.12 (Continued) Build-up of total tunnel effect for the 1-inch jet. (b) Effect of adding along-surface elements.

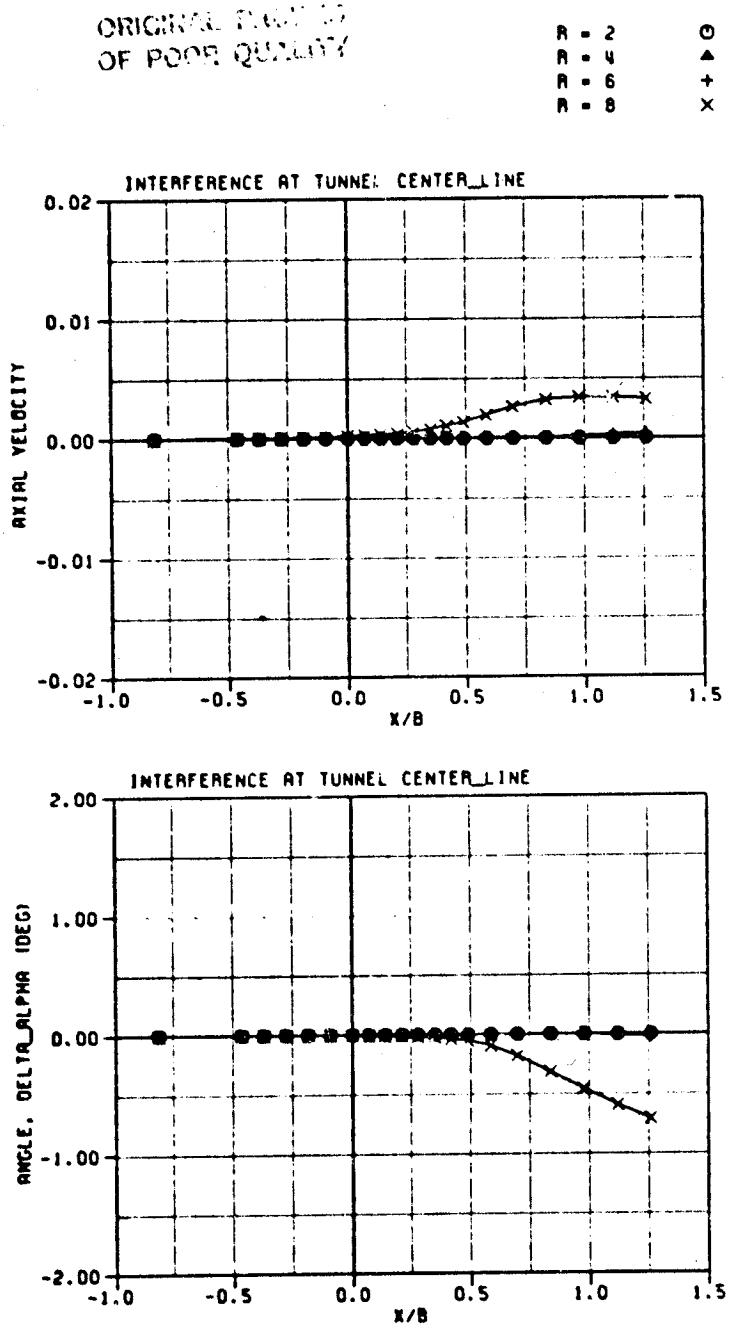

Figure 5.12 (Continued) Build-up of total tunnel effect for the 1-inch jet. (c) Plume redirection increments.

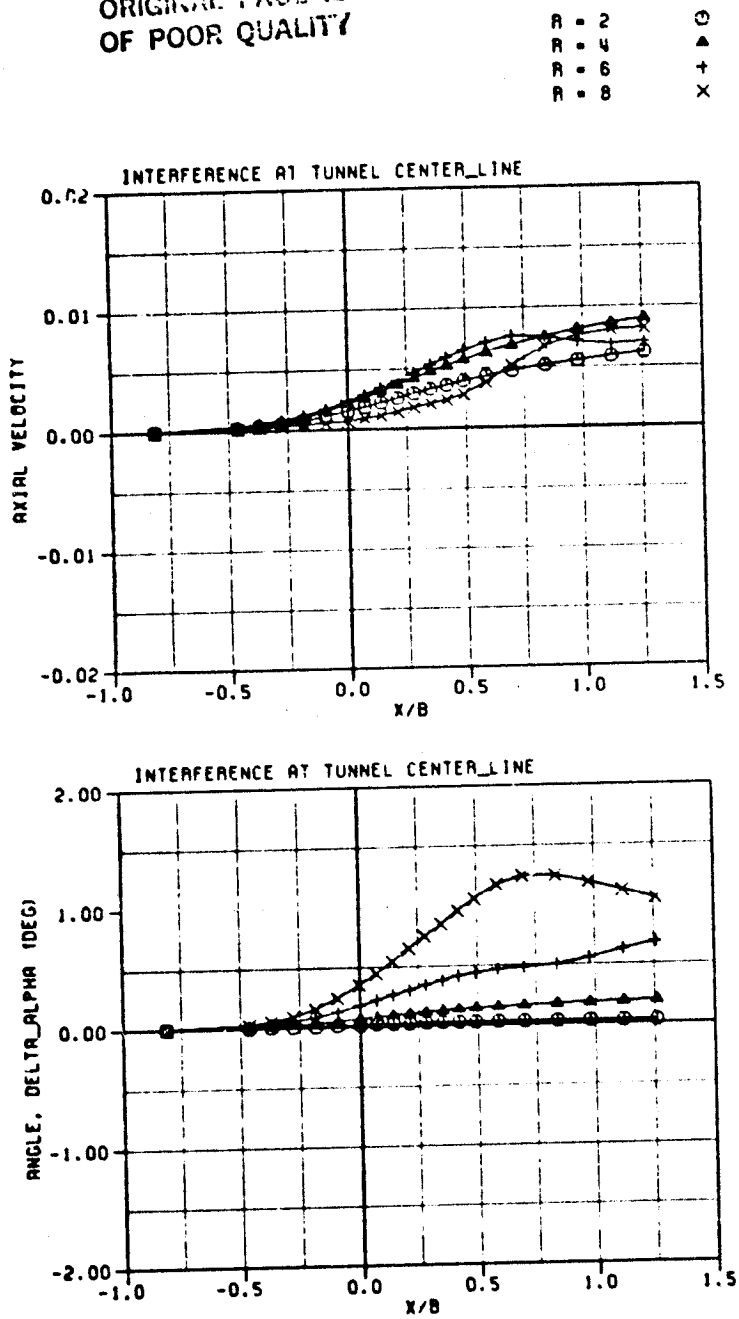

Figure 5.12 (Concluded) Build-up of total tunnel effect for the 1-inch jet.
(d) Total tunnel effect.

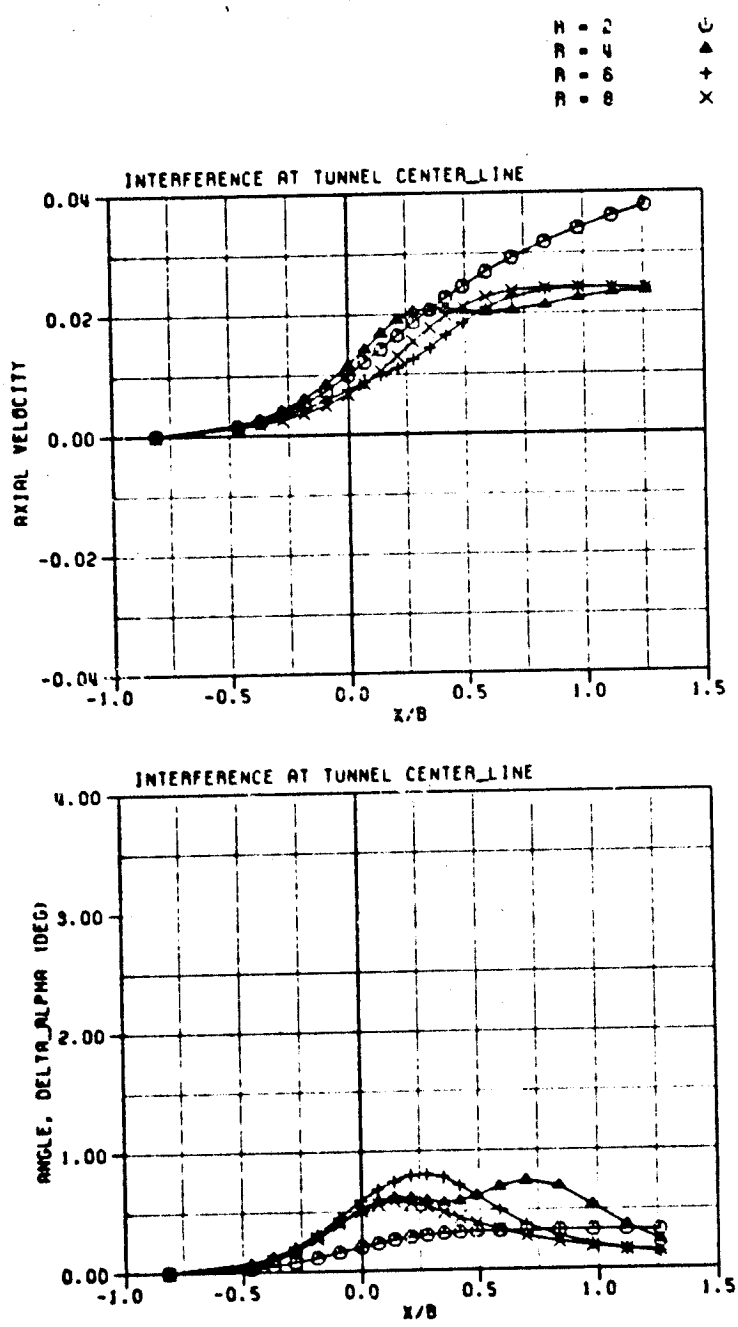

Figure 5.13 Build-up of total tunnel effect for the 3-inch jet.
(a) Effect of within-tunnel images.

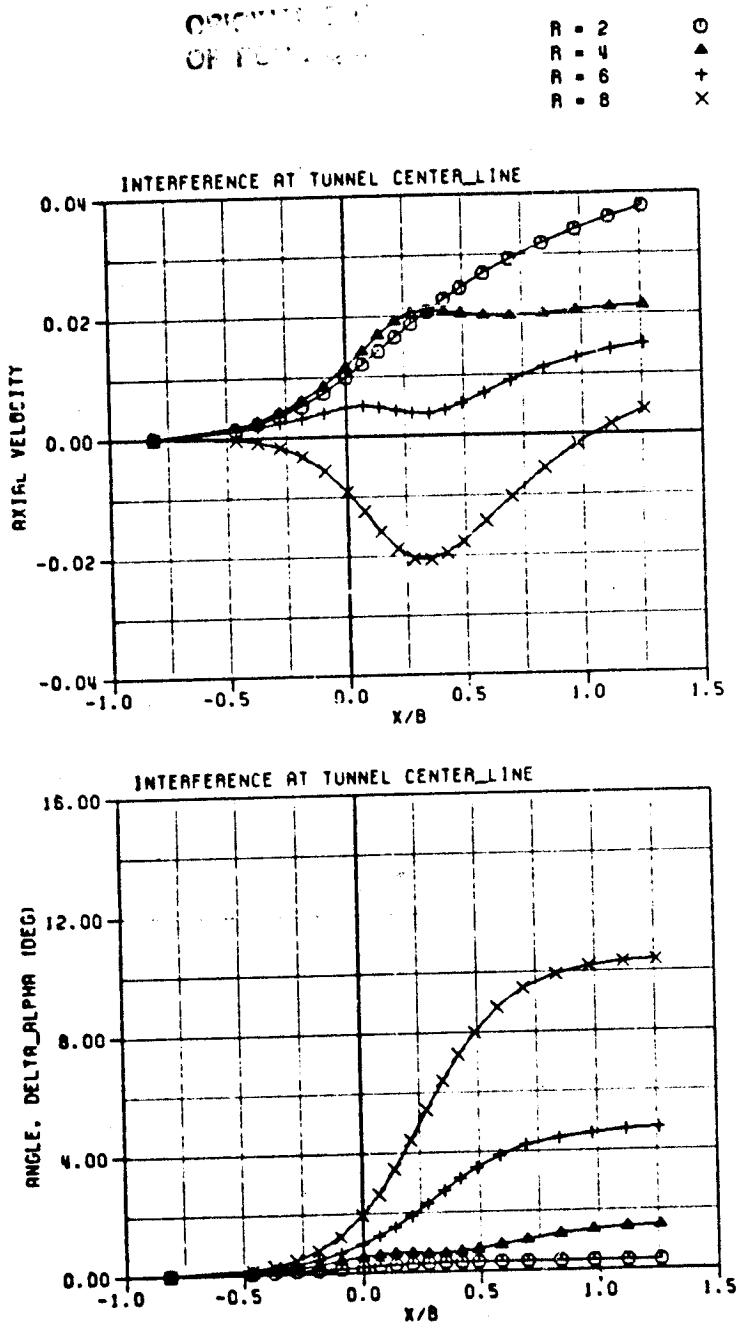

Figure 5.13 (Continued) Build-up of total tunnel effect for the 3-inch jet. (b) Effect of adding along-surface elements.

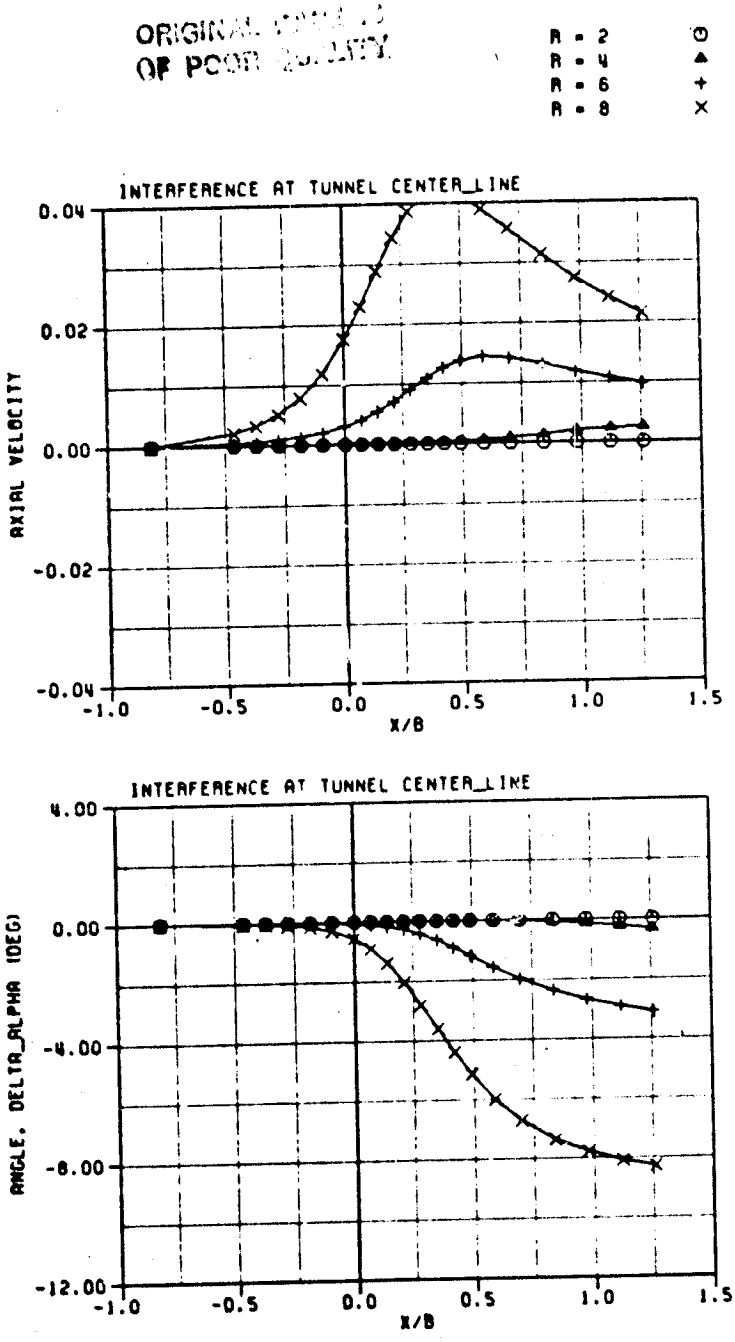

Figure 5.13 (Continued) Build-up of total tunnel effect for the 3-inch jet. (c) Plume redirection increments.

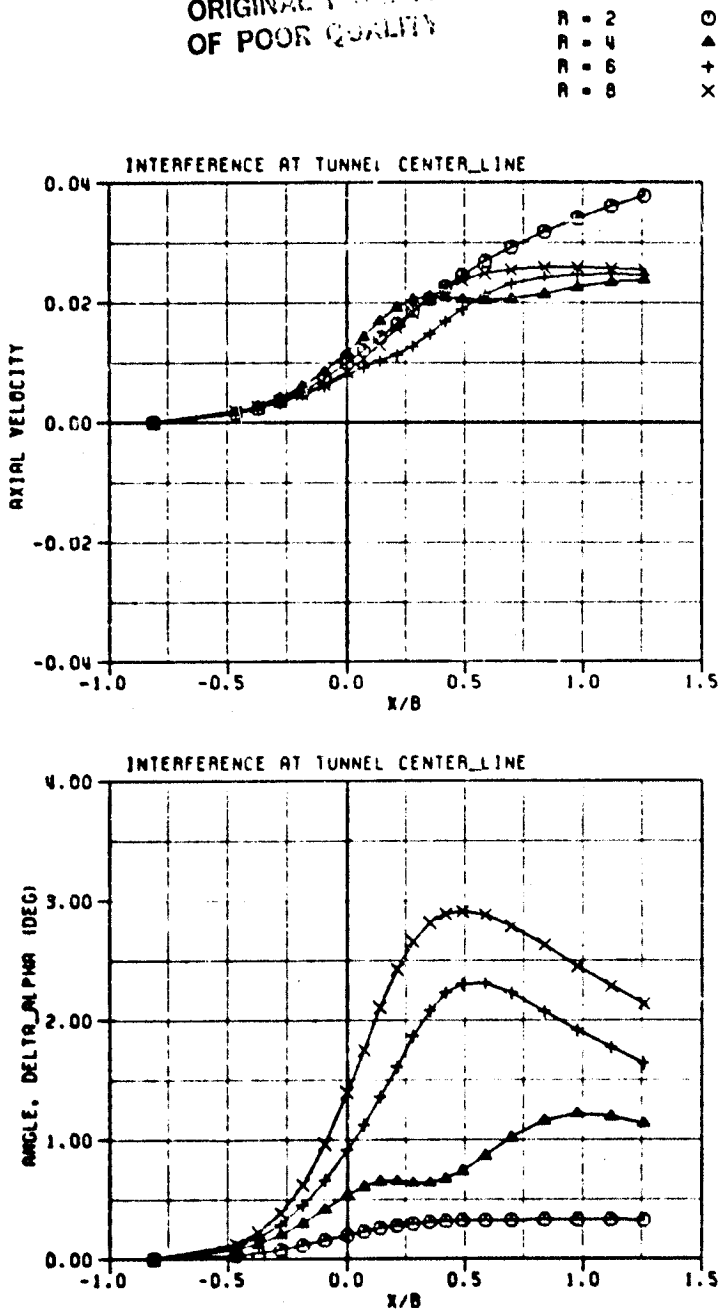

Figure 5.13 (Concluded) Build-up of total tunnel effect for the 3-inch jet.
(d) Total tunnel effect.

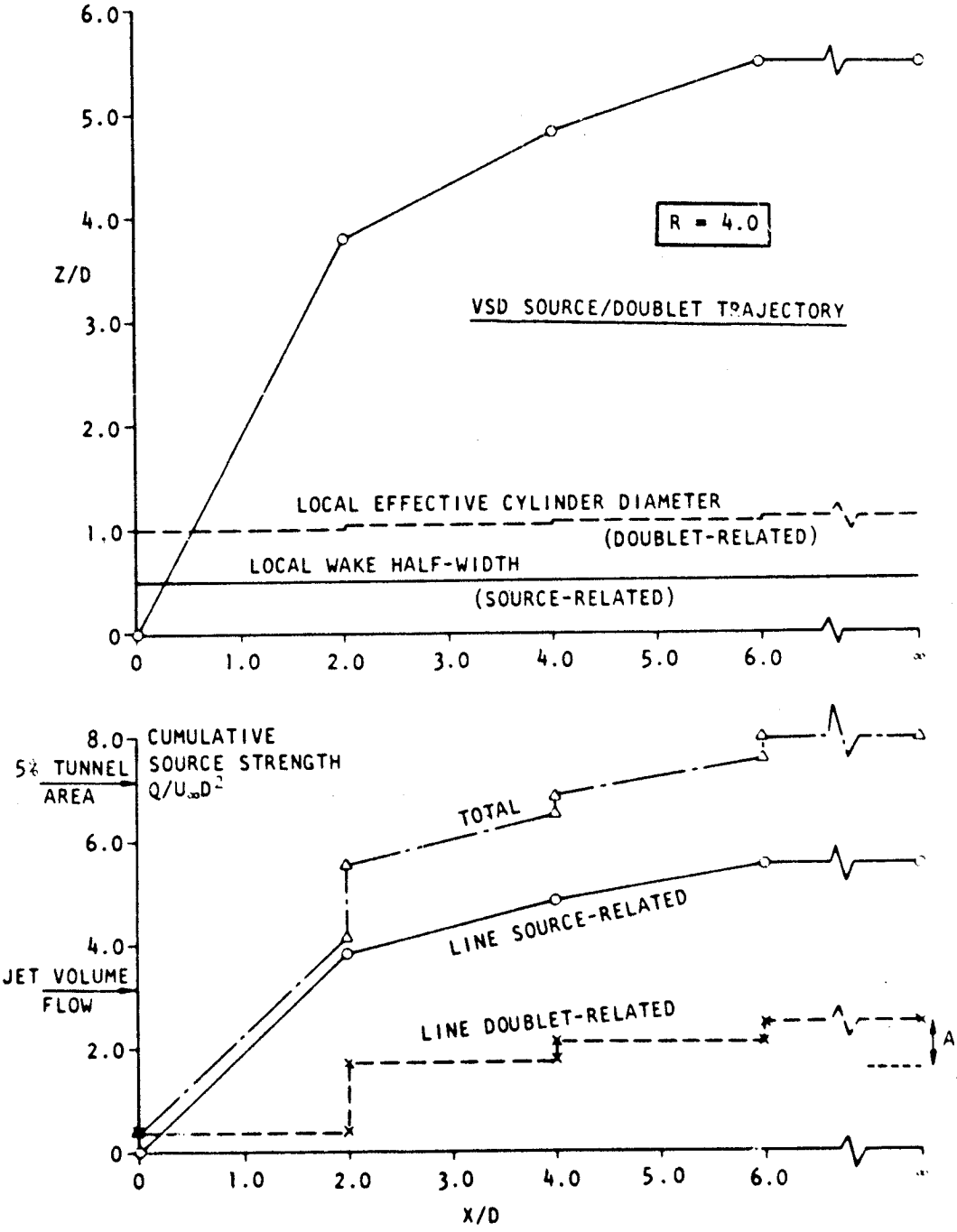

5.14 Comparison between jet-in-crossflow models.
(a) Present, 'VSD' flow model.

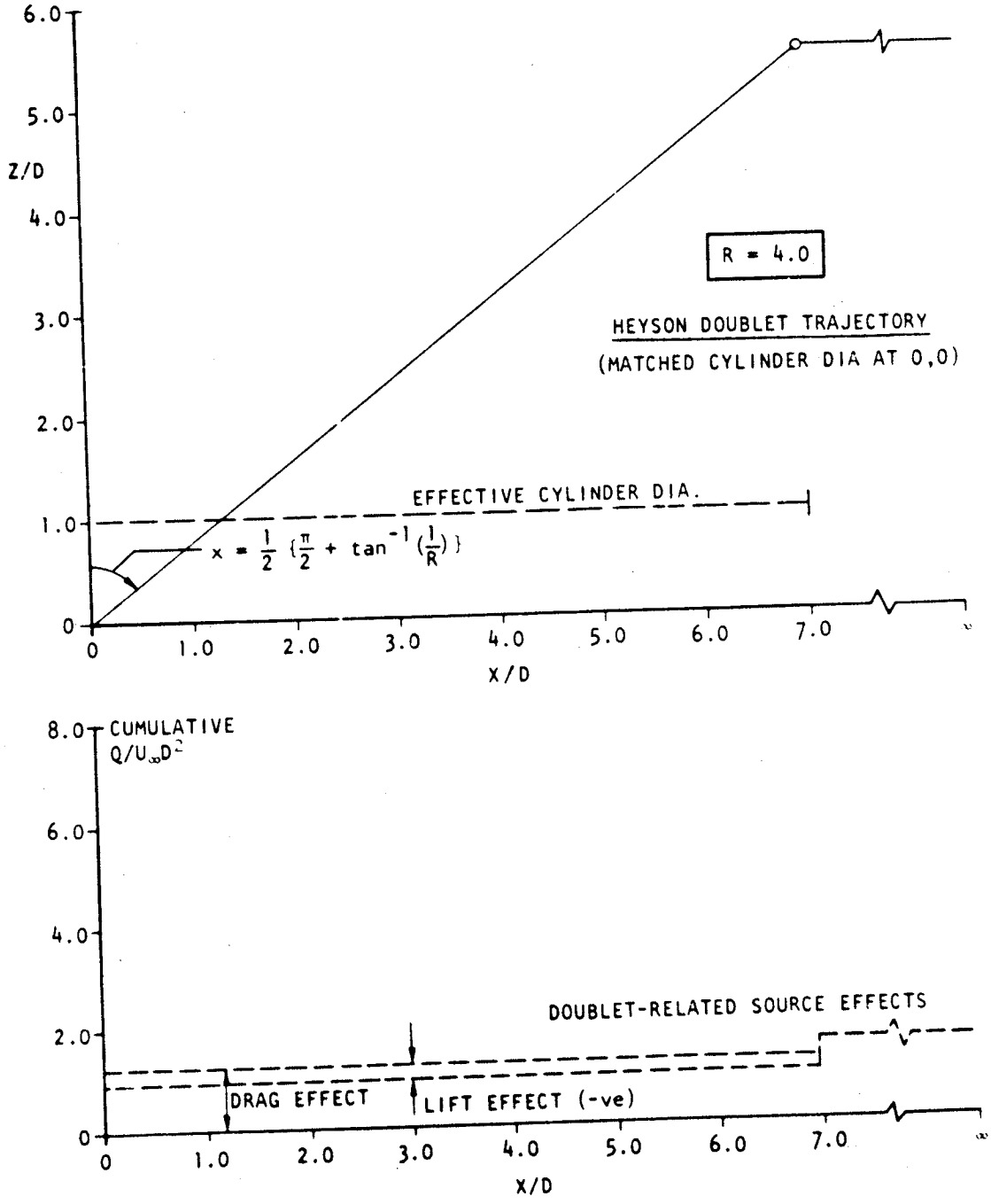

5.14 (Concluded) Comparison between jet-in-crossflow models.
(b) Heyson's flow model.

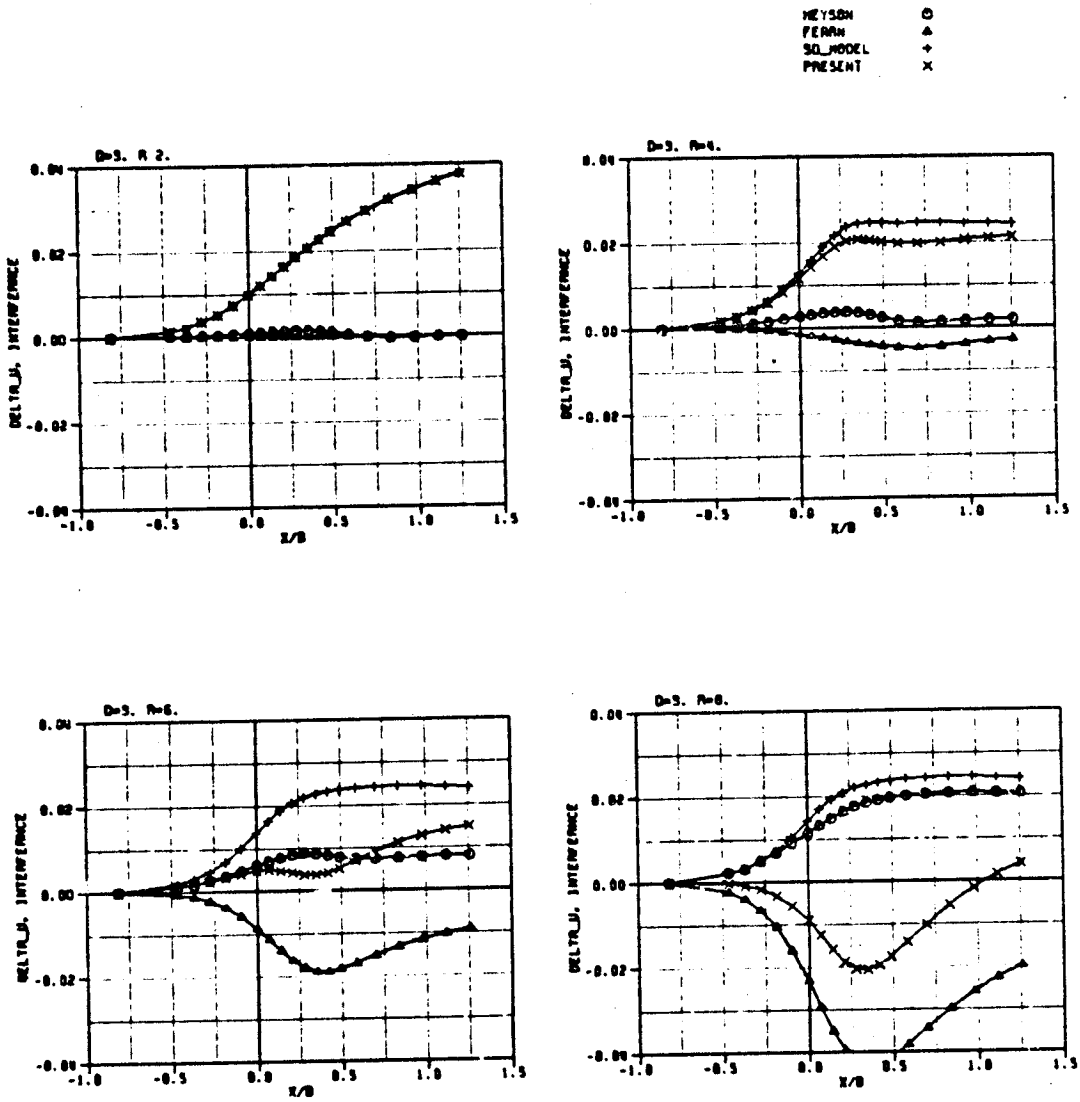

Figure 5.15 Comparisons between present blockage corrections and other methods. (a) Image effects.

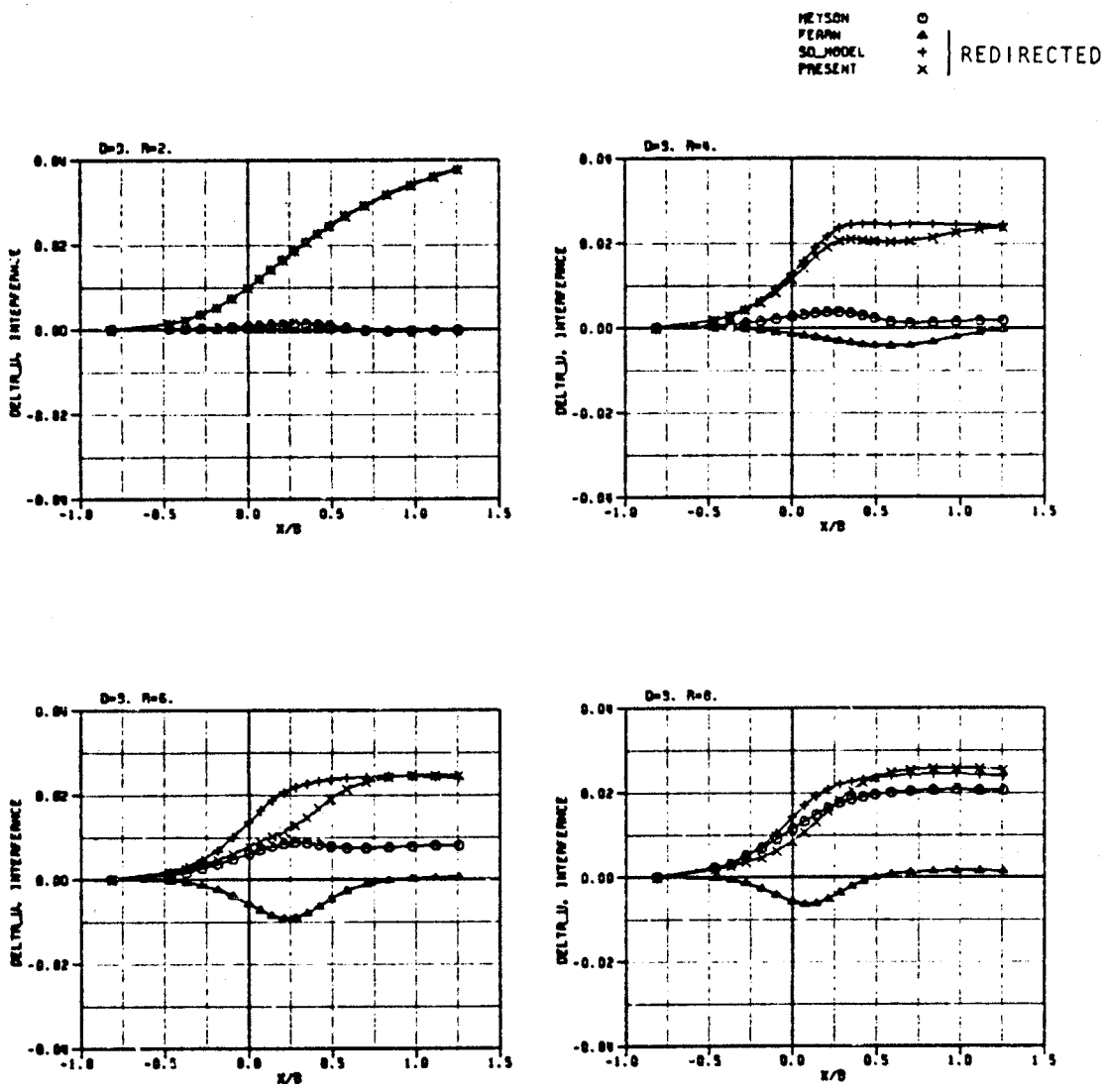

Figure 5.15 (Concluded) Comparisons between present blockage corrections and other methods.
(b) Total tunnel effects.

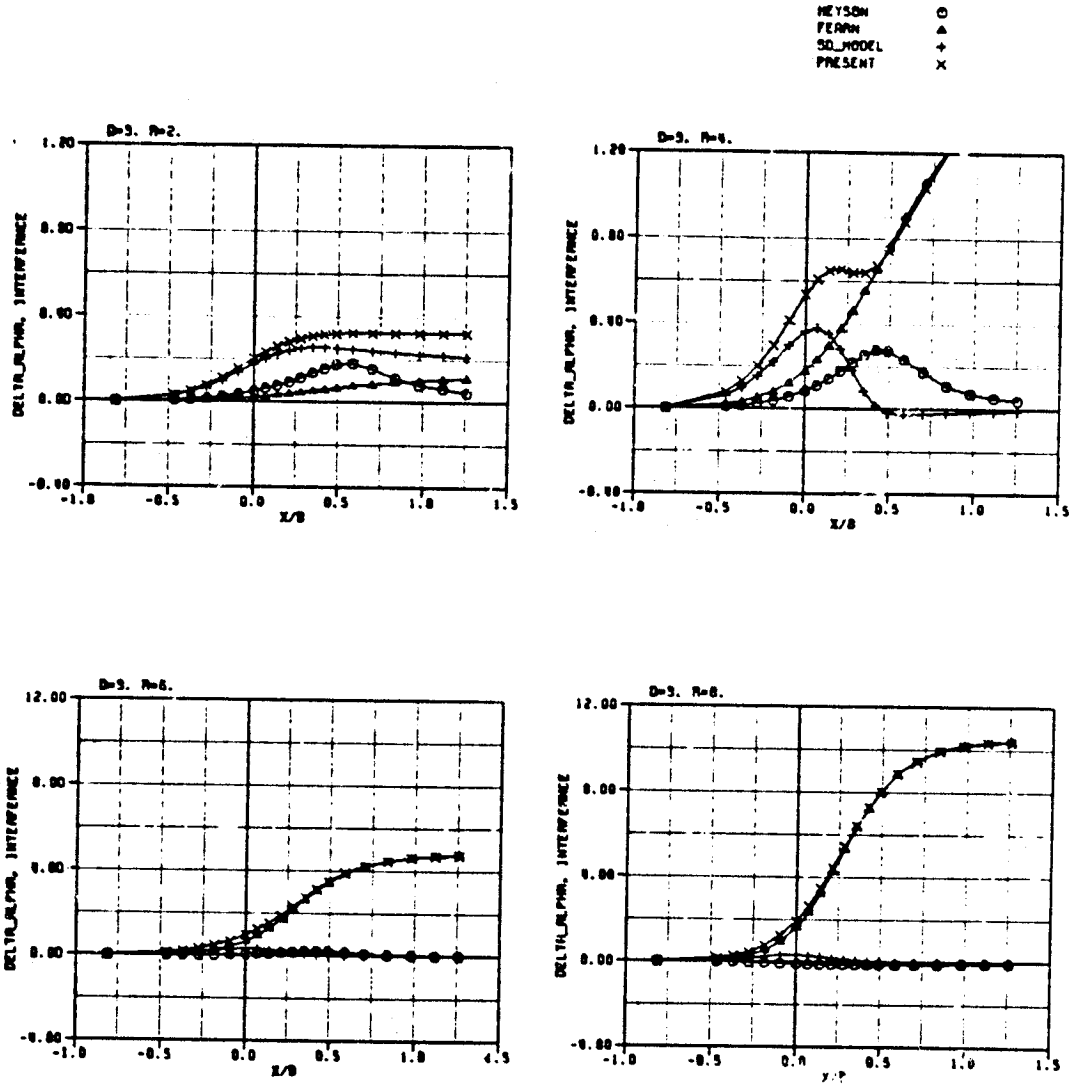

Figure 5.16 Comparisons between present angle-of-attack corrections and other methods.
(a) Image effects

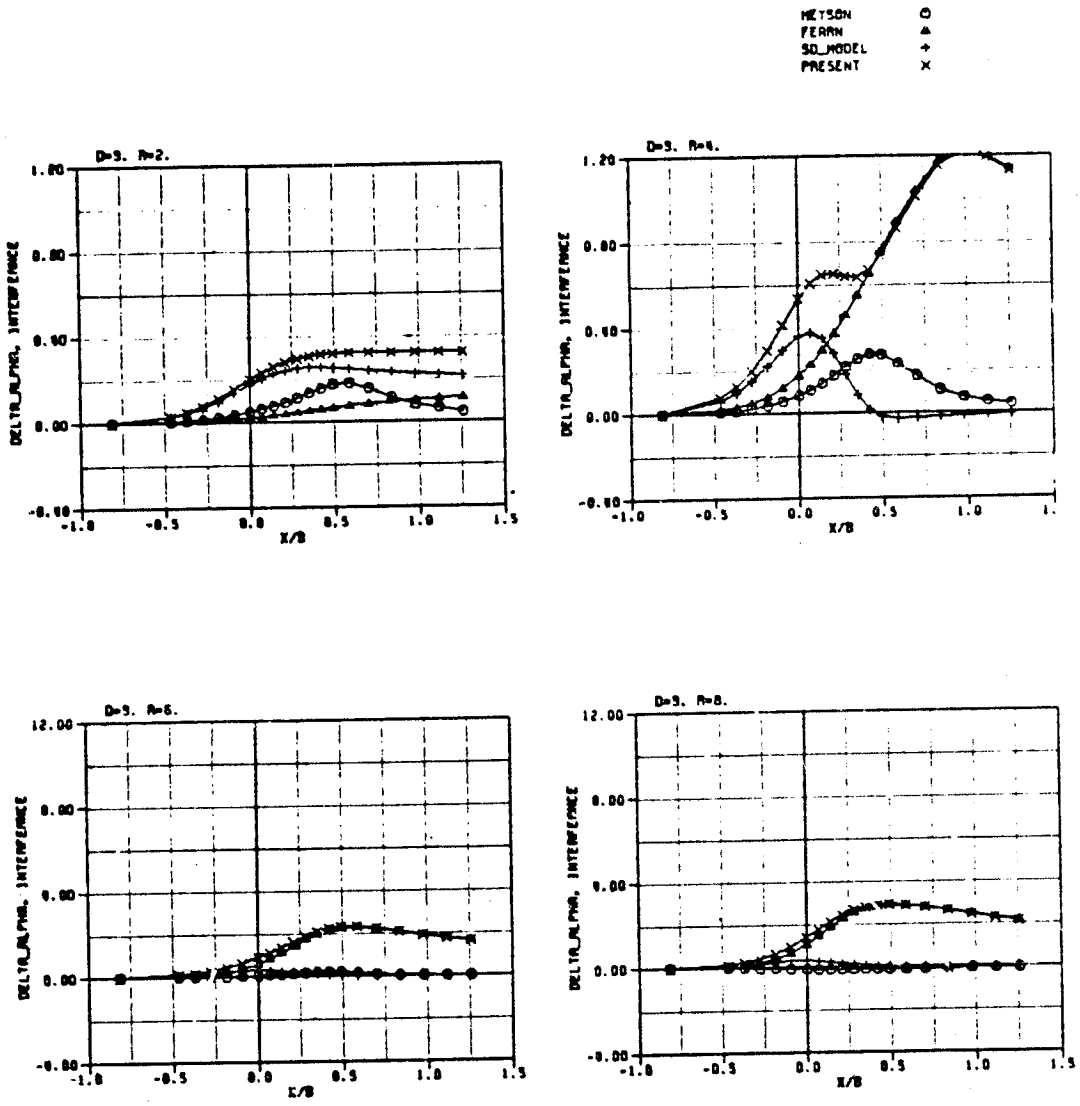

Figure 5.16 (Concluded) Comparisons between present angle-of-attack corrections and other methods.
(b) Total tunnel effects.

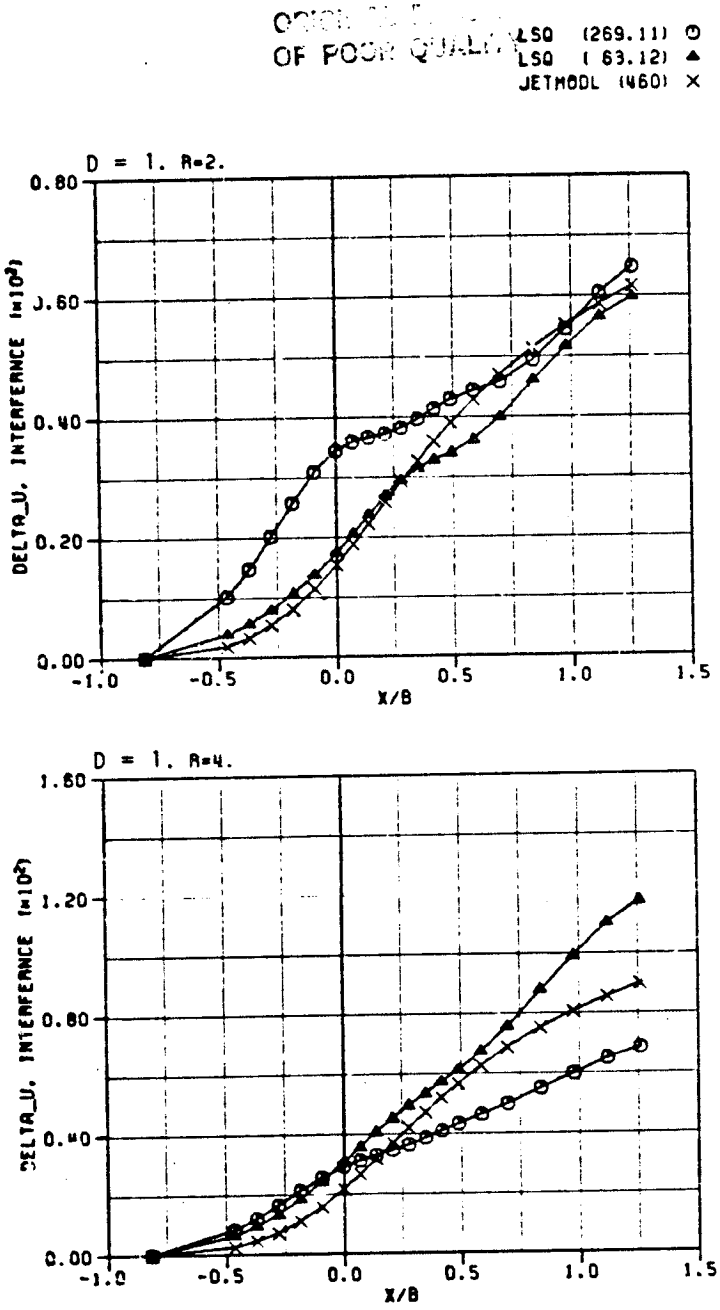

Figure 5.17 Comparisons between 'planar' and 'VSD' blockage estimates.
(a) 1-inch jet

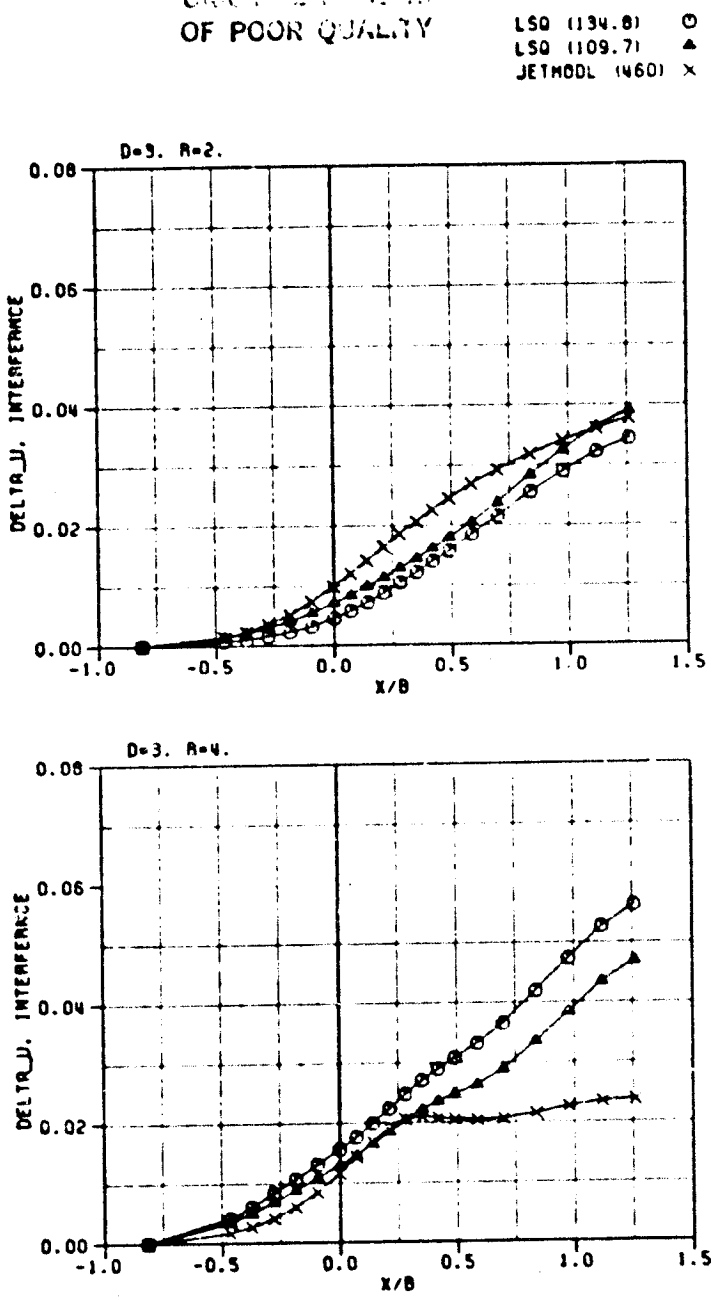

Figure 5.17 (Concluded) Comparisons between 'planar' and 'VSD' blockage estimates. (b) 3-inch jet.

APPENDIX A

WAKE TRAVERSE DATA FOR ONE-INCH JET AT -30°, 0° AND +30° TO THE VERTICAL

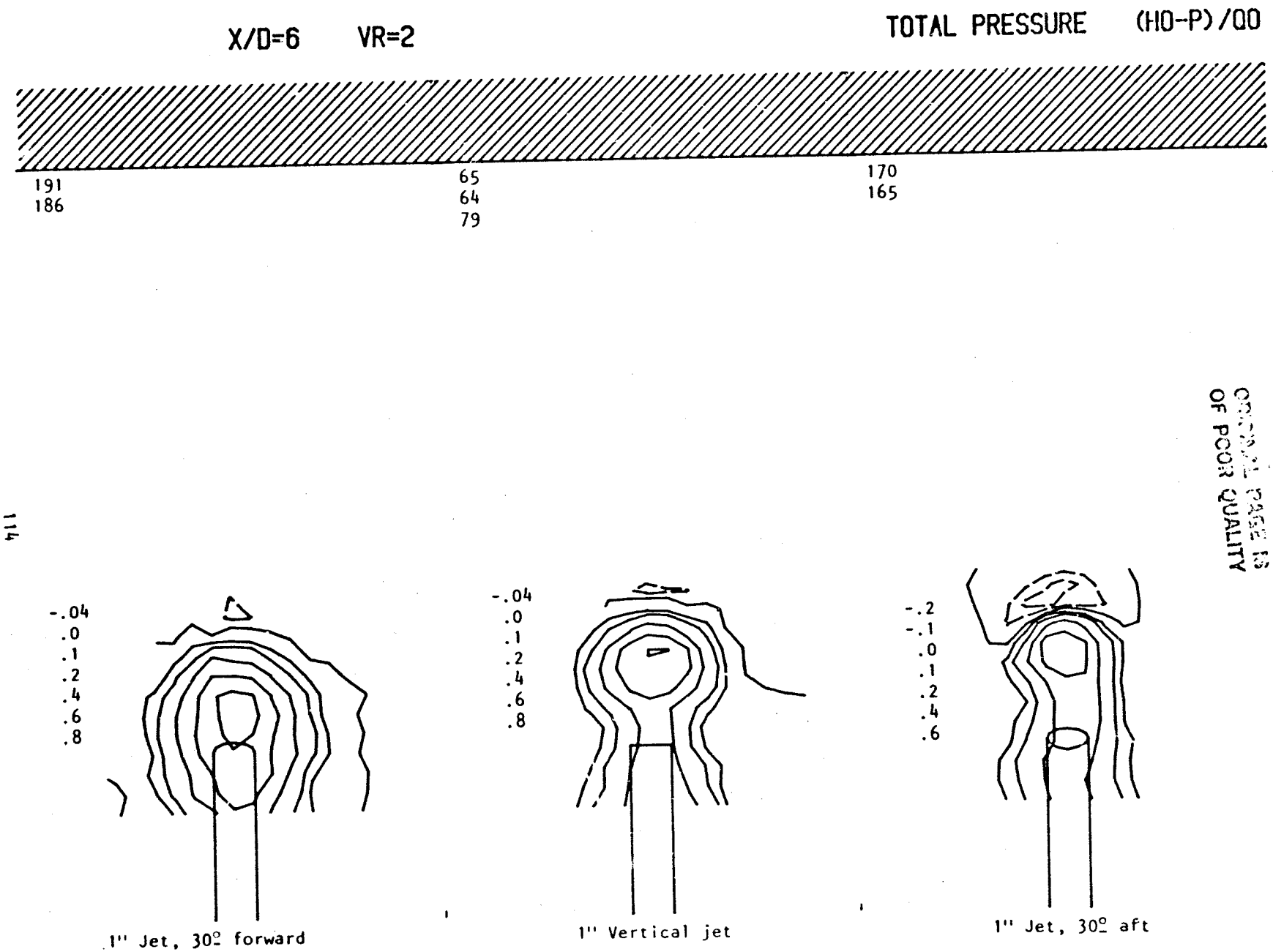

Figure A1 Effect of jet inclination on total pressures: R = 2

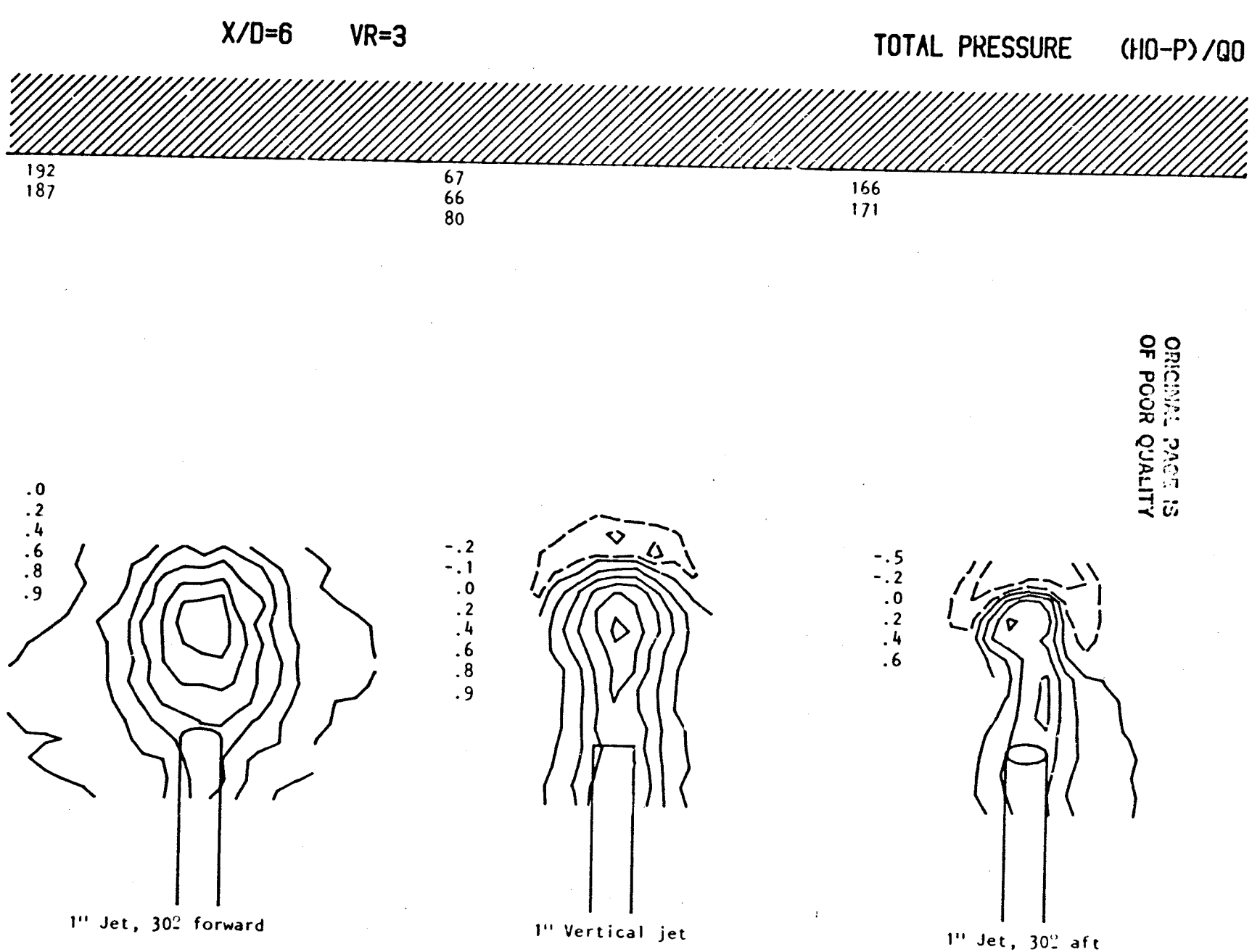

Figure A1 (continued) Effect of jet inclination on total pressures: R = 3

X/D=6 VR=4 TOTAL PRESSURE (H0-P)/Q0

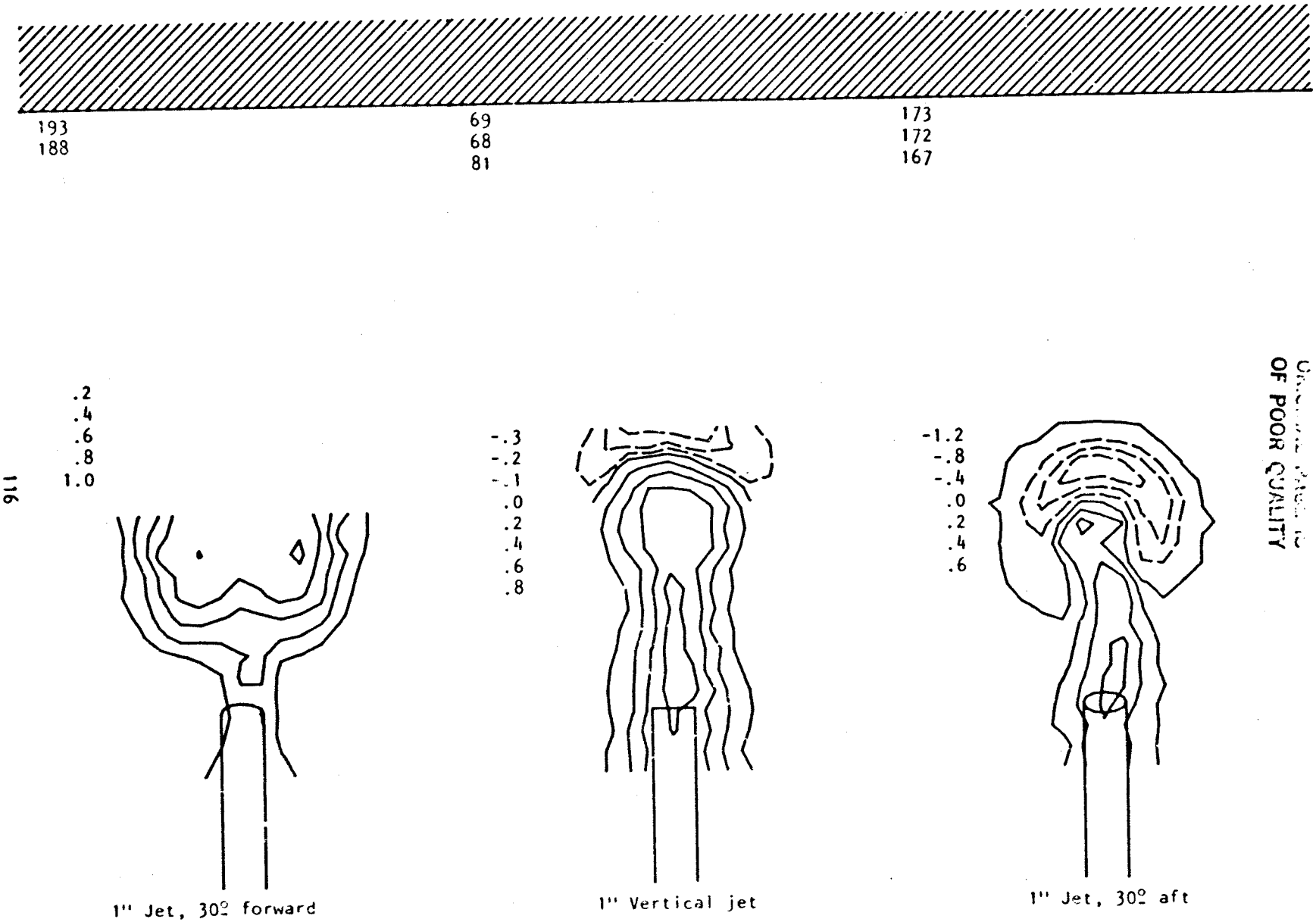

Figure A1 (continued) Effect of jet inclination on total pressures: R = 4

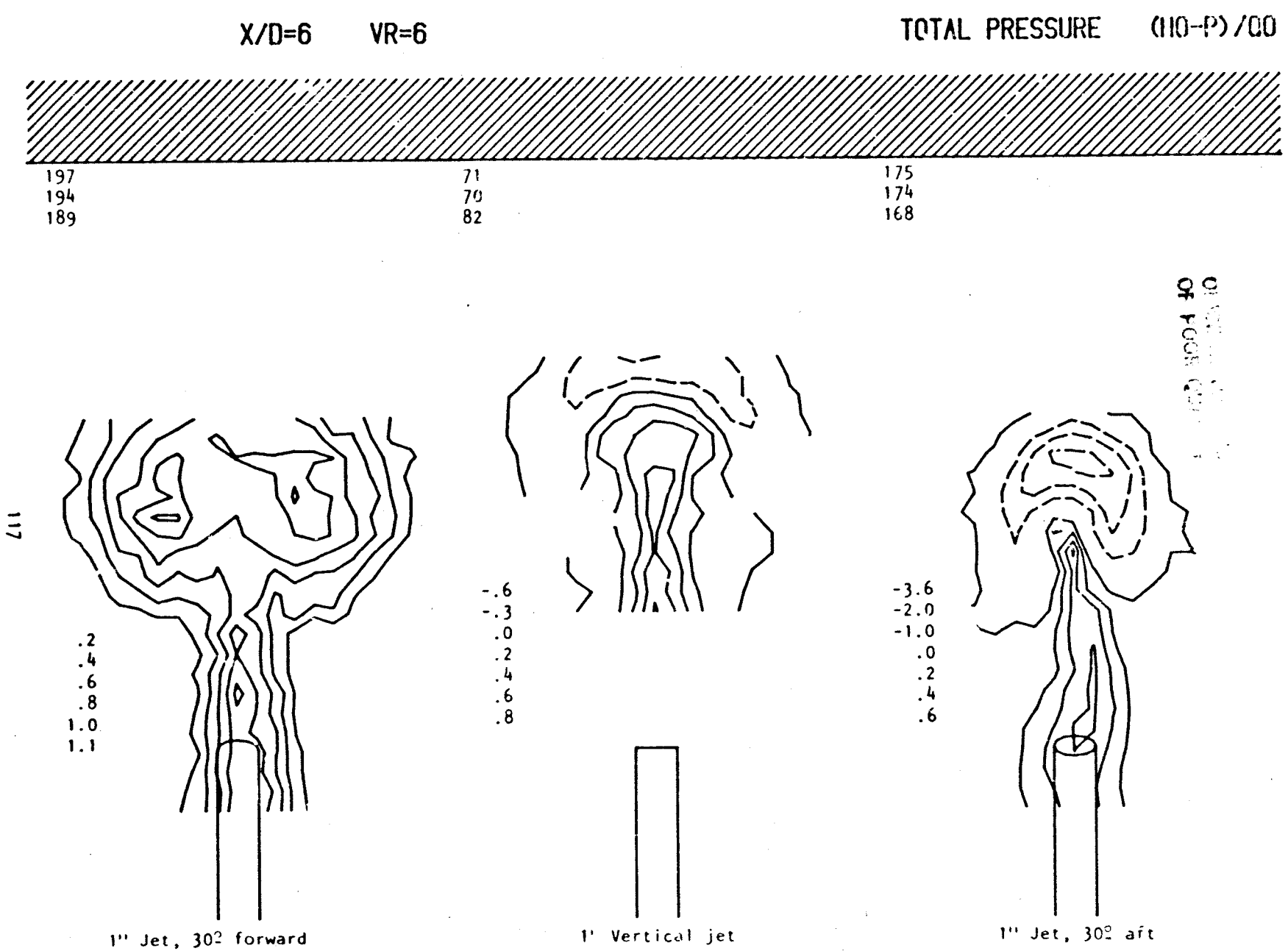

Figure A1 (continued) Effect of jet inclination on total pressures: R = 6

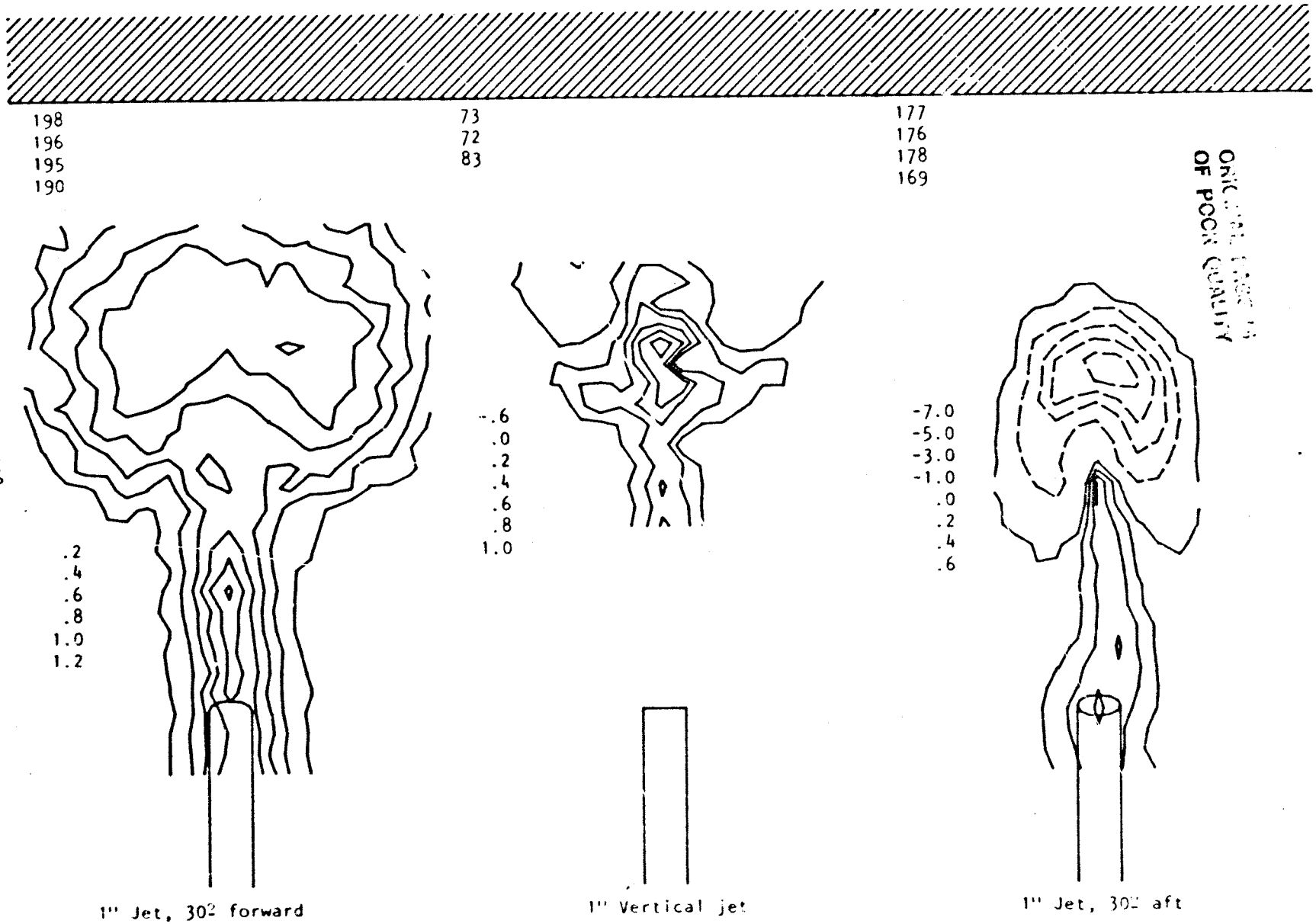

Figure A1 (concluded) Effect of jet inclination on total pressures: R = 8

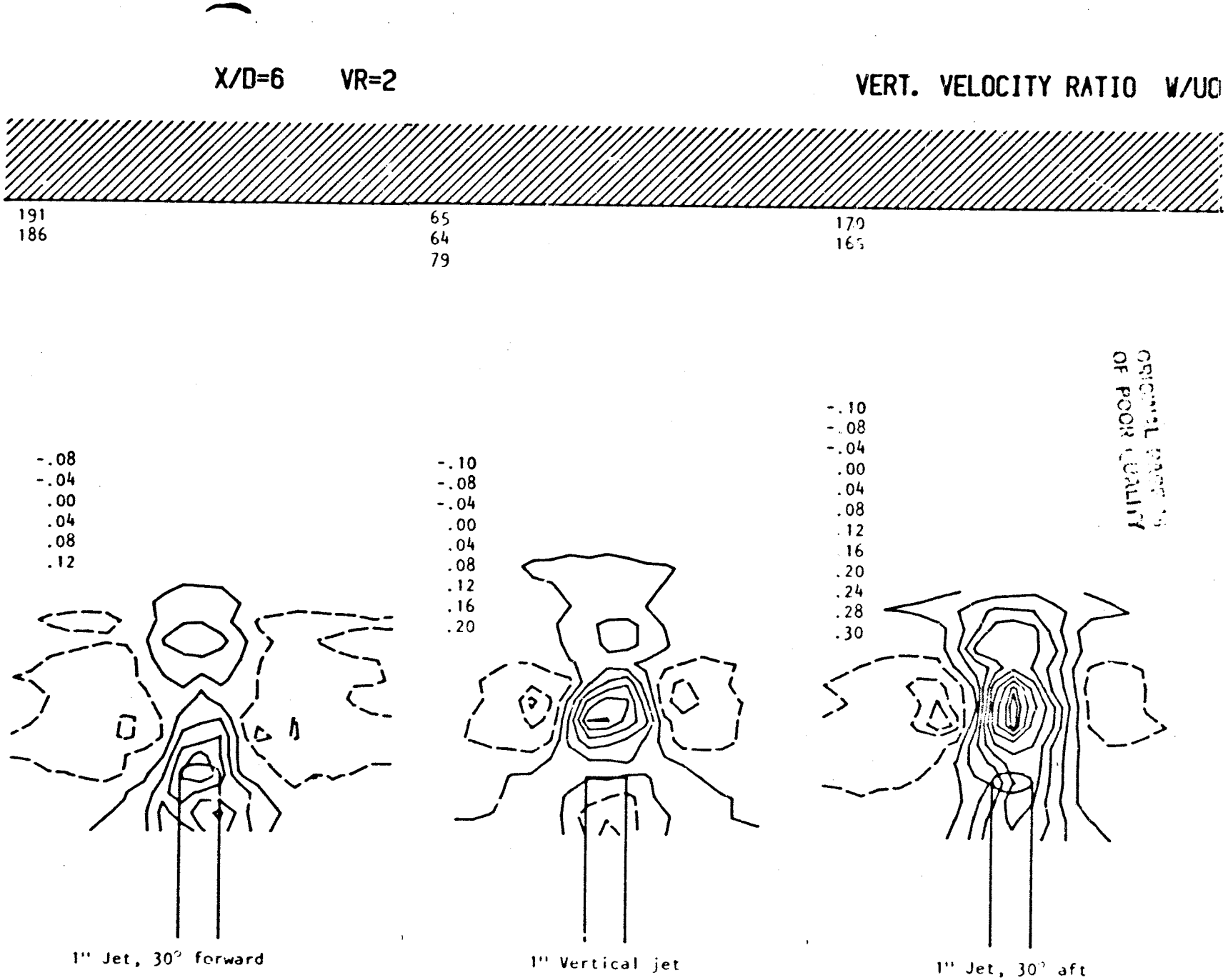

Figure A2 Effect of jet inclination on vertical velocities: R = 2

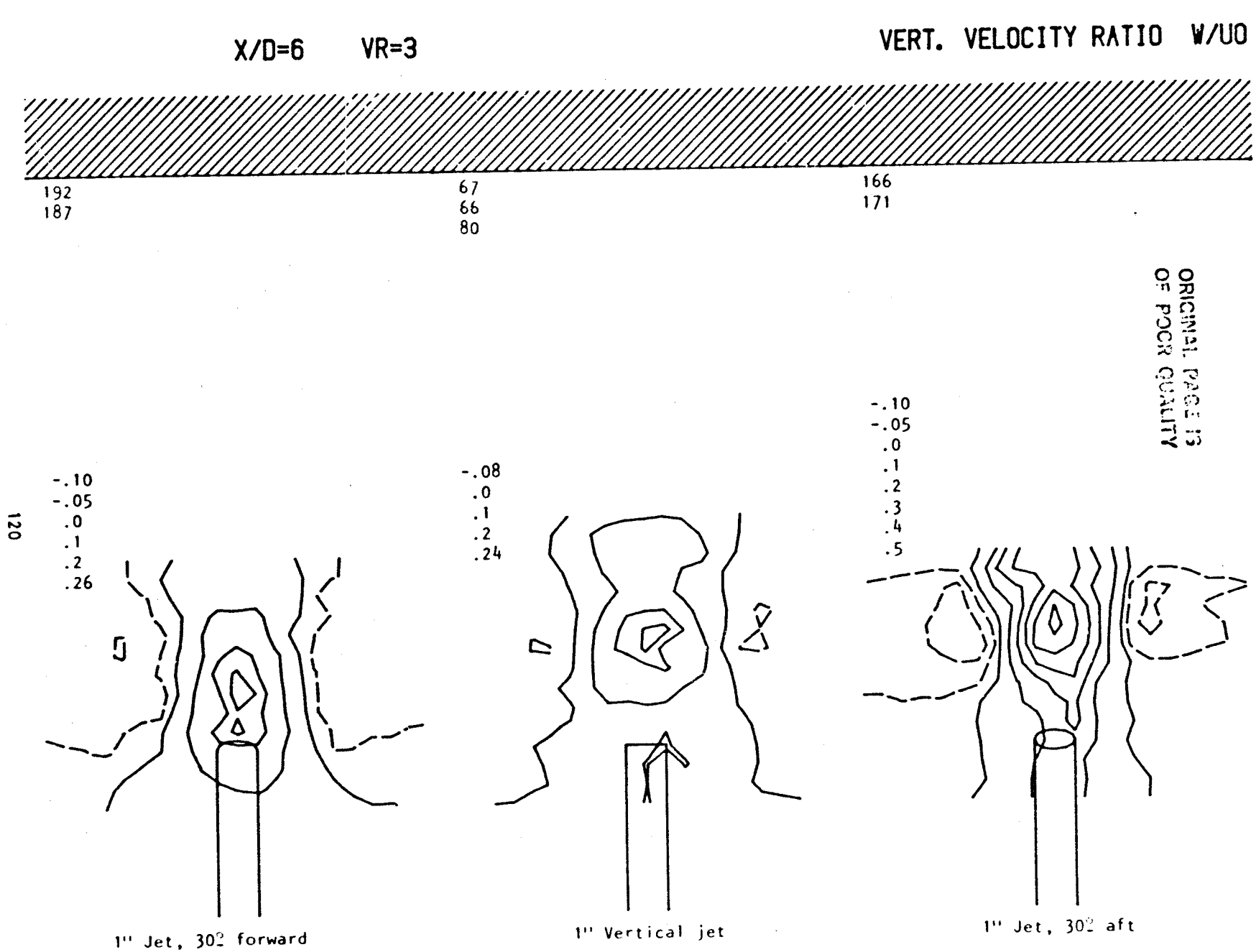

Figure A2 (continued) Effect of jet inclination vertical velocities: R = 3

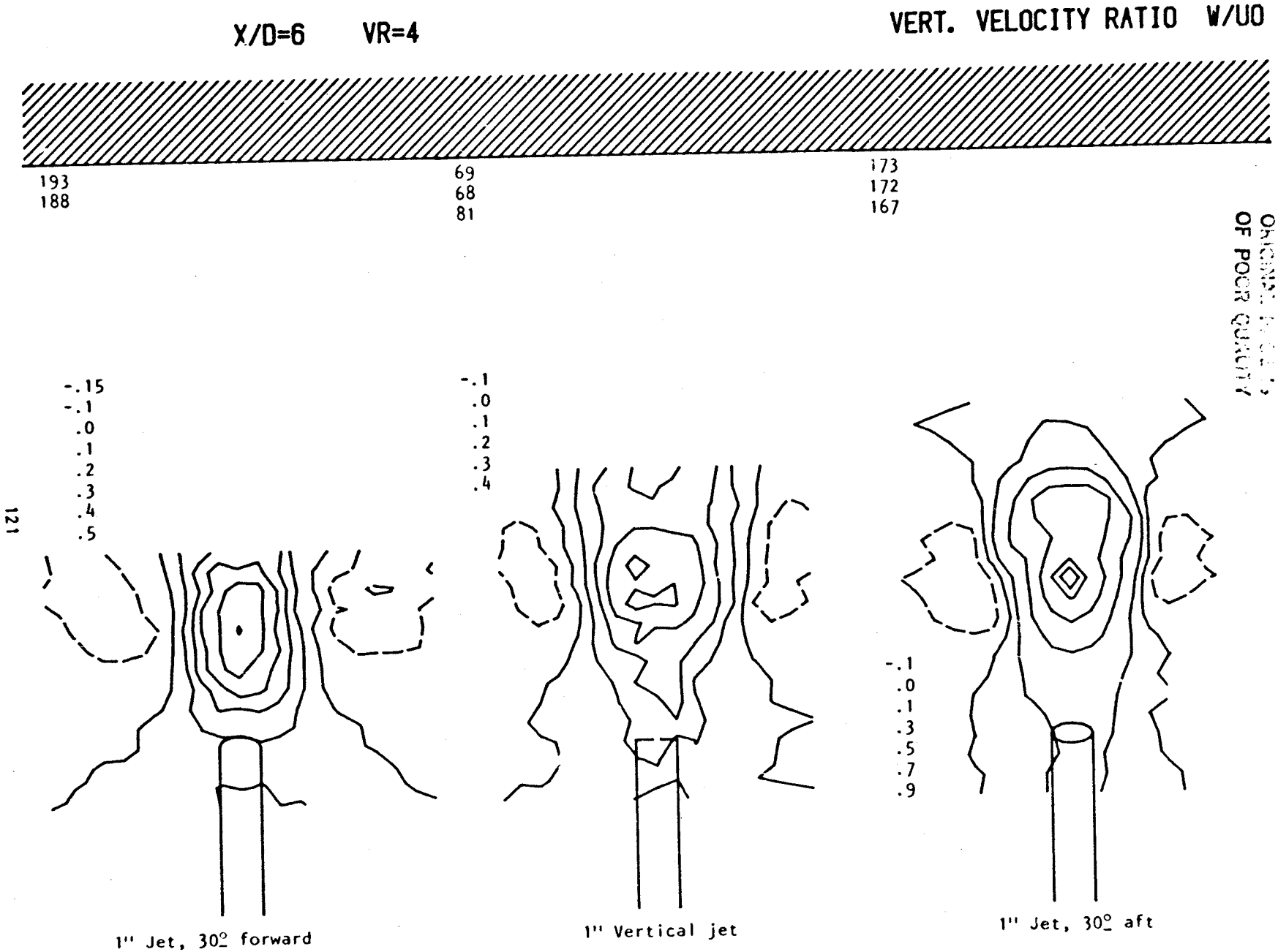

Figure A2 (continued) Effect of jet inclination on vertical velocities: R = 4

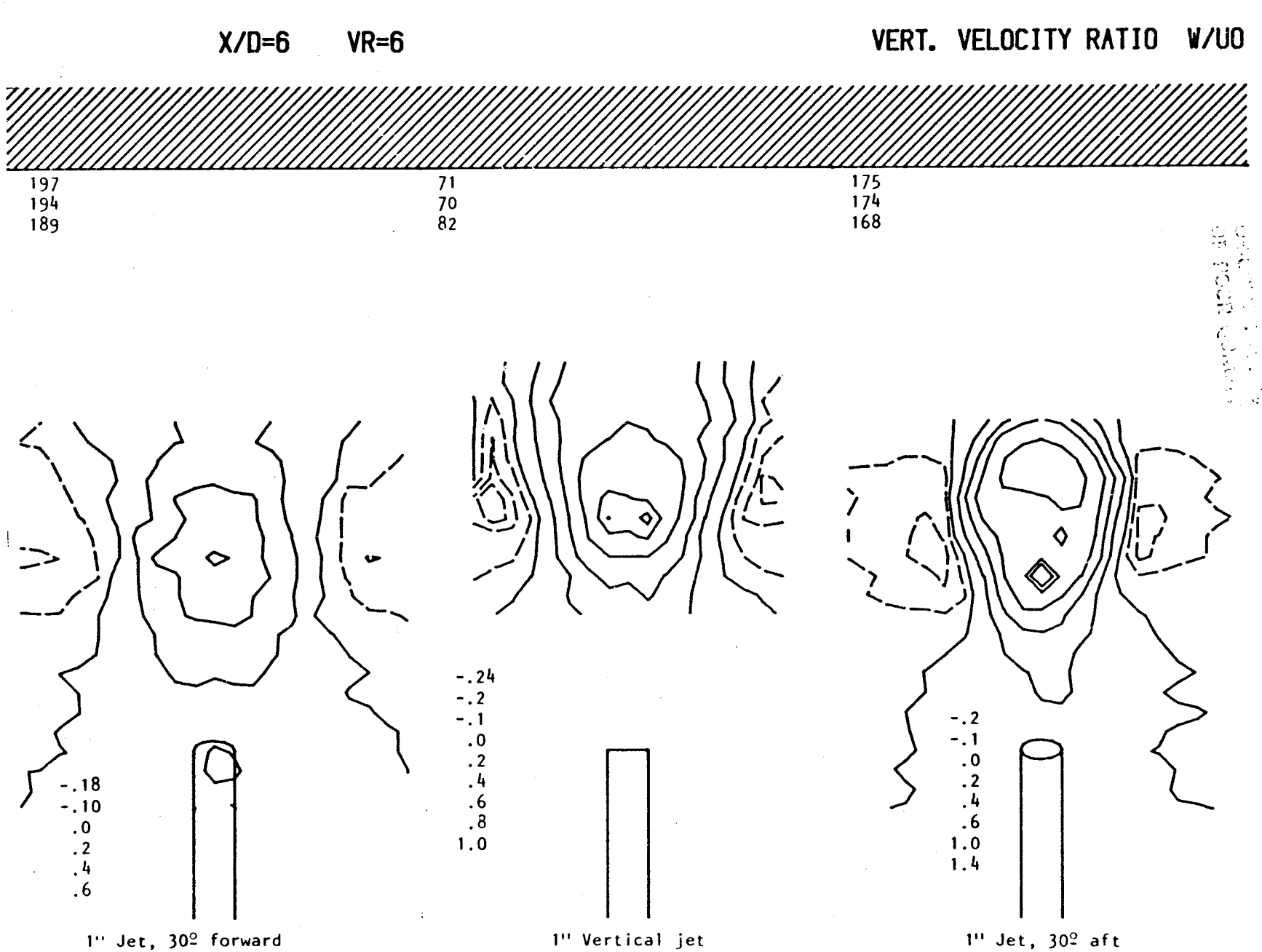

Figure A2 (continued) Effect of jet inclination on vertical velocities: R = 6

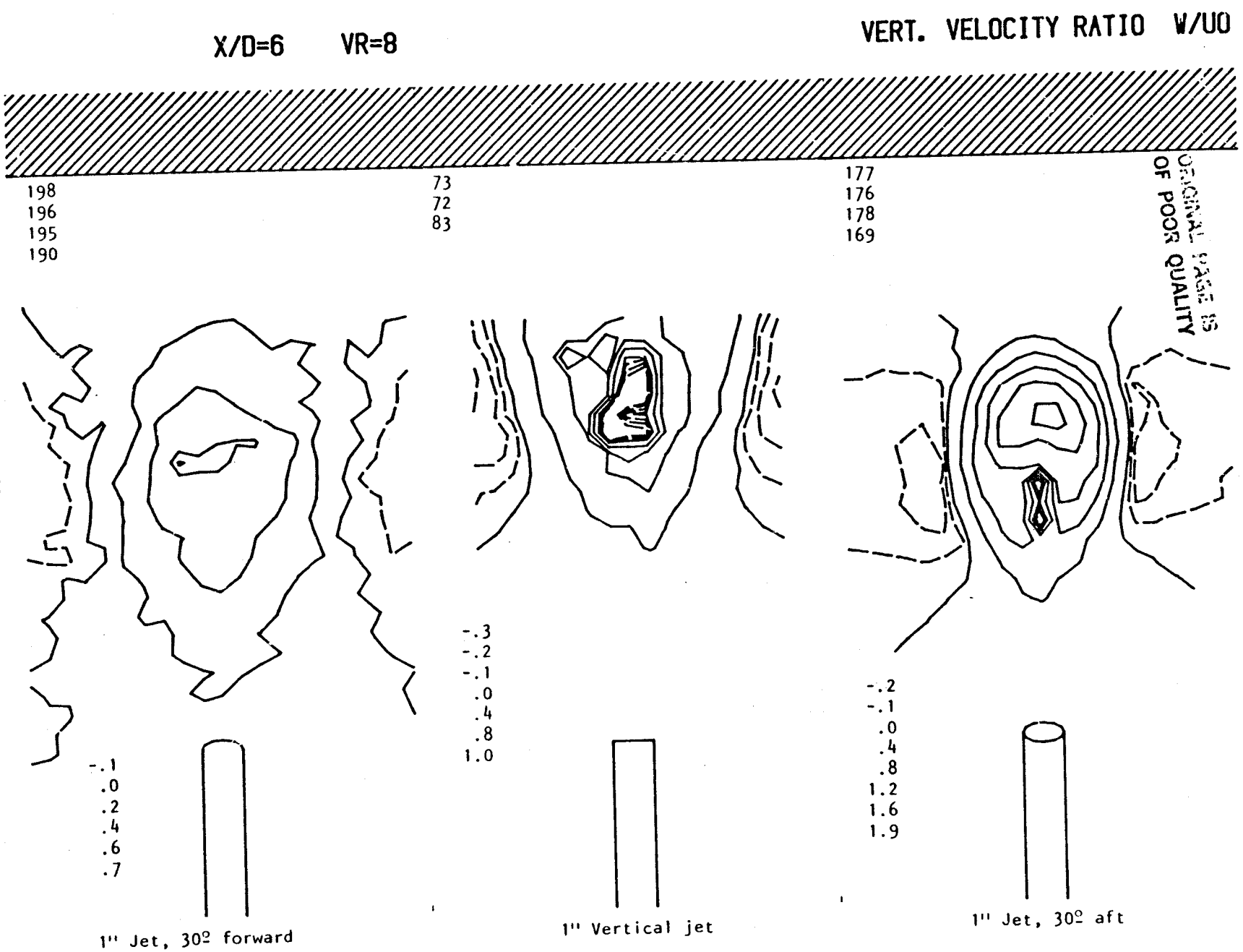

Figure A2 (concluded) Effect of jet inclination on vertical velocities: R = 8

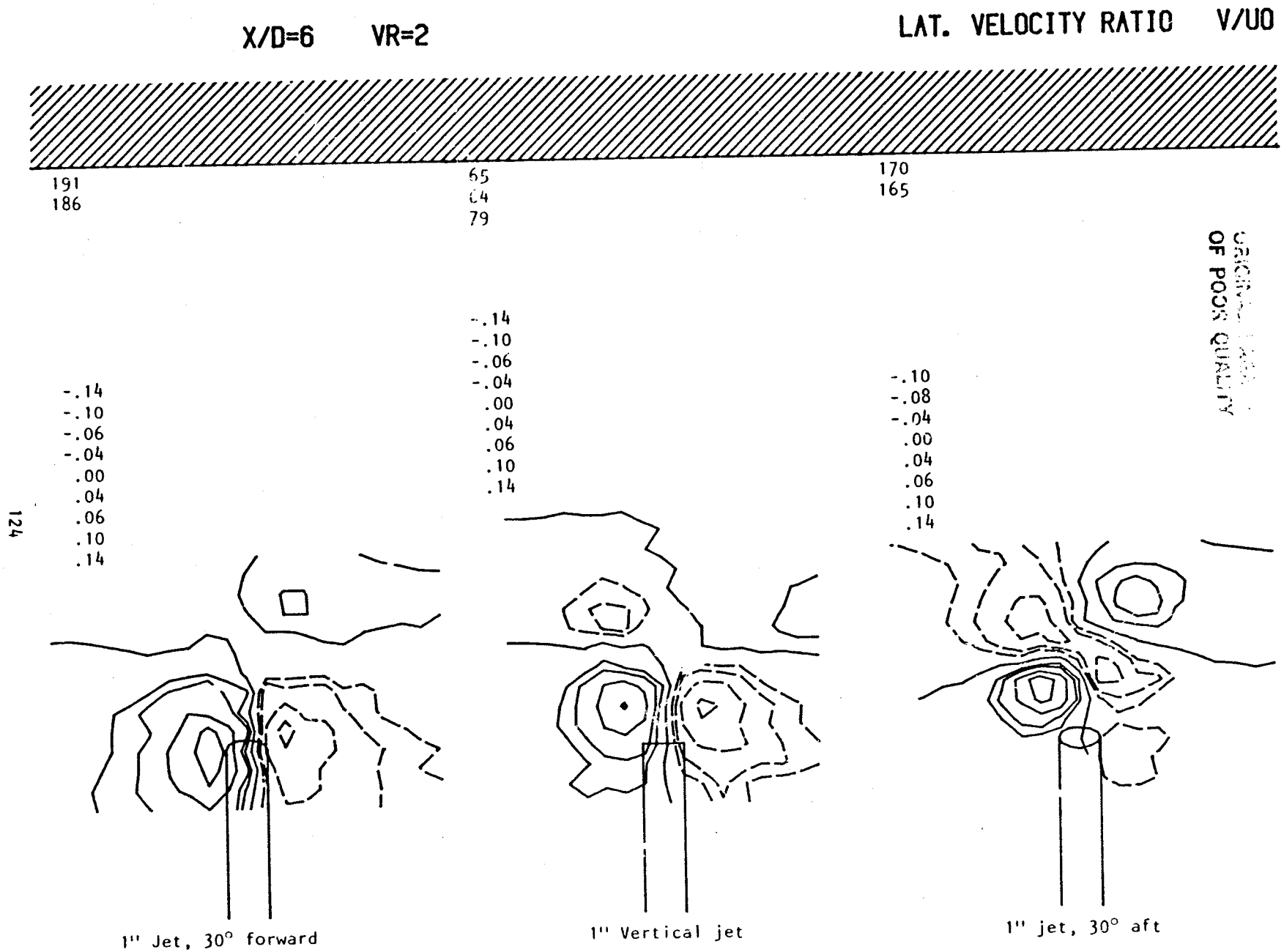

Figure A3 Effect of jet inclination on lateral velocities: R = 2

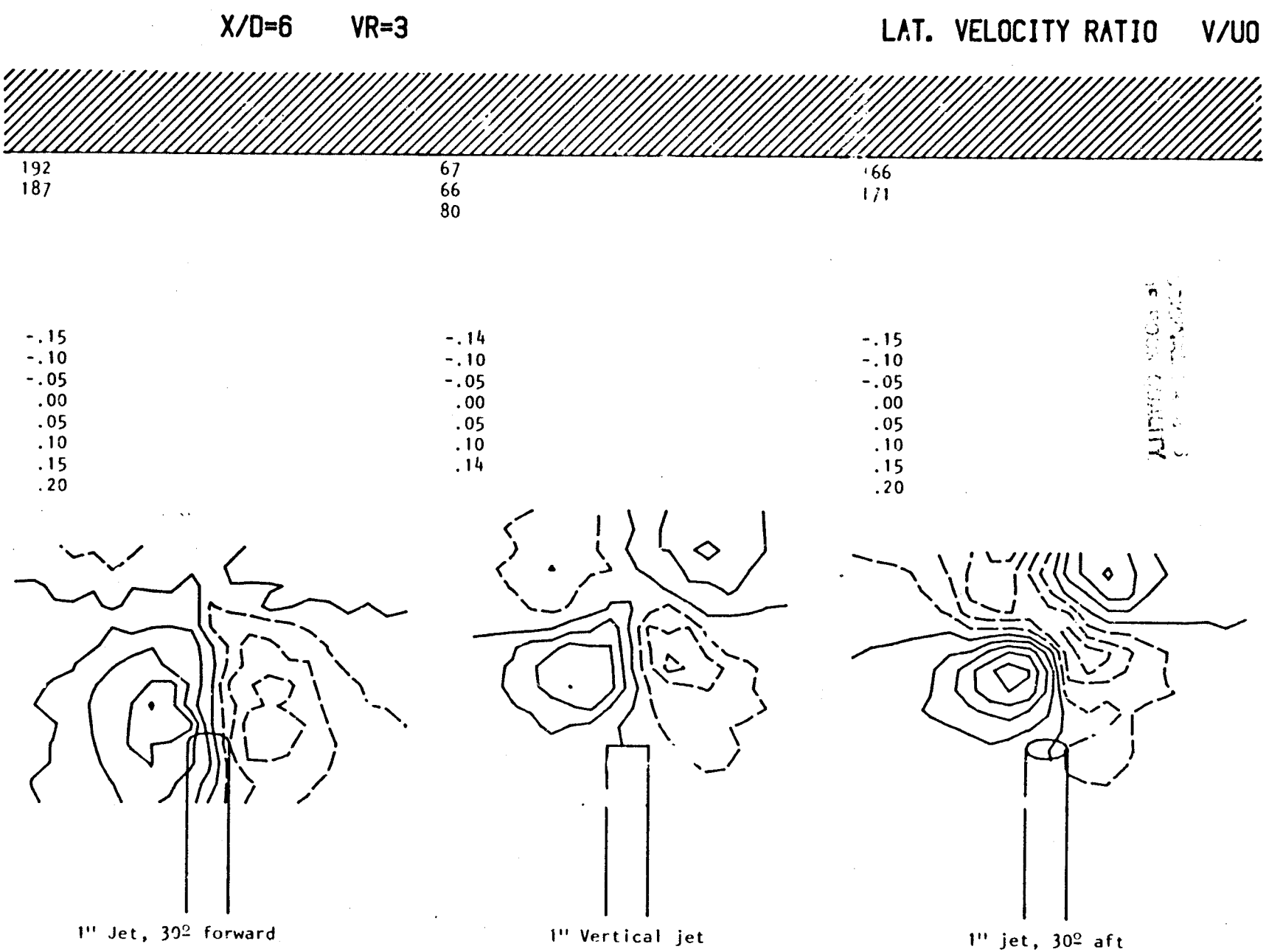

Figure A3 (continued) Effect of jet inclination on lateral velocities: R = 3

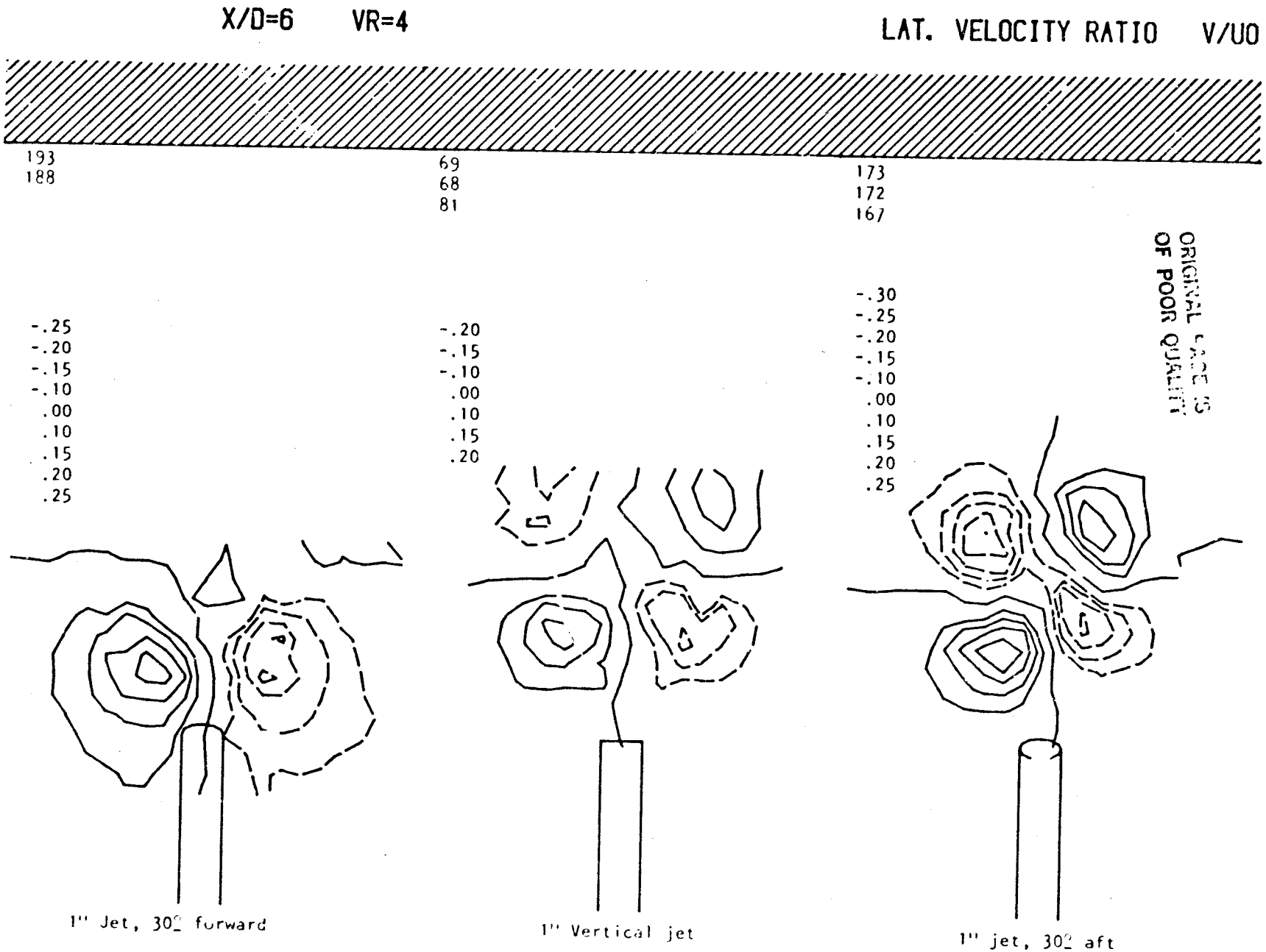

Figure A3 (continued) Effect of jet inclination on lateral velocities: R = 4

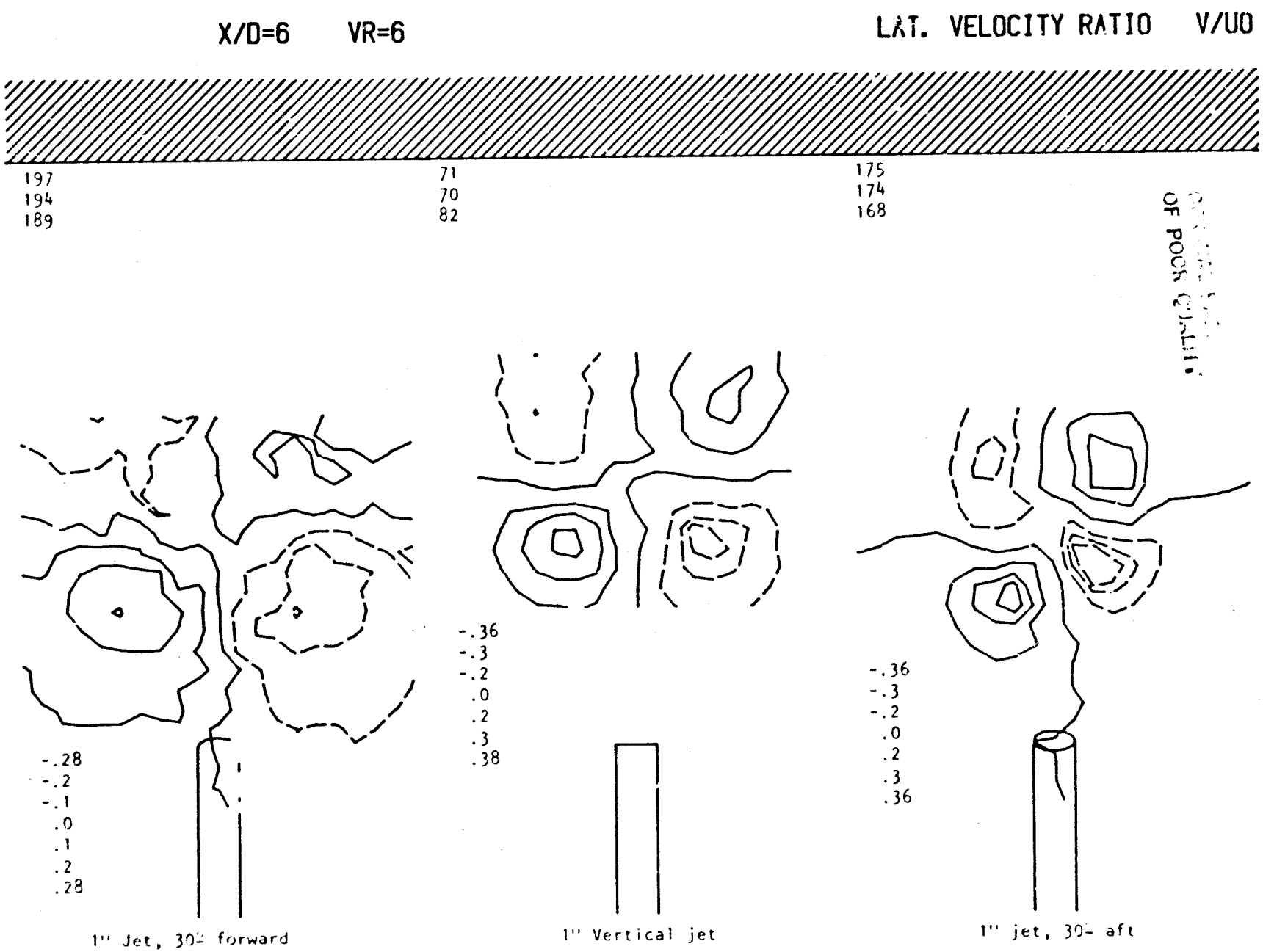

F'gure A3 (continued) Effect of jet inclination on lateral velocities: R = 6

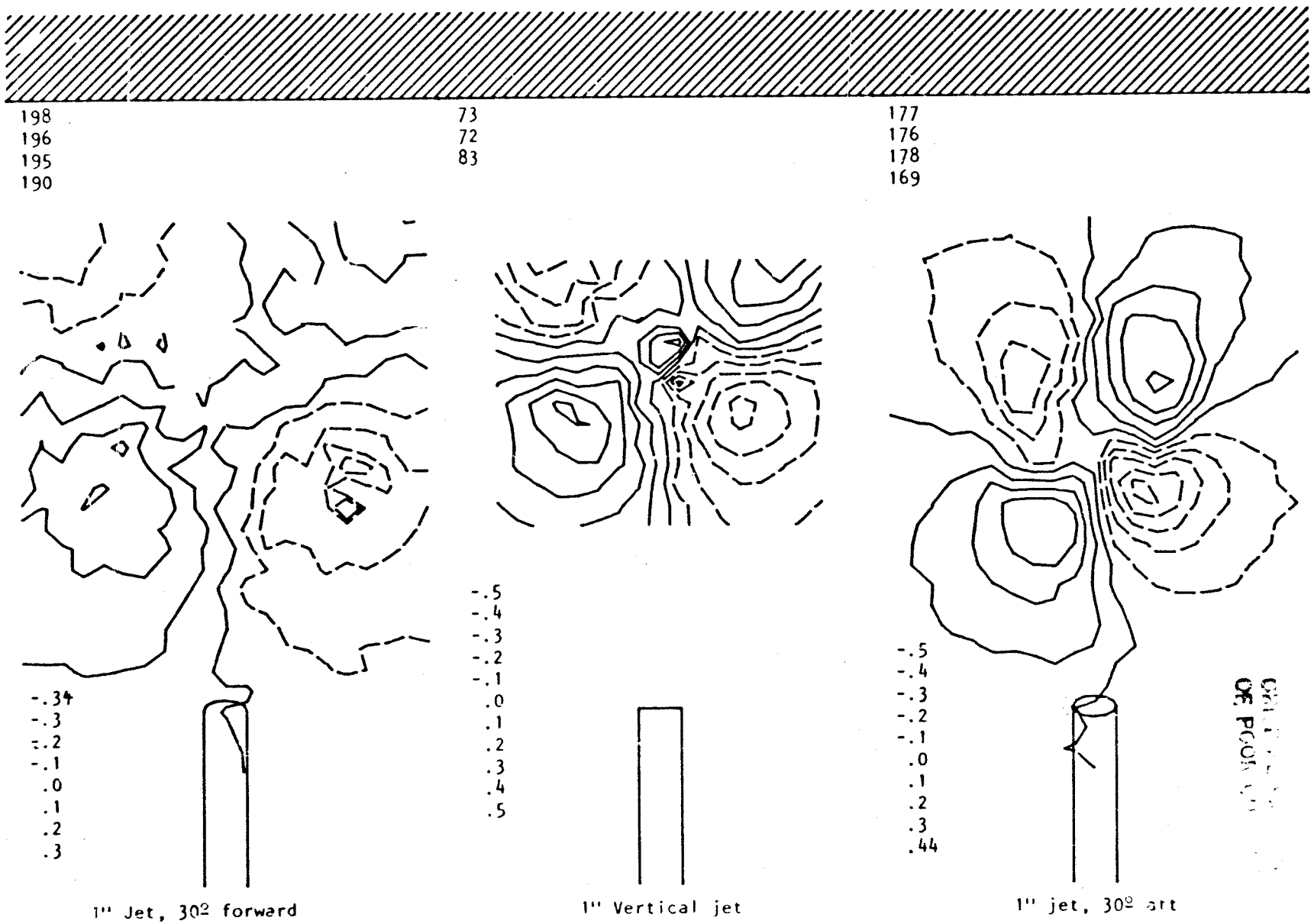

Figure A3 (concluded) Effect of jet inclination on lateral velocities: R = 8

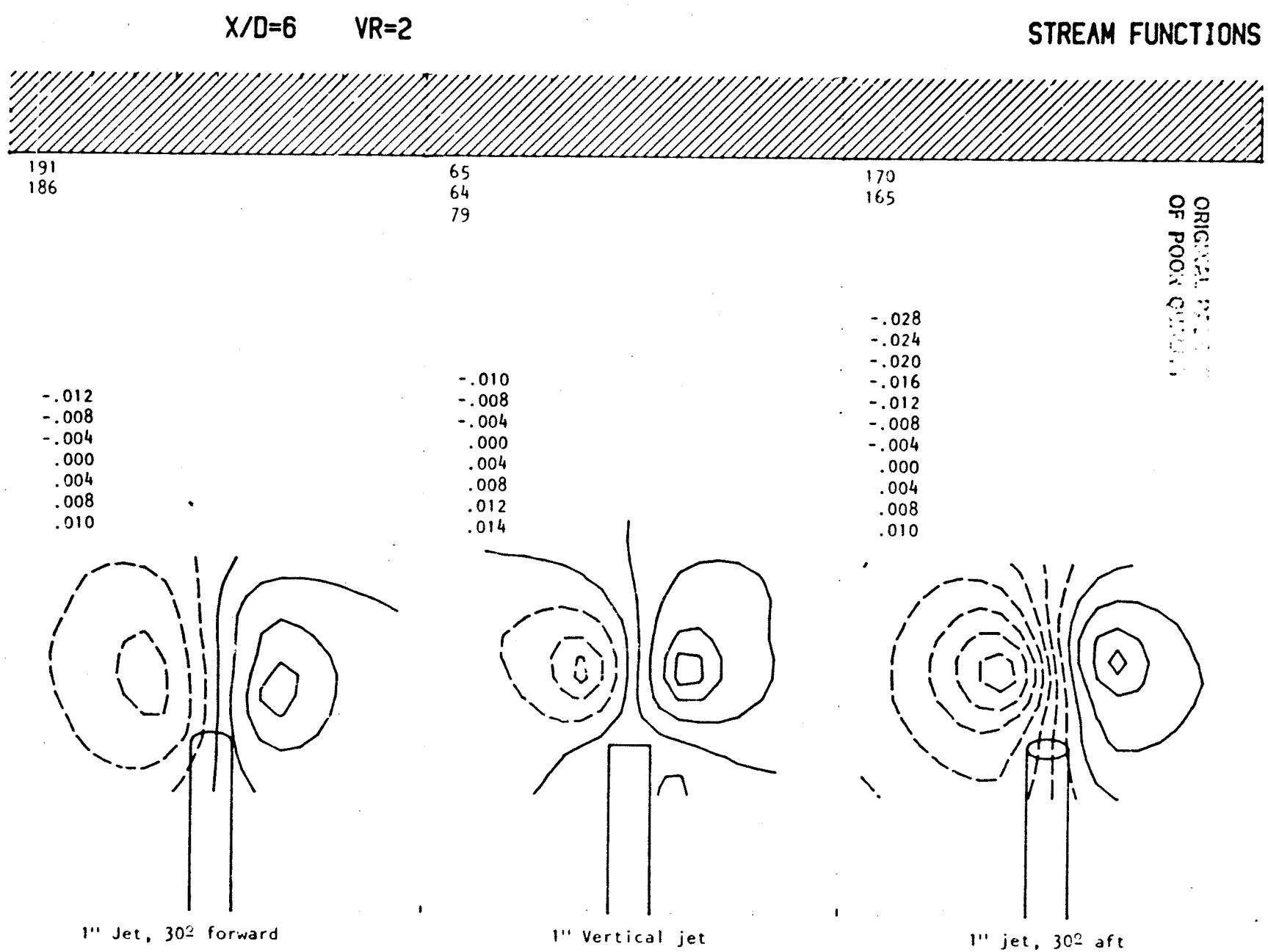

Figure A4 Effect of jet inclination on streamlines: R = 2

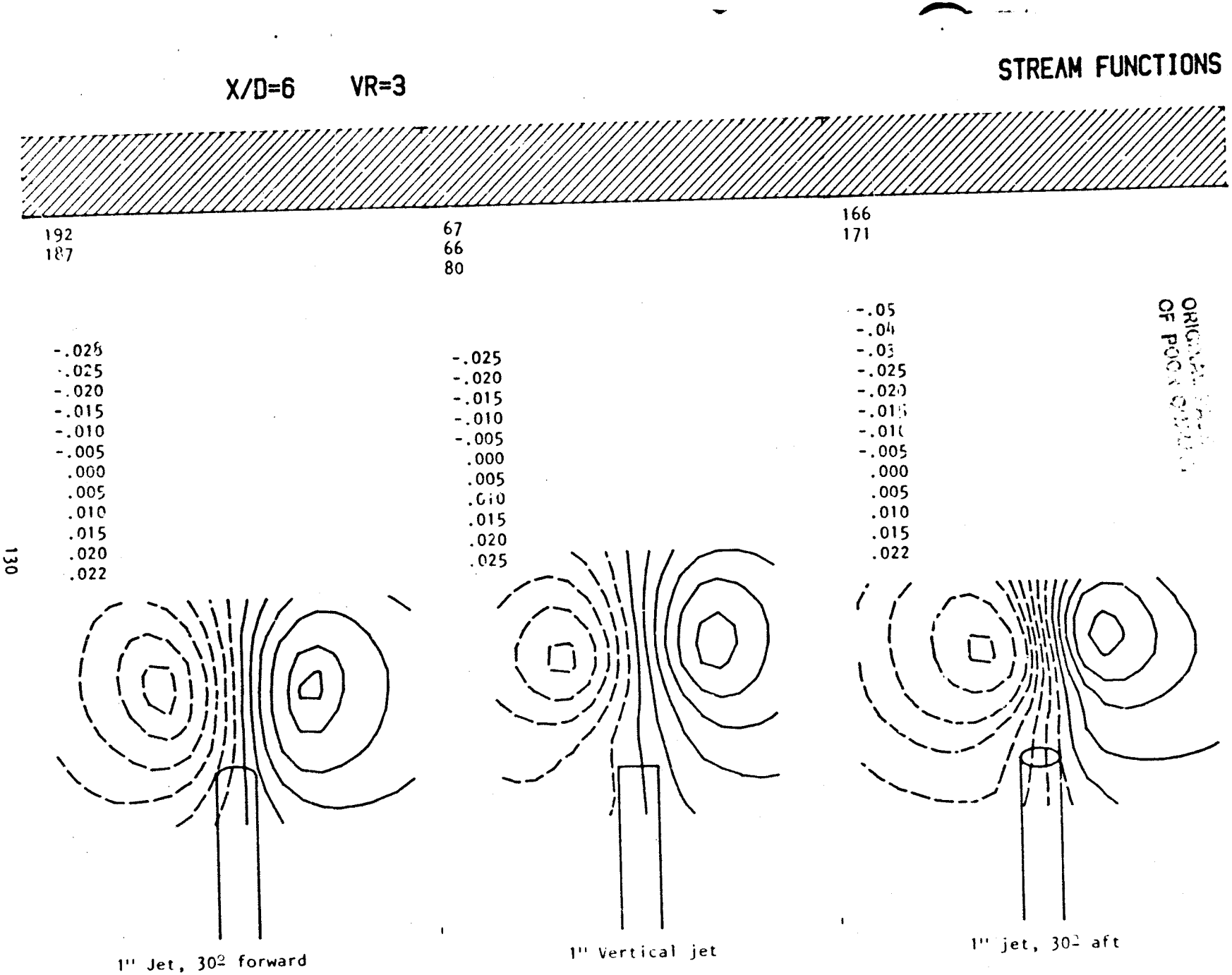

Figure A4 (continued) Effect of jet inclination on streamlines: R = 3

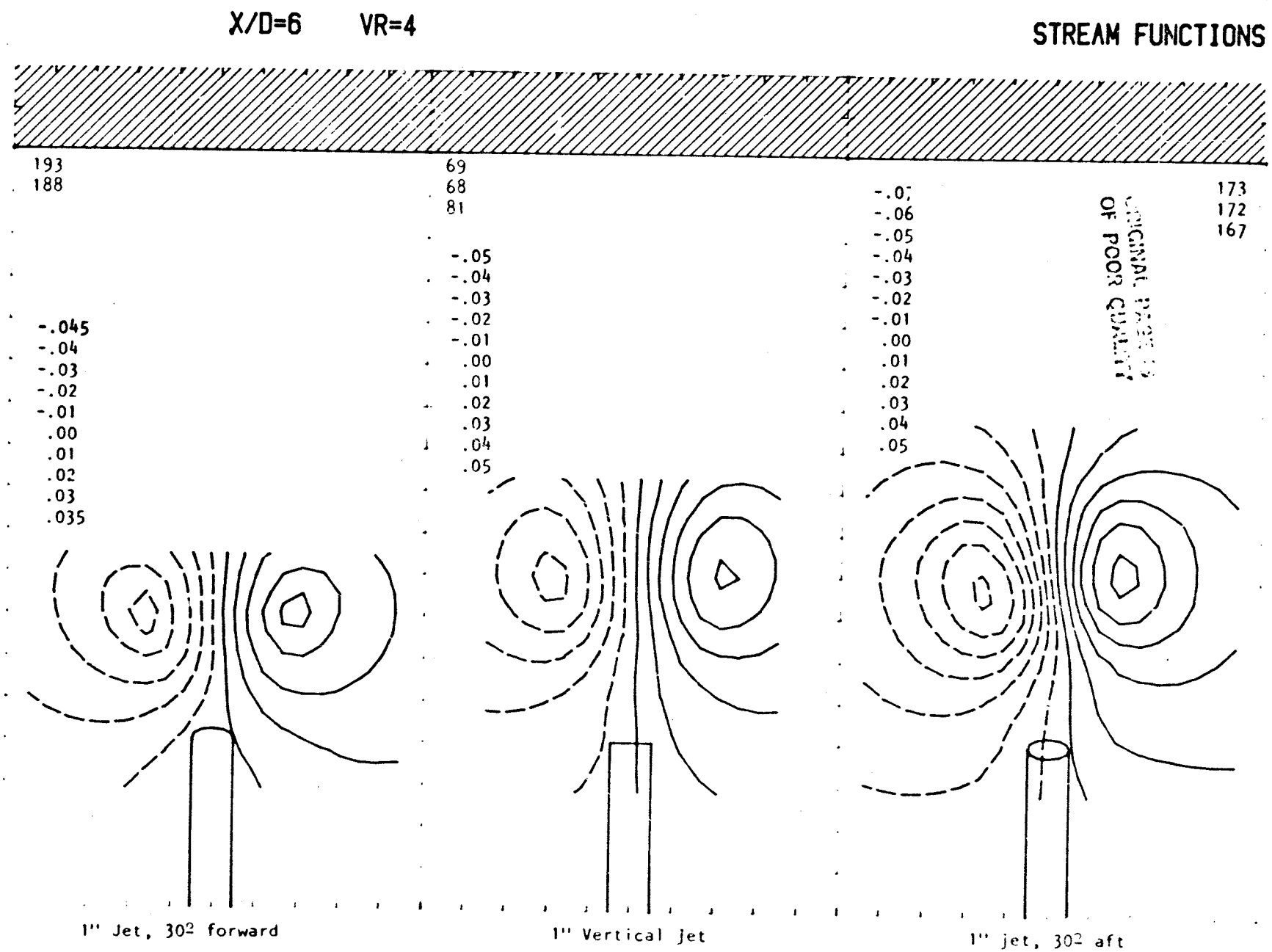

Figure A4 (continued) Effect of jet inclination on streamlines: R = 4

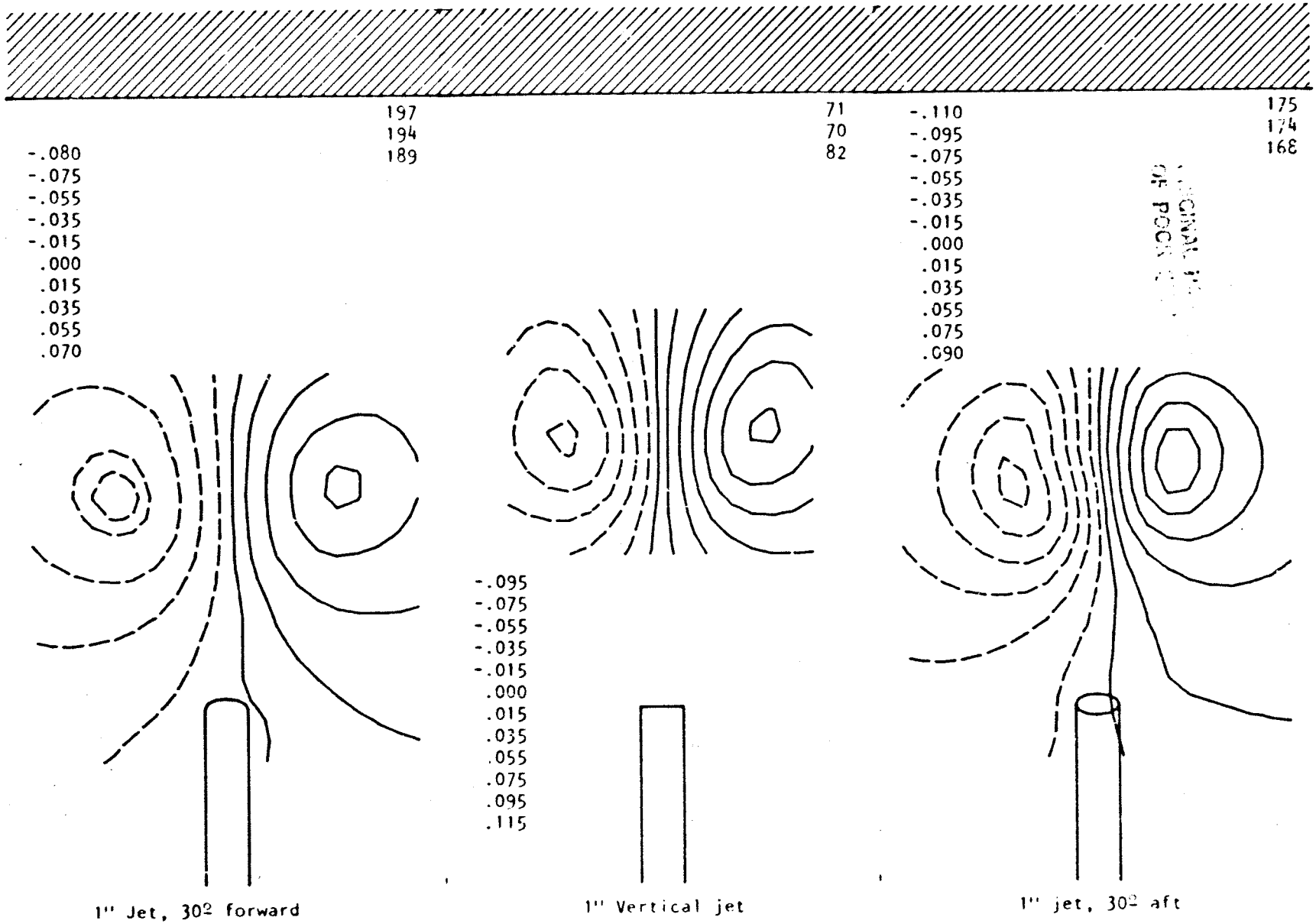

Figure A4 (continued) Effect of jet inclination on streamlines: R = 6

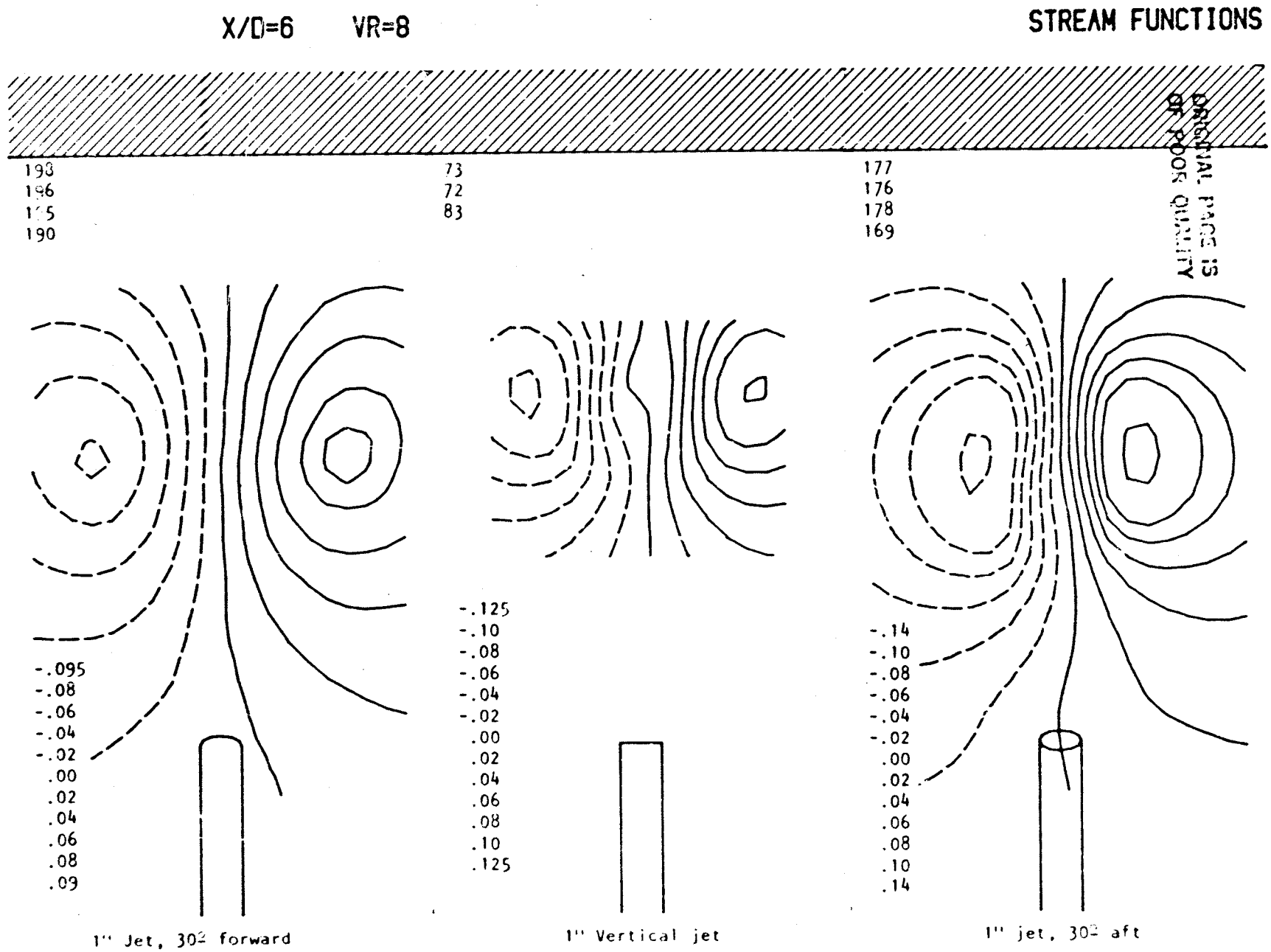

Figure A4 (concluded) Effect of jet inclination on streamlines: R = 8

APPENDIX B

WAKE TRAVERSE DATA FOR ONE-INCH, THREE-INCH AND SQUARE-PROFILE JETS

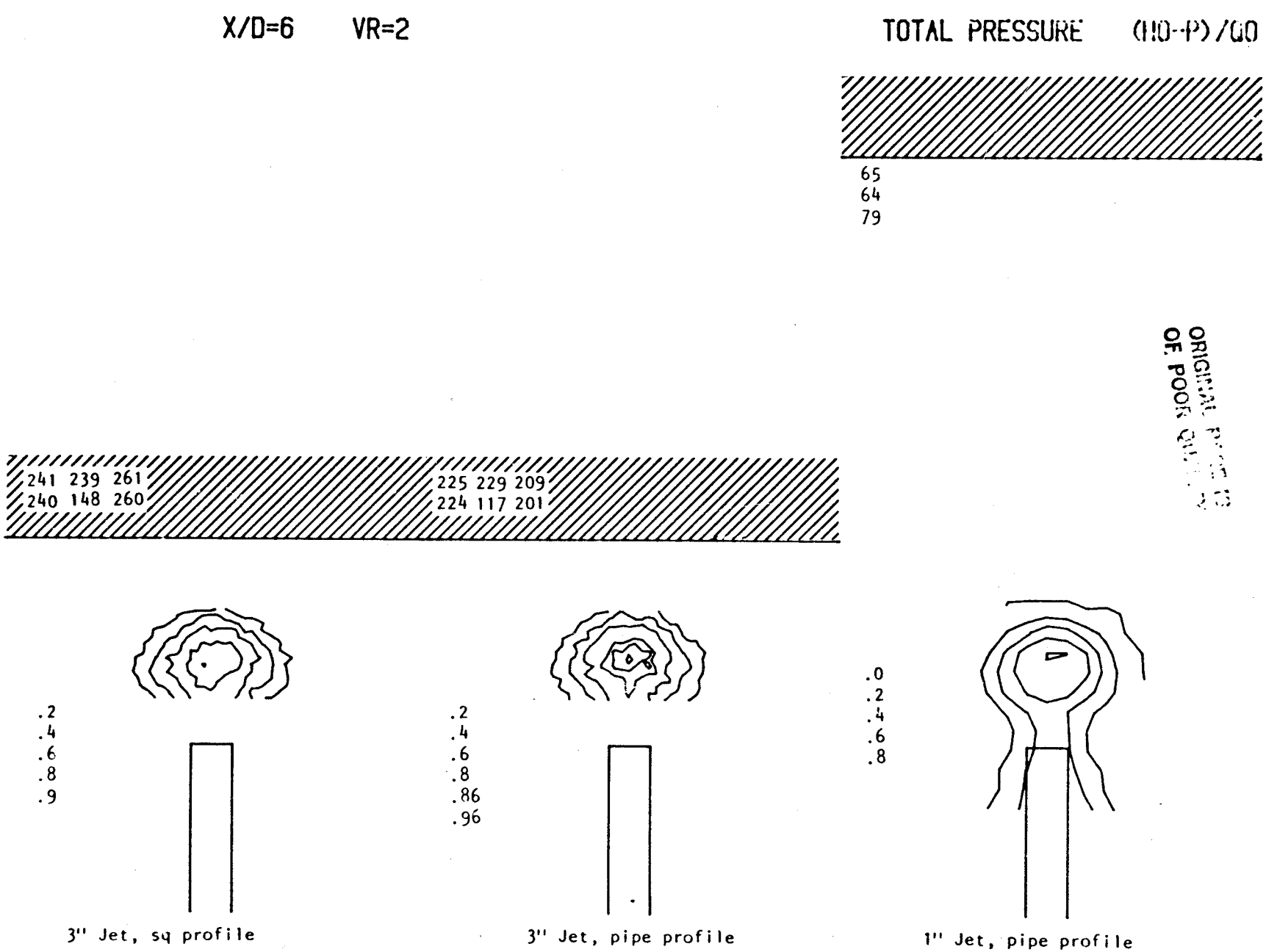

Figure B1 Effect of jet profile and size on total pressures: R = ?

VR=3

TOTAL PRESSURE (110-P)/00

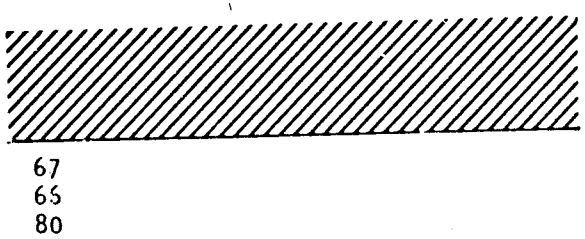

67
65
80

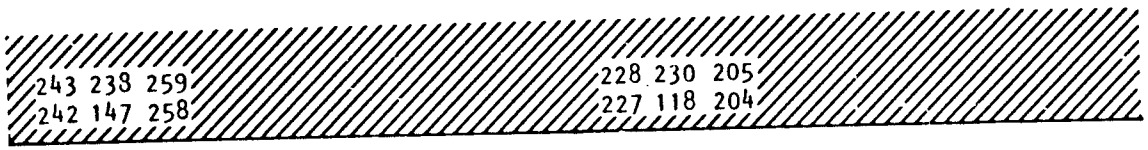

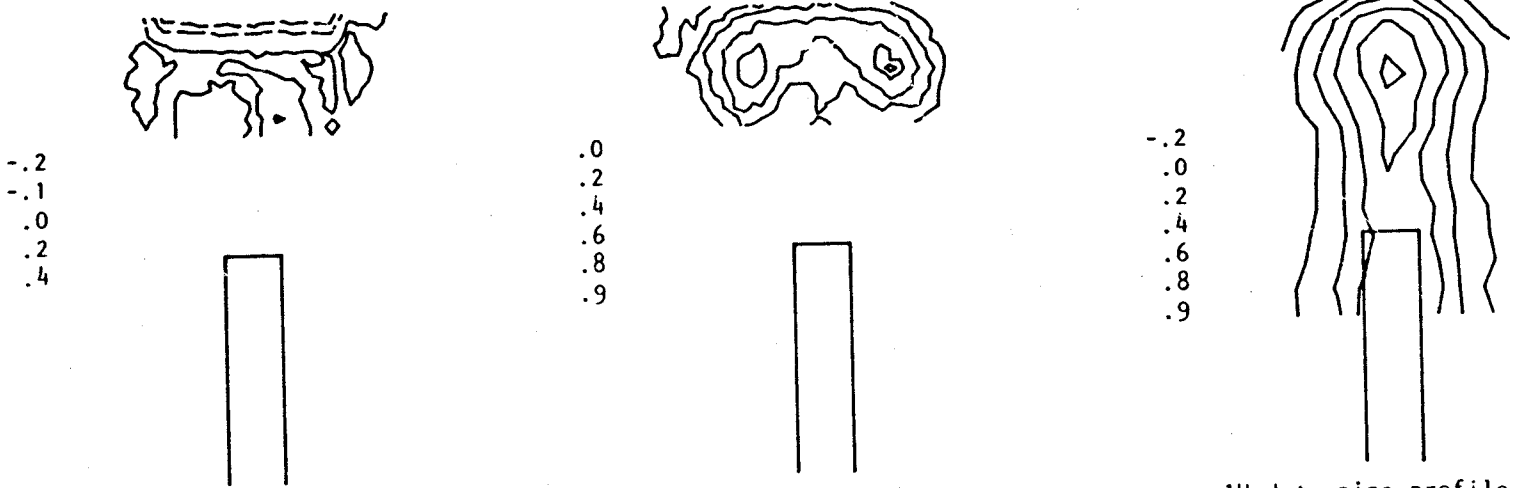

3" Jet, sq profile

3" Jet, pipe profile

1" Jet, pipe profile

Figure B1 (continued) Effect of jet profile and size on total pressures: R = 3

X/D=6 VR=4

TOTAL PRESSURE (110-P)/Q0

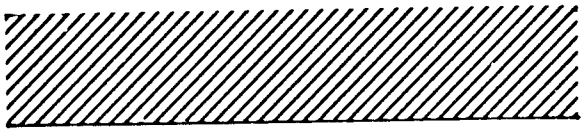

69
68
81

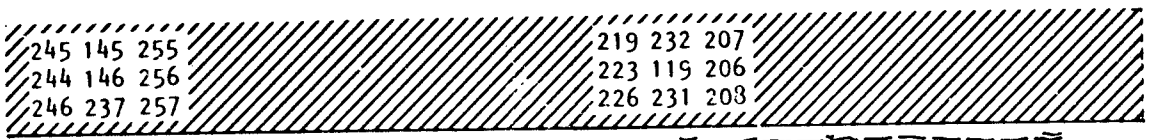

245 145 255
244 146 256
246 237 257

219 232 207
223 119 206
226 231 208

-1.2
-.6
.0
.2
.4
.6
.8

-1.0
-.6
.0
.2
.4
.6
.8

-.3
.0
.2
.4
.6
.8

3" Jet, sq profile

3" Jet, pipe profile

1" Jet, pipe profile

Figure B1 (continued) Effect of jet profile and size on total pressures: R = 4

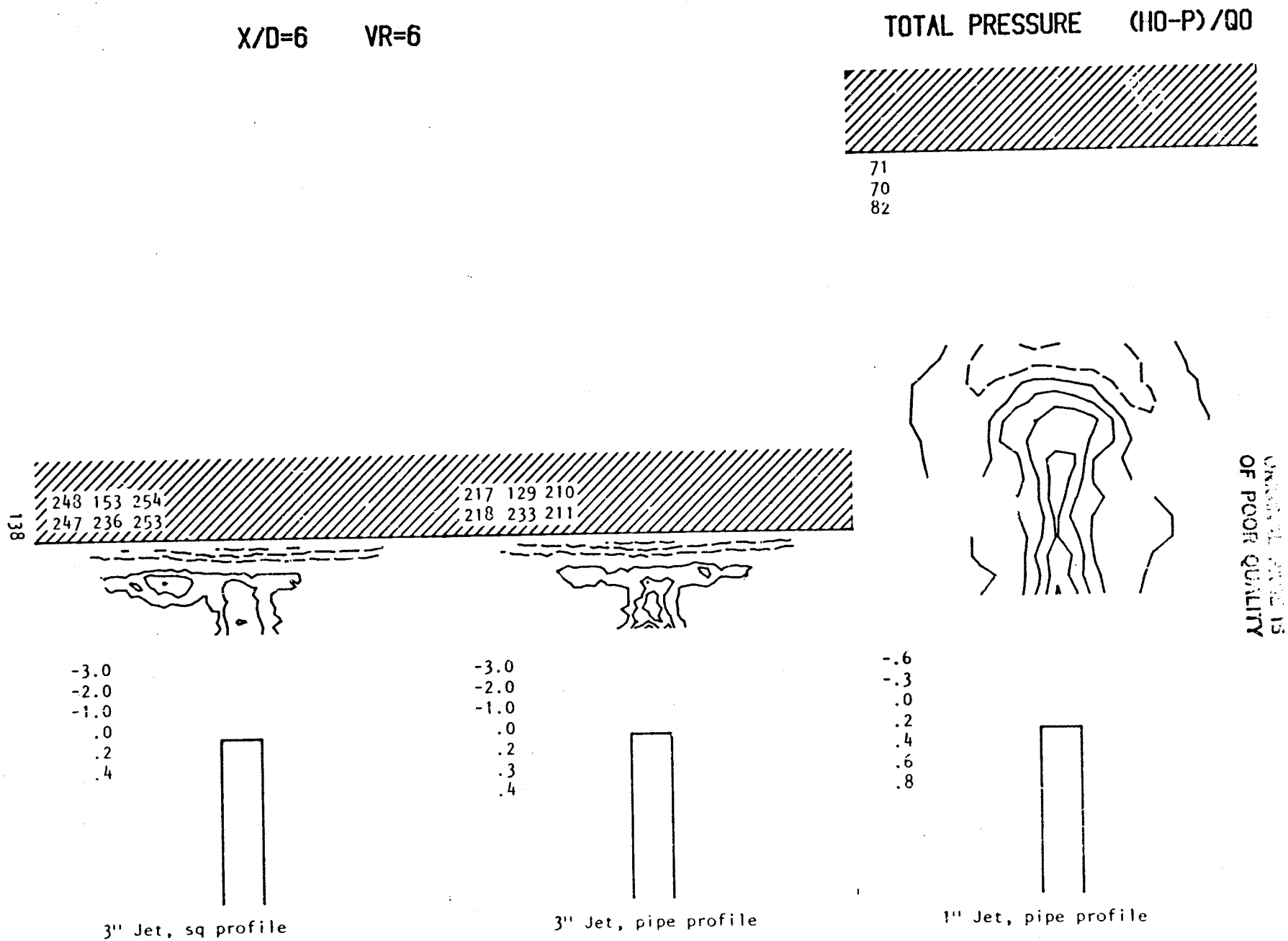

Figure B1 (continued) Effect of jet profile and size on total pressures: R = 6

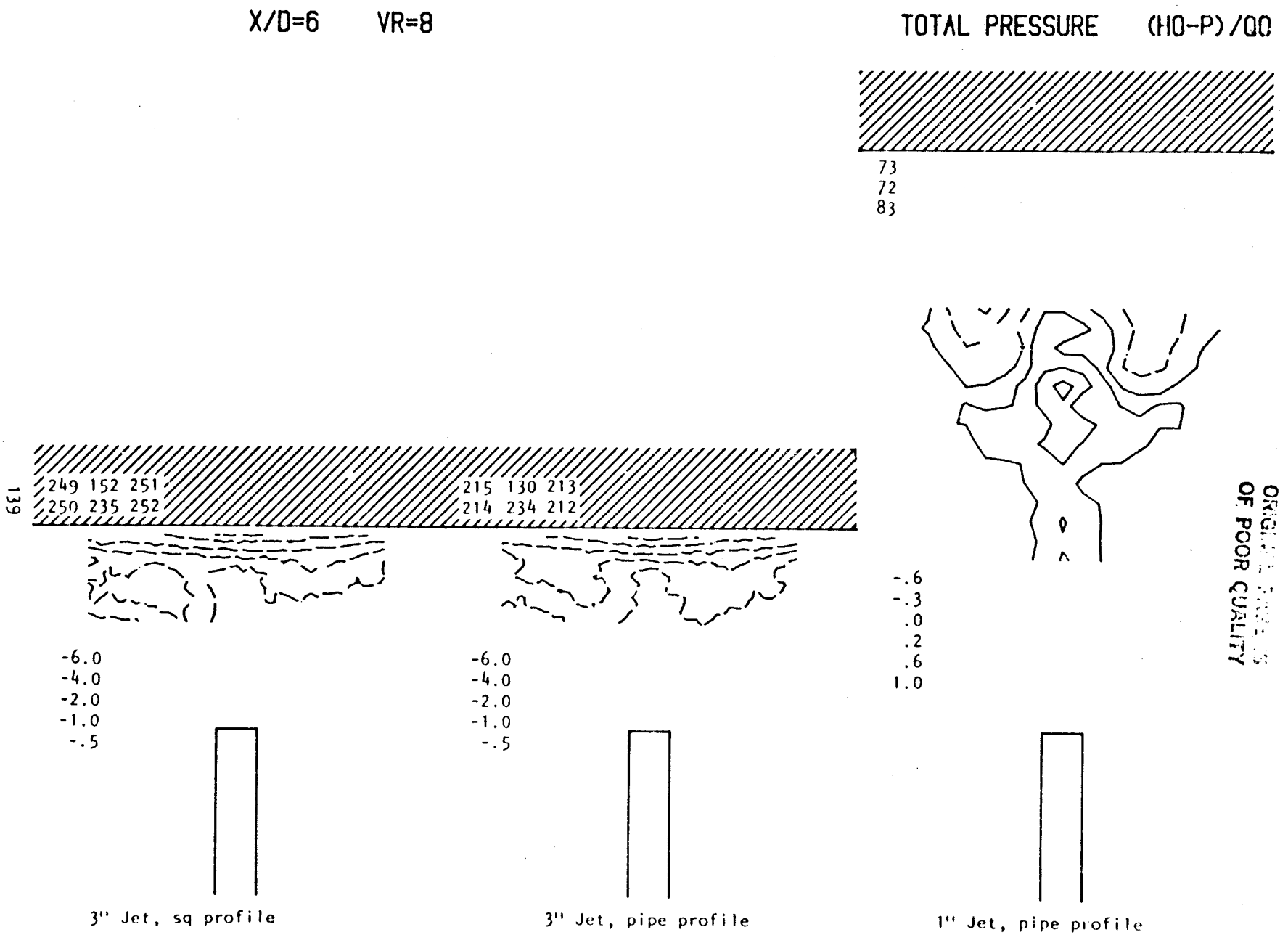

Figure B1 (concluded) Effect of jet profile and size on total pressures: R = 8

X/D=6 VR=2

VERT. VELOCITY RATIO W/UO

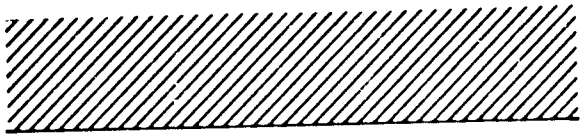

65
64
79

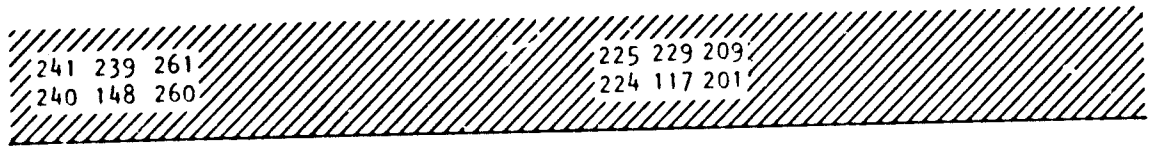

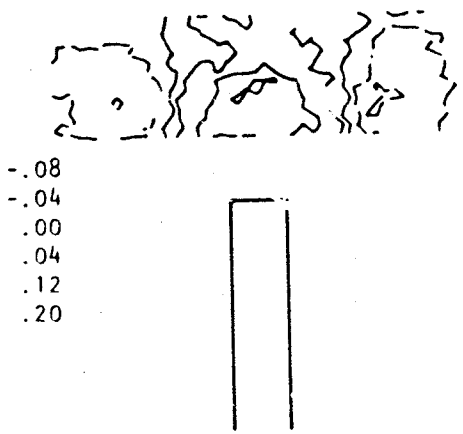

3" Jet, sq profile

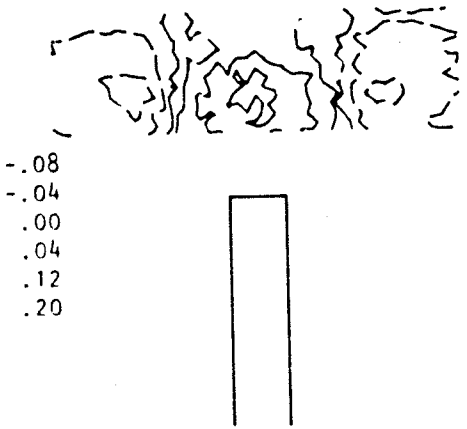

3" Jet, pipe profile

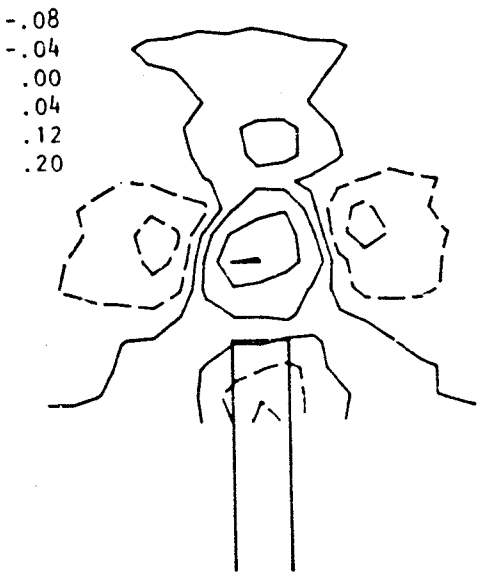

1" Jet, pipe profile

Figure B2 Effect of jet profile and size on vertical velocities: R = 2

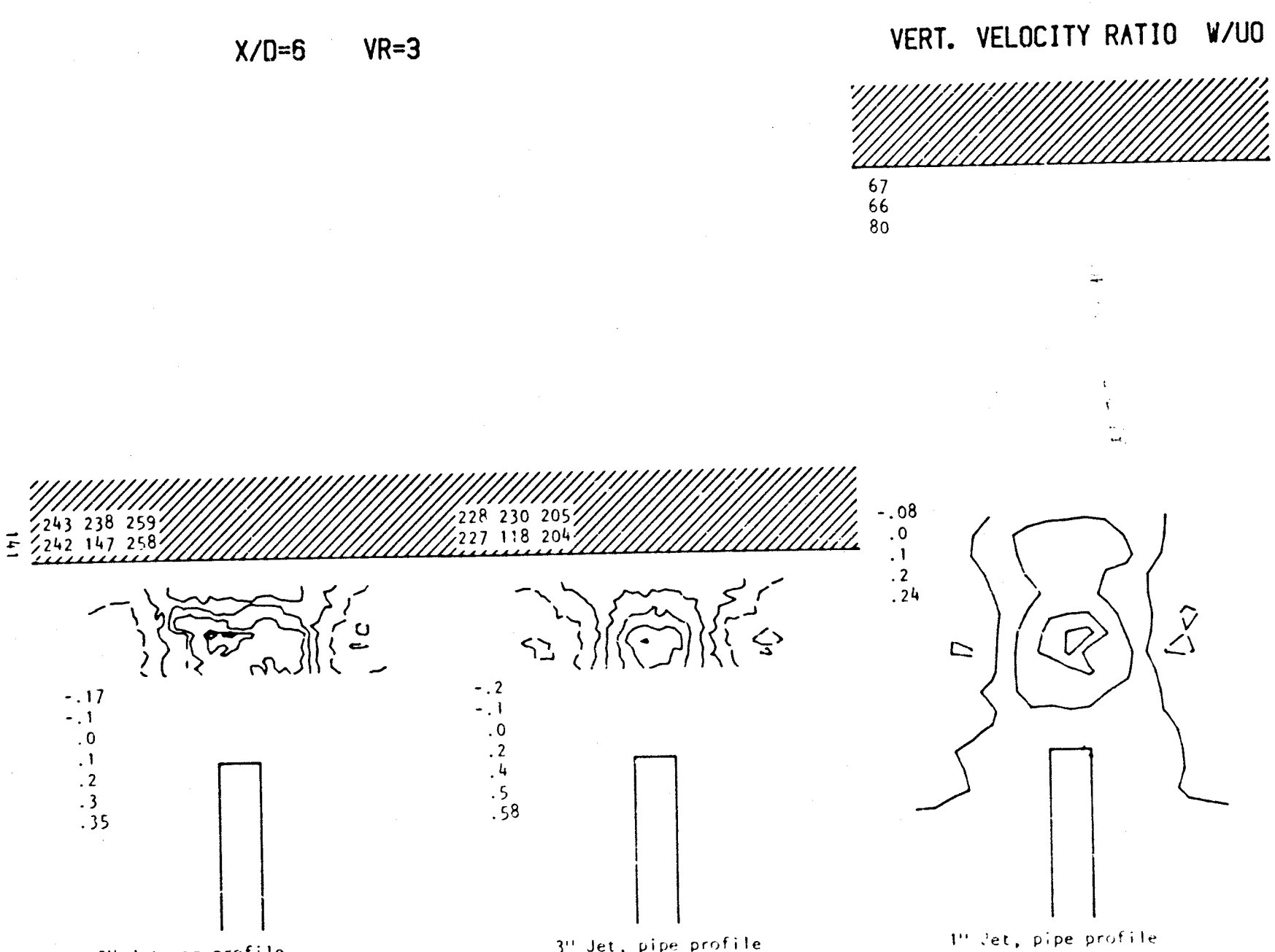

Figure 82 (continued) Effect of jet profile and size on vertical velocities: R = 3

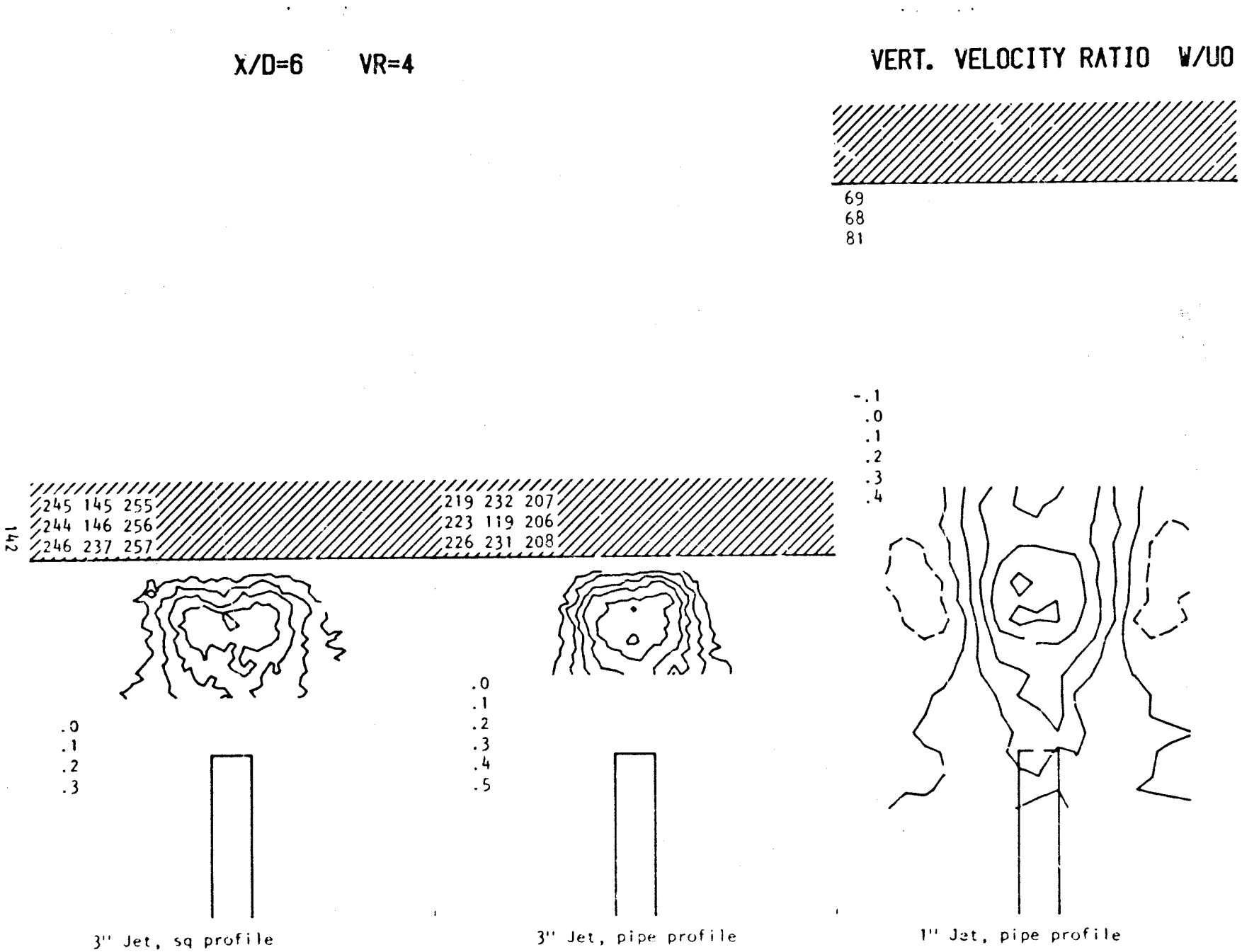

Figure B2 (continued) Effect of jet profile and size on vertical velocities: R = 4

X/D=6 VR=6

VERT. VELOCITY RATIO W/UO

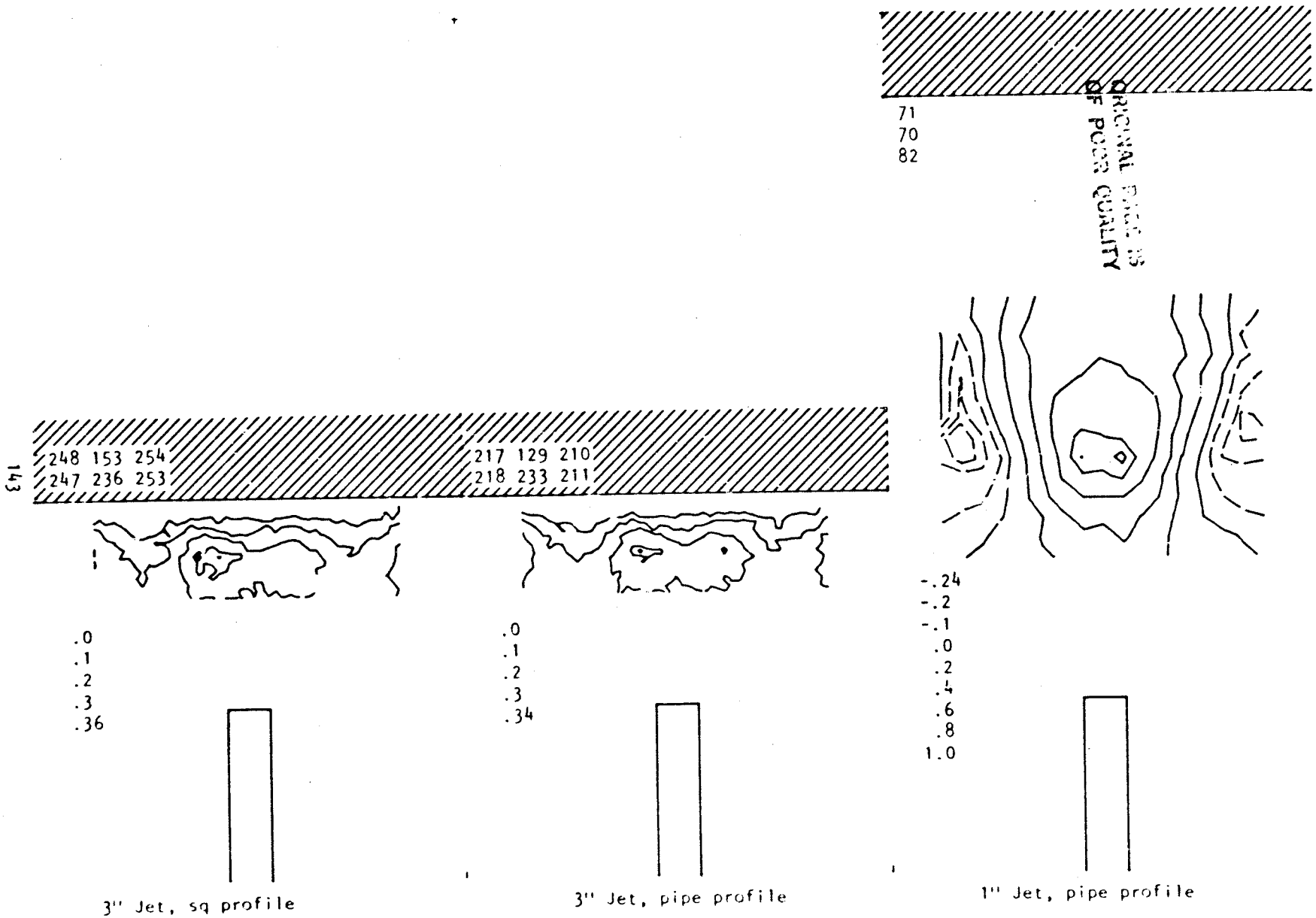

Figure B2 (continued) Effect of jet profile and size on vertical velocities: R = 6

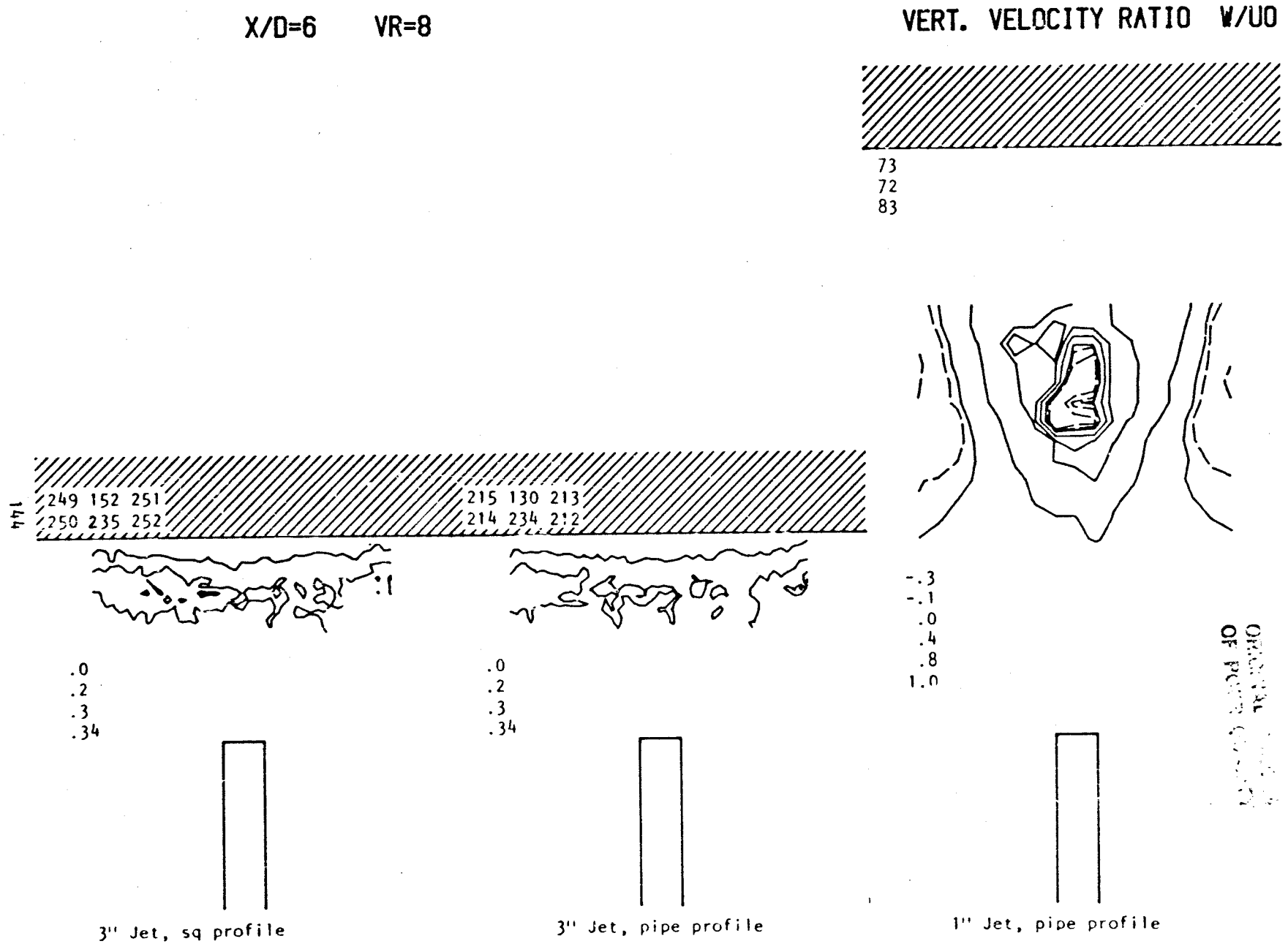

Figure B2 (concluded) Effect of jet profile and size on vertical velocities: R = 8

X/D=6 VR=2

LAT. VELOCITY RATIO V/UO

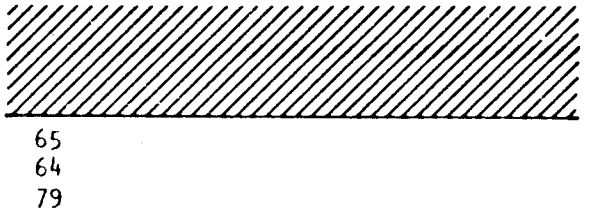

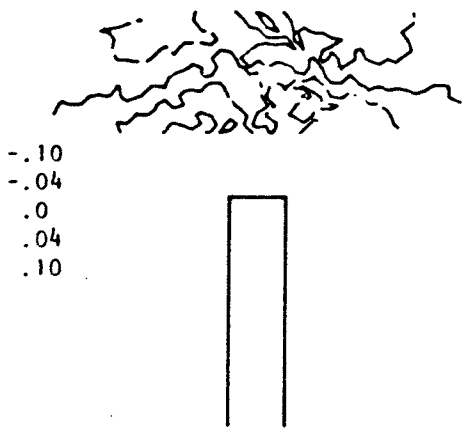

3" Jet, sq profile

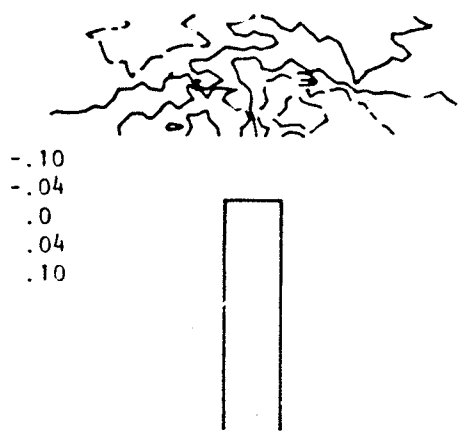

3" Jet, pipe profile

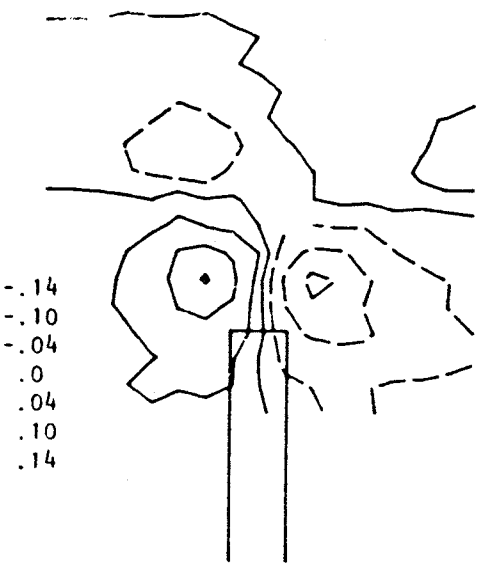

1" Jet, pipe profile

Figure B3 Effect of jet profile and size on lateral velocities: R = 2

X/D=6 VR=3

LAT. VELOCITY RATIO V/UO

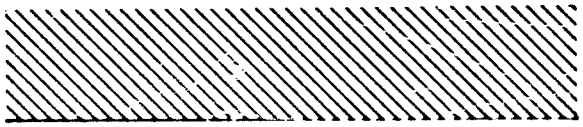

67
66
80

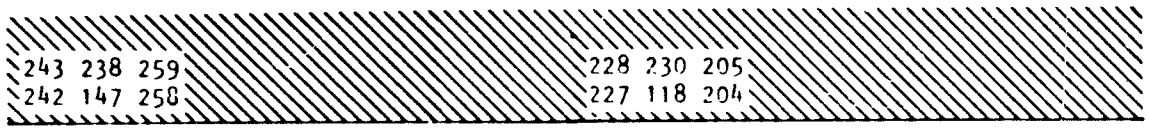

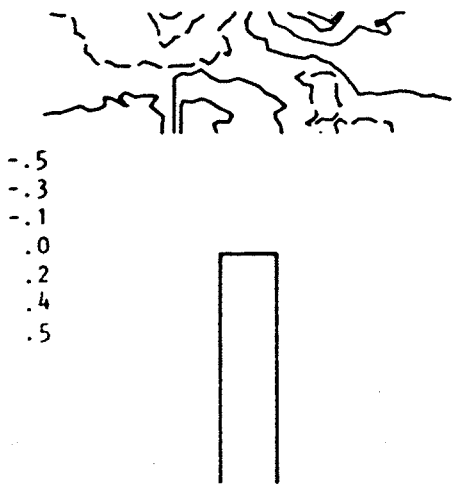

3" Jet, sq profile

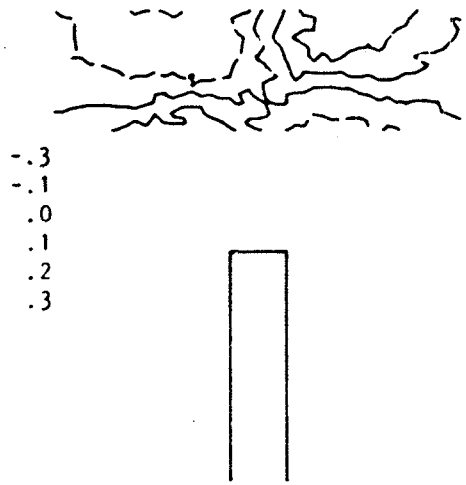

3" Jet, pipe profile

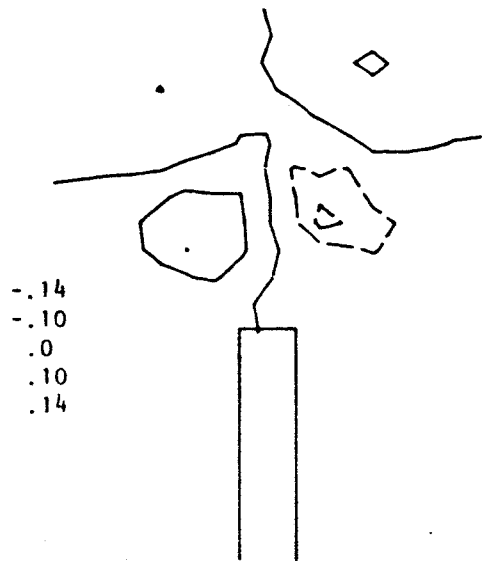

1" Jet, pipe profile

Figure B3 (continued) Effect of jet profile and size on lateral velocities: R = 3

X/D=6 VR=4

LAT. VELOCITY RATIO V/UO

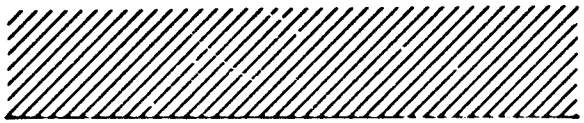

69
68
81

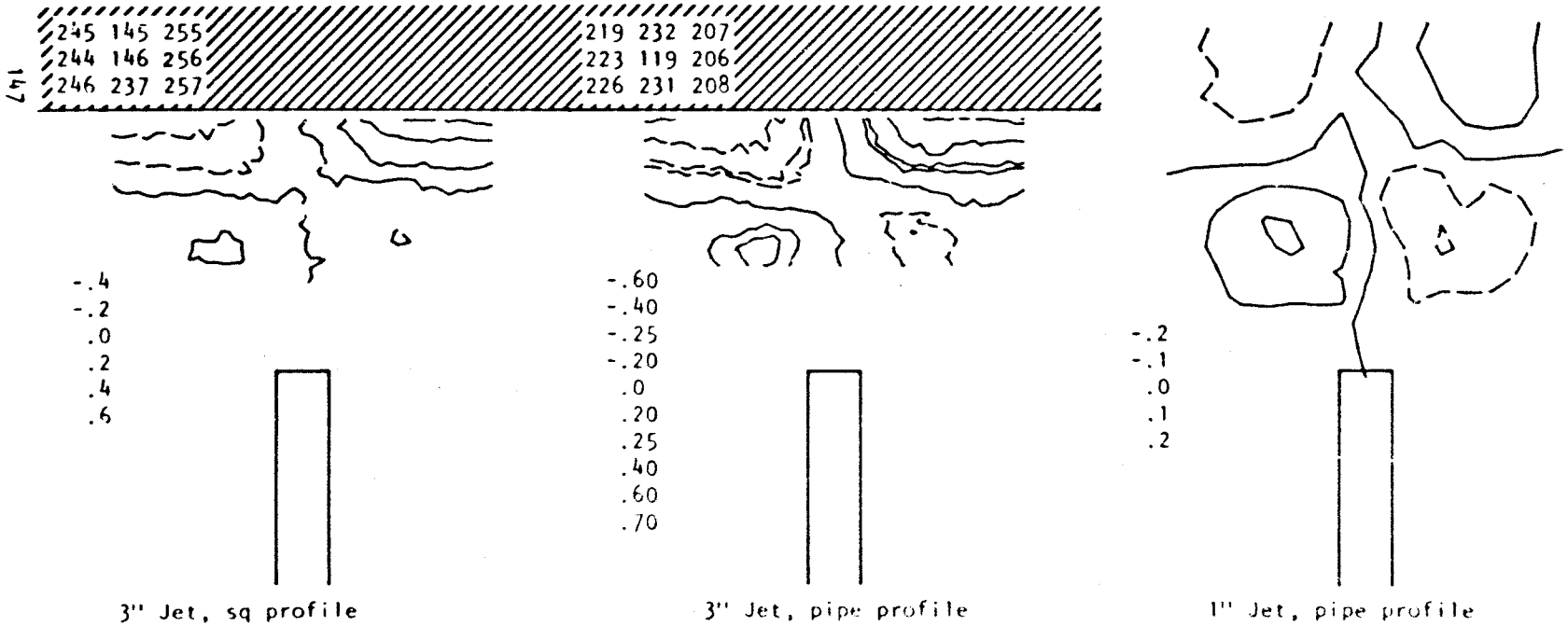

3" Jet, sq profile

3" Jet, pipe profile

1" Jet, pipe profile

Figure B3 (continued) Effect of jet profile and size on lateral velocities: R = 4

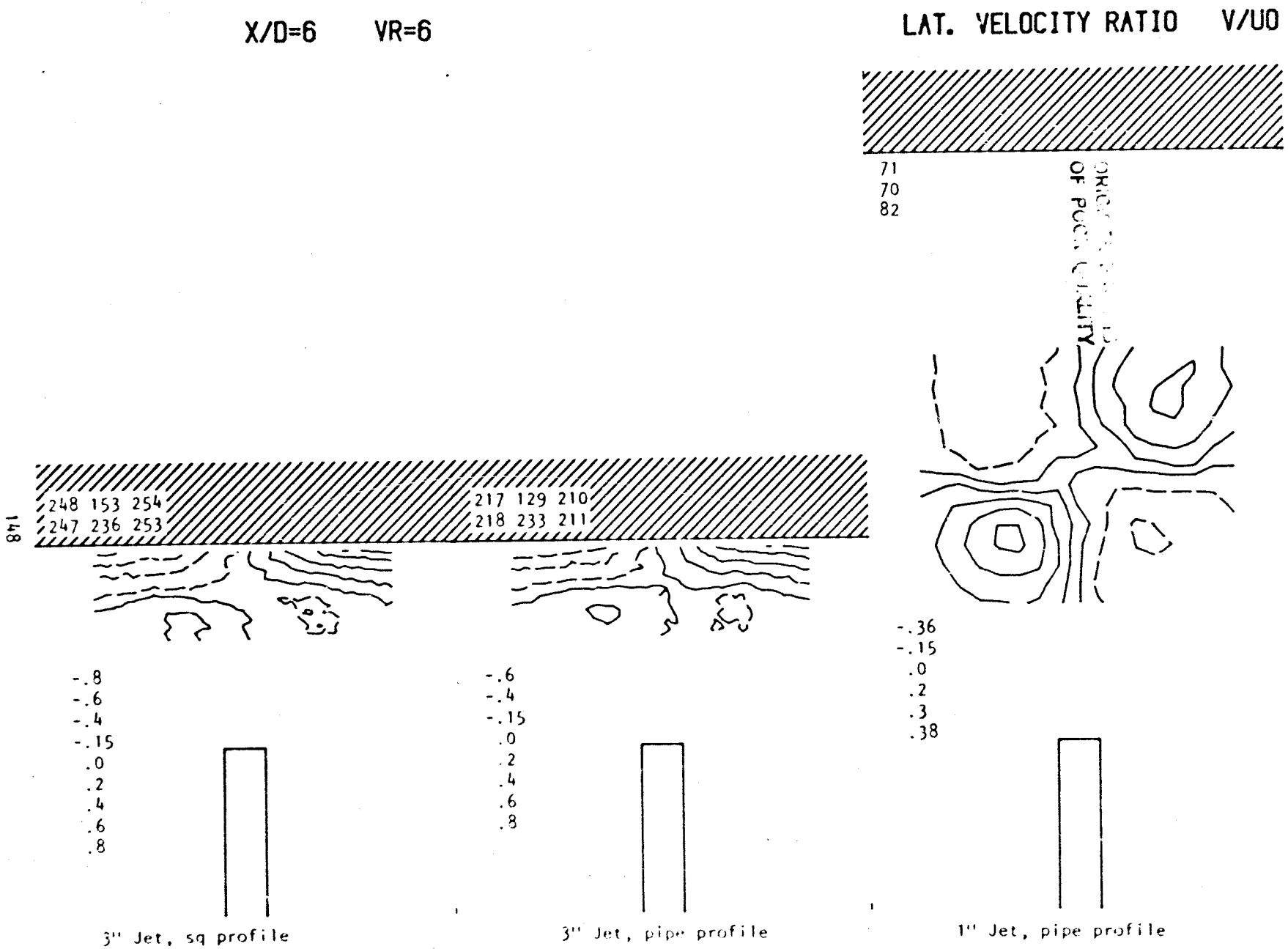

Figure B3 (continued) Effect of jet profile and size on lateral velocities: R = 6

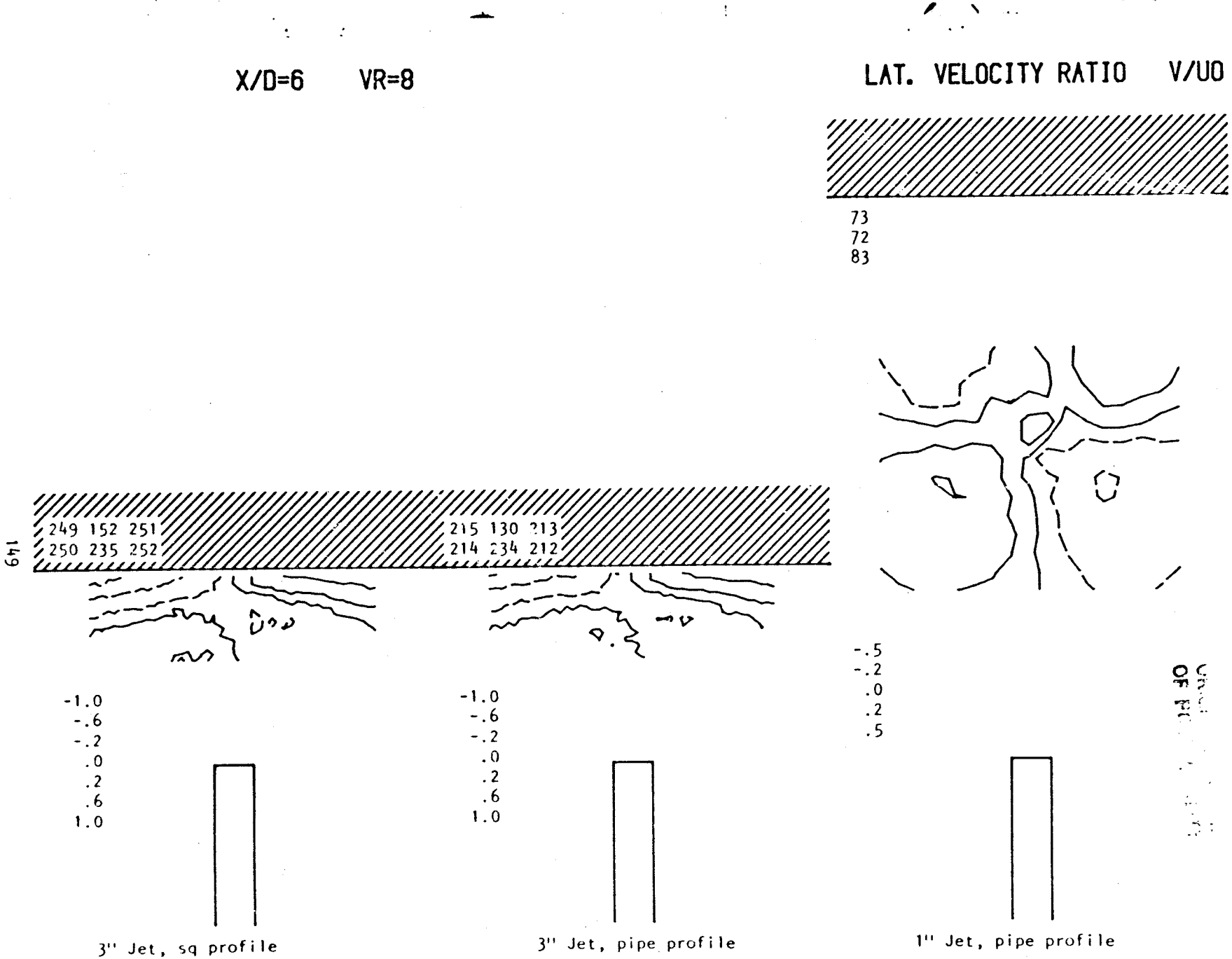

Figure B3 (concluded) Effect of jet profile and size on lateral velocities: R = 8

X/D=6 VR=2

STREAM FUNCTIONS

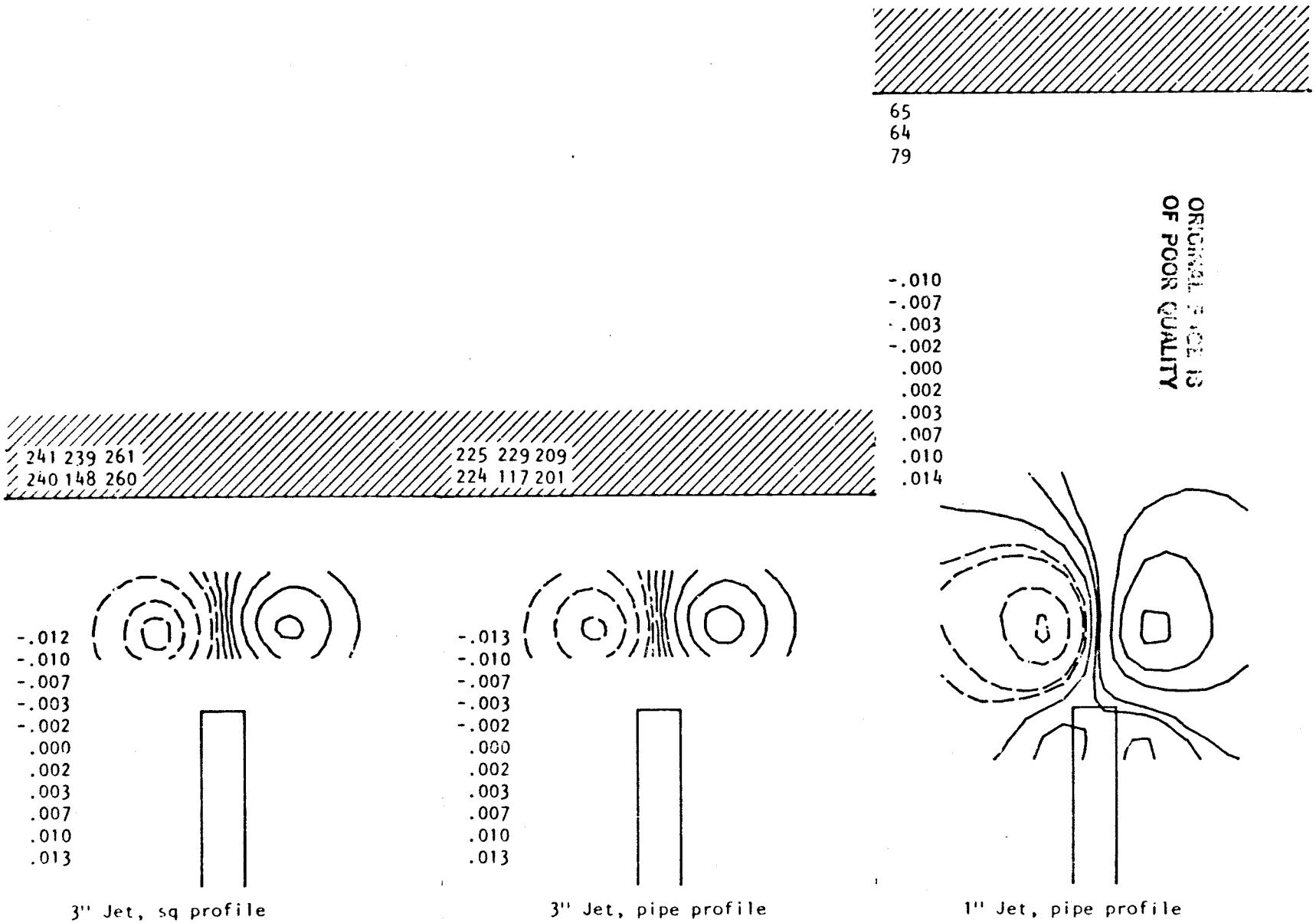

Figure B4 Effect of jet profile and size on streamlines: R = 2

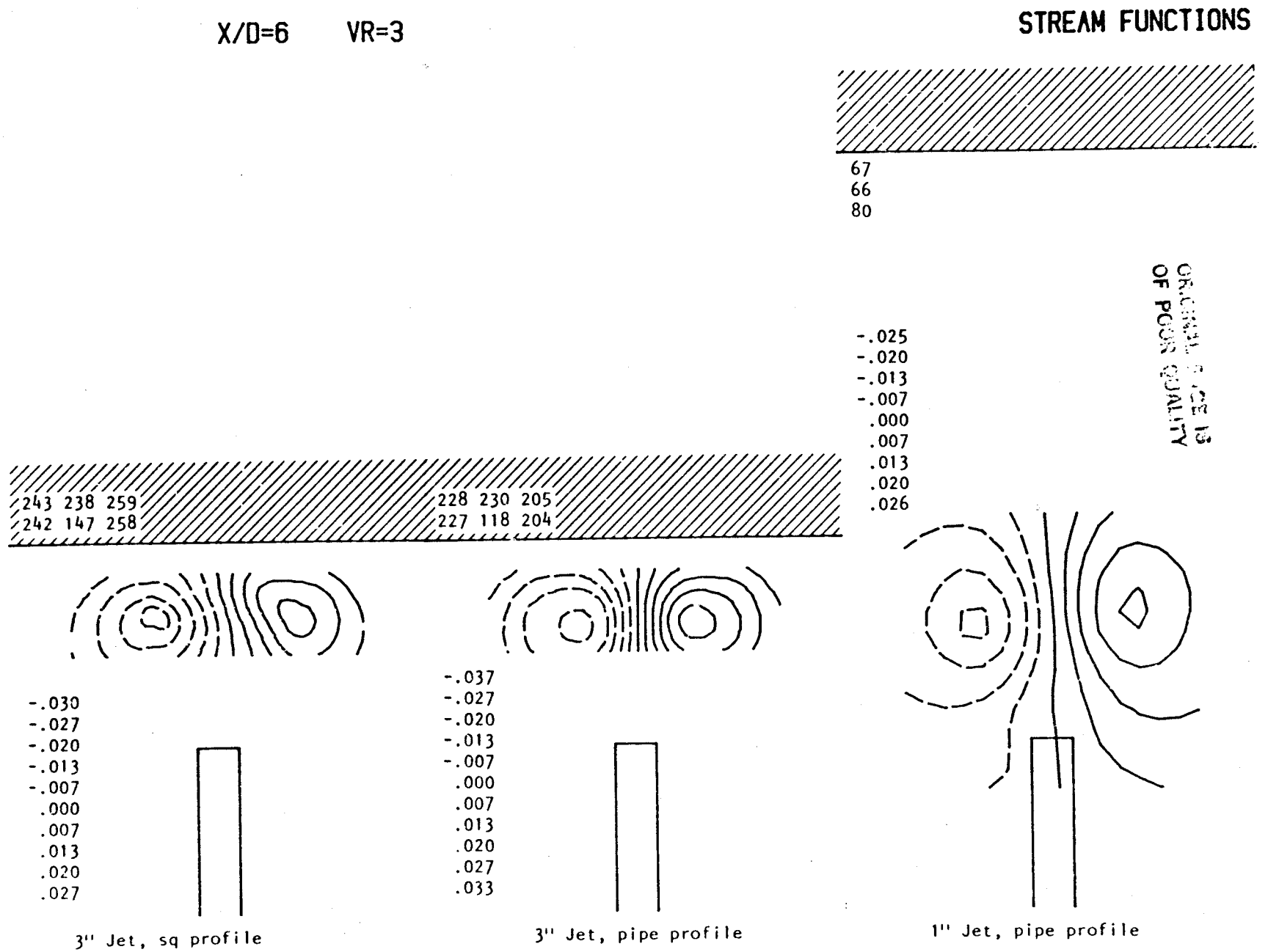

Figure B4 (continued) Effect of jet profile and size on streamlines: R = 3

X/D=6 VR=4

STREAM FUNCTIONS

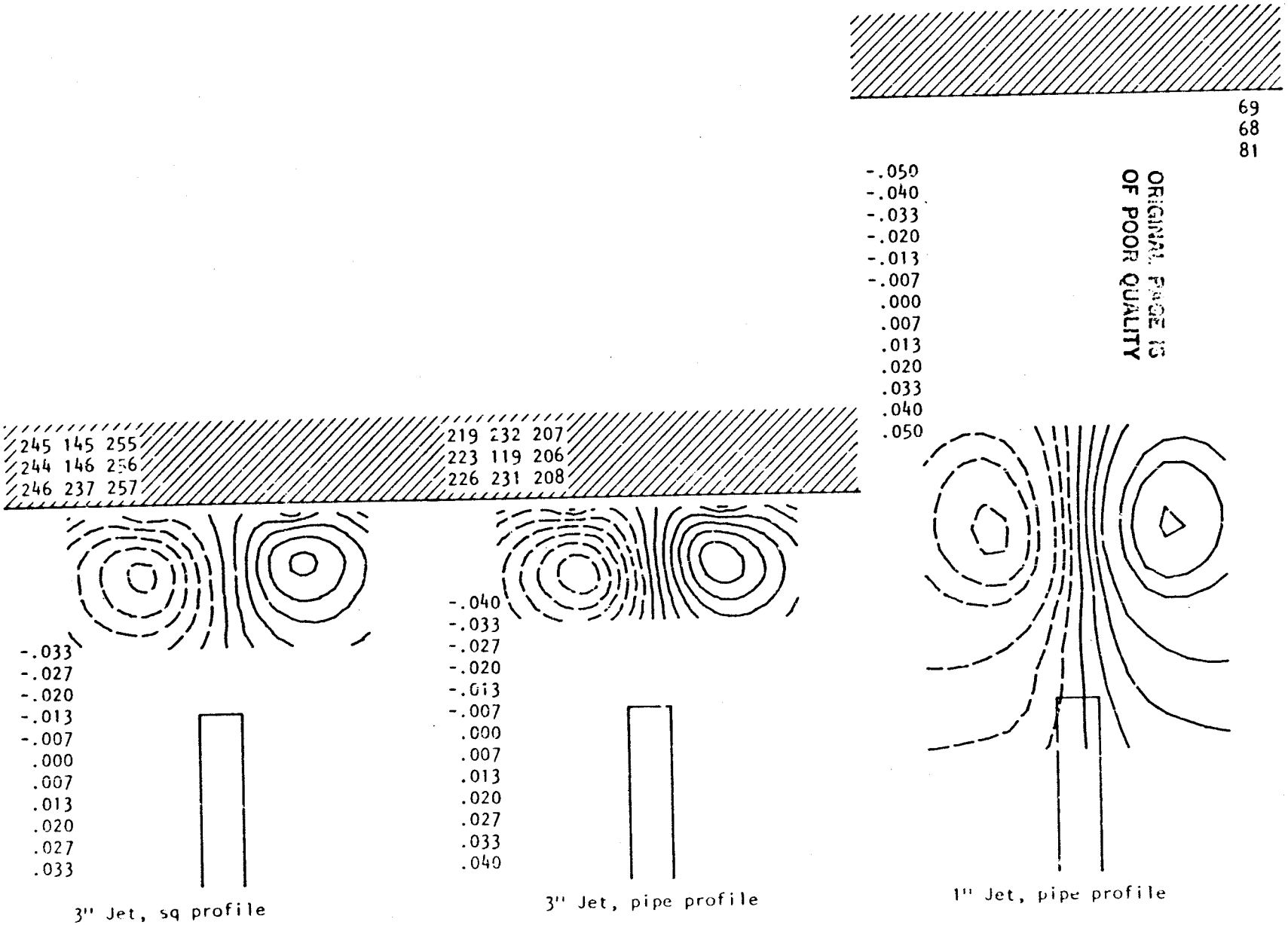

Figure B4 (continued) Effect of jet profile and size on streamlines: R = 4

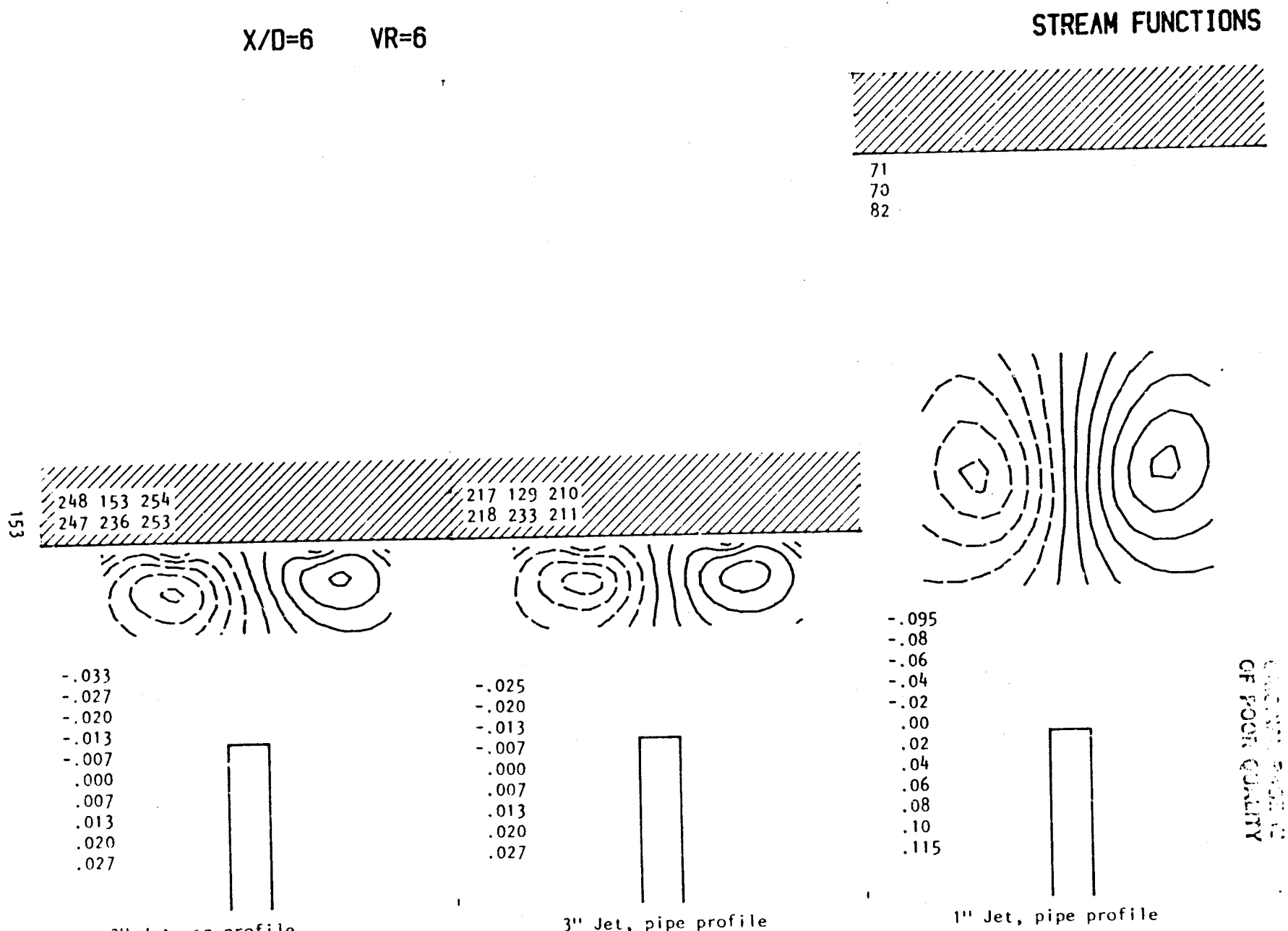

Figure B4 (continued) Effect of jet profile and size on streamlines: R = 6

X/D=6 VR=8

STREAM FUNCTIONS

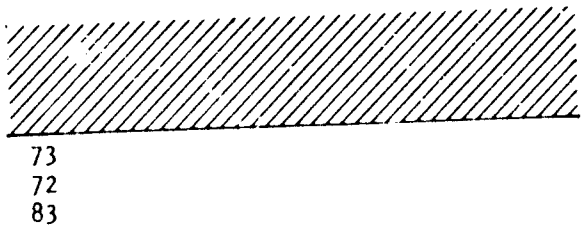

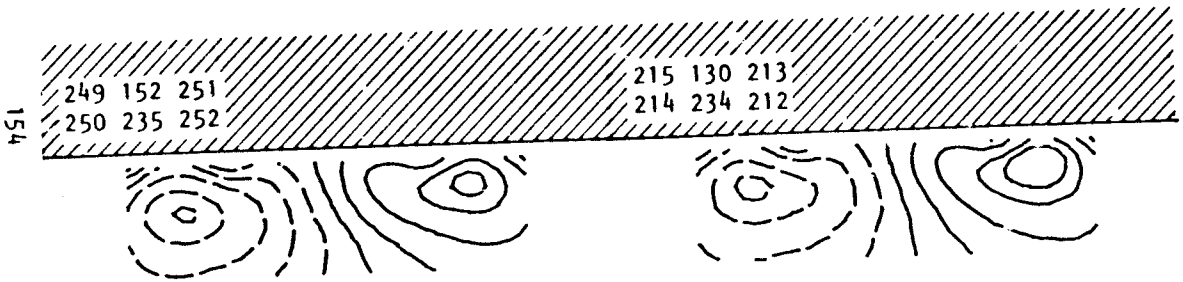

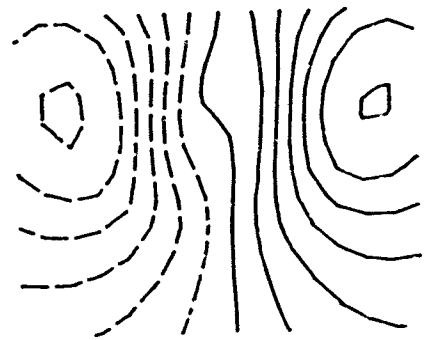

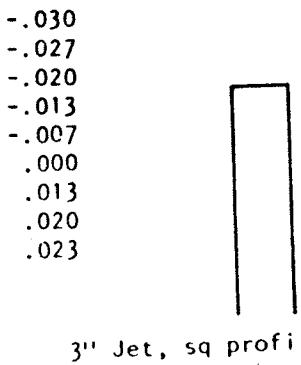

3" Jet, sq profile

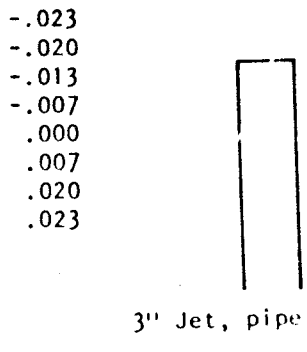

3" Jet, pipe profile

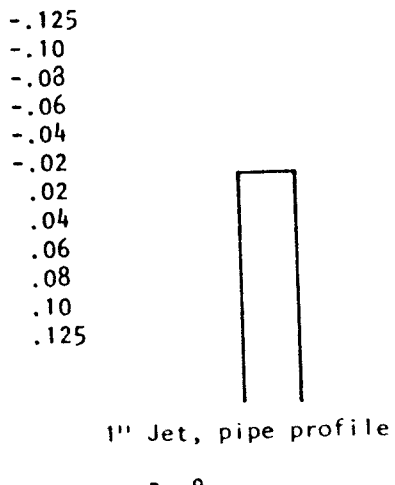

1" Jet, pipe profile

Figure B4 (concluded) Effect of jet profile and size on streamlines: R = 8

APPENDIX C

SOME COMMENTS UPON HEYSON'S METHOD

APPENDIX C

SOME COMMENTS UPON HEYSON'S METHOD

Heyson's model differs from the VSD model not only geometrically (see Figures 5.1(a) and C1) but also because it relies entirely upon doublets. A further significant factor is that, as a result of being force-based, the form of dependence upon R may differ.

Properties of line doublets

Heyson's model involves only line doublets. However, these can have source-like properties which permit for example, a non-zero, wake-blockage-like asymptote far downstream. The simplest example of this concerns the drag-related line doublet which streams along the tunnel wall from the impingement point. The upstream-directed doublet vector aligned with this line element becomes in effect, a long thin ring-vortex tube which pumps fluid along it's center in the upstream direction. It may be shown mathematically that the induced flow field is identical to that for a source situated at the upstream end plus a sink far downstream. The volume flow Q, ft^3/sec is numerically equal to the line doublet strength μ $ft^4/sec/ft$. The inclined doublet line from the jet exit may be regarded similarly, giving a source at the upstream end and an equal sink at the impingement point each with a strength proportional to the doublet strength component parallel to the line between them. However, these contributions create the equivalent of positive solid blockage (rather than wake blockage) since the net source strength within the test section is zero. A vertical doublet component, corresponding to lift, has no wake-like contribution. It has a negative solid blockage effect when considered as above.

The behavior for angle-of-attack interference is the converse of that just described: lift-related doublets generate a positive $\Delta\alpha$ asymptote downstream and drag-related doublets give an antisymmetric pattern of upwash and downwash.

Though the individual elements have the properties just mentioned; i.e. appropriate asymptotic behavior and the ability to provide 'peaky' behavior near the model, the geometric restrictions of Heyson's model are quite severe - particularly with regard to the limited range of jet skew angle, which is found in practical cases. (For $2 \leq R \leq 8$, $58.3° \leq \chi \leq 48.6°$ where χ is from the vertical.

Dependency upon jet-velocity ratio, R

The form adopted by Heyson is a generalization of the familiar $\Delta\varepsilon = \delta$, $\delta\alpha = \delta$, $S/C \cdot C_L$ equation to include cross effects. Thus

$$\frac{\Delta u}{U_\infty} = \delta_{11} f_1 + \delta_{3.1} f_3 \qquad (C1)$$

$$\frac{\Delta w}{U_\infty} = \delta_{13} f_1 + \delta_{3.3} f_3$$

where δ_{11} and δ_{33} are the influence factors for drag on u and lift on w and f_1 and f_3 are related to drag and lift respectively. These take the form of the product of model-to-tunnel area ratio and a characteristic velocity. Thus

$$f_1 = \frac{A_M}{C} \cdot \frac{U_o}{U_\infty} \quad \text{and} \quad f_3 = \frac{A_M}{C} \cdot \frac{W_o}{U_\infty} \tag{C2}$$

U_o and W_o are defined via

$$D = -\rho A_M V_R U_o \quad \text{and} \quad L = -\rho A_M V_R W_o$$

where the product $\rho A_M V_R$ represents the jet mass flow in the present case. So

$$D = -\dot{m} U_o \quad \text{and} \quad L = -\dot{m} W_o$$

$$\text{giving } U_o = -D/\dot{m} \quad \text{and} \quad W_o = -L/\dot{m} \tag{C3}$$

$$\text{If } A_M \text{ is taken here as jet exit area, then } V_R = V_J \text{ and } A_M = \dot{m}/\rho V_J \tag{C4}$$

Substituting into Equations (C2) from (C4) and (C3) gives

$$f_1 = \frac{(\dot{m}/\rho V_J)}{C} \cdot \frac{-D}{\dot{m} U_\infty} \quad \text{and} \quad f_3 = \frac{\dot{m}/\rho V_J}{C} \cdot \frac{-L}{\dot{m} U_\infty}$$

$$f_1 = \frac{-D}{\rho V_J U_\infty C} \quad \text{and} \quad f_3 = \frac{-L}{\rho V_J U_\infty C} \tag{C5}$$

Lift

L is the net lift on the model, which we shall assume equals jet gross thrust for the present vertical jet. Thus

$$L = \rho A_J V_J^2$$

giving from (C5)

$$f_3 = \frac{-\rho A_J V_J^2}{\rho V_J U_\infty C} = -\frac{A_j}{C} R. \tag{C6}$$

This is the form needed if Heyson's program is used directly. For the calculation of wall pressures, however, a special version of the present program is used which reproduces the Heyson model. This requires input of doublet strength, μ_3, given by

$$\mu_3 = \frac{A_m}{2\pi} w_o = \frac{A_j}{2\pi} \frac{-\rho A_J V_J^2}{\dot{m}} \quad \text{from (C3)}$$

$$= -\frac{1}{2\pi} A_J V_J \tag{C7}$$

Drag

For the most meaningful application of Heyson's method to the present case it would be preferable to employ balance data. In it's absence, jet drag will be estimated from the traverse data at X/D = 6, since experimental vortex strengths and core sizes are available. For a solid-body vortex core, which is a reasonable approximation to the present case:

$$D = \frac{\rho\Gamma^2}{2\pi}\left\{\log_e\left(\frac{b}{a} - 1\right) + \frac{1}{4}\right\} \tag{C8}$$

where b is the vortex spacing and a is the core radius. It was noted from experiments described in Section 4.3 that the vortex cores touch, implying that b = 2a. For this case, the argument of the log in Equation (C8) is unity and the first term becomes zero. Thus

$$D = \frac{\rho\Gamma^2}{8\pi} \tag{C9}$$

Substituting Equation (C9) into Equation (C5)

$$f_1 = \frac{-\rho\Gamma^2}{8\pi\rho V_J U_\infty C}$$

Now $\Gamma = \frac{L}{\rho b U_\infty} = \frac{\rho A_J V_J^2}{\rho b U_\infty} = \frac{A_J U_\infty}{b} R^2$

and $\Gamma^2 = \frac{A_J^2 U_\infty^2}{b^2} R^4$

giving $f_1 = -\frac{1}{8\pi}\frac{A_J^2 U_\infty^2}{b^2 V_J U_\infty C} R^4$

$$= -\frac{1}{8\pi}\frac{A_J}{C}\frac{A_J}{b^2} R \tag{C10}$$

and $\mu_1 = \frac{A_m}{2\pi} U_o = \frac{-A_J}{2\pi}\frac{\rho\Gamma^2}{8\pi}\frac{1}{m}$

$$= \frac{-A_J}{(4\pi)^2}\frac{\rho}{8\pi}\frac{A_J^2 U_\infty^2}{b^2} R^4 \frac{1}{\rho A_J V_J}$$

$$= \frac{-1}{(4\pi)^2}\frac{A_J}{b^2} R^3 A_J U_\infty \tag{C11}$$

The R- cubed power in Equation (C11) is unexpectedly high. However the dependency is weaker than this (though still greater than R-squared) because the relationship for b takes the empirical form

$$b = (\alpha + \beta R)\, D \qquad (C12)$$

where $\alpha = 3$ and $\beta = 0.3$ for the 1-inch jet dat at X/D = 6 in Figure 4.8(a). It is found upon suostituting (C12) into (C11) that the resulting values of μ, are far too small: the implied cylinder diameter values are an order of magnitude less than the jet. The assumption was therefore made that b = D: this gave a match to the jet diameter for R = 7.38. Because of the cubic dependency (Equation (C11)), the effective diameter decreases very rapidly with R. On making the substitution b = D and clearing, we obtain

$$f_1 = \frac{1}{32}\,\frac{A_J}{C}\,R^3 \qquad (C13)$$

and $$\frac{\mu_1}{U_\infty D^2} = \frac{1}{4}\,\frac{R}{4}^3$$

Unless stated otherwise, Equation (C13) or (C14) was used to determine doublet strength for the Heyson examples quoted in the main text of this report.

The jet skew angle χ

The sweep-back of the jet doublet line, from the vertical, is related to the velocity ratio R by the equation

$$\chi = \frac{1}{2}\left\{\frac{\pi}{2} + \tan^{-1}\frac{1}{R}\right\} \qquad (C15)$$

APPENDIX D

PROGRAM DOCUMENTATION

PROGRAM DESCRIPTION

Capabilities

This program computes the effect of a single jet of an arbitrary diameter at an arbitrary location with respect to the global, tunnel coordinates. Using the model described in the main text and using an imaging technique, the additional jet effects are calculated at the specified wall points and at the tunnel centerline.

A limited option is provided via the flag ICAL (see Input Description below) to study the effects of individual components of the theoretical model, if so desired. An option flag JMOD also lets this program be run to study the effects of jet only when it is not desired to run the Part I program for further analysis using the modified wall signatures.

As of now the theoretical jet model is restricted to jets issuing at 90° to the mainstream. To consider the effects of jets at other angles, the input constants as well as the program coding defining the geometry and strengths of singularities will have to be appropriately modified.

Compatibility with the Part-I Program

To obtain the total interference of a model with a lifting jet, the Part II program must be run first as a pre-processor. This program creates two mass storage files via FORTRAN UNITS 10 and 11, which subsequently become part of the input files for the Part I program, with the same FORTRAN UNIT-numbers. Additionally, the Part I program must be "signalled" to expect the pre-processed jet-effect output. This is done by assigning a non-zero value to a variable JETEFCT, which is the last variable of Input Card Number-2 in the Part I program.

Input Description

1 | ICAL | JMOD |

Format --- 1615

ICAL: A calculation index ($0 \leq ICAL \leq 4$)

0 - No calculations are to be performed. Print the model geometry and singularity strengths.

1 - Calculate jet effects using vortex pair singularity only.

2 - Calculate jet effect using source singularity only

3 - Calculate jet effect using doublet singularity only.

4 - Use all three singularities (Recommended value)

JMOD: A non-zero value implies that the effects of jet should be taken out of existing wall pressure signatures. The wall pressure signatures to be modified should be available in UNIT - 7. The modified signatures will be written to UNIT - 10, and the interference effect due to jet alone will be written to UNIT - 11.

If JMOD = 0, no input is sought from UNIT - 7. The wall pressure signatures due to the jet alone are written to UNIT - 10, and the interference velocities due to the jet alone are written to UNIT - 11.

2 | TITL | Format --- (20A4)

TITL: A title with no more than 80 characters.

3 | B | H | Format --- (8F10.6)

B: Tunnel width

H: Tunnel height in same units as that of B.

4 | AZ | BZ | CZ | Format (810.6)

AZ, BZ, CZ: Non-dimensional constants for definition of Z-coordinate of vortex curve (see Eq. 5.1). See sample input for recommended values.

5 | AY | BY | Format --- (8F10.6)

AY, BY: Non-dimensional constants for the definition of Y-coordinate of vortex curve. (See Eq. 5.3) See sample input for recommended values.

6 | AG | GB | CG | Format --- (8F10.6)

AG, BG, CG: Non-dimensional constants for the definition of circulation strengths. (See Eq. 5.4) See sample input for recommended values.

7 | ACL | BCL | CCL | Format --- (8F10.6)

ACL, BCL, CCL: Non-dimensional constants for the definition of Z-coordinate of jet centerline. (See Eq. 5.2). See sample imput for recommended values.

8 | NSPV | NCAL | NWALL | LAYER | Format --- (1615)

NSPV: Number of singularity points in the X-direction on the vortex line. (Note: These points will be connected by straight line segments to produce the required links. The same number of points are used for sources and doublets)

NCAL: Number of calculation points in the X-direction for both wall pressures and the centerline interference velocity points.

NWALL: Number of rails on tunnel surfaces.

LAYER: Number of image layers to be used. (Recommended value: 5)

9 | XNG_1 | XNG_2 | ... | XNG_{NSPV} | Format --- (8F10.6)

XNG_i: X-coordinate of i-th singularity point normalized with respect to tunnel breadth, B

10 | XC_1 | XC_2 | ... | XC_{NCAL} | Format --- (8F10.6)

XC_i: X-coordinate of i-th calculation point normalized with respect to tunnel breadth, B.

11 | $YWALL_1$ | $YWALL_2$ | ... | $YWALL_{NWALL}$ | Format --- (8F10.6)

$YWALL_i$: Y-coordinate of i-th rail on tunnel surface normalized with respect to tunnel breadth, B.

12 | $ZWALL_1$ | $ZWALL_2$ | ... | $ZWALL_{NWALL}$ | Format --- (8F10.6)

$ZWALL_i$: Z-coordinate of i-th rail on tunnel surface normalized with respect to tunnel height, H.

13 | IFLOR | IROOF | IWAL1 | IWAL2 | Format --- (1615)

IFLOR: The rail number for floor signature.

IROOF: The rail number for roof signature

IWAL1: The rail number for the signature on sidewall 1.

IWAL2: The rail number for the signature on sidewall 2.

(Note: These should be compatible with the values defined in Card No. 10 of the input for Part I program)

14 | ITEST | IRUN | IPOINT | Format --- (1615)

ITEST: Test Number

IRUN: Run Number

IPOINT: Point Number

15 | R | D | YJET | ZJET | Format --- (8F10.6)

R: Velocity ratio, V_{jet}/U_{∞}

D: Jet diameter, normalized with respect to tunnel height, H.

YJET: Y-coordinate of jet origin normalized with respect to tunnel breadth, B.

ZJET: Z-coordinate of jet origin normalized with respect to the tunnel height, H.

Mass Storage Requirements

In addition to the standard input and output files (UNITS 5 and 6), the coding also requires that three more mass storage files be pre-assigned to UNITS 7, 10 and 11. The purpose and format of these data files are as follows:

UNIT-7 — Input file. This file should have the measured wall pressure data for the tests done with the model and the jet. The format of the data is the same as the corresponding wall pressure data file used by the PART I program. This file need not be assigned if the jet alone option is used (i.e., JMOD = 0) in running this program.

UNIT-10 — Output file. This file will contain the wall pressure signatures as modified by the presence of the jet. This will be in the same format as UNIT-7 and can be used as it is for the auxillary input file for Part I program. If the option JMOD = 0 is employed, the file will contain the wall pressures due to the jet alone.

UNIT-11 — Output file. This will contain the interference velocity at the tunnel centerline due to the jet. The Part I program will add these values to the model interference to obtain the total interference due to the model with jet. This file should be assigned to UNIT-11 again while running the Part I program for further analysis.

Output Description

The output produced by this program consists of the following sections: (1) Tunnel geometry and the values of constants used for defining the model as specified in the input to the program. (2) For a given jet diameter and R-value, the complete definition of the model. (3) The velocities induced by the jet at the pressure rails on tunnel surface and the new values of wall pressures as modified by the jet. (4) The interference velocity due to the jet alone.

A listing of the program, a sample input and output are given below. The following list of subroutines are the same as in Part-I program and they have to be additionally linked with the present program: INFLU, CRDTEG, LNVXGN, LNVXEQ, LNSCGN, LNSCEQ, LNDBGN, LNDBEQ, CPREAD,

```
      PROGRAM JETEFFCT
C
C FILE... JETEFFCT.FOR;1
C
C      Calcualtes effect of a jet on tunnel wa'ls and modifies the wall
C      pressure signature accordingly. Also, determ nes the interference
C      velocity components at the tunnel center_line due the jet.
C
C      INPUT files :
C                    UNIT_5  : Flow parameters and otler key values.
C                    UNIT_7  : Measured Wall_pressure data.
C      OUTPUT Files:
C                    UNIT_6  : Print ou
C                    UNIT_10 : Modified Wall_pressure data.
C                    UNIT_11 : Interference velocit's due to the jet
C
      DIMENSION XPV(30),YPV(30),ZPV(30),XPR(30,YPR(3E),ZPR(30),XNG(30),
     1          XPS(30),YPS(30),ZPS(30), XC(30, VC(30), ZC(30),
     1          VMS(30),GAM(30),VMU(30), U(30) V(30),W(30),CP(30,3),
     1          UWL(30),URF(30),YWALL(10),ZWALL(10) ITYP(4 ,TITL(20)
      COMMON /IMAG/ B,H,LAYER,MINIT,IBUG
      COMMON /DIRC/ DCXO, DCYO, DCZO
      COMMON /LOAD/ ALFU,POU,QOU,CMUU,CLU,CDU,CMU
C
C
      PI = 3.141592654
      IBUG = 0
C
C-    READ_IN GEOMETRICAL PARAMETERS FOR THE JET_MODEL
C
      READ (5,510) ICAL,JMOD
      READ (5,520) TITL
      READ  (5,500) B,H
      WRITE (6,600) B,H
      WRITE (6,601) TITL
      READ  (5,500) AZ,BZ,CZ
      WRITE (6,612)
      WRITE (6,630) AZ,BZ,CZ
      READ  (5,500) AY,BY
      WRITE (6,614)
      WRITE (6,630) AY,BY
      READ  (5,500) AG,BG,CG
      WRITE (6,616)
      WRITE (6,630) AG,BG,CG
      READ  (5,500) ACL,BCL,CCL
      WRITE (6,618)
      WRITE (6,630) ACL,BCL,CCL
C
C-    READ_IN CALCULATION PARAMETERS
C
      READ (5,510) NSPV,NCAL,NWALL,LAYER
      READ (5,500) (XNG(I),I=1,NSPV)
      READ (5,500) (XC(I),I=1,NCAL)
      READ (5,500) (YWALL(I),I=1,NWALL)
```

```
JTEFCT 001
JTEFCT 002
JTEFCT 003
JTEFCT 004
JTEFCT 005
JTEFCT 006
JTEFCT 007
JTEFCT 008
JTEFCT 009
JTEFCT 010
JTEFCT 011
JTEFCT 012
JTEFCT 013
JTEFCT 014
JTEFCT 015
JTEFCT 016
JTEFCT 017
JTEFCT 018
JTEFCT 019
JTEFCT 020
JTEFCT 021
JTEFCT 022
JTEFCT 023
JTEFCT 024
JTEFCT 025
JTEFCT 026
JTEFCT 027
JTEFCT 028
JTEFCT 029
JTEFCT 030
JTEFCT 031
JTEFCT 032
JTEFCT 033
JTEFCT 034
JTEFCT 035
JTEFCT 036
JTEFCT 037
JTEFCT 038
JTEFCT 039
JTEFCT 040
JTEFCT 041
JTEFCT 042
JTEFCT 043
JTEFCT 044
JTEFCT 045
JTEFCT 046
JTEFCT 047
JTEFCT 048
JTEFCT 049
JTEFCT 050
JTEFCT 051
JTEFCT 052
JTEFCT 053
JTEFCT 054
```

```
      READ (5,500) (ZWALL(I),I=1,NWALL)
      READ (5,510) IFLOR,IROOF,IWAL1,IWAL2
      NWALL = NWALL+1
      YC(NWALL) = 0.
      ZC(NWALL) = 0.
C
      DO 10 I = 1,NSPV
   10 XNG(I) = XNG(I)*B
      DO 11 I = 1,NCAL
   11 XC(I) = XC(I)*B
      DO 12 I = 1,NWALL
      YWALL(I) = YWALL(I)*B
      ZWALL(I) = ZWALL(I)*H
   12 CONTINUE
C
C     READ_IN TEST PARAMETERS
C
   22 READ (5,510,END=99) ITEST,IRUN,IPOINT
      READ (5,500) R,D,VJET,ZJET
      IF(IMOD .NE. 0) CALL CPREAD (ITEST,IRUN,IPOINT, CP, NCAL)
C
C     DEFINE VORTEX CURVE , SOURCE/DOUBLET_LINE AND CIRCULATION STRENGTHS
C
      D = D*H
      VJET = VJET*B
      ZJET = ZJET*H
      ISECT = NSPV+1
      CEIL = 0.5*H
      IF(LAYER .EQ. 0) CEIL = 0.1E+32
      XPV(1) = 0.25*D + VJET
      ZPV(1) = ZJET
      GAM(1) = 0.0
      XPP(1) = XPV(1)
      YPP(1) = YPV(1)
      ZPP(1) = ZPV(1)
      XPS(1) = XPV(1)
      YPS(1) = YPV(1)
      ZPS(1) = ZPV(1)
   35 DO 40 I = 2,NSPV
      XX = XNG(I)/D
      XPV(I) = XNG(I)
      YPV(I) = AY*(XX**BY)/R.0*D*R + VJET
      ZPV(I) = AZ*(XX**CZ)*EXP(R**BZ) + ZJET
      XPP(I) = XPV(I)
      YPP(I) = YPV(I)
      ZPP(I) = CEIL
      XPS(I) = XPV(I)
      YPS(I) = YPV(I)
      ZPS(I) = ACL*(XX**CCL)*D*(R**BCL) + ZJET
      GAMA = AG/XX*(1.0-EXP(-CG*XX)) + BG*TANH(XX)
      GAM(I) = GAMA*2.0*D*R*R/61.0
C
      IF(I .GT. ISECT) GO TO 40
      ZPP(I) = ZPV(I)
      IF(ZPV(I) .LT. CEIL) GO TO 40
```

```
JTEFCT 055
JTEFCT 056
JTEFCT 057
JTEFCT 058
JTEFCT 059
JTEFCT 060
JTEFCT 061
JTEFCT 062
JTEFCT 063
JTEFCT 064
JTEFCT 065
JTEFCT 066
JTEFCT 067
JTEFCT 068
JTEFCT 069
JTEFCT 070
JTEFCT 071
JTEFCT 072
JTEFCT 073
JTEFCT 074
JTEFCT 075
JTEFCT 076
JTEFCT 077
JTEFCT 078
JTEFCT 079
JTEFCT 080
JTEFCT 081
JTEFCT 082
JTEFCT 083
JTEFCT 084
JTEFCT 085
JTEFCT 086
JTEFCT 087
JTEFCT 088
JTEFCT 089
JTEFCT 090
JTEFCT 091
JTEFCT 092
JTEFCT 093
JTEFCT 094
JTEFCT 095
JTEFCT 096
JTEFCT 097
JTEFCT 098
JTEFCT 099
JTEFCT 100
JTEFCT 101
JTEFCT 102
JTEFCT 103
JTEFCT 104
JTEFCT 105
JTEFCT 106
JTEFCT 107
JTEFCT 108
JTEFCT 109
```

```
      ISECT = I                                                          JTEFCT 110
      YPR(I) = XPR(I-1) + (CEIL-ZPR(I-1))/(ZPR(I)-ZPR(I-1))*             JTEFCT 111
     1                    (XPR(I)-XPR(I-1))                             JTEFCT 112
      YPR(I) = YPR(I-1) + (CEIL-ZPR(I-1))/(ZPR(I)-ZPR(I-1))*             JTEFCT 113
     1                    (YPR(I)-YPR(I-1))                             JTEFCT 114
      ZPR(I) = CEIL                                                      JTEFCT 115
      XX = XPV(I)                                                        JTEFCT 116
      GAMA = AG/XX*(1.0-EXP(-CG*X**XX)) + BG*TANH(XX)                    JTEFCT 117
      GAM(I) = GAMA*2.0*D*R*R/64.0                                       JTEFCT 118
      XPV(I) = XPR(I)                                                    JTEFCT 119
      YPV(I) = YPR(I)                                                    JTEFCT 120
      ZPV(I) = ZPR(I)                                                    JTEFCT 121
   40 CONTINUE                                                           JTEFCT 122
C                                                                        JTEFCT 123
      NSV = NSPV-1                                                       JTEFCT 124
      JMAX = NSV                                                         JTEFCT 125
      DO 43 I = 1,JMAX                                                   JTEFCT 126
   43 GAM(I) = 0.5*(GAM(I) + GAM(I+1))                                   JTEFCT 127
      IF(JMAX .GE. ISECT) JMAX = ISECT-1                                 JTEFCT 128
C                                                                        JTEFCT 129
C     CHECK FOR INTERSECTION OF SOURCE/DOUBLET LINE WITH ROOF            JTEFCT 130
C                                                                        JTEFCT 131
      XINT = ((CEIL-ZJET)/(ACL*D*R**BCL))**(1.0/CCL)                     JTEFCT 132
      XINT = XINT*D                                                      JTEFCT 133
      JMAX2 = NSV                                                        JTEFCT 134
      IF(XINT .GT. XPS(NSV)) GO TO 50                                    JTEFCT 135
      DO 45 J = 1,NSV                                                    JTEFCT 136
      IF(XPS(J) .GT. XINT) GO TO 46                                      JTEFCT 137
   45 CONTINUE                                                           JTEFCT 138
   46 JMAX2 = J                                                          JTEFCT 139
      XPS(JMAX2) = XINT                                                  JTEFCT 140
      XX = XINT/D                                                        JTEFCT 141
      YPS(JMAX2) = ACL*(XX**BCL)/3.0*D*R + YJET                          JTEFCT 142
      ZPS(JMAX2) = CEIL                                                  JTEFCT 143
      JMAX2 = JMAX2-1                                                    JTEFCT 144
C                                                                        JTEFCT 145
C-    DEFINE SOURCE AND DOUBLET STRENGTHS                                JTEFCT 146
C                                                                        JTEFCT 147
   50 DO 51 J = 1,JMAX2                                                  JTEFCT 148
      DL = SQRT((XPS(J+1)-XPS(J))**2 + (YPS(J+1)-YPS(J))**2 +            JTEFCT 149
     *          (ZPS(J+1)-ZPS(J))**2 )                                  JTEFCT 150
      VPS(J) = D*(ZPS(J+1)-ZPS(J))*SQRT(1.+0.125*(XPS(J+1)+XPS(J))/D)/DL JTEFCT 151
   51 CONTINUE                                                           JTEFCT 152
      DOXO = -1.                                                         JTEFCT 153
      DOZO = 0.                                                          JTEFCT 154
      DOYO = 0.                                                          JTEFCT 155
      VMU(1) = 2.0*PI*(0.5*D)**2                                         JTEFCT 156
      DO 56 J = 2,JMAX2                                                  JTEFCT 157
   56 VMU(J) = VMU(1)*SQRT(1.0 + 0.250*XPS(J)/D)                         JTEFCT 158
C                                                                        JTEFCT 159
C-    PRINT OUT JET_MODEL                                                JTEFCT 160
C                                                                        JTEFCT 161
      WRITE (6,610)                                                      JTEFCT 162
      WRITE (6,650) R,D/H, YJET/B,ZJET/H                                 JTEFCT 163
      WRITE (6,620)                                                      JTEFCT 164
```

```
      JJ = JMAX+1                                                       JTEFCT 165
      DO 60 J = 1,JJ                                                    JTEFCT 166
      GAMA = GAM(J)/D                                                   JTEFCT 167
      WRITE (6,640) J, XPV(J)/D,YPV(J)/D,ZPV(J)/D, GAM(J)/D             JTEFCT 168
   60 CONTINUE                                                          JTEFCT 169
      WRITE (6,621)                                                     JTEFCT 170
      JJ = JMAX2+1                                                      JTEFCT 171
      DO 62 J = 1,JJ                                                    JTEFCT 172
      WRITE (6,640) J, XPS(J)/D,YPS(J)/D,ZPS(J)/D, VMS(J)/D,VMU(J)/D/D  JTEFCT 173
   62 CONTINUE                                                          JTEFCT 174
C                                                                       JTEFCT 175
      IF(ICAL .EQ. 0) GO TO 22                                          JTEFCT 176
C                                                                       JTEFCT 177
C-    DEFINE COMPONENTS OF MODEL                                        JTEFCT 178
C                                                                       JTEFCT 179
      WRITE (6,622)                                                     JTEFCT 180
      DO 70 I = 1,3                                                     JTEFCT 181
      ITYP(I) = 0                                                       JTEFCT 182
      IF(ICAL.EQ.1 .OR. ICAL.EQ.4) ITYP(I) = 1                          JTEFCT 183
      GO TO (65,66,67),I                                                JTEFCT 184
   65 IF(ITYP(I) .NE. 0) WRITE(6,623)                                   JTEFCT 185
      GO TO 70                                                          JTEFCT 186
   66 IF(ITYP(I) .NE. 0) WRITE(6,624)                                   JTEFCT 187
      GO TO 70                                                          JTEFCT 188
   67 IF(ITYP(I) .NE. 0) WRITE(6,625)                                   JTEFCT 189
   70 CONTINUE                                                          JTEFCT 190
C                                                                       JTEFCT 191
C-    COMPUTE WALL_PRESSURE AND CENTERLINE INTERFERENCE                 JTEFCT 192
C                                                                       JTEFCT 193
      DO 95 NW = 1,NWALL                                                JTEFCT 194
C                                                                       JTEFCT 195
      DO 75 I = 1,NCAL                                                  JTEFCT 196
      YC(I) = YWALL(NW)                                                 JTEFCT 197
      ZC(I) = ZWALL(NW)                                                 JTEFCT 198
   75 CONTINUE                                                          JTEFCT 199
      MINIT = 0                                                         JTEFCT 200
      IF(NW .EQ. NWALL) MINIT = 1                                       JTEFCT 201
C                                                                       JTEFCT 202
      WRITE (6,626) LAYER,MINIT                                         JTEFCT 203
      IF(MINIT .EQ. 0) WRITE (6,627) NW                                 JTEFCT 204
      IF(MINIT .NE. 0) WRITE (6,628)                                    JTEFCT 205
      WRITE (6,629)                                                     JTEFCT 206
      IYW = 0.0                                                         JTEFCT 207
      IZW = 0.0                                                         JTEFCT 208
      DO 80 I = 1,NCAL                                                  JTEFCT 209
      U(I) = 0.0                                                        JTEFCT 210
      V(I) = 0.0                                                        JTEFCT 211
      W(I) = 0.0                                                        JTEFCT 212
      UWL(I) = 0.                                                       JTEFCT 213
      UP(I) = 0.                                                        JTEFCT 214
C                                                                       JTEFCT 215
      DO 80 J = 1,NSV                                                   JTEFCT 216
      DU1 = 0.                                                          JTEFCT 217
      DV1 = 0.                                                          JTEFCT 218
      DW1 = 0.                                                          JTEFCT 219
```

```
      DU2 = 0.                                                          JTEFCT 220
      DV2 = 0.                                                          JTEFCT 221
      DW2 = 0.                                                          JTEFCT 222
C                                                                       JTEFCT 223
C-    COMPUTE THE EFFECT OF VORTEX PAIR (ICAL=1 OR 4)                   JTEFCT 224
C                                                                       JTEFCT 225
      IF(ITYP(1) .EQ. 0) GO TO 76                                       JTEFCT 226
      IF(J .GT. JMAX(1)) GO TO 76                                       JTEFCT 227
      CALL INFLU(XPR(J),YPR(J),ZPR(J), XPR(J+1),YPR(J+1),ZPR(J+1),      JTEFCT 228
     1           -GAM(J),2,IYW,IZW, XC(I),YC(I),ZC(I), DU1,DV1,DW1 )    JTEFCT 229
      YPR1 = 2.0*YJET-YPR(J)                                            JTEFCT 230
      YPR2 = 2.0*YJET-YPR(J+1)                                          JTEFCT 231
      CALL INFLU(XPR(J),YPR1,ZPR(J), XPR(J+1),YPR2,ZPR(J+1),            JTEFCT 232
     1           GAM(J),2,IYW,IZW, XC(I),YC(I),ZC(I), DU2,DV2,DW2 )     JTEFCT 233
      U(I) = U(I) + DU1 + DU2                                           JTEFCT 234
      V(I) = V(I) + DV1 + DV2                                           JTEFCT 235
      W(I) = W(I) + DW1 + DW2                                           JTEFCT 236
C                                                                       JTEFCT 237
C-    COMPUTE  AND ADD THE EFFECT OF SOURCE PAIR (ICAL=2 OR 4)          JTEFCT 238
C                                                                       JTEFCT 239
   76 IF(ITYP(2) .EQ. 0) GO TO 77                                       JTEFCT 240
      IF(J .GT. JMAX(2)) GO TO 80                                       JTEFCT 241
      CALL INFLU(XPS(J),YPS(J),ZPS(J), XPS(J+1),YPS(J+1),ZPS(J+1),      JTEFCT 242
     1       0.5*VMS(J),1,IYW,IZW, XC(I),YC(I),ZC(I), DU1,DV1,DW1 )     JTEFCT 243
      YPR1 = 2.0*YJET-YPS(J)                                            JTEFCT 244
      YPR2 = 2.0*YJET-YPS(J+1)                                          JTEFCT 245
      CALL INFLU(XPS(J),YPR1,ZPS(J), XPS(J+1),YPR2,ZPS(J+1),            JTEFCT 246
     1       0.5*VMS(J),1,IYW,IZW, XC(I),YC(I),ZC(I), DU2,DV2,DW2)      JTEFCT 247
C.....FOR SOURCES, ADD A DOWNSTREAM SINK.                               JTEFCT 248
      DL = SQRT((XPS(J+1)-XPS(J)  **2 + (YPS(J+1)-YPS(J))**2            JTEFCT 249
     *          + (ZPS(J+1)-ZPS(J)  **2)                                JTEFCT 250
      DU1 = DU1 + 0.5*VMS(J)*DL/(8*H)                                   JTEFCT 251
      U(I) = U(I) + DU1 + DU2                                           JTEFCT 252
      V(I) = V(I) + DV1 + DV2                                           JTEFCT 253
      W(I) = W(I) + DW1 + DW2                                           JTEFCT 254
C                                                                       JTEFCT 255
C-    COMPUTE AND ADD THE EFFECT OF DOUBLET PAIR (ICAL=3 OR 4)          JTEFCT 256
C                                                                       JTEFCT 257
   77 IF(ITYP(3) .EQ. 0) GO TO 80                                       JTEFCT 258
      IF(J .GT. JMAX(2)) GO TO 80                                       JTEFCT 259
      CALL INFLU(XPS(J),YPS(J),ZPS(J), XPS(J+1),YPS(J+1),ZPS(J+1),      JTEFCT 260
     1           0.5*VMU(J),3,IYW,IZW, XC(I),YC(I),ZC(I), DU1,DV1,DW1 )  JTEFCT 261
      YPR1 = 2.0*YJET-YPS(J)                                            JTEFCT 262
      YPR2 = 2.0*YJET-YPS(J+1)                                          JTEFCT 263
      CALL INFLU(XPS(J),YPR1,ZPS(J), XPS(J+1),YPR2,ZPS(J+1),            JTEFCT 264
     1           0.5*VMU(J),3,IYW,IZW, XC(I),YC(I),ZC(I), DU2,DV2,DW2 )  JTEFCT 265
      U(I) = U(I) + DU1 + DU2                                           JTEFCT 266
      V(I) = V(I) + DV1 + DV2                                           JTEFCT 267
      W(I) = W(I) + DW1 + DW2                                           JTEFCT 268
   80 CONTINUE                                                          JTEFCT 269
C                                                                       JTEFCT 270
C-    SUBTRACT "FREE_AIR_LEG" FOR INTERFERENCE CALCULATION (ICAL=1 OR 4)  JTEFCT 271
C                                                                       JTEFCT 272
      IF(ITYP(1) .EQ. 0) GO TO 82                                       JTEFCT 273
      IF(MINIT .NE. 0) GO TO 82                                         JTEFCT 274
```

```
      LHOLD = LAYER
      LAYER = 0
      DO 81 J = ISECT, NSV
      CALL INFLU(XPR(J),YPR(J),ZPR(J), XPR(J+1),YPR(J+1),ZPR(J+1),
     1           -GAM(J),2,IYW,IZW, XC(I),YC(I),ZC(I), DU1,DV1,DW1 )
      YPR1 = 2.0*YJET-YPR(J)
      YPR2 = 2.0*YJET-YPR(J+1)
      CALL INFLU(XPR(J),YPR1,ZPR(J), XPR(J+1),YPR2,ZPR(J+1),
     1           GAM(J),2,IYW,IZW, XC(I),YC(I),ZC(I), DU2,DV2,DW2 )
      U(I) = U(I) - DU1 - DU2
      V(I) = V(I) - DV1 - DV2
      W(I) = W(I) - DW1 - DW2
   81 CONTINUE
      LAYER = LHOLD
   82 CONTINUE
C
      UEFF = U(I)
      IF(JMOD .NE. 0) UEFF = SQRT(ABS(1.-CP(I,NW)))-1.0 - U(I)
      CP(I,NW) = -UEFF*(2.0+UEFF) - V(I)**2 - W(I)**2
      IF(MINIT.EQ.0) WRITE (6,610) I,XC(I)/B,YC(I)/B,ZC(I)/H,
     *                              U(I),V(I),W(I),CP(I,NW)
      IF(MINIT.NE.0) WRITE (6,640) I,XC(I)/B,YC(I)/B,ZC(I)/H,
     *                              U(I),V(I),W(I)
      IF(NW.EQ.IWAL1 .OR. NW.EQ.IWAL2) UWL(I) = UWL(I) + U(I)
      IF(NW.EQ.IROOF) URF(I) = URF(I) + U(I)
      IF(NW.EQ.IFLOR) URF(I) = URF(I) - U(I)
   90 CONTINUE
   95 CONTINUE
C
C-    WRITE RESULTS TO MASS_STORAGE FILES
C
      CALL JETINT(ITEST,IRUN,IPOINT,B, XC, UWL URF, U,V,W, NCAL)
      CALL CPWRIT(ITEST,IRUN,IPOINT, CP, NCAL)
      GO TO 20
C
   99 STOP
C
  500 FORMAT (8F10.5)
  510 FORMAT (16I5)
  520 FORMAT (20A4)
C
  600 FORMAT (1H1,' TUNNEL GEOMETRY:  B=',F5.2,',    H=',F6.2/)
  601 FORMAT (/1X,20A4/)
  610 FORMAT (/'1*** JET MODEL ***'//' SIZE AND LOCATIONS :-',12X,1HR,
     1       7X,3HD/H,4X,6HYJET/B,4X,6HZJET/H
  612 FORMAT (/' CONSTANTS FOR. .'/3X,'VORTEX CURVE. Z(X)',12X,2HAZ,
     1       8X,2HBZ,8. ,2HCZ)
  614 FORMAT (/3X,'VORTEX CURVE. Y(X)',12X,2HAY,8X,2HEY)
  616 FORMAT (/3X,'VORTEX STRENGTH',15X,2HAS,6X,2HBG,6X,2HCG)
  618 FORMAT (/3X,'SECONDARY LINE, Z(X)',6X,'HACL', ,3HBCL,7X,3HCCL)
  620 FORMAT (/' VORTEX GEOMETRY AND STRENGTHS :'/ ,'I',6X,'X/D',
     *       7X,'Y/D',7X,'Z/D',5X,'GAM/(D*U0)'/)
  621 FORMAT(//' GEOMETRY AND STRENGTHS FOR... ,10X 'SOURCE AND DOUBLET'
     *       //3X,'I',6X,'X/D',7X,'Y/D',7X,'Z/D' ,
     *       ' M/(D*U0)    MU/(D*D*U0)'/)
```

```
  622  FORMAT (//' COMPUTATIONAL MODEL INCLUDES:'/' THE FOLLOWING '
     *          'SING LARITIES:')
  623  FORMAT (30X,'VORTEX PAIR')
  624  FORMAT (30X,'SOURCES')
  625  FORMAT (30X,'DOUBLETS')
  626  FORMAT (/,' IMAGE LAYERS =',I2,',    M-INITIAL =',I2)
  627  FORMAT (' JET EFFECT ON RAIL =',I2)
  628  FORMAT (' JET INTERFERENCE VELOCITY AT TUNNEL CENTER_LINE :'
  629  FORMAT (/3X,'I',6X,'X/B',7X,'Y/B',7X,'Z/H',7X,'DELW/UO',5X,
     *          'DELV/UO',5X,'U=W/UO',4X,'CP_MODED')
C
  630  FORMAT (25X,5F10.6)
  640  FORMAT (I4,1X,3F10.4,1X,4F12.4)
C
       END
```

```
JTEFCT 329
JTEFCT 331
JTEFCT 332
JTEFCT 333
JTEFCT 334
JTEFCT 335
JTEFCT 336
JTEFCT 337
JTEFCT 338
JTEFCT 339
JTEFCT 340
JTEFCT 341
JTEFCT 342
JTEFCT 343
JTEFCT 344
```

```
      SUBROUTINE CPREAD(ITEST,IRUN,IPNT, CP, NO)                        CPREAD 001
C                                                                       CPREAD 002
C-    READS IN EXPERIMENTAL CP VALUES FROM UNIT 7.                      CPREAD 003
C                                                                       CPREAD 004
      COMMON /LOAD/ ALFU,POU,QOU,CMUU,CLU,CDU,CMU                       CPREAD 005
      DIMENSION CP(30,8)                                                CPREAD 006
      IREW = 0                                                          CPREAD 007
   10 READ (7,560,END=30) NTEST,NRUN,NPNT                               CPREAD 008
      DO 20 J = 1,8                                                     CPREAD 009
   20 READ (7,510) (CP(I,J),I=1,NO)                                     CPREAD 010
      READ (7,520) ALFU,POU,QOU,CMUU,CLU,CDU,CMU                        CPREAD 011
      IF(ITEST.EQ.ITEST .AND. NRUN.EQ.IRUN .AND.                        CPREAD 012
     *   NPNT .EQ. IPNT ) RETURN                                        CPREAD 013
      GO TO 10                                                          CPREAD 014
C                                                                       CPREAD 015
   30 IF(IREW .NE. 0) GO TO 90                                          CPREAD 016
      IREW = 1                                                          CPREAD 017
      GO TO 10                                                          CPREAD 018
C                                                                       CPREAD 019
   90 WRITE (6,600) ITEST,IRUN,IPNT, NTEST,NRUN,NPNT                    CPREAD 020
      STOP                                                              CPREAD 021
C                                                                       CPREAD 022
  500 FORMAT (16I5)                                                     CPREAD 023
  510 FORMAT (2X,9F8.4)                                                 CPREAD 024
  520 FORMAT (7E10.2)                                                   CPREAD 025
  600 FORMAT (///' *** NO DATA IN UNIT_7 WITH ITEST/IRUN/IPOINT =',     CPREAD 026
     *        3(I3/),' ***'//4X,'LAST DATA POINT READ IS : ',          CPREAD 027
     *        'ITEST,IRUN/IPOINT =',3(I3,'/'))                         CPREAD 028
      END                                                               CPREAD 029
```

```
      SUBROUTINE JETINT(ITEST,IRUN,IPNT, B,XC, UWL,URF, U,V,W, NO)
C
C-    WRITE_OUT JET INTERFERENCE VELOCITIES TO UNIT_11
C
      DIMENSION XC(30), UWL(30),URF(30), U(30),V(30),W(30)
C
      WRITE (11,1000) ITEST,IRUN,IPNT
      DO 30 I = 1,NO
      WRITE (11,1100) I, XC(I)/B, UWL(I),URF(I), U(I),V(I),W(I)
   30 CONTINUE
      RETURN
C
 1000 FORMAT (16I5)
 1100 FORMAT (I5,7E12.4)
      END
```

```
JETINT 001
JETINT 002
JETINT 003
JETINT 004
JETINT 005
JETINT 006
JETINT 007
JETINT 008
JETINT 009
JETINT 010
JETINT 011
JETINT 012
JETINT 013
JETINT 014
JETINT 015
```

```
      SUBROUTINE CPWRIT(ITEST,IRUN,IPNT, CP, NO)                        CPWRIT 001
      DIMENSION CP(30,8),UCP(30                                         CPWRIT 002
      COMMON /LOAD/ ALFU,POU,QOU,CMUU,CLU,CDU,CMU                       CPWRIT 003
C                                                                       CPWRIT 004
C-    CONVERTS CP_VALUES TO SUPER VELOCITY AND WRITES TO UNIT_10        CPWRIT 005
C                                                                       CPWRIT 006
      WRITE (10,500) ITEST,IRUN,IPNT                                    CPWRIT 007
      DO 20 J = 1,8                                                     CPWRIT 008
      DO 10 I = 1,NO                                                    CPWRIT 009
   10 UCP(I) = SQRT(ABS(1.-CP(I,J))) - 1.E                              CPWRIT 010
   20 WRITE (10,510) (UCP(I),I=1,NO)                                    CPWRIT 011
      WRITE (10,520) ALFU,POU,QOU,CMUU,CLU,CDU,CMU                      CPWRIT 012
C                                                                       CPWRIT 013
  500 FORMAT (16I5)                                                     CPWRIT 014
  510 FORMAT (2X,9F8.4)                                                 CPWRIT 015
  520 FORMAT (7F10.2)                                                   CPWRIT 016
C                                                                       CPWRIT 017
      RETURN                                                            CPWRIT 018
      END                                                               CPWRIT 019
```

```
   4     Ø
JET EFFECT CALCULATIONS FOR 3"_JET AT R = 2.
   43.0       [illegible]
 Ø.352ØØØ   1.122ØØØ   Ø.429668
 Ø.Ø76555   Ø.447Ø16
 [illegible]   [illegible]   Ø.Ø349ØØ
 Ø.757572   1.ØØ[illegible]   Ø.333333
  17    21     2     5
 Ø.ØØØØØØ   Ø.139535   Ø.27907Ø   Ø.4186Ø5   Ø.55814Ø   Ø.697674   Ø.8372Ø9   Ø.976744
 1.116279   1.255814   1.395349   1.744185   2.Ø93Ø23   2.44186Ø   2.79Ø698   3.139535
 3.488372
-Ø.613953  -Ø.465116  -Ø.372Ø93  -Ø.27907Ø  -Ø.186Ø47   Ø.Ø93Ø23   Ø.2Ø93Ø2   Ø.Ø69767
 Ø.139535   Ø.2Ø93Ø2   Ø.27907Ø   Ø.348837   Ø.4186Ø4   Ø.488372   [illegible]   Ø.697674
 Ø.8372Ø9   Ø.976744   1.116279   1.255814   1.395349
-Ø.[illegible]   Ø.ØØØØØØ
 Ø.[illegible]   Ø.5[illegible]
   Ø     2      1     Ø
 999     1      1
 2.ØØØØØØ   Ø.1ØØØØØ     Ø.ØØ[illegible]ØØ     Ø.Ø3ØØØØ
```

SAMPLE INPUT

TUNNEL GEOMETRY: B= 43.00, H= 32.00

JET MODEL.

CONSTANTS FOR...			
VORTEX CURVE, Z(X)	AZ	BZ	CZ
	0.352000	1.122000	0.429556
VORTEX CURVE, Y(X)	AY	BY	
	0.276955	0.440046	
VORTEX STRENGTH	AG	BG	CG
	0.606311	0.006554	0.004300
SRC/DBLT LINE, Z(X)	ACL	BCL	CCL
	0.757572	1.000000	0.333333

SAMPLE OUTPUT

(GEOMETRICAL CONSTANTS)

*** JET MODEL ***

SIZE AND LOCATIONS :-	R	D/H	YJET/B	ZJET/H
	2.000000	0.100000	0.000000	0.000000

SAMPLE OUTPUT

(JET MODEL DEFINITION)

VORTEX GEOMETRY AND STRENGTHS :

I	X/D	Y/D	Z/D	GAMA/(D*UO)
1	0.0000	0.2500	0.0000	0.2451E+00
2	2.0000	0.2088	1.0019	0.5765E+00
3	4.0000	0.2833	1.3899	0.[illegible]77E+00
4	6.0000	0.33[illegible]	1.6544	0.[illegible]234E+00
5	8.0000	0.3843	1.8721	0.5[illegible]E+00
6	10.0000	0.4242	2.0685	0.5[illegible]20E+00
7	12.0000	0.4594	2.2284	0.5[illegible]13E+00
8	14.0000	0.4916	2.3810	0.5869E+00
9	16.0000	0.5214	2.5216	0.[illegible]79E+00
10	18.0000	0.5491	2.6525	0.4[illegible]20E+00
11	20.0000	0.5752	2.7753	0.4543E+00
12	25.0000	0.6345	3.0546	0.[illegible]43E+00
13	[illegible]0.0000	0.6875	3.3015	0.[illegible]5E+00
14	[illegible].0000	0.7356	3.5797	0.[illegible]65E+00
15	4[illegible].0000	0.7803	3.7381	0.[illegible]29E+00
16	45.0000	0.8218	3.9322	0.[illegible]69E+00
17	50.0000	0.8608	4.1143	0.3942E+00

130

GEOMETRY AND STRENGTHS FOR... SOURCE AND DOUBLET

I	X/D	Y/D	Z/D	M (D*UO)	MU/(D**2*UO)
1	0.0000	0.2500	0.0000	0.[illegible]57E+00	0.15[illegible]E+01
2	2.0000	0.2088	1.9899	0.3128E+00	0.18[illegible]E+01
3	4.0000	0.283[illegible]	2.4[illegible]	0.[illegible]513E+00	0.21[illegible]E+01
4	6.0000	0.338[illegible]	2.7[illegible]	0.[illegible]17E+00	0.24[illegible]E+01
5	8.0000	0.384[illegible]	3.0[illegible]3	0.[illegible]6E+00	0.26[illegible]E+01
6	10.0000	0.424[illegible]	3.2643	0.[illegible]11E+00	0.28[illegible]E+01
7	12.0000	0.4594	3.4[illegible]68	0.[illegible]19E+00	0.3[illegible]E+01
8	14.0000	0.4916	3.6[illegible]17	0.[illegible]47E+00	0.3[illegible]E+01
9	16.0000	0.5214	3.[illegible]179	0.[illegible]9E+00	0.[illegible]E+01
10	18.0000	0.5491	3.9[illegible]	0.[illegible]40E+00	0.3[illegible]E+01
11	20.0000	0.575[illegible]	4.1[illegible]7	0.[illegible]E+00	0.3[illegible]E+01
12	[illegible]	0.634[illegible]	4.4[illegible]	0.[illegible]E+00	0.[illegible]E+01
13	[illegible]	0.6875	4.7[illegible]79	0.[illegible]43E+00	0.4[illegible]E+01
14	[illegible]	0.7354	4.[illegible]1	0.[illegible]414E+00	0.4[illegible]E+01
15	[illegible]	0.7444	[illegible].0000	0.[illegible]E+00	0.[illegible]E+01

COMPUTATIONAL MODEL INCLUDES
THE FOLLOWING SINGULARITIES:

VORTEX PAIR
SOURCES
DOUBLETS

SAMPLE OUTPUT

(JET EFFECT ON TUNNEL SURFACE)

IMAGE LAYERS = 5,   M-INITIAL = 0
JET EFFECT ON RAIL - 1

I	X/B	Y/B	Z/H	DELU/UO	DELV/UO	DELW/UO	CP_MODFD
1	-0.8140	-0.5000	0.0000	0.4907E-02	-0.3634E-03	-0.4056E-03	-0.9839E-02
2	-0.4651	-0.5000	0.0000	0.1027E-02	-0.3972E-03	-0.1486E-02	-0.8033E-02
3	-0.3721	-0.5000	0.0000	0.4429E-02	-0.3918E-03	-0.2106E-02	-0.8883E-02
4	-0.2791	-0.5000	0.0000	0.5514E-02	-0.3956E-03	-0.2915E-02	-0.1107E-01
5	-0.1860	-0.5000	0.0000	0.7564E-02	-0.3967E-03	-0.3954E-02	-0.1520E-01
6	0.0930	-0.5000	0.0000	0.2030E-01	-0.1903E-02	-0.7546E-02	-0.4640E-01
7	0.0000	-0.5000	0.0000	0.1511E-01	-0.1002E-02	-0.6416E-02	-0.3049E-01
8	0.0698	-0.5000	0.0000	0.1876E-01	-0.1003E-02	-0.7277E-02	-0.3793E-01
9	0.1395	-0.5000	0.0000	0.2246E-01	-0.1003E-02	-0.8014E-02	-0.4550E-01
10	0.2093	-0.5000	0.0000	0.2600E-01	-0.1002E-02	-0.8535E-02	-0.5274E-01
11	0.2791	-0.5000	0.0000	0.2923E-01	-0.1001E-02	-0.8987E-02	-0.5940E-01
12	0.3486	-0.5000	0.0000	0.3215E-01	-0.1000E-02	-0.9235E-02	-0.6543E-01
13	0.4186	-0.5000	0.0000	0.3477E-01	-0.3981E-03	-0.9365E-02	-0.7084E-01
14	0.4884	-0.5000	0.0000	0.3714E-01	-0.9957E-03	-0.9396E-02	-0.7574E-01
15	0.5874	-0.5000	0.0000	0.4015E-01	-0.9915E-03	-0.9322E-02	-0.8201E-01
16	0.6977	-0.5000	0.0000	0.4315E-01	-0.3857E-03	-0.9138E-02	-0.8924E-01
17	0.8372	-0.5000	0.0000	0.4655E-01	-0.9767E-03	-0.9821E-02	-0.9535E-01
18	0.9767	-0.5000	0.0000	0.4965E-01	-0.9660E-03	-0.8401E-02	-0.1016E+00
19	1.1163	-0.5000	0.0000	0.5252E-01	-0.9535E-03	-0.8116E-02	-0.1079E+00
20	1.2558	-0.5000	0.0000	0.5518E-01	-0.9395E-03	-0.7733E-02	-0.1135E+00
21	1.3953	-0.5000	0.0000	0.5766E-01	-0.9239E-03	-0.7331E-02	-0.1187E+00

181

IMAGE LAYERS = 5,   M-INITIAL = 0
JET EFFECT ON RAIL - 2

I	X/B	Y/B	Z/H	DELU/UO	DELV/UO	DELW/UO	CP_MODFD
1	-0.8140	0.0000	0.5000	0.1240E-02	0.9391E-09	0.1263E-02	-0.8500E-02
2	-0.4651	0.0000	0.5000	-0.4185E-03	0.7860E-09	0.1317E-02	0.8351E-03
3	-0.3721	0.0000	0.5000	-0.2736E-02	0.7139E-09	0.1321E-02	0.5582E-02
4	-0.2791	0.0000	0.5000	-0.5943E-02	0.3086E-09	0.1337E-02	0.1185E-01
5	-0.1860	0.0000	0.5000	-0.9546E-02	0.1182E-08	0.1345E-02	0.1900E-01
6	0.0930	0.0000	0.5000	0.1086E-02	0.4011E-06	0.1355E-02	-0.2174E-02
7	0.0000	0.0000	0.5000	-0.9681E-02	0.1244E-08	0.1356E-02	0.1927E-01
8	0.0698	0.0000	0.5000	-0.3251E-02	0.1703E-08	0.1351E-02	0.4695E-02
9	0.1395	0.0000	0.5000	0.8474E-02	0.1762E-08	0.1359E-02	-0.1702E-01
10	0.2093	0.0000	0.5000	0.1796E-01	0.1002E-08	0.1361E-02	-0.3625E-01
11	0.2791	0.0000	0.5000	0.2416E-01	0.1630E-09	0.1359E-02	-0.4890E-01
12	0.3488	0.0000	0.5000	0.2768E-01	0.1303E-02	0.1357E-02	-0.5614E-01
13	0.4186	0.0000	0.5000	0.3053E-01	0.4817E-08	0.1354E-02	-0.6156E-01
14	0.4884	0.0000	0.5000	0.3211E-01	-0.1516E-06	0.1356E-02	-0.6525E-01
15	0.5874	0.0000	0.5000	0.3497E-01	0.2732E-08	0.1342E-02	-0.7117E-01
16	0.6977	0.0000	0.5000	0.3753E-01	0.7913E-08	0.1332E-02	-0.7647E-01
17	0.8372	0.0000	0.5000	0.4081E-01	-0.1249E-06	0.1315E-02	-0.8329E-01
18	0.9767	0.0000	0.5000	0.4410E-01	0.7863E-08	0.1294E-02	-0.9014E-01
19	1.1163	0.0000	0.5000	0.4754E-01	0.8829E-08	0.1276E-02	-0.9735E-01
20	1.2558	0.0000	0.5000	0.5166E-01	0.2951E-09	0.1242E-02	-0.1066E+00
21	1.3953	0.0000	0.5000	0.5927E-01	-0.1462E-07	0.1211E-02	-0.1221E+00

IMAGE LAYERS = 5,   M-INITIAL = 1
JET INTERFERENCE VELOCITY AT TUNNEL CENTER_LINE :

I	X/R	Y/B	Z/H	DELU/UO	DELV/UO	DELW/UO	CP_MODFD
1	-0.8140	0.0000	0.0000	0.7783E-02	0.8688E-09	-0.2588E-06	
2	-0.4651	0.0000	0.0000	0.3825E-02	0.5780E-09	-0.5455E-03	
3	-0.3721	0.0000	0.0000	0.3696E-02	0.6780E-09	-0.5112E-03	
4	-0.2791	0.0000	0.0000	0.1895E-01	0.8527E-09	-0.1425E-02	
5	-0.1860	0.0000	0.0000	0.1267E-01	0.1252E-08	-0.3092E-02	
6	0.0930	0.0000	0.0000	0.2061E-01	0.1257E-08	-0.4586E-02	
7	0.0000	0.0000	0.0000	0.1756E-01	0.1029E-08	-0.3767E-02	
8	0.0930	0.0000	0.0000	0.1982E-01	0.1357E-08	-0.4391E-02	
9	0.1395	0.0000	0.0000	0.2022E-01	0.9404E-09	-0.4252E-02	
10	0.2093	0.0000	0.0000	0.2409E-01	0.9763E-09	-0.5418E-02	
11	0.2791	0.0000	0.0000	0.2714E-01	0.1438E-08	-0.5785E-02	
12	0.3488	0.0000	0.0000	0.2952E-01	0.1156E-08	-0.6064E-02	
13	0.4186	0.0000	0.0000	0.3161E-01	0.1042E-08	-0.6273E-02	
14	0.4884	0.0000	0.0000	0.3398E-01	0.1000E-08	-0.6438E-02	
15	0.5874	0.0000	0.0000	0.3688E-01	0.1052E-08	-0.6597E-02	
16	0.6977	0.0000	0.0000	0.3985E-01	0.8595E-09	-0.6738E-02	
17	0.8372	0.0000	0.0000	0.4328E-01	0.1045E-08	-0.6876E-02	
18	0.9767	0.0000	0.0000	0.4640E-01	0.5412E-09	-0.6990E-02	
19	1.1163	0.0000	0.0000	0.4927E-01	0.1230E-08	-0.7086E-02	
20	1.2558	0.0000	0.0000	0.5188E-01	0.5567E-09	-0.7177E-02	
21	1.3953	0.0000	0.0000	0.5423E-01	0.3895E-09	-0.7164E-02	

SAMPLE OUTPUT

(INTERFERENCE DUE TO JET)